LOCKHEED MARTIN ENERGY RESEARCH LIBRARIES
3 4456 0515062 6

CENTRAL RESEARCH LIBRARY
DOCUMENT COLLECTION

cy. 200

ORNL-4705
UC-34 – Physics

NEUTRON PHYSICS DIVISION
ANNUAL PROGRESS REPORT
FOR PERIOD ENDING MAY 31, 1971

OAK RIDGE NATIONAL LABORATORY
CENTRAL RESEARCH LIBRARY
DOCUMENT COLLECTION
LIBRARY LOAN COPY
DO NOT TRANSFER TO ANOTHER PERSON
If you wish someone else to see this document, send in name with document and the library will arrange a loan.
UCN-7969
(9 3-67)

OAK RIDGE NATIONAL LABORATORY
operated by
UNION CARBIDE CORPORATION
for the
U.S. ATOMIC ENERGY COMMISSION

Printed in the United States of America. Available from
National Technical Information Service
U.S. Department of Commerce
5285 Port Royal Road, Springfield, Virginia 22151
Price: Printed Copy $3.00; Microfiche $0.95

This report was prepared as an account of work sponsored by the United States Government. Neither the United States nor the United States Atomic Energy Commission, nor any of their employees, nor any of their contractors, subcontractors, or their employees, makes any warranty, express or implied, or assumes any legal liability or responsibility for the accuracy, completeness or usefulness of any information, apparatus, product or process disclosed, or represents that its use would not infringe privately owned rights.

ORNL-4705
UC-34 – Physics

Contract No. W-7405-eng-26

NEUTRON PHYSICS DIVISION
ANNUAL PROGRESS REPORT
For Period Ending May 31, 1971

F. C. Maienschein, Director
R. G. Alsmiller, Associate Director
C. E. Clifford, Associate Director
R. W. Peelle, Associate Director

OCTOBER 1971

OAK RIDGE NATIONAL LABORATORY
Oak Ridge, Tennessee 37830
operated by
UNION CARBIDE CORPORATION
for the
U.S. ATOMIC ENERGY COMMISSION

LOCKHEED MARTIN ENERGY RESEARCH LIBRARIES
3 4456 0515062 6

Reports previously issued in this series are as follows:

ORNL-2081	Period Ending September 10, 1956
ORNL-2389	Period Ending September 1, 1957
ORNL-2609	Period Ending September 1, 1958
ORNL-2842	Period Ending September 1, 1959
ORNL-3016	Period Ending September 1, 1960
ORNL-3193	Period Ending September 1, 1961
ORNL-3360	Period Ending September 1, 1962
ORNL-3499, Vols. I and II	Period Ending August 1, 1963
ORNL-3714, Vols. I and II	Period Ending August 1, 1964
ORNL-3858, Vols. I and II	Period Ending August 1, 1965
ORNL-3973, Vols. I and II	Period Ending May 31, 1966
ORNL-4134	Period Ending May 31, 1967
ORNL-4280	Period Ending May 31, 1968
ORNL-4433	Period Ending May 31, 1969
ORNL-4592	Period Ending May 31, 1970

Contents

1. NEUTRON CROSS SECTIONS 1

1.0 Introduction – R. W. Peelle 1

1.1 ^{238}U Cross-Section Measurements by Transmission and Self-Indication Techniques – E. G. Silver, G. de Saussure, R. B. Perez, and R. Ingle 2

1.2 Measurement of Neutron Cross Sections of ^{238}U and ^{235}U Below 100 keV at the ORELA – E. G. Silver, G. de Saussure, R. B. Perez, and R. Ingle 4

1.3 Measurements of the Neutron Absorption and Fission Cross Sections of ^{239}Pu and ^{235}U Over the Energy Range from 0.02 eV to 400 keV – R. Gwin, E. G. Silver, R. W. Ingle, and H. Weaver 4

1.4 Neutron Multiplicity for ^{239}Pu Resonance Fission – L. W. Weston and J. H. Todd 9

1.5 Measurement of the Neutron Capture and Fission Cross Sections for ^{241}Pu – L. W. Weston and J. H. Todd 9

1.6 Simultaneous Measurements of the Neutron Fission and Capture Cross Sections for ^{235}U for Incident Neutron Energies up to 100 keV – R. B. Perez, G. de Saussure, E. G. Silver, R. W. Ingle, and H. Weaver 10

1.7 Multilevel Analysis of the ^{233}U and ^{235}U Capture and Fission Cross Sections and Statistical Properties of the Kapur-Peierls Type Resonance Parameters for the S-Wave Cross Sections of the Fissile Isotopes – G. de Saussure, R. B. Perez, and H. Derrien 16

1.8 Multilevel Analysis of the ^{235}U Fission and Capture Cross Sections – G. de Saussure, R. B. Perez, and W. Kolar 16

1.9 Preparations for Precision Measurements of Fission Cross Sections for ^{235}U and ^{239}Pu in the Neutron Energy Range Above 30 keV – R. W. Peelle and L. W. Weston 21

1.10 Neutron Fission and Capture Cross-Section Measurements for Uranium-233 in the Energy Region 0.02 to 1 eV – L. W. Weston, R. Gwin, G. de Saussure, R. W. Ingle, J. H. Todd, C. W. Craven, R. W. Hockenbury, and R. C. Block 22

1.11 The Use of the Computer Program HYFITS to Generate Approximate Resonance Parameters – E. G. Silver, R. S. Booth, R. B. Perez, and G. de Saussure 23

1.12 Invariant Imbedding Approach to the Kapur-Peierls Nuclear Reaction Formalism – R. B. Perez 23

1.13 Variation of the R Matrix – A. J. Mockel and R. B. Perez 25

1.14 MSC, A Program to Evaluate Multiple Scattering Corrections in Thick Samples – N. M. Greene, R. B. Perez, G. de Saussure, and S. K. Penny 25

1.15 High-Resolution Inelastic Cross-Section Measurements for Na, Si, and Fe – F. G. Perey, W. E. Kinney, and R. L. Macklin 28

1.16 Status Report of the Oak Ridge Electron Linear Accelerator (ORELA) – N. A. Betz, J. A. Harvey, T. A. Lewis, F. C. Maienschein, J. W. Reynolds, and H. A. Todd 28

1.17 Pulse-Shape Measurements for the Oak Ridge Electron Linear Accelerator with Gamma-Ray Detection Techniques – L. W. Weston and J. H. Todd 31

1.18 Spectrum of Photons Emitted in Coincidence with Fission of ^{235}U by Thermal Neutrons – R. W. Peelle and F. C. Maienschein 31

1.19 Neutron Elastic- and Inelastic-Scattering Cross Sections for Yttrium in the Energy Range 4.19 to 8.56 MeV – F. G. Perey and W. E. Kinney 31

1.20 Elastic and Inelastic Scattering of Neutrons from Carbon in the Energy Range of 5–8.7 MeV – F. G. Perey and W. E. Kinney 31

1.21 V Neutron Elastic- and Inelastic-Scattering Cross Sections from 4.19 to 8.56 MeV – F. G. Perey and W. E. Kinney 31

1.22 Al Neutron Elastic- and Inelastic-Scattering Cross Sections from 4.19 to 8.56 MeV – W. E. Kinney and F. G. Perey 32

1.23 Scattering of Neutrons from Fe, Cu, and Pb – F. G. Perey and W. E. Kinney 32

1.24 Nucleon-Nucleus Optical Model Potential – F. G. Perey 32

1.25 Compilation of Optical Model Parameters – C. M. Perey 32

1.26 11-MeV Proton Inelastic Scattering from Even-Even Medium-Weight Nuclei – C. M. Perey, R. J. Silva, J. K. Dickens, and F. G. Perey 32

1.27 Measurements of the Neutron Fission and Absorption Cross Sections of ^{239}Pu Over the Energy Region 0.02 eV to 30 keV, Part II – R. Gwin, L. W. Weston, G. de Saussure, R. W. Ingle, J. H. Todd, F. E. Gillespie, R. W. Hockenbury, and R. C. Block 33

1.28 Fast Fission Chamber Amplifier-Discriminator System – R. W. Ingle, F. E. Gillespie and L. W. Weston 33

2. REACTOR AND WEAPONS RADIATION SHIELDING 34

2.0 Introduction – C. E. Clifford 34

2.1 Shielding for Advanced Reactors in the United States – F. C. Maienschein, C. E. Clifford, F. R. Mynatt, and L. S. Abbott 35

2.2 FFTF Related Studies in the ORNL-LMFBR Shielding Program – F. R. Mynatt, C. E. Clifford, F. J. Muckenthaler, R. E. Maerker, M. L. Gritzner, L. R. Williams, and J. L. Rathbun 36

2.3 Measurements of the Transport of Reactor Neutrons Through Iron Shields – C. E. Clifford, F. J. Muckenthaler, P. N. Stevens, K. M. Henry, L. B. Holland, J. L. Hull, J. J. Manning, and J. N. Money 37

2.4 Comparison of Monte Carlo Calculations with Measurements of Neutron Transport in Iron – R. E. Maerker, R. Q. Wright, G. W. Morrison, R. M. Freestone, Jr., and M. B. Emmett 38

2.5 Measurements of the Transport of Reactor Neutrons Through Iron Shields Containing Plane and Annular Slits – C. E. Clifford, F. J. Muckenthaler, P. N. Stevens, K. M. Henry, L. B. Holland, J. L. Hull, J. J. Manning, and J. N. Money 42

2.6 Experimental Investigation of Neutron Streaming Through the Grid Plate Shield of the Fast Flux Test Facility – C. E. Clifford, F. J. Muckenthaler, P. N. Stevens, K. M. Henry, L. B. Holland, J. L. Hull, J. J. Manning, and J. N. Money 43

2.7 Calculated Neutron Flux Distribution Resulting from a Fission Source Located at the Center of a 10-meter-diam Sphere of Sodium – C. L. Thompson 43

2.8 The Low-Energy Neutron Spectrum of the ORNL Tower Shielding Reactor Beam – R. M. Freestone, Jr., F. J. Muckenthaler, K. M. Henry, and C. E. Clifford 43

2.9 Response Functions for Bonner Ball Neutron Detectors – R. E. Maerker, L. R. Williams, F. R. Mynatt, and N. M. Greene 44

2.10 Calibration of the Bonner Ball Neutron Detectors Used at the Tower Shielding Facility – R. E. Maerker, F. J. Muckenthaler, J. J. Manning, J. L. Hull, J. N. Money, K. M. Henry, and R. M. Freestone, Jr. 44

2.11 The Energy Spectrum of Photoneutrons Produced by 140-MeV Electrons Incident on Tantalum – C. E. Burgart, E. A. Straker, T. A. Love, and R. M. Freestone, Jr. 44

2.12 Simultaneous Determination of Fast-Neutron Spectra by Time-of-Flight and Pulse-Height Unfolding Techniques – E. A. Straker, C. E. Burgart, T. A. Love, and R. M. Freestone, Jr. 44

2.13 Measurements and Calculations of the Time-Dependent Spectra of Gamma Rays Emerging from Polyethylene Slabs Pulsed with Neutrons – C. E. Burgart, E. A. Straker, T. A. Love, G. L. Morgan, and R. M. Freestone, Jr. 45

2.14 TAKER – Data Acquisition Program for a PDP-9 Computer – C. E. Burgart and R. M. Freestone, Jr. 46

2.15 A Study of the Overlap Conditions Required in Sequential Discrete Ordinates Transport Calculations for a 14-MeV Neutron Source in a 5000-m Radius Cylinder of Air – J. V. Pace, III, F. R. Mynatt, and L. S. Abbott 47

2.16 Neutron and Secondary Gamma-Ray Induced Heat in the Ground Due to Point 12.1–15-MeV and Fission Sources at an Altitude of 50 Feet – E. A. Straker, M. B. Emmett, and M. L. Gritzner 47

2.17 Neutron and Gamma-Ray Fluences Transmitted Through a Slab of Borated Polyethylene – C. E. Burgart 47

2.18 Gamma-Ray Spectra Arising from Fast-Neutron Interactions in Elements Found in Soils, Concretes, and Structural Materials – R. E. Maerker and F. J. Muckenthaler 48

2.19 Gamma-Ray Spectra Arising from Thermal-Neutron Capture in Elements Found in Soils, Concretes, and Structural Materials – R. E. Maerker and F. J. Muckenthaler 48

2.20 Time-Dependent Neutron and Photon Transport Calculations Using the Method of Discrete Ordinates – S. A. Dupree, H. A. Sandmeier, G. E. Hansen, W. W. Engle, Jr., and F. R. Mynatt 48

2.21 Bracketing the Peak Primary Gamma-Ray Dose Rate from Nuclear Devices by Steady-State Transport Calculations – H. C. Claiborne and W. W. Engle, Jr. 48

2.22 The Ca($n,x\gamma$) Reaction at E_n = 5.9 MeV –
J. K. Dickens and F. G. Perey 49

2.23 Pb($n,x\gamma$) Reactions for E_n Between 4.9 and 8.0 MeV –
J. K. Dickens 49

2.24 Survey of ($n,x\gamma$) Gamma Production Cross Sections for E_n = 6 MeV –
J. K. Dickens 49

2.25 Deterioration of Large Ge(Li) Diodes Caused by Fast Neutrons –
P. H. Stelson, S. Raman, J. K. Dickens, and R. C. Trammell 50

2.26 Evaluation of Natural Lead Neutron and Gamma-Ray Production Cross Sections –
C. Y. Fu and F. G. Perey 50

2.27 A Calculation of Neutron Energy-Dependent Capture Gamma-Ray Yield Spectra for Iron and Comparisons with Experiments –
J. E. White, C. Y. Fu, and K. J. Yost 51

2.28 Fe($n,x\gamma$) Reaction for E_n Between 4.0 and 9.0 MeV –
J. K. Dickens and F. G. Perey 51

2.29 Weapons Radiation Shielding Handbook: Status Report – L. S. Abbott, H. C. Claiborne, and C. E. Clifford, Editors 53

2.30 A Re-Evaluation of Natural Iron Neutron and Gamma-Ray Production Cross Sections – ENDF/B Material 1124 – S. K. Penny and W. E. Kinney 53

2.31 Evaluation of the Cross Sections of Iron: ENDF/B MAT 1101 –
D. C. Irving and E. A. Straker 53

2.32 Energy Calibration of a Proton-Recoil Proportional Counter –
G. L. Morgan, T. A. Love, E. A. Straker, R. M. Freestone, Jr., and C. E. Burgart 54

2.33 INTRIGUE-II: An IBM-360 Subroutine Package for Making Linear, Logarithmic and Semilogarithmic Graphs Using the CALCOMP Plotter – M. B. Emmett 54

2.34 A Calculation of Neutron-Induced Physical Doses in Human Tissues –
J. J. Ritts, M. Solomito, and P. N. Stevens 54

2.35 Heat Generation by Neutrons in Some Moderating and Shielding Materials –
H. C. Claiborne, M. Solomito, and J. J. Ritts 54

2.36 Use of the Discrete Ordinates S_n Method in Radiation Shielding Calculations –
P. N. Stevens 55

2.37 MORSEC, A Revised Cross-Section Module for the MORSE Multigroup Monte Carlo Code – E. A. Straker and M. B. Emmett 55

2.38 Methods of Biasing Secondary Gamma-Ray Production in Coupled Neutron Gamma-Ray Monte Carlo Calculations – M. Solomito, P. N. Stevens, E. A. Straker, C. E. Burgart, and S. N. Cramer 55

2.39 A General Method of Importance Sampling the Angle of Scattering in Monte Carlo Calculations – C. E. Burgart and P. N. Stevens 56

2.40 Collision Density Plotting Routines and Collision Density Fluence Estimates for the MORSE Monte Carlo Code – E. A. Straker and M. B. Emmett 56

2.41 XCHEKR – A Multigroup Cross-Section Editing and Checking Code –
C. E. Burgart and E. A. Straker 56

2.42 NNNGAM: A Code for Calculating Gamma-Ray Spectra from Competing (n,n') and $(n,2n)$ Reactions – C. Y. Fu 57

2.43 A Comparison of Folding and Unfolding Techniques for Determining the Gamma Spectrum from Thermal Neutron Capture in Aluminum – R. S. Booth 57

2.44 The ORNL-SNAP Shielding Program – F. R. Mynatt, C. E. Clifford, F. J. Muckenthaler, and M. L. Gritzner 58

2.45 The Design of Asymmetric 4π Shields for Space Reactors – W. W. Engle, Jr., R. L. Childs, and F. R. Mynatt 58

2.46 Optimization of a Shield for a Heat-Pipe-Cooled Fast Reactor Designed as a Nuclear Electric Space Power Plant – W. W. Engle, Jr., R. L. Childs, F. R. Mynatt, and L. S. Abbott 58

2.47 Development of Shield Optimization Techniques – R. L. Childs 58

2.48 MORSE Monte Carlo Shielding Calculations for the Zirconium Hydride Reference Reactor – C. E. Burgart 59

2.49 Application of DOT-MORSE Coupling to the Analysis of Three-Dimensional SNAP Shielding Problems – E. A. Straker, R. L. Childs, and M. B. Emmett 59

2.50 Comparisons of Monte Carlo Calculations to Measurements of Neutron Leakage from the TSF-SNAP Reactor – V. R. Cain 59

2.51 Examination of the Code ERF (Extended R-Matrix Formalism) with a Coupled Square-Well Potential – C. Y. Fu 60

2.52 A Unified Model of Deformed Odd-Odd Nuclei for Nuclear Data Generation and Analysis – C. Y. Fu and K. J. Yost 61

2.53 The POPOP4 Library and Codes for Preparing Secondary Gamma-Ray Production Cross Sections – W. E. Ford, III 61

2.54 The Testing of ^{238}U Secondary Gamma-Ray Production Data Sets from the POPOP4 Library – W. E. Ford, III, and J. S. Gillen 62

2.55 Gamma-Ray Spectra from Inelastic Neutron Scattering in ^{181}Ta – C. Y. Fu and K. J. Yost 62

2.56 Neutron Energy-Dependent Capture Gamma-Ray Yields in Tantalum and Tungsten – K. J. Yost, J. E. White, C. Y. Fu, and W. E. Ford, III 63

2.57 The Total Gamma-Ray Energy Spectrum Above 1 MeV from Neutron Interactions in ^{235}U and ^{238}U – R. S. Booth and F. J. Muckenthaler 63

2.58 Calculated Perturbations in Threshold Foil Measurements Due to Neutron Interactions in B_4C Shells – W. E. Ford, III, and J. S. Gillen 63

2.59 Al$(n,x\gamma)$ Reactions for $5.3 \leqslant E_n \leqslant 9.0$ MeV – J. K. Dickens 64

2.60 $^{28-30}$Si$(n,x\gamma)$ Reactions for $5.3 \leqslant E_n \leqslant 9.0$ MeV – J. K. Dickens 64

2.61 A Monoenergetic 6130-keV Gamma-Ray Source for Detector Calibration – J. K. Dickens and R. D. Baybarz 64

2.62 Pairing-Plus-Quadrupole Model Calculation of Band-Mixing Anomalies in ^{152}Sm – K. Kumar 65

2.63 The Adjoint Boltzmann Equation and Its Simulation by Monte Carlo – D. C. Irving 65

2.64 LEGCK, A Subroutine to Analyze Legendre Coefficients for Negativity in the Angular Distribution – D. C. Irving 65

3. RADIATION SHIELDING INFORMATION CENTER 66

3.1 Introduction, Functions, and Summary of Operations – B. F. Maskewitz, R. W. Roussin, H. C. Claiborne, J. Gurney, H. E. Comolander, H. R. Hendrickson, J. B. Wright, M. W. Landay, M. P. Guthrie, V. A. Jacobs, A. B. Gustin, C. M. Anthony, and J. D. Needham 66

3.2 The Space Shielding Handbook – R. T. Santoro, R. G. Alsmiller, Jr., H. C. Claiborne, and J. Barish 76

3.3 Bibliography, Subject Index, and Author Index of the Literature Examined by the Radiation Shielding Information Center (Reactor and Weapons Radiation Shielding) – H. C. Claiborne, R. W. Roussin, J. Gurney and A. B. Gustin 77

3.4 Bibliography, Subject Index, and Author Index of the Literature Examined by the Radiation Shielding Information Center (Space and Accelerator Shielding) – M. P. Guthrie, R. G. Alsmiller, Jr., J. Gurney and A. B. Gustin 78

3.5 Abstracts of the Literature Examined by the Radiation Shielding Information Center (Space and Accelerator Shielding) – M. P. Guthrie, R. G. Alsmiller, Jr., J. Gurney, and A. B. Gustin 78

3.6 A Review of the Monte Carlo Method for Radiation Transport Calculations (Collected Papers of a Seminar, October 5–7, 1970) – B. F. Maskewitz and V. Z. Jacobs, Compilers 78

3.7 Recent Developments in the Shielding of Neutron Sources – H. C. Claiborne 79

3.8 Shielding Against Neutrons in the Energy Range 15 to 75 MeV – R. W. Roussin, R. G. Alsmiller, Jr., and J. Barish 79

3.9 Computer Codes for Shielding Calculations – 1970 – B. F. Maskewitz and D. K. Trubey 80

3.10 The INDEX Data System: An Index of Nuclear Data Libraries Available at ORNL – J. L. Lucius, J. D. Jenkins, and R. Q. Wright 80

3.11 Adjoint S_n Calculations of Coupled Neutron and Gamma-Ray Transport Through Concrete Slabs – R. W. Roussin and F. A. R. Schmidt 80

3.12 Preparation of Data Sets in ENDF Format for Na, Mg, Cl, and K for Use in Shielding Calculations – R. W. Roussin, S. K. Penny, V. A. Singletary, and J. B. Wright 80

3.13 User's Manual for Programs to Edit and Combine DLC-5/Hallmark Calculational Results of Neutron and Secondary Gamma-Ray Transport in Air-Over-Ground Geometry – C. L. Thompson, I. J. Brown, and R. W. Roussin 81

3.14 Activities of the ANS-6 Subcommittee on Radiation Shielding Standards – H. C. Claiborne, D. J. Dudziak, and N. M. Schaeffer 81

3.15 A Computer Code Center – Experience and Operations – B. F. Maskewitz 81

3.16 Kernel Methods for Radiation Shielding Calculations – D. K. Trubey 81

3.17 Gamma-Ray Buildup Factor Coefficients for Concrete and Other Materials – D. K. Trubey 82

4. THEORETICAL STUDIES FOR MEDIUM- AND HIGH-ENERGY RADIATION SHIELDING 83

4.0 Introduction – R. G. Alsmiller, Jr. 83

4.1 Calculation of Nuclear Reactions for Incident Nucleons and π-Mesons in the Energy Range 30 to 2700 MeV – H. W. Bertini 83

4.2 Results from Medium-Energy Intranuclear-Cascade Calculation – H. W. Bertini and M. P. Guthrie 84

4.3 HECC-1, A Code to Calculate High-Energy Particle-Nucleus Reactions by the Method of Intranuclear Cascades – H. W. Bertini, A. H. Culkowski, N. B. Gove, and M. P. Guthrie 84

4.4 Calculation of the Photon-Production Spectrum from Proton-Nucleus Collisions in the Energy Range 15 to 150 MeV and Comparison with Experiment – Y. Shima and R. G. Alsmiller, Jr. 85

4.5 An Approximate High-Energy Alpha-Particle-Nucleus-Collision Model – T. A. Gabriel, R. T. Santoro, and R. G. Alsmiller, Jr. 85

4.6 Phenomenologically Determined Isobar Angular Distributions for Nucleon-Nucleon and Pion-Nucleon Reactions Below 3 GeV – H. W. Bertini, M. P. Guthrie, and A. H. Culkowski 86

4.7 Instructions for the Operation of Codes Associated with MECC-3, a Preliminary Version of an Intranuclear-Cascade Calculation for Nuclear Reactions – H. W. Bertini, M. P. Guthrie, and O. W. Hermann 86

4.8 EVAP-4: Another Modification of a Code to Calculate Particle Evaporation from Excited Compound Nuclei – M. P. Guthrie 86

4.9 Instructions for the Operation of the Program Package PICA, an Intranuclear-Cascade Calculation for High-Energy (30 to 400 MeV) Photon-Induced Nuclear Reactions – T. A. Gabriel, M. P. Guthrie, and O. W. Hermann 87

4.10 The Nucleon-Meson Transport Code NMTC – W. A. Coleman and T. W. Armstrong 87

4.11 Electromagnetic- and Nuclear-Cascade Calculations and Their Application in Shielding and Dosimetry – R. G. Alsmiller, Jr. 87

4.12 An Approximate Density-Effect Correction for the Ionization Loss of Charged Particles – T. W. Armstrong and R. G. Alsmiller, Jr. 88

4.13 The Absorbed Dose and Dose Equivalent from Neutrons in the Energy Range 60 to 3000 MeV and Protons in the Energy Range 400 to 3000 MeV – R. G. Alsmiller, Jr., T. W. Armstrong, and W. A. Coleman 88

4.14 Calculation of the Absorbed Dose and Dose Equivalent Induced by Medium-Energy Neutrons and Protons and Comparison with Experiment – T. W. Armstrong and B. L. Bishop 88

4.15 The Absorbed Dose and Dose Equivalent from Negatively and Positively Charged Pions in the Energy Range 10 to 2000 MeV – R. G. Alsmiller, Jr., T. W. Armstrong, and B. L. Bishop 88

4.16 Calculation of Depth-Dose Distributions Produced in Tissue by Negative Pions – T. W. Armstrong, R. G. Alsmiller, Jr., and K. C. Chandler 89

4.17 Calculation of the Radiation Hazard at Supersonic Aircraft Altitudes Produced by an Energetic Solar Flare–II. – T. W. Armstrong and H. S. Moran 91

4.18 Calculation of the Dose, Radionuclide Production, and Delayed Photon Leakage Due to Solar-Proton Bombardment of Tissue with Application to Astronaut Dosimetry – T. W. Armstrong and K. C. Chandler 91

4.19 Primary- and Secondary-Particle Contributions to the Depth-Dose Distribution in a Phantom Shielded from Solar-Flare and Van Allen Protons – R. T. Santoro, H. C. Claiborne, and R. G. Alsmiller, Jr. 91

4.20 Calculation of Cosmogenic Radionuclides in the Moon and Comparison with Apollo Measurements – T. W. Armstrong and R. G. Alsmiller, Jr. 92

4.21 Calculation of the Lunar Photon Albedo and Induced Dose Rate from Galactic and Solar Proton Bombardment – T. W. Armstrong 92

4.22 Monte Carlo Calculations of High-Energy Nucleon-Meson Cascades and Applications to Galactic Cosmic-Ray Transport – T. W. Armstrong, R. G. Alsmiller, Jr., and K. C. Chandler 92

4.23 The Lateral Spread of High-Energy (≤400 MeV) Neutron Beams and Earthshine – R. G. Alsmiller, Jr., F. R. Mynatt, M. L. Gritzner, J. V. Pace, and J. Barish 93

4.24 Calculated Activation of Copper and Iron by 3-GeV Protons – T. W. Armstrong and J. Barish 93

4.25 Calculation of the Long-Lived Induced Activity in Soil Produced by 200-MeV Protons – T. A. Gabriel 93

4.26 Calculation of the Long-Lived Induced Activity in the Soil Around High-Energy Accelerator Target Areas – T. A. Gabriel 93

4.27 Calculation of the Long-Lived Induced Activity in the Soil Around High-Energy Accelerator Target Areas – II – T. A. Gabriel, R. G. Alsmiller, Jr., and J. Barish 94

4.28 Calculation of the Long-Lived Activity in Soil Produced by 500-GeV Protons – T. A. Gabriel and R. T. Santoro 94

4.29 Nucleon and Pion Star Production from High-Energy (>40 GeV) Protons Incident on Iron – R. T. Santoro and T. A. Gabriel 94

4.30 Calculation of the Nucleon- and Pion-Induced Star and Flux Distributions from 400-GeV Proton Interactions in Iron – R. T. Santoro and T. A. Gabriel 94

4.31 Nucleon and Charged-Pion Albedo Spectra in an Accelerator Cave from 200-GeV Proton Interactions in Iron – T. A. Gabriel and R. T. Santoro 94

4.32 Muon Transport and the Shielding of High-Energy (≤500 GeV) Proton Accelerators – R. G. Alsmiller, Jr., F. S. Alsmiller, J. Barish, and Y. Shima 95

4.33 Low-Energy Electron Transport with the Method of Discrete Ordinates – D. E. Bartine, R. G. Alsmiller, Jr., F. R. Mynatt, W. W. Engle, Jr., and J. Barish 95

4.34 Energy Deposition by 45-GeV Photons in Be and Al – R. G. Alsmiller, Jr., and H. S. Moran 96

5. MEDIUM-ENERGY NUCLEON SPECTROSCOPIC STUDIES 97

5.0 Introduction – R. W. Peelle 97

5.1 Experimental Nuclear Cross Sections for Spacecraft Shield Analysis – R. W. Peelle 97

5.2 Neutron Spectral Measurements in the Upper Atmosphere – W. Zobel, T. A. Love, J. T. Delorenzo, and C. O. McNew 97

5.3 Hydrogen and Helium Particles Produced by 59-MeV Alpha Particle Bombardment of ^{12}C, ^{16}O, and ^{54}Fe – F. E. Bertrand and R. W. Peelle 98

5.4 Differential Cross Sections at Forward Angles for Hydrogen and Helium Particles from 62-MeV Protons Incident on ^{60}Ni – R. W. Peelle and F. E. Bertrand 99

5.5 Cross Sections for Hydrogen and Helium Particles Produced by 62- and 39-MeV Protons on ^{209}Bi – F. E. Bertrand and R. W. Peelle 99

5.6 Evidence from 62-MeV Proton Scattering for Extending the Weak Coupling Model in ^{209}Bi – F. E. Bertrand and M. B. Lewis 100

5.7 Differential Cross Sections for Neutrons from 40- and 60-MeV Protons on Nuclei – J. W. Wachter, R. T. Santoro, T. A. Love, and W. Zobel 101

5.8 A Pre-Target Monitor for the Intensity and Time Distribution of a Proton Beam – R. T. Santoro, J. W. Wachter, and T. A. Love 103

PUBLICATIONS AND PAPERS PRESENTED AT SCIENTIFIC MEETINGS 104

1. Neutron Cross Sections

1.0 INTRODUCTION

R. W. Peelle

This section reports experimental cross-section measurements, theoretical studies, and instrument development performed in support of the AEC's fast breeder reactor program. The measurements, performed at Van de Graaff and linear accelerator installations, span the entire energy region of interest to the engineering of reactors and their shields. Related measurements of $(n,x\gamma)$ reactions for 5- to 9-MeV neutrons, formerly reported in this section, may now be found in Sect. 2.

The first fourteen and last two reports in this section relate primarily to the program at the Oak Ridge Electron Linear Accelerator (ORELA) for measurement of cross sections for the important fertile and fissile nuclides, though the theoretical work in papers 1.12 and 1.13 has broad application in nuclear reaction theory. One or more studies are reported involving nuclides ^{233}U, ^{235}U, ^{238}U, ^{239}Pu, ^{240}Pu, and ^{241}Pu, with general emphasis on simultaneous measurements of fission and capture cross sections for the various nuclides under conditions sufficiently comparable that some errors should cancel in ratio determinations. The largest share of the work is performed with ORELAST, the large scintillator tank which serves to detect photons from fission and from neutron capture. These experiments are arduous because high (3-5%) accuracy must be sought, but this year preliminary results have been released which are useful to cross-section evaluators.

Papers 1.3 and 1.6 each present results for the average fission cross section of ^{235}U in the region from 10 to 80 keV and for α (the ratio of average capture and fission cross sections) for ^{235}U in the energy range from 0.1 to 10 keV. Both sets of data used similar experimental techniques with ORELAST, but the data and analyses are independent. The deadline for this report did not allow a full study of the output differences, but the average +4% difference between the fission cross-section values in reports 1.6 and 1.3 and the rms 7% difference between the values of α may reflect some of the current uncertainties in results obtained using ORELAST. Other sets of data obtained with ORELAST show greater differences. Experimental uncertainties for energies near and above 100 keV are expected to be reduced when ORELAST is moved to the new flight station 150 m from ORELA's neutron-producing target.

Paper 1.5 describes early efforts on ^{241}Pu using a completely different method for observing capture and fission cross sections. We anticipate that this method will be sufficiently successful that its application to other isotopes will provide a good check on the results obtained using ORELAST.

Papers 1.19 through 1.26 result from the productive program of fast-neutron inelastic-scattering cross sections carried out at the ORNL Van de Graaff facility over the past several years. The experimental part of this program is now complete. Abstract 1.15, which refers to the very narrow-resolution studies of neutron inelastic scattering which are now to be carried out at the ORELA, represents the opportunity afforded by the conclusion of the Van de Graaff work. Our knowledge of the energy dependence of inelastic neutron scattering has generally been disturbed so much by poor experimental resolution that a user could carelessly come to believe that inelastic cross sections are smooth even when the total cross section is known to have structure!

Paper 1.16 reviews the operation and continued development of the ORELA facility. Appropriate beams were available for 4400 hr, 78% of the hours scheduled. The scheduled time does not include the six weeks required to repair a mechanical failure of the pressure tank which houses the electron gun and its associated electronics. The ORELA data-handling system is approaching completion, and experience with the completed portion of the data-acquisition system has proven both hardware and software to be powerful and reliable.

1.1 ^{238}U CROSS-SECTION MEASUREMENTS BY TRANSMISSION AND SELF-INDICATION TECHNIQUES

E. G. Silver R. Perez
G. de Saussure R. Ingle[1]

In addition to the measurements of the capture cross section of ^{238}U in the large scintillator tank ORELAST,[2] cross-section measurements for ^{238}U are being made by transmission and self-indication techniques at the 40-m station of flight path No. 6 of the Oak Ridge Electron Linear Accelerator. Figure 1.1.1 shows the experimental arrangements in schematic form. The results obtained by these methods have not yet been analyzed extensively, but the work is currently in progress.

Both the transmission (T) measurements, which yield total cross sections, and the self-indication (SI) measurements used transmission samples consisting of ^{238}U-metal disks of high isotopic purity. These samples, 4.125 in. in diameter, are described in Table 1.1.1. These were located at the 20-m station of the flight path in a sample changer that permitted cooling the material to about -190°C. The SI measurements were made with the transmission samples both at room temperature and at the low temperature; the T measurements were made with the samples at room temperature only. The sample thicknesses (obtained by combining disks in some cases) ranged from 3 to 1300 mils in the SI runs and from 10 to 1455 mils in the T runs.

In the SI measurements the beam filtered through the samples at the 20-m station was observed at the 40-m station exactly as it was in the capture cross-section measurements.[2] That is, the beam passed through the beryllium-walled BF_3 chamber (which in these measurements monitored the total transmission) into the ORELAST, where capture events were detected with the same 25-mil ^{238}U sample used in the capture cross-section measurements.

For the T measurements the filtered neutron beam was detected at the 40-m station by a 3-in.-diam, l-mm thick ^{6}Li glass detector viewed by two RCA 7585

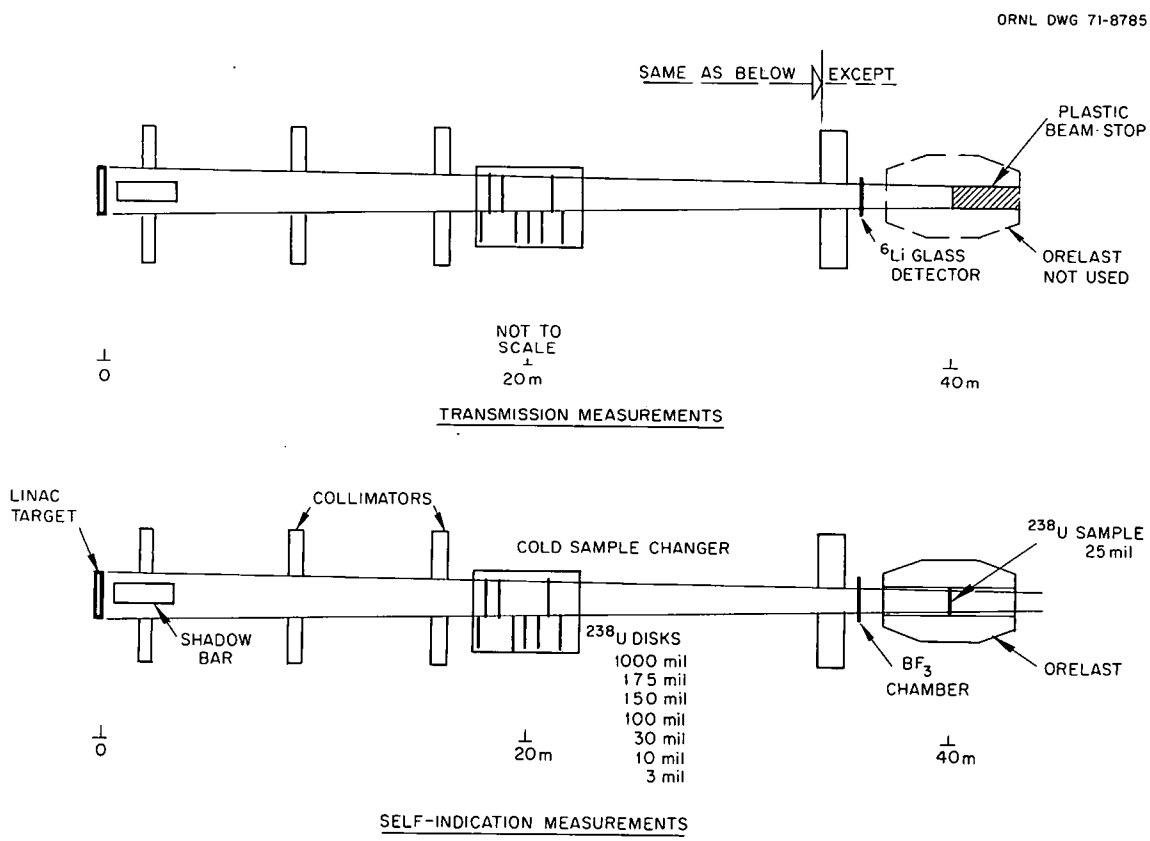

Fig. 1.1.1. Schematic Diagram of Experimental Arrangement Used for Transmission and Self-Indication Measurements on ^{238}U (Not to Scale).

Table 1.1.1. ^{238}U Transmission Samples[a]

Nominal Thickness (mil)	Weight (g)	Diameter (cm)	Areal Density (g/cm^2)	Isotopic Composition
1000	4724.8	11.13	48.560	99.92% ^{238}U; 0.042% ^{235}U; 0.012% ^{236}U; 0.026% ^{234}U
100	475.18	11.11	4.900	
30	144.11	11.12	1.483	
10	47.92	11.18	0.488	99.973% ^{238}U; 0.268% ^{235}U; 0.0003% ^{236}U; 0.0003% ^{234}U
3	12.80	11.18	0.130	
175[b]	694.40	11.10	7.176	99.9991% ^{238}U; 9 ppm ^{235}U; 100% ^{238}U (<6 ppm impurities)
150[b]	826.7	11.09	8.557	

[a]Appreciation is expressed to L. Love and H. Guinn for performing the isotope separations and to G. Mitchell (Y-12) and E. H. Kobisk for reducing the material to metal and machining all the finished samples.

[b]These disks were made from material separated by the Stable Isotopes Division especially for these measurements.

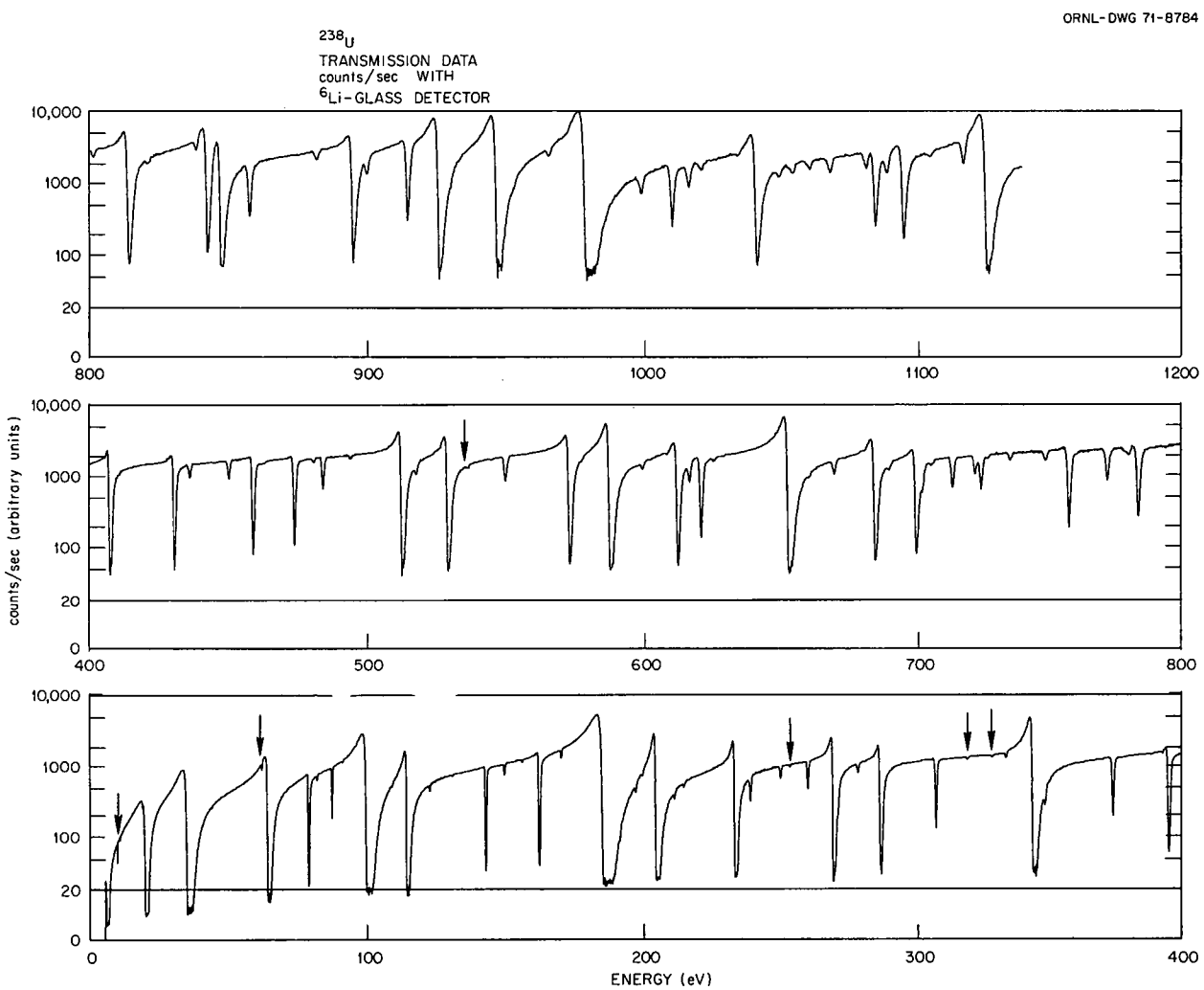

Fig. 1.1.2. ^{238}U Transmission Data Obtained with 1.355-in. Sample Thickness from 0 to 1140 eV.

phototubes. With this detector, much higher count rates can be observed than with the BF_3 chamber. The T measurements were made at a time when the ORELAST was not usable as a detector because of construction work extending the flight path to a 150-m station. During these measurements the through-tube of the tank was plugged with plastic and lead, which allowed ORELAST to serve as a beam dump. Very long runs, ranging from 54 to 88 hr divided into 2-hr sample-in-sample-out cycles, were used in order to obtain good statistics. An automatic sample changer was built to control the sample moving and to route the experimental data accordingly.

In addition to yielding total cross sections, the T measurements are serving to establish the existence of a number of small levels which seemed to appear in the earlier capture measurements[2] but which were obscured by multiple scattering effects. Figure 1.1.2 shows the T measurement results up to 1140 eV. The arrows indicate some of the levels not present in the ENDF/BII compilation but seen in the capture experiments.

The theoretical work in progress to enable an analysis of the SI measurements is described elsewhere in this report.[3]

Both the T measurements and the SI measurements will be resumed at the 150-m station with higher resolution and covering higher energies.

References

1. Instrumentation and Controls Division.
2. G. de Saussure, E. G. Silver, R. W. Ingle, R. B. Perez, and H. Weaver, "Measurement of the Capture Cross Section of ^{238}U up to 100 keV," *Neutron Phys. Div. Ann. Progr. Rept. May 31, 1970,* ORNL-4592, p. 6; see also Sect. 1.2, this report.
3. N. M. Greene et al., Sect. 1.14, this report.

1.2 MEASUREMENT OF NEUTRON CROSS SECTIONS OF ^{238}U AND ^{235}U BELOW 100 keV AT THE ORELA[1]

E. G. Silver R. B. Perez
G. de Saussure R. W. Ingle[2]

The ^{238}U(n,γ) and ^{235}U(n,f) cross sections have been measured for neutron energies up to 100 keV with a large scintillation detector in a split-halves coincidence mode. Special care was taken in making sample-thickness corrections to the observed ^{238}U(n,γ) data, with significant results. The ^{235}U(n,f) cross section has been measured both with a fission chamber and by the two-bias technique. Results are presented and compared with other work. Fission-to-capture ratio measurements are presented for ^{235}U, including measurements in a gap hitherto found between 2 and 20 keV.

References

1. Abstract of a paper presented at the Third Conference on Neutron Cross Sections and Technology, March 15-18, 1971, Knoxville, Tennessee.
2. Instrumentation and Controls Division.

1.3 MEASUREMENTS OF THE NEUTRON ABSORPTION AND FISSION CROSS SECTIONS OF ^{239}Pu AND ^{235}U OVER THE ENERGY RANGE FROM 0.02 eV TO 400 keV

R. Gwin R. W. Ingle[1]
E. G. Silver H. Weaver

Experiments have been performed in which the neutron absorption rates of ^{239}Pu and ^{235}U were measured over the energy region from 0.02 eV to 400 keV. The main goal of this investigation was to provide values of $\bar{\alpha}$, the ratio of the average neutron capture cross section $\bar{\sigma}_c$ to the average neutron fission cross section $\bar{\sigma}_f$, for ^{239}Pu over the neutron energy region of interest for fast breeder reactors. The full energy region from 0.02 eV to 400 keV was covered in one measurement, enabling a single normalization of the data, and values of $\bar{\alpha}$ for ^{239}Pu are given over this energy region. An additional object of the experiments was to provide values of the ratio of the ^{239}Pu fission cross section to the ^{235}U fission cross section in the energy region from 10 to 100 keV. A knowledge of the ratio of these fission cross sections is useful in obtaining a set of neutron cross sections which is consistent with critical experiments. Values of the ^{235}U neutron fission cross sections $\bar{\sigma}_f$ are also presented for the energy region from 10 to 80 keV.

These measurements are a continuation of those reported previously.[2] A pulsed source of neutrons produced by the Oak Ridge Electron Linear Accelerator (ORELA) is collimated to strike a sample centered in a beam tube in the large liquid scintillator ORELAST.[3] Prompt gamma rays resulting from neutron absorption in the sample are detected by ORELAST. In these experiments the samples were ^{239}Pu and ^{235}U contained in ionization chambers. Absorption events detected by ORELAST which are in coincidence with pulses from the ionization chamber are fission events, while absorption events not in coincidence with pulses from the fission chamber correspond to capture events

plus those fission events not recorded by the ionization chamber. The background spectrum from ORELAST was measured by performing an experiment in which a mock ionization chamber containing no sample material was used. In order to check the time-dependent background measured with the mock chamber, "notch" filters were used to remove essentially all of the neutrons from the beam at the energies of the prominent resonances of the filter materials. In the present experiments both Au and Na were used as notch filters. The Na was in the form of NaF and the Au was a metallic sample. A Co notch filter was used in some of the experiments.

For the present experiments ORELAST was optically separated into two sections. The data were divided into two groups according to whether the absorption event was detected by both sections of ORELAST (CO-MODE) or by only one section (XOR-MODE). The data obtained by using the CO-MODE have a much higher signal-to-background ratio than data obtained without the optical divider in ORELAST (see ref. 2). The improvement in signal-to-background permits the measurement of α for ^{239}Pu above 100 keV with the ionization chamber technique whereas previous measurements with the chamber could not extend above about 3 keV.

The neutron flux for these experiments for energies <100 keV was measured with an ionization chamber filled with BF_3. The $^{10}B(n,\alpha)$ cross section used to obtain the neutron flux was that suggested by Sowerby et al.[4]

The ^{239}Pu data obtained using ORELAST in the CO-MODE were normalized to the ENDF/B II (ref. 5) values for ^{239}Pu (Mat-1104) over the neutron energy range extending from 0.02 to 0.7 eV in such a way that the scale was fixed over the energy interval 0.02 to 0.03 eV. Table 1.3.1 shows that the results of the present work agree very well with the results of the ENDF/B II evaluation (the average difference is <1%).

Also shown in Table 1.3.1 are the results of the ORNL-RPI[6] experiments for ^{239}Pu. Again good agreement exists (the average difference is ~1.5%).

The fission cross-section results obtained with ORELAST in the XOR-MODE are also in good agreement with the CO-MODE results shown in Table 1.3.1 up to 0.7 eV. In the neutron energy region between 7 and 60 eV, the data for the two modes differ on the average by about 5%, between 6.0 to 24.7 eV they differ by 1.3%, and between 6.0 to 9.0 eV they differ by about 5%. Because of the relative size of the count rates, the analysis of the combined CO-MODE and XOR-MODE data leads to an average neutron fission cross section which differs by only 1.6% from that obtained using CO-MODE data only.

Figure 1.3.1 shows values of $\bar{\alpha}$ of ^{239}Pu obtained at ORELA for energy intervals extending from 0.1 to 400

Table 1.3.1. Energy Integrals of the Neutron Fission and Absorption Cross Sections of ^{239}Pu

Energy Interval (eV)	$\int \sigma_a dE$ (b·eV)			$\int \sigma_f dE$ (b·eV)		
	ENDF/B Mat. 1104	This Work, CO-MODE	ORNL-RPI, 1968	ENDF/B Mat. 1104	This Work, CO-MODE	ORNL-RPI, 1968
0.02–0.03	10.23	10.23	10.23	7.50	7.50	7.49
0.03–0.04	8.88	8.84	8.89	6.43	6.42	6.44
0.04–0.05	8.06	8.08	8.12	5.77	5.81	5.80
0.05–0.06	7.55	7.60	7.64	5.34	5.33	5.37
0.06–0.07	7.22	7.27	7.33	5.06	5.06	5.09
0.07–0.08	7.03	7.07	7.17	4.87	4.88	4.90
0.08–0.09	6.95	7.02	7.12	4.75	4.74	4.81
0.09–0.10	6.97	6.80	7.10	4.71	4.69	4.73
0.10–0.20	92.6	92.8	93.0	58.0	58.2	57.9
0.20–0.30	335.1	337.7	333.4	198.9	200.7	197.0
0.30–0.40	282.2	281.0	289.6	168.4	170.3	174.3
0.40–0.50	54.5	54.5	55.7	35.5	34.9	36.4
0.50–0.60	21.4	21.2	21.9	14.6	14.49	15.0
0.60–0.70	12.21	12.06	12.2	8.59	8.67	8.85
6.0–9.0		326.0	340.0		178.4	180.8
9.0–12.6		756.0	773.0		492.9	495.5
12.6–20.0		1095.0	1196.0		540.0	547.2
20.0–24.7		457.0	495.0		224.0	225.4

keV. Also included in Fig. 1.3.1 are the results of the ENDF/B II evaluation for ^{239}Pu (Mat-1104),[5] the ORNL-RPI results, and the data from the Van de Graaff measurements of Lottin et al.[7] With a few notable exceptions, the present data (those obtained with ORELAST in the CO-MODE) agree with the ORNL-RPI results within 10%. The results are consistent with the Van de Graaff measurements above 20 keV. Although the data have been corrected for the effects of the notch filters on the neutron flux, some uncertainty in $\bar{\sigma}_c/\bar{\sigma}_f$ is introduced in the energy region of the resonances of the filters.

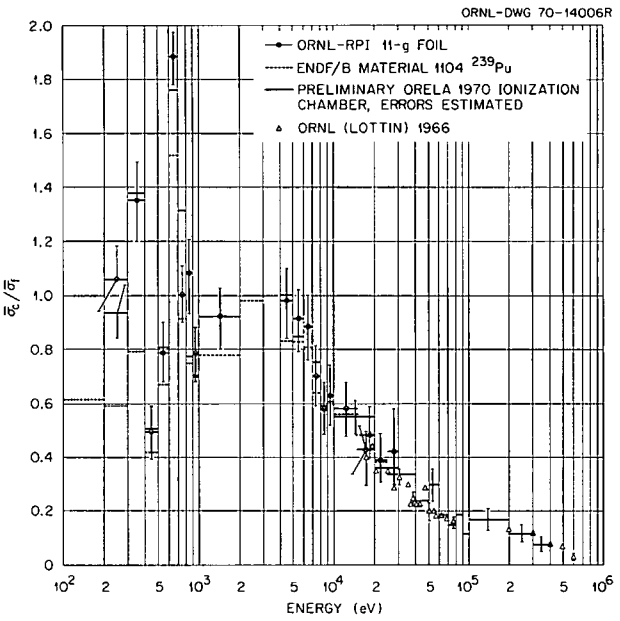

Fig. 1.3.1. Ratio of the Average Values of $\bar{\sigma}_c$ and $\bar{\sigma}_f$ of ^{239}Pu for Energy Intervals Between 0.1 and 400 keV.

Measurements similar to those presented above for ^{239}Pu have been made for ^{235}U. The data were normalized to the ENDF/B II values for ^{235}U (Mat-1102)[5] in the thermal-neutron energy region. Table 1.3.2 shows values of the energy integrals of the neutron fission and absorption cross sections for energy intervals extending from 0.02 to 20.5 eV. Also shown are the ENDF/B values, the 1966 ORNL-RPI values of de Saussure et al.,[8] and some results of Deruytter and Wagemans.[9]

The general agreement of the various values shown in Table 1.3.2 for ^{235}U is good. One of the known uncertainties in the present data is the amount of ^{10}B in the neutron flux monitor. This uncertainty introduces a variation in the neutron cross sections of about 1% over the energy range shown in Table 1.3.2. The experimental data indicate that the ENDF/B II values for fission may be high (~2%) above 0.4 eV. The results for the XOR-MODE operation of ORELA are in good agreement with the CO-MODE results shown in the table.

Figure 1.3.2 shows values of $\bar{\alpha}$ obtained for ^{235}U over the energy range from 0.02 eV to 300 keV. The figure also presents the ENDF/B values, the 1966 ORNL-RPI data of de Saussure et al.,[8] and the Van de Graaff results of Weston[10] and of Lottin.[7]

Table 1.3.2. Energy Integrals of the Neutron Fission and Absorption Cross Sections of ^{235}U

Energy Interval (eV)	$\int \sigma_f(E)dE$ (b·eV)				$\int \sigma_a(E)dE$ (b·eV)		
	ENDF/B MAT 1102	This Work, CO-MODE	Deruytter and Wagemans	ORNL-RPI, 1966	ENDF/B MAT 1102	This Work, CO-MODE	ORNL-RPI, 1966
0.02–0.03	5.87	5.87			6.87	6.87	
0.03–0.04	4.83	4.88			5.65	5.70	
0.04–0.05	4.16	4.21			4.86	4.91	
0.05–0.06	3.68	3.72			4.30	4.35	
0.06–0.07	3.31	3.35			3.87	3.93	
0.07–0.08	3.02	3.07			3.54	3.59	
0.08–0.09	2.78	2.83			3.26	3.30	
0.09–0.10	2.59	2.61			3.05	3.07	
0.10–0.20	20.14	20.2			24.11	24.00	
0.20–0.30	18.47	18.5			22.98	22.76	
0.30–0.40	15.03	15.1			18.13	18.14	
0.40–0.50	9.66	9.58			10.94	11.09	
0.50–0.70	13.69	13.48	13.26	13.45	15.14	15.38	
0.70–1.00	17.39	17.01	16.66	17.09	19.32	19.67	
1.0–1.8		29.42	29.11	29.09		38.46	36.57
10.5–15.0		214.2	214.4	215.6		441.6	445.0
15.0–20.5		313.9	316.0	320.1		506.4	510.5

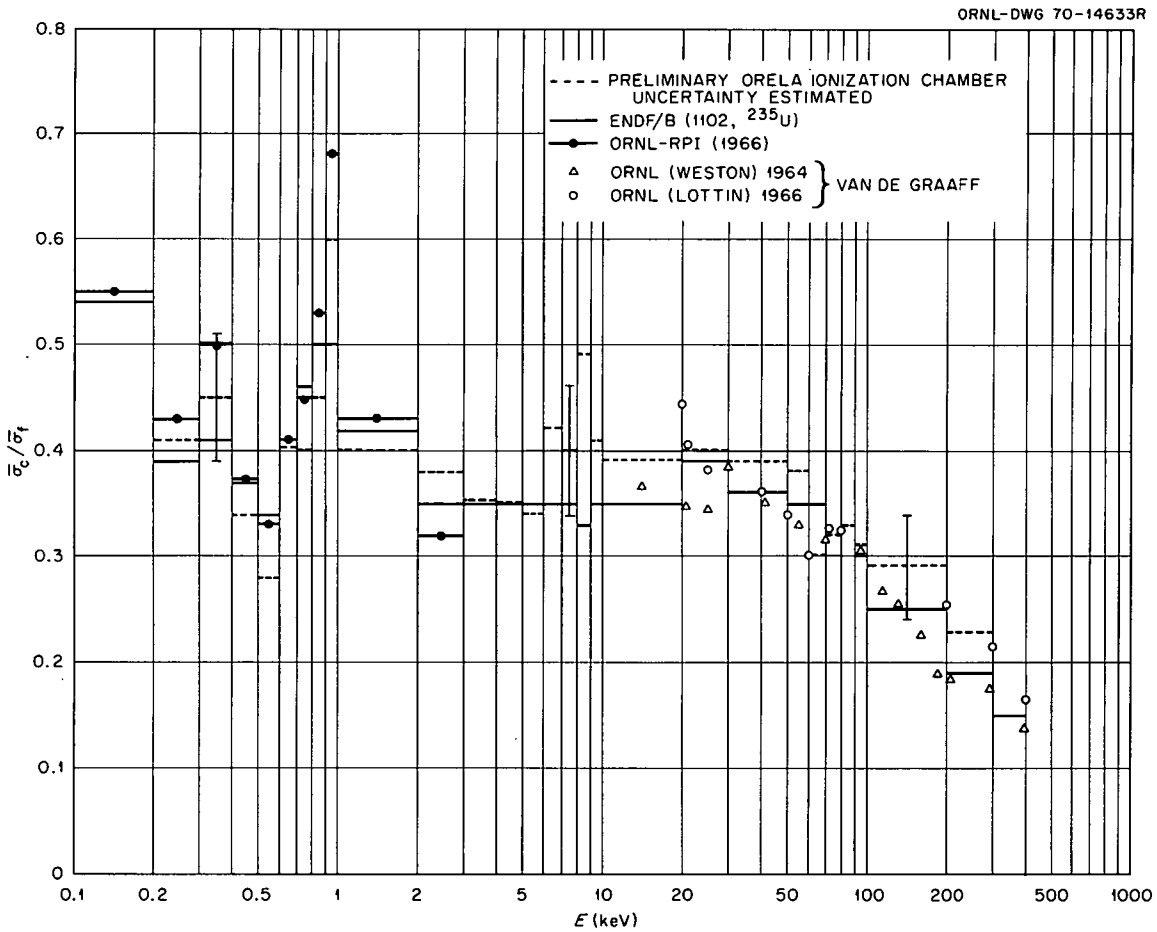

Fig. 1.3.2. Ratio of the Average Values of $\bar{\sigma}_c$ to $\bar{\sigma}_f$ for ^{235}U Energy Intervals from 0.1 to 400 keV.

The results from the measurements on ^{235}U and ^{239}Pu, together with those from similar measurements, have been combined to yield the ratio of the average fission cross section for ^{239}Pu to that for ^{235}U. The present ORELA values for the region above 10 keV are compared with the ENDF/B II values[5] and the results of Szabo et al.[11] in Fig. 1.3.3. The ORELA results are about 8 to 10% higher than the ENDF/B values. This may be partially attributable to a difference in the thicknesses of the Al plates used in the ^{239}Pu and ^{235}U ionization chambers. The plates in the ^{239}Pu chamber were 0.005 in. thick, whereas those in the ^{235}U chamber were only 0.001 in. thick. Since there are prominent Al resonances at 35 keV and at above 85 keV, no uncertainty has been assigned to the present ratio between 30 and 40 keV nor above 80 keV.

Figure 1.3.4 shows average values of the neutron fission cross section for ^{235}U as obtained in these experiments for energies between 10 and 80 keV. Also shown are the ENDF/B II evaluation for ^{235}U (Mat-1102) and the results of the recent measurements of Lemley et al.[12] and Szabo et al.[11] The experimental data in the figure are in general lower than the ENDF/B values for ^{235}U. The interpretation of the present data in terms of an absolute neutron cross section in the keV region is complicated both by fluctuations in the energy dependence of the neutron flux and by instrumental difficulties in the measurement of the neutron flux. For these reasons the neutron fission cross section for ^{235}U is not given above 80 keV. The present data and that of Szabo et al. suggest that the ENDF/B II results for the ^{235}U (Mat-1102) fission cross sections are too high and that this is reflected in the ratio of the fission cross section of ^{239}Pu to that of ^{235}U.

In summary, it can be stated that the present experiments have provided values of the neutron absorption and fission cross sections for ^{239}Pu and ^{235}U over an energy interval which extends from 0.02

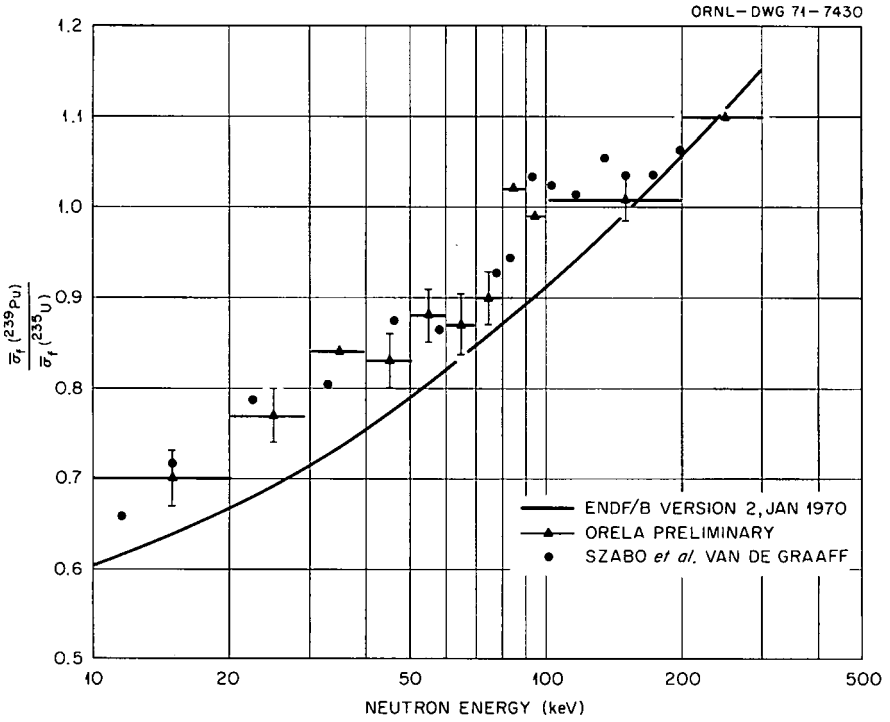

Fig. 1.3.3. Ratio of the Fission Cross Sections of ^{239}Pu and ^{235}U vs. Energy.

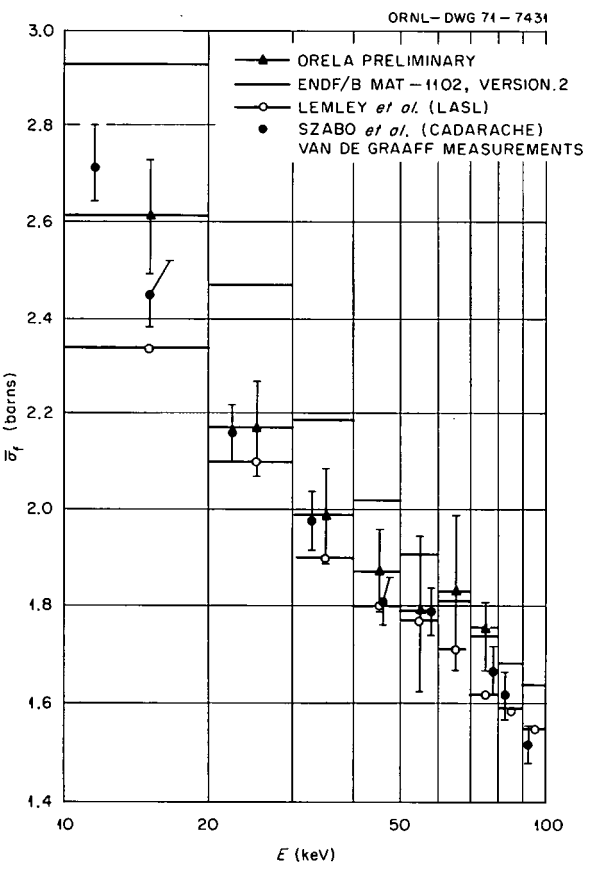

Fig. 1.3.4. Fission Cross Section of ^{235}U vs. Energy.

eV to 80 keV and gives values of $\bar{\alpha}$ to 400 keV for ^{239}Pu. In general the values of $\bar{\alpha}$ measured for both ^{239}Pu and ^{235}U are in reasonable agreement with the corresponding ENDF/B II results. Results on the ^{235}U neutron fission cross section shown in Table 1.3.2 indicate a possible discontinuity of 1 to 2% in the results of the ENDF/B evaluation at 0.4 eV. For the neutron energy region above 10 keV, the neutron fission cross section of ^{235}U and the ratio $\bar{\sigma}_f(^{239}\text{Pu})/\bar{\sigma}_f(^{235}\text{U})$ as derived in these experiments are not consistent with the ENDF/B II evaluation. The present experiments yield a lower fission cross section for ^{235}U and a higher ratio of the ^{239}Pu fission cross section to that of ^{235}U than the ENDF/B II results. Recent measurements by Lemley et al.[12] and Szabo et al.[11] also yield lower values of the ^{235}U neutron fission cross section than the results given by ENDF/B II for Mat-1102.

References

1. Instrumentation and Controls Division.

2. R. Gwin et al., "Measurements of the Neutron Fission and Absorption Cross Sections of ^{239}Pu Over the Energy Region 0.02 eV to 30 keV, Part II," Sec. 1.1 in *Neutron Phys. Div. Ann. Progr. Rept. May 31, 1970,* ORNL-4592.

3. E. G. Silver, J. H. Todd, and J. Lewin, "Assembly and Initial Operation of the ORELAST," Sec. 1.11 in

Neutron Phys. Div. Ann. Progr. Rept. May 31, 1969, ORNL-4443.

4. M. G. Sowerby et al., *Proc. Conf. Nuclear Data for Reactors, Helsinki,* Vol. I, p. 161, International Atomic Energy Agency (1970).

5. Evaluated Nuclear Data File (ENDF/B) of the National Neutron Cross Section Center (NNCSC), ^{239}Pu data, Material (MAT) 1104 and for ^{235}U data Material (MAT) 1102, Tape 201 (revised April 1970). A detailed list of the evaluators for the ENDF/B information is given in File 1 of the data tape which is available from NNCSC. The code SUPERTOG was used to obtain the data on the ENDF/B tape.

6. R. Gwin et al., *Nucl. Sci. Eng.* **45**, 25 (1971).

7. A Lottin, et al. in *Proc. Intern. Conf. on Fast Critical Experiments and Their Analysis,* p. 22, ANL-7320 (1966).

8. G. de Saussure et al. in *Proc. Conf. on Nuclear Data for Reactors, Vienna* Vol. II, International Atomic Energy Agency (1967).

9. A. J. Deruytter, in *Proc. Conf. on Nuclear Data for Reactors, Helsinki,* Vol. I, p. 127, International Atomic Energy Agency (1970).

10. L. W. Weston et al., *Nucl. Sci. Eng.* **20**, 80 (1964).

11. I. Szabo et al., "^{235}U Fission Cross Section from 10 keV to 200 keV," paper presented at Third Conference on Neutron Cross Sections and Technology, March 15–18, 1971, Knoxville, Tennessee.

12. J. R. Lemley, *Nucl. Sci. Eng.* **43**, 281 (1971).

1.4 NEUTRON MULTIPLICITY FOR ^{239}Pu RESONANCE FISSION[1]

L. W. Weston J. H. Todd[2]

Measurements were carried out in an attempt to resolve the discrepancy in the spin dependence of the fission neutron multiplicity (ν) for resonances in ^{239}Pu between the works of Weinstein et al.[3] at Rensselaer Polytechnic Institute and Ryabov et al.[4] at Dubna. For the present measurements fission neutrons from a fission chamber were detected with low efficiency by fast-neutron detectors rather than with high efficiency by thermal-neutron detectors. Our data do not indicate any statistically significant separation into two groups of multiplicity values according to spin state of the resonances between 14 and 200 eV. Where previous results indicated an average difference of 3% to 5% in neutron multiplicity for resonances of different spin, the present results indicate no difference outside the ~1/4% uncertainty of the experiment.

References

1. Abstract of a paper presented at the Third Conference on Neutron Cross Sections and Technology, March 15–18, 1971, Knoxville, Tennessee; also abstract of ORNL-TM-3331 (1971).

2. Instrumentation and Controls Division.

3. S. Weinstein, R. Reed, and R. C. Block, *Proc. Symp. Physics and Chemistry of Fission, p. 477,* International Atomic Energy Agency, Vienna, SM-122/113 (1969).

4. Yu. V. Ryabov et al., Report P3-5297, Neutron Physics Laboratory, Joint Institute of Nuclear Research, Dubna, 1970.

1.5 MEASUREMENT OF THE NEUTRON CAPTURE AND FISSION CROSS SECTIONS FOR ^{241}Pu

L. W. Weston J. H. Todd[1]

Since a fast breeder reactor such as the Liquid Metal Fast Breeder Reactor may have ~12%[2] of its Pu fuel as ^{241}Pu, the knowledge of the ^{241}Pu cross sections is of importance in the economics of such a reactor. Most previous differential measurements above a few eV consist of total or fission cross sections measured under different conditions so that no really consistent set of data is available.

The fission and absorption cross sections for ^{241}Pu are being measured simultaneously under the same conditions at the Oak Ridge Electron Linear Accelerator. Two sets of detectors view the ^{241}Pu sample. The fast-neutron detectors used in the earlier $\bar{\nu}$ measurements[3] detect the fast neutrons following fission, and nonhydrogeneous liquid scintillators detect the prompt gamma rays from capture and fission events. The pulse height as well as the time of flight is recorded for each event in the gamma-ray detectors. With the pulse-height information, a Moxon-Rae detector efficiency can be constructed at a later time with the pulse-height-weighting techniques developed by Macklin and Gibbons.[4] The gamma-ray detectors do not measure the absorption cross section exactly because of the different efficiencies for the detection of capture and fission events. Since the fission cross section is also measured, the gamma-ray detector response can be corrected for this difference in efficiency. The signal-to-background ratio and the count rates achieved at the 20-m flight station are quite good. An example of the count rates with a 2-g ^{241}Pu sample is shown in Fig. 1.5.1. The signal-to-background ratio is comparable to that of the liquid scintillator tank when it is operated in

the mode where a coincidence is demanded between the two halves. The present technique should be less sensitive to changes in gamma-ray multiplicity than the technique of operating the tank in the coincidence mode.

Data are now being taken for this experiment. Data reduction has not progressed to the point where results can be presented. No major problems have developed in the data reduction and none are foreseen.

The normalization of the data will be based on the total cross section. Since the scattering cross section is small and known with an acceptable accuracy, the total cross section can be used for a normalization. The present fission and capture cross sections, plus the previously measured scattering cross section, should add to form the total cross section. This procedure will furnish the relative efficiency of the gamma-ray detectors for fission and capture as well as provide a normalization for the cross sections. If the previously measured total cross sections for ^{241}Pu are not sufficient for this procedure, additional total cross sections could be measured at ORELA.

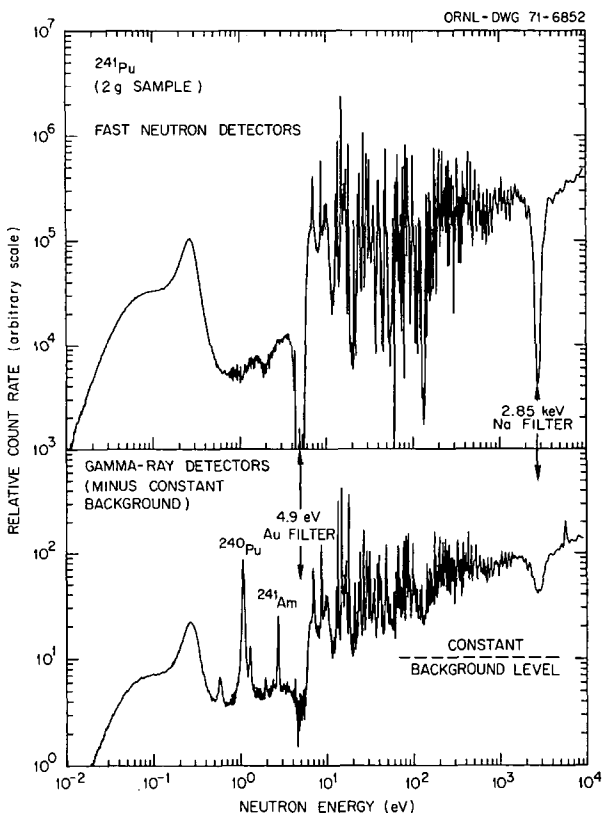

Fig. 1.5.1. Count Rate vs. Neutron Energy Obtained with a 2-g ^{241}Pu Sample. Resonance absorption filters used to determine background level are indicated.

Since our ^{241}Pu samples contain 3% ^{240}Pu, the capture and fission rates from a ^{240}Pu sample will also be measured to correct the data. Similar measurements will be done on ^{241}Am, a daughter product with a 13-yr half life that builds up in the sample. Since this technique is new to our group, measurements are first being carried out on ^{239}Pu in order to correlate the present results with the previous results using the large liquid scintillator tank as a capture and fission detector.

The goal of this experiment is to produce a consistent set of cross sections for ^{241}Pu. Extensive comparisons will be carried out with the ENDF evaluated data as well as with other measurements.

References

1. Instrumentation and Controls Division.

2. P. Greebler, B. A. Hutchins, and C. L. Cowan, "Implications of Nuclear Data Uncertainties to Reactor Design," *Proc. Conf. on Nuclear Data for Reactors, Helsinki,* Vol. 1, p. 19, International Atomic Energy Agency (1970).

3. L. W. Weston and J. H. Todd, *Neutron Multiplicity for ^{239}Pu Resonance Fission,* ORNL-TM-3331 (1971); see also Sec. 1.4.

4. R. L. Macklin and J. H. Gibbons, *Phys. Rev.* **159**, 1007 (1967).

1.6 SIMULTANEOUS MEASUREMENTS OF THE NEUTRON FISSION AND CAPTURE CROSS SECTIONS FOR ^{235}U FOR INCIDENT NEUTRON ENERGIES UP TO 100 keV

R. B. Perez E. G. Silver
G. de Saussure R. W. Ingle[1]
H. Weaver

The design and optimization of fast reactors such as the Liquid Metal Fast Breeder Reactor require a detailed knowledge of the neutron cross sections of both fertile and fissile materials in the energy range covered by the reactor neutron spectrum. This fact, together with the use of the ^{235}U fission cross section as a standard, has resulted in accurate measurements of the fission and capture cross sections of ^{235}U being given a high priority rating in the LMFBR cross-section request list.[2] In response to the LMFBR needs, simultaneous measurements of the fission and capture cross sections of ^{235}U have been carried out at the Oak Ridge Electron Linear Accelerator (ORELA) for incident neutron energies up to 100 keV.

1.6.1 Experimental Methods

The measurements utilized the scintillator tank ORELAST[3] as a capture detector at the 40-m station of flight path No. 6 at ORELA.[4] Two types of measurements were carried out, following techniques which have been explained in some detail previously.[5-7] For the first set of measurements, a 21-plate fission chamber containing 1.802×10^{-4} atoms/b of ^{235}U was placed in a central location in the ORELAST, and data were collected both with and without coincidence between the fission chamber and the ORELAST system. For the second set, the fission chamber was replaced by a solid sample of highly purified ^{235}U (nominal thicknesses of 2.5 and 9 mils), and the technique used was the two-bias technique suggested by Diven and Hopkins.[8] The low-bias interval was set to include the gamma-ray energy range from 3 to 10 MeV, and the high-bias interval was set for the range from 10 to 15 MeV.

1.6.2 Data Analysis

The first step in the data reduction procedure is the background subtraction. To this end runs were performed with a blank fission chamber and also with lead samples having thicknesses equivalent to those of the ^{235}U samples used in the second set of measurements. From these runs the shape of the background was obtained as a function of the time of flight. The curve labelled *B* in Fig. 1.6.1 shows a typical background run, and the smooth solid line is the result of a polynomial fit to this background below 20 keV. Curve *A* shows the counting rate obtained from the ^{235}U solid sample when several black resonance absorbers were placed in the neutron beam. The background spectrum is established by a least-squares fit of the background shape (curve *B*) to the notches in the foreground (curve *A*) and normalization to the foreground without filters in the region below 1 keV. (At these energies the filters have a negligible effect.) Figure 1.6.2 shows the low-bias counting rate obtained for the 2.5-mil ^{235}U sample in the energy region between 0.02 and 1.5 keV after the background has been subtracted.

The ^{235}U cross sections, relative to the ^{10}B cross section, were obtained by dividing the background-subtracted counting rate by the neutron flux per unit energy, $\Phi(E)$, incident upon the BF_3 detector that was utilized as a flux monitor. Due to the aluminum canning of the neutron moderator of the ORELA target, there is a marked structure in the neutron flux at 6 keV and above 20 keV. These effects were taken into account by fitting the counting rate of the BF_3 monitor to the function

$$C(E) = \frac{\sigma(E)\,F(E)}{\sqrt{E}}$$

$$= S(E)\left\{1 + \sum_{k=1}^{15} \frac{G_k + [(E-\mu_k)/\nu_k]H_k}{1 + [(E-\mu_k)/\nu_k]^2}\right\},$$

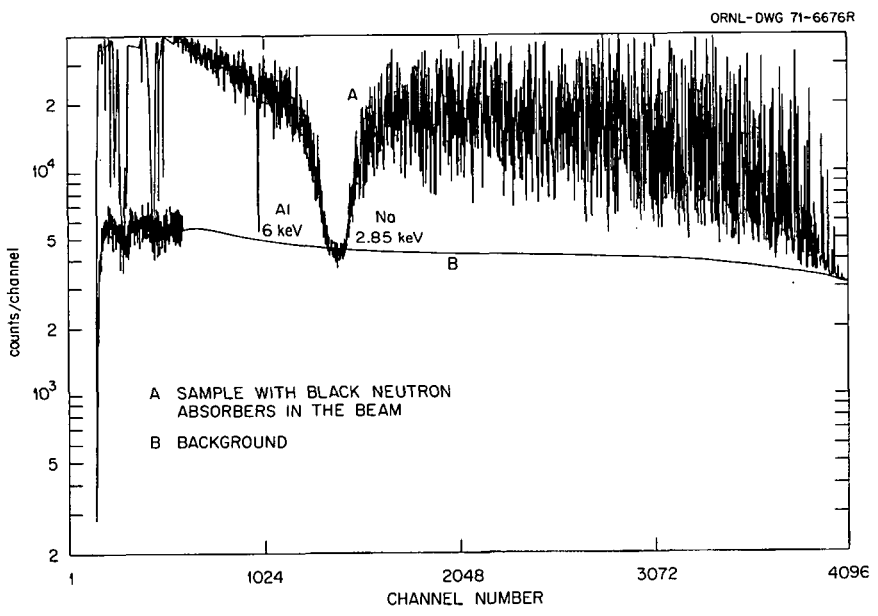

Fig. 1.6.1. Fit of the Background Shape to the Sample Data with Black Absorbers in the Neutron Beam.

where $F(E)$ is a "non-(1/v)" correction to the ^{10}B cross section, and $S(E) = k\ E^{\alpha}\exp\ (-\beta/\sqrt{E})$ is the neutron spectrum below roughly 10 keV where the structure arising from the presence of aluminum and other structural materials in the beam is considered to be negligible. The parameters G_k, H_k, μ_k, and ν_k were obtained by fitting the BF_3 chamber output to the equation with the hybrid computer program "HYFITS."[9]

1.6.3 Results and Discussion

Fission Cross Sections. The fission cross sections obtained from these ORELA measurements are compared in Fig. 1.6.3 with those based on earlier measure-

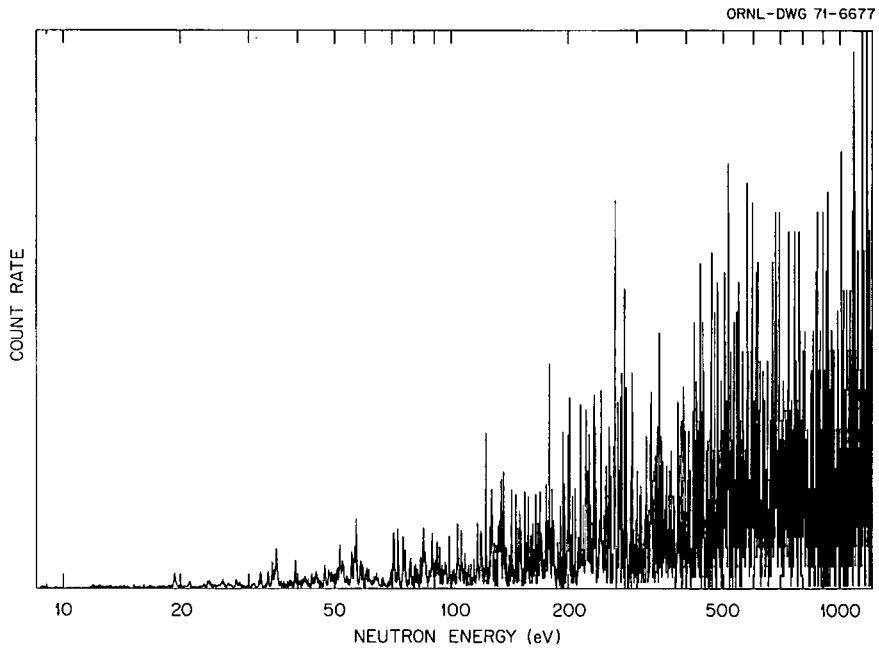

Fig. 1.6.2. The Background-Subtracted Low-Bias Data.

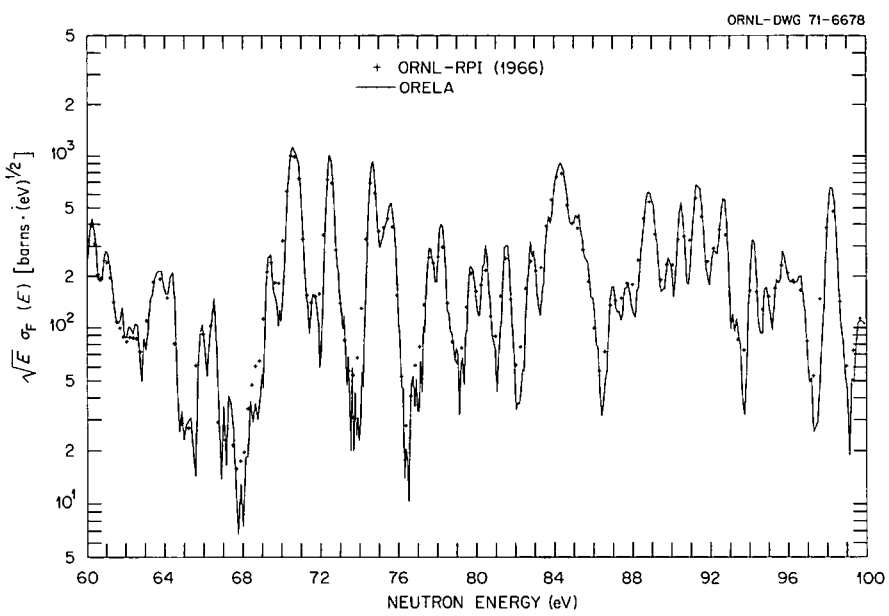

Fig. 1.6.3. Comparison of ^{235}U Fission Cross Sections from ORNL-RPI and ORELA Results.

ments made by an ORNL and Rensselaer Polytechnic Institute team at the RPI linac in the energy region from 60 to 100 eV. Very good agreement exists, especially in the important region around the peaks of the neutron resonances. A similar comparison with the results of Blons et al.[10] from measurements at liquid-nitrogen temperature at the Saclay linac in the energy region from 120 to 136 eV is shown in Fig. 1.6.4. Except for a small difference in the adjustment of the energy scale, the ORELA data and Saclay data also compare very well. Both figures show that the present data give a better definition of the smaller size resonances owing to the improved resolution available at ORELA (0.1-nsec/m nominal resolution).

For the purpose of our discussion, it is convenient to divide the energy interval between 0.1 and 100 keV into three regions: from 0.1 to 1 keV, from 1 to 10 keV, and from 10 and 100 keV. The comparisons of the three linac measurements (ORNL-RPI, Saclay, and ORELA) have been made by normalizing all the data to a value of 2103 b·eV for the fission integral between 100 and 200 eV. The data were also corrected for the "non-(1/v)" behavior of the ^{10}B cross section following the prescription of Sowerby et al.[11]

The ^{235}U results from the three linacs in the 0.1- to 1-keV region are shown in Fig. 1.6.5, where the vertical bars on the histogram representing the ORELA data correspond to a 3% error. Similar measurements between 1 and 10 keV are exhibited in Fig. 1.6.6, together with data from the Los Alamos Scientific Laboratory[12] and an evaluation by Davey.[13] The three linac measurements agree within a 4% error band, and there is a general agreement with the evaluated data of Davey; however, the LASL data, which were obtained in a recent nuclear explosion, appear to be systematically lower.

In the 10- to 100-keV region linac measurements are scarce. Except for the ORELA results, the only linac data available are from Saclay for energies below 30 keV. Most of the data for these energies have been obtained with Van de Graaff machines, specifically by White[14] and by Szabo et al.,[15] and it is these data, particularly White's, which form the basis of Davey's evaluation. However, the entire energy region is covered by the LASL measurements,[12] which are compared in Fig. 1.6.7 with the Davey evaluation, the linac measurements, and the Van de Graaff measurements by Szabo et al. There are quite apparent discrepancies among the various sets of data. The LASL measurements are consistently lower than Davey's evaluation but agree very well with the results of Szabo et al.,[15] especially at the high-energy end. The ORELA data lie between the Davey evaluation and the LASL results and show only a somewhat spotty agreement with the data of Szabo et al.[15]

The Capture-to-Fission Ratio, α. Very few direct measurements of the ^{235}U capture cross section are presently available. The only linac measurement is the

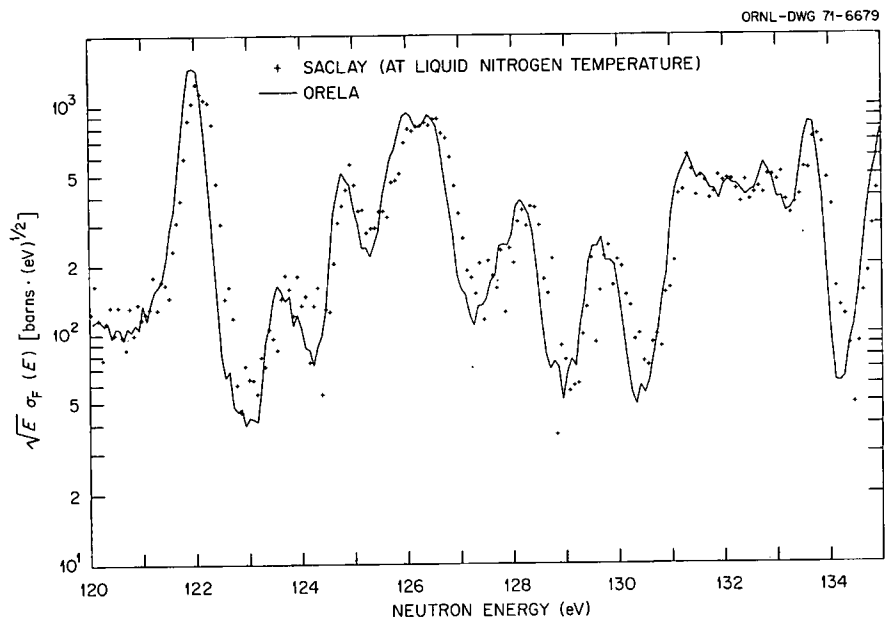

Fig. 1.6.4. Comparison of ^{235}U Fission Cross Sections from ORELA Room-Temperature Data and Saclay Cold-Sample Data.

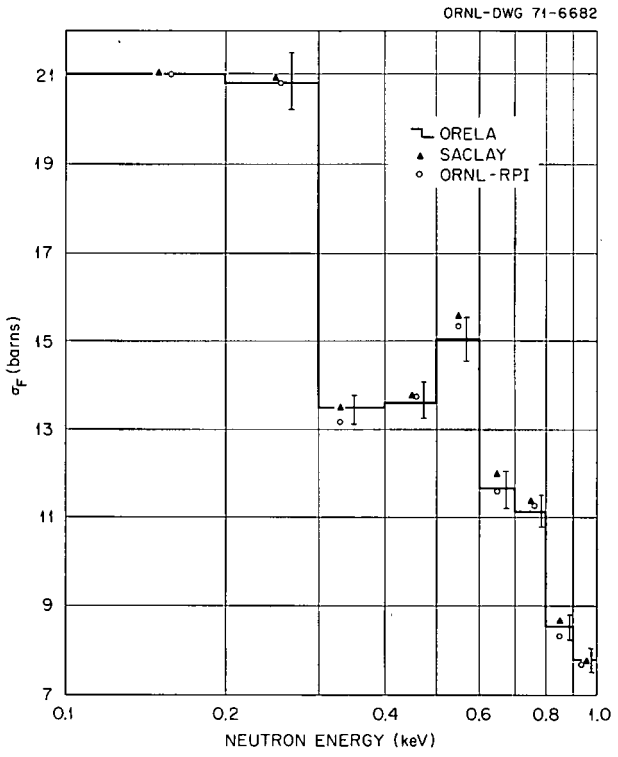

Fig. 1.6.5. The ^{235}U Fission Cross Section Between 0.1 and 1.0 keV.

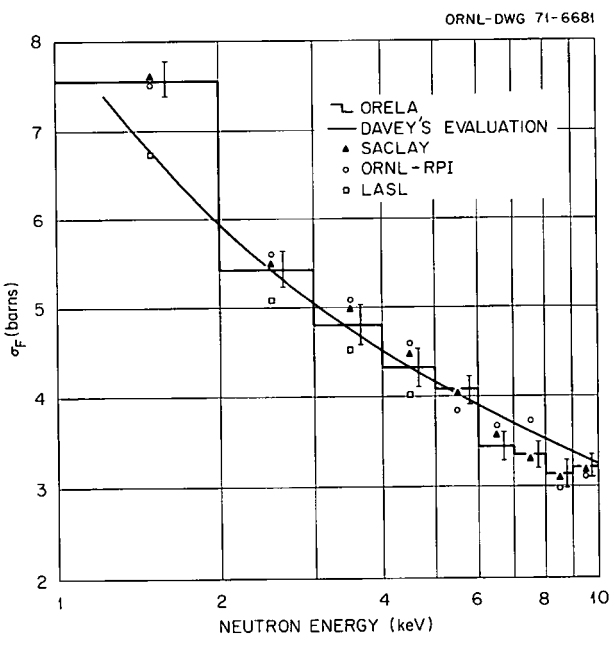

Fig. 1.6.6. The ^{235}U Fission Cross Section Between 1 and 10 keV.

one performed by the ORNL-RPI[4] group for incident neutron energies between thermal and 3 keV. Beyond this limit, most of the data consist of measurements of α, the capture-to-fission ratio, which have been performed either with Van de Graaff machines, by Weston et al.[16] among others, or with pulsed reactors, by Van Shi-Di et al.,[17] for example. The ORELA ^{235}U capture results, expressed in terms of the parameter, α, are shown in Fig. 1.6.8. Shown also for comparison are the

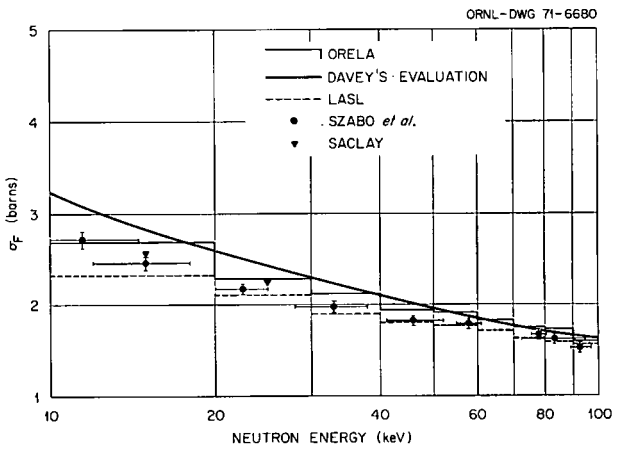

Fig. 1.6.7. The ^{235}U Fission Cross Section Between 10 and 100 keV.

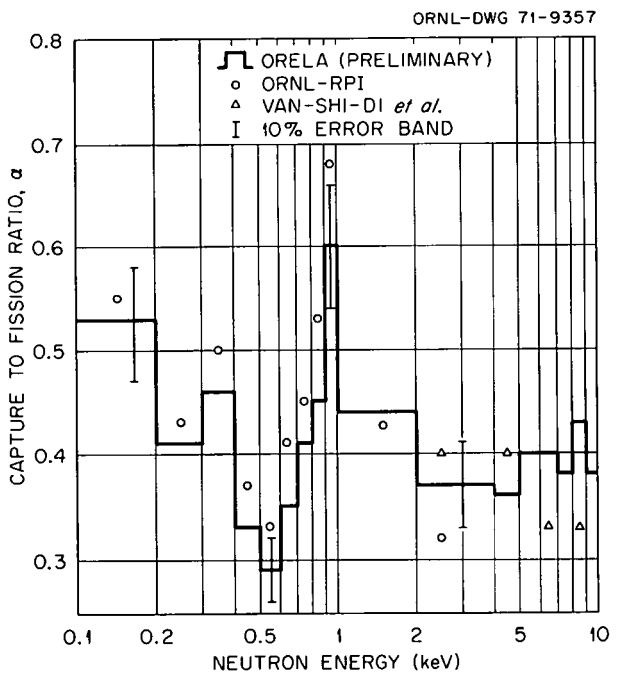

Fig. 1.6.8. Average Values of α, the Capture-to-Fission Ratio, in ^{235}U. The ORELA and ORNL-RPI results are averages over the intervals shown. The Van de Graaff and the Van Shi-Di data are point values.

ORNL-RPI data and the measurements of Van Shi-Di et al.[17] Although there is a general agreement within a 10% to 15% error, the significance of the observed discrepancies cannot be evaluated until all the available data have been reduced.

1.6.4 Conclusions

From the present measurements and comparisons with other sets of data, it can be concluded that all the presently available linac measurements agree within 3% in the energy region between 100 eV and 1 keV. In the energy interval from 1 up to 10 keV, the agreement is also excellent (within 4%). This conclusion is substantiated by Table 1.6.1, which gives values of the fission integrals collected from various sources by James,[18] together with the weighted errors assigned to them. Also shown are the ORELA results and their deviation from James' "best values." With only two exceptions, the two sets of data agree over the entire energy region (0.1 to 10 keV) within the errors quoted, which are less than 3% on the average.

Hence, from the viewpoint of the reactor designer, the present situation in regard to group cross sections for the fission of the ^{235}U nucleus is well defined, with an overall accuracy of about 3% in the energy region between 0.1 and 10 keV. However, the region above 10 keV still needs a rather substantial amount of work.

Table 1.6.1. ^{235}U Fission Cross Section Data from 0.1 eV to 10 keV

Energy Range (keV)	σ_F (b·eV) ORELA	$\langle\sigma_F\rangle$ (b·eV) (James)	Percent Error (James)	Percent Deviation[a]
0.1–0.2	2103	2084	1.47	0.9
0.2–0.3	2087	2031	2.45	3.0
0.3–0.4	1348	1279	3.70	5.0
0.4–0.5	1359	1362	3.00	0.2
0.5–0.6	1511	1463	2.18	3.0
0.6–0.7	1165	1134	2.75	3.0
0.7–0.8	1109	1084	1.82	2.0
0.8–0.9	850	826	2.66	3.0
0.9–1.0	777	771	2.65	0.7
1.0–2.0	7567	7525	1.10	0.5
2.0–3.0	5412	5562	1.40	3.0
3.0–4.0	4771	4842	0.87	2.0
4.0–5.0	4304	4392	2.21	2.0
5.0–6.0	4099	3883	3.35	5.0
6.0–7.0	3424	3521	3.27	3.0
7.0–8.0	3337	3407	4.08	2.0
8.0–9.0	3121	3159	3.04	1.0
9.0–10.0	3199	3246	2.00	1.0
0.1–1.0	12309	12035	1.90	2.0
1.0–10.0	39234	39537	2.50	0.8

[a]Percent deviation between ORELA and James values of $\langle\sigma_F\rangle$.

References

1. Instrumentation and Controls Division.
2. *Liquid Metal Fast Breeder Reactor Program Plan,* Vol. 9, *Physics* WASH-1109 (1968).
3. E. G. Silver, J. H. Todd, and J. Lewin, *Neutron Phys. Div. Ann. Progr. Rept. May 31, 1969,* ORNL-4433, p. 11.
4. A. L. Boch et al., ORNL-4433, *op. cit.,* p. 9.
5. G. de Saussure et al., *Simultaneous Measurements of the Neutron Fission and Capture Cross Sections for ^{235}U for Incident Neutron Energies from 0.4 eV to 3 keV.* ORNL-TM-1804 (1967).
6. G. de Saussure et al., *Neutron Phys. Div. Ann. Progr. Rept. May 31, 1970,* ORNL-4592, p. 6.
7. E. G. Silver et al., Sec. 1.2, this report.
8. B. C. Diven and J. C. Hopkins, *Neutron Time-of-Flight Methods,* J. Spaepen, Ed., Geel, Belgium, p. 1107 (1971).
9. The HYFITS program was written by R. S. Booth, Instrumentation and Controls Division (see Sec. 1.11).
10. J. Blons et al., in *Proc. Conf. on Nuclear Data for Reactors, Helsinki,* Vol. 1, p. 469, International Atomic Energy Agency (1970).
11. M. G. Sowerby et al. *Ratio of the $^{6}Li(n,\alpha)$ $^{10}B(n,\alpha)$ Cross Section from 10 eV to 80 keV and Recommended Values of $^{10}B(n,\alpha)$ Cross Sections,* AERE-R-6316 (1970).
12. J. R. Lemley, *Nucl. Sci. Eng.* **43**, 281 (1971).
13. W. G. Davey, *Nucl. Sci. Eng.* **26**, 149 (1966).
14. P. H. White, *J. Nucl. Energy* **19**, 325 (1965).
15. I. Szabo et al., DRP/SMPNF/70/21, Cadarache Report (1970).
16. L. W. Weston et al., *Nucl. Sci. Eng.* **20**, 80 (1964).
17. Van Shi-Di et al., *Proc. Salzburg Symp. Physics and Chemistry of Fission,* International Atomic Energy Agency, Vienna, 1965.
18. G. D. James, in *Proc. Conf. on Nuclear Data for Reactors, Helsinki,* Vol. 1, p. 267, International Atomic Energy Agency (1970).

1.7 MULTILEVEL ANALYSIS OF THE ^{233}U AND ^{235}U CAPTURE AND FISSION CROSS SECTIONS AND STATISTICAL PROPERTIES OF THE KAPUR-PEIERLS TYPE RESONANCE PARAMETERS FOR THE S-WAVE CROSS SECTIONS OF THE FISSILE ISOTOPES[1]

G. de Saussure R. B. Perez
H. Derrien[2]

At the 1966 Conference on Nuclear Data for Reactors, simultaneous measurements of the capture and fission cross sections of ^{233}U and ^{235}U were presented. Those measurements have now been analyzed with the multilevel formalism developed by Adler and Adler. To obtain consistent sets of resonance parameters, the capture and fission data were least square fitted simultaneously. This analysis was carried out to 60 eV for ^{233}U and to 100 eV for ^{235}U.

References

1. Abstract of paper published in *Proc. Conf. Nuclear Data for Reactors, Helsinki,* Vol. II, p. 757, International Atomic Energy Agency (1970).
2. Centre d'Etudes Nucléaires de Saclay, France.

1.8 MULTILEVEL ANALYSIS OF THE ^{235}U FISSION AND CAPTURE CROSS SECTIONS

G. de Saussure R. B. Perez
W. Kolar[1]

The ^{235}U fission and capture cross section data[2] obtained in 1966 at the Renssalaer Polytechnic Institute linac have been analyzed in the energy region up to 60 eV by using the Reich and Moore multilevel formalism[3] and the computer program MULTI developed at LASL by Auchampaugh.[4] There were three main motivations for this analysis:

1. Multilevel parameters are required to extrapolate statistically the behavior of the cross sections to the unresolved resonance region.[5] Multilevel parameters for ^{235}U are requested with Priority I in the 1971 Compilation of Requests for Nuclear Cross Sections.[5,6]

2. The R-matrix parameters are transformed into equivalent Kapur-Peierls parameters through the expansion of the R-matrix.[7] The Kapur-Peierls parameters so obtained can then be compared with the previously reported parameters[8] obtained directly by the Adler and Adler formalism.[9] The comparison will indicate to what extent the data define a unique set of Kapur-Peierls parameters.

3. The resonance parameters obtained by analyzing RPI linac data will be used as "initial guesses" for a fit to new data recently obtained at ORELA.[10] The new data have a better energy resolution and a higher precision than the earlier data, but they were not yet fully reduced when this analysis started.

Figure 1.8.1 shows some preliminary results obtained in this analysis. The dots in the figure are the capture and fission cross sections obtained from the linac data. The solid lines are the cross sections computed with the parameters listed in Table 1.8.1. Two open fission channels were assumed. The levels were not divided into two spin groups, as sufficient information for such a

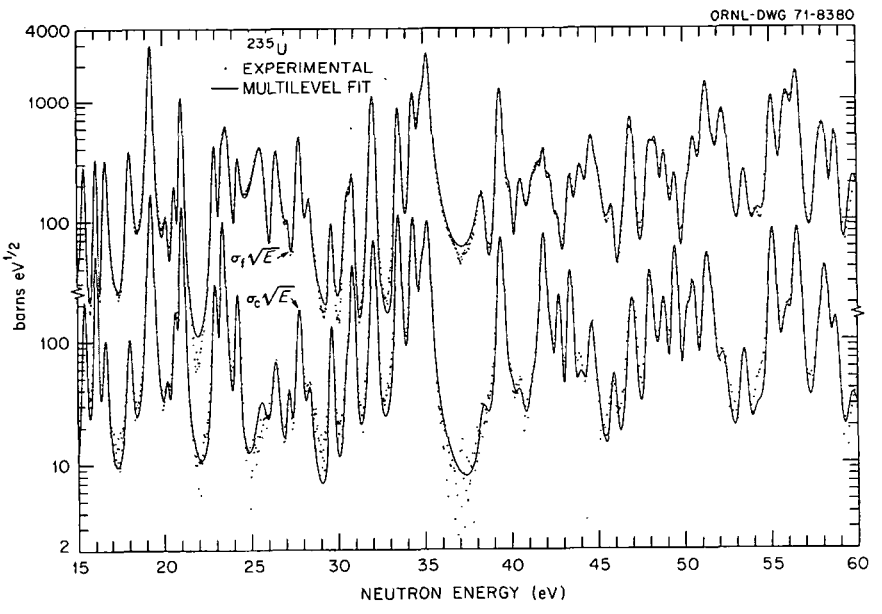

Fig. 1.8.1. Reich-Moore Type Multilevel Fit to the ^{235}U Capture and Fission Cross Sections.

Table 1.8.1. Low-Energy Reich-Moore Parameters.

E_0 (eV)	Γ_γ (eV)	Γ_n^o (mV)	Γ_{f1} (eV)	Γ_{f2} (eV)
-1.447	0.021	2.581	0.179	-0.024
-0.020	0.034	0.000	-0.003	-0.576
1.140	0.034	0.013	-0.042	-0.063
2.029	0.042	0.005	-0.002	-0.010
2.736	0.044	0.000	0.010	-0.063
3.135	0.033	0.014	-0.007	0.112
3.605	0.039	0.027	-0.043	-0.023
4.840	0.044	0.029	0.000	0.006
5.351	0.025	0.018	-0.230	0.682
6.222	0.038	0.011	0.105	-0.015
6.379	0.045	0.114	0.002	-0.014
7.079	0.041	0.049	-0.000	-0.036
7.753	0.040	0.001	-0.390	-0.416
8.777	0.037	0.383	0.119	-0.016
8.976	0.041	0.001	-0.020	1.113
9.335	0.040	0.076	-0.007	-0.277
10.155	0.030	0.014	-0.018	-0.024
11.409	0.040	0.065	-0.109	1.482
11.664	0.049	0.136	0.000	-0.057
12.407	0.047	0.344	0.002	-0.051
12.935	0.040	0.021	0.208	-0.001
13.291	0.040	0.043	0.170	-0.402
13.813	0.040	0.142	0.619	-0.078
14.381	0.040	0.002	-0.032	1.004
14.581	0.040	0.024	-0.048	0.179
15.418	0.050	0.062	-0.071	-0.001
16.088	0.050	0.096	0.017	0.018
16.676	0.039	0.070	0.121	-0.027
18.053	0.043	0.094	0.003	-0.170
19.016	0.040	0.033	0.024	0.028
19.298	0.042	0.693	-0.059	0.015
20.189	0.039	0.012	0.068	0.017
20.650	0.040	0.037	0.044	-0.002
21.064	0.050	0.316	-0.000	-0.040
22.942	0.040	0.099	0.057	0.001
23.409	0.040	0.169	0.002	0.012
23.572	0.038	0.150	-0.006	0.175
24.234	0.040	0.059	-0.021	0.016
25.612	0.040	0.223	0.049	-0.597
26.439	0.045	0.117	0.211	-0.042
27.204	0.036	0.009	-0.030	-0.013
27.801	0.040	0.125	-0.109	-0.011
28.414	0.046	0.042	0.174	-0.062
28.431	0.040	0.000	-0.011	-0.125
29.663	0.040	0.029	0.016	0.011
30.602	0.050	0.047	-0.019	0.112
30.888	0.041	0.086	-0.007	-0.016
31.936	0.050	0.110	0.195	0.023

Table 1.8.1. Low-Energy Reich-Moore Parameters

E_0 (eV)	Γ_γ (eV)	Γ_n^o (mV)	Γ_{f1} (eV)	Γ_{f2} (eV)
32.124	0.033	0.206	-0.049	0.016
33.529	0.050	0.317	0.040	-0.000
34.364	0.050	0.365	-0.063	0.001
34.880	0.050	0.233	0.172	-0.001
35.196	0.039	0.686	0.009	-0.092
35.498	0.037	0.106	-0.709	-0.235
38.388	0.050	0.063	-0.024	0.367
39.426	0.050	0.399	0.086	0.001
40.014	0.026	0.049	-0.059	0.183
40.494	0.050	0.090	0.130	0.250
41.286	0.050	0.067	-0.142	0.129
41.607	0.025	0.050	-0.038	-0.028
41.902	0.049	0.187	0.003	0.019
42.275	0.050	0.053	0.104	0.000
42.746	0.050	0.042	-0.011	0.000
43.417	0.050	0.097	-0.024	-0.001
43.964	0.050	0.114	0.000	-0.376
44.618	0.029	0.122	0.048	0.093
44.974	0.026	0.080	0.054	-0.269
45.911	0.050	0.023	-0.002	0.095
46.878	0.026	0.076	0.049	1.069
46.970	0.050	0.175	-0.186	-0.016
48.015	0.050	0.109	0.007	-0.053
48.391	0.032	0.164	-0.252	-0.028
48.801	0.050	0.122	-0.082	-0.008
49.474	0.050	0.132	-0.000	0.017
50.157	0.050	0.061	0.002	0.051
50.505	0.035	0.117	-0.040	-0.007
51.315	0.050	0.473	0.134	-0.008
51.617	0.025	0.067	-0.003	0.080
52.294	0.028	0.343	0.033	-0.385
53.446	0.047	0.077	-0.129	-0.018
54.254	0.050	0.026	0.287	-0.012
55.123	0.050	0.404	-0.034	0.033
55.945	0.037	0.469	0.235	0.082
56.559	0.043	0.561	-0.070	0.018
57.796	0.037	0.110	-0.104	-0.045
58.144	0.050	0.189	0.042	-0.023
58.731	0.026	0.157	0.038	0.074
59.750	0.045	0.072	0.305	0.000
60.220	0.029	0.008	0.000	-0.200
60.950	0.045	0.620	0.000	-0.202
0.300	0.040	0.001	0.049	0.050
5.446	0.037	0.001	0.0	0.0

Table 1.8.2. Kapur-Peierls Resonance Parameters Corresponding to the R-Matrix Parameters of Table 1.8.1.

μ (eV)	ν (eV)	α (barn·eV$^{3/2}$)	β (barn·eV$^{3/2}$)	G_F (barn·eV$^{3/2}$)	H_F (barn·eV$^{3/2}$)	G_C (barn·eV$^{3/2}$)	H_C (barn·eV$^{3/2}$)
-1.426	0.105	1679.749	22.385	1510.158	20.637	168.718	5.908
0.090	0.263	0.508	-0.500	0.495	-0.518	0.010	0.018
1.146	0.069	8.253	2.419	6.104	2.410	2.144	-0.013
2.030	0.027	3.639	0.014	0.768	0.012	2.867	-0.007
2.753	0.048	0.104	-0.468	-0.126	-0.442	0.228	-0.025
3.158	0.066	8.410	0.762	6.156	0.733	2.249	0.005
3.612	0.052	17.169	1.458	10.520	1.418	6.634	-0.006
4.842	0.024	18.088	0.433	1.449	0.381	16.607	-0.002
5.558	0.385	12.229	-14.836	11.255	-14.425	0.915	-0.438
6.225	0.080	6.380	10.649	4.464	10.125	1.950	0.480
6.379	0.029	73.895	2.438	16.742	2.398	56.768	-0.187
7.087	0.031	30.723	2.468	10.464	2.384	20.191	-0.011
7.890	0.365	-0.636	-0.294	-0.657	-0.213	0.021	-0.078
8.777	0.070	244.623	-5.783	175.366	-6.205	67.158	-0.396
9.408	0.667	24.767	16.972	23.734	15.982	1.028	0.898
10.152	0.036	8.803	-2.838	4.858	-2.734	3.927	-0.125
11.656	0.028	113.136	4.686	14.203	4.013	97.692	0.164
13.514	0.201	-26.928	-0.346	-27.683	0.090	0.790	-0.375
12.398	0.046	233.911	26.044	105.755	24.068	124.861	1.365
12.976	0.083	-0.294	7.852	-1.857	7.785	1.570	0.059
14.082	0.301	72.746	42.814	66.399	40.715	6.318	1.860
15.414	0.060	40.745	4.232	22.986	4.103	17.671	0.001
14.552	0.031	16.569	3.961	5.420	3.906	11.118	0.018
16.656	0.085	45.191	-8.839	34.632	-8.875	10.436	-0.082
16.086	0.041	62.019	0.542	23.934	0.346	37.779	0.005
18.026	0.099	55.288	-10.280	42.579	-10.362	12.517	-0.172
19.015	0.045	25.094	-6.115	12.317	-5.925	12.545	-0.470
19.293	0.058	452.136	16.689	273.832	15.412	166.090	0.109
20.190	0.062	7.335	2.262	4.868	2.206	2.459	0.046
20.647	0.043	24.919	2.006	13.180	1.915	11.669	-0.004
21.061	0.045	205.764	-0.319	88.370	-0.313	114.018	-0.188
22.944	0.049	64.301	1.723	37.930	1.480	26.021	-0.028
23.411	0.026	100.784	16.842	23.541	14.425	75.649	1.909
23.572	0.113	108.670	-34.106	91.314	-31.660	16.712	-2.200
24.235	0.039	37.205	-12.584	16.580	-12.289	20.429	-0.287
25.579	0.355	160.438	53.279	150.619	52.398	9.488	0.534
26.426	0.139	65.541	-36.253	53.846	-35.789	11.455	-0.497
27.208	0.039	4.719	3.010	2.198	2.952	2.520	0.046
27.810	0.080	82.510	-0.942	60.103	-0.889	22.023	-0.216
28.389	0.145	22.626	-7.495	18.420	-7.516	4.161	-0.002
28.428	0.080	0.840	2.702	-0.041	2.505	0.883	0.192
29.663	0.034	18.739	0.781	7.495	0.726	11.195	-0.009
30.591	0.089	30.336	3.183	21.070	3.189	9.208	-0.174
30.888	0.031	56.732	1.333	18.358	0.986	37.908	0.121
31.960	0.135	52.948	-37.355	36.894	-30.727	15.364	-6.782
32.115	0.047	153.192	36.789	86.875	29.367	63.776	6.635

Table 1.8.2. Kapur-Peierls Resonance Parameters Corresponding to the R-Matrix Parameters of Table 1.8.1.

μ (eV)	ν (eV)	α (barn·eV$^{3/2}$)	β (barn·eV$^{3/2}$)	G_F (barn·eV$^{3/2}$)	H_F (barn·eV$^{3/2}$)	G_C (barn·eV$^{3/2}$)	H_C (barn·eV$^{3/2}$)
33.532	0.045	211.171	-9.306	88.682	-10.238	117.887	-0.392
34.373	0.054	235.553	-10.612	114.729	-11.066	115.594	-1.051
34.910	0.097	197.022	37.729	142.625	33.780	51.556	2.261
35.191	0.067	399.767	-72.740	275.546	-66.117	112.084	-3.451
35.470	0.525	70.355	24.682	66.074	23.062	3.536	1.678
38.405	0.224	34.863	26.120	29.825	25.908	5.007	0.102
39.428	0.070	260.545	-0.526	160.728	-0.421	94.965	-0.442
40.018	0.135	27.613	28.756	23.907	28.356	3.557	0.378
40.488	0.223	67.299	-26.838	60.276	-26.654	6.842	-0.112
41.268	0.162	44.164	-4.127	37.247	-4.132	6.767	-0.072
41.605	0.046	31.981	0.173	21.720	0.367	10.084	-0.300
41.900	0.036	120.777	-4.253	34.616	-4.378	83.985	0.149
42.267	0.076	34.616	-5.001	22.660	-4.711	11.823	-0.199
42.745	0.031	27.635	2.115	4.767	2.065	22.715	0.062
43.415	0.037	61.958	1.952	19.605	1.872	41.771	0.025
44.006	0.219	76.412	1.711	65.631	2.371	10.521	-0.709
44.622	0.088	79.246	-1.719	61.782	-1.426	16.975	-0.324
44.946	0.185	46.557	-9.471	41.660	-10.078	4.738	0.680
45.915	0.073	14.807	11.354	8.219	11.042	6.565	0.277
46.963	0.103	147.078	29.891	110.218	29.033	35.668	0.433
46.727	0.602	8.391	-25.178	8.199	-24.300	0.109	-0.796
48.003	0.047	82.285	5.407	36.715	5.126	44.660	-0.051
48.377	0.158	122.715	21.289	110.949	20.118	11.082	0.954
48.782	0.062	63.431	-35.178	34.982	-34.144	27.922	-0.933
49.472	0.033	87.473	-0.660	20.087	-0.745	66.047	-0.013
50.150	0.050	37.552	-6.667	17.656	-6.632	19.655	-0.165
50.502	0.041	77.180	-14.301	41.149	-14.287	34.992	-0.203
51.315	0.098	307.918	42.874	219.198	42.525	82.820	-0.410
51.615	0.055	40.126	-9.832	27.101	-9.637	12.711	0.133
52.228	0.208	228.288	-9.051	210.448	-8.456	16.050	0.216
53.449	0.098	47.155	-7.694	34.525	-7.464	12.443	-0.178
54.234	0.176	14.482	-1.814	11.788	-1.835	2.648	-0.011
55.113	0.057	270.463	13.327	142.335	12.457	120.456	-0.199
55.921	0.178	292.073	-35.091	253.667	-33.698	34.379	-1.403
56.548	0.065	376.878	26.020	234.318	27.487	128.547	1.158
57.784	0.092	68.564	-11.040	52.671	-10.029	15.402	-0.741
58.137	0.057	128.571	21.731	68.169	21.858	58.255	0.634
58.720	0.068	102.776	-2.423	81.413	-1.602	20.363	-0.014
59.712	0.166	43.475	-10.546	37.548	-10.246	5.824	-0.081
60.205	0.114	1.952	18.248	0.511	18.588	1.390	-0.388
60.914	0.114	410.441	-15.170	318.694	-12.609	82.892	0.189
13.346	0.855	114.564	-80.177	111.652	-77.856	2.518	-2.416
11.623	1.149	-12.784	-9.957	-12.545	-8.862	-0.242	-1.034
9.263	0.059	36.366	-5.381	21.831	-4.578	14.435	-0.835
0.300	0.069	0.385	0.000	0.274	0.000	0.111	0.000
5.446	0.019	0.398	-0.000	-0.000	-0.000	0.398	-0.000

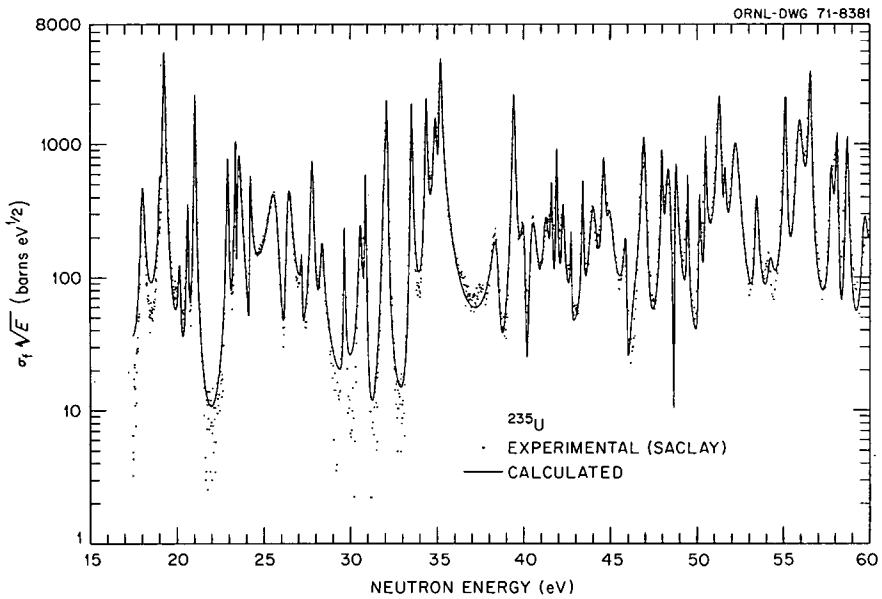

Fig. 1.8.2. Comparison of ^{235}U Fission Cross Sections Computed with Multilevel Parameters with the Low-Temperature Measurements of Blons et al.

division is not yet available. It is clear that for the energy region covered by Fig. 1.8.1 the resonance parameters describe the fission and capture cross sections with an accuracy comparable to that of the data.

An interesting test of the validity of the analysis is illustrated in Fig. 1.8.2. The data on that figure are from the measurement of the fission cross section made at Saclay[11] at a sample temperature of 77°K. The line was obtained from the parameters of Table 1.8.1, with a Doppler broadening corresponding to the Saclay experimental conditions. The consistency between the calculation and the experimental data is fair.

In Table 1.8.2 are listed the Kapur-Peierls parameters obtained from the R-matrix parameters of Table 1.8.1. There are rather large differences between these parameters and those obtained directly by the Adler and Adler formalism.[8] These differences illustrate the non-uniqueness of this type of multilevel analysis.

References

1. Central Bureau for Nuclear Measurements, Euratom, Geel, Belgium.

2. G. de Saussure et al., *Simultaneous Measurements of the Neutron Fission and Capture Cross Sections for ^{235}U for Incident Neutron Energies from 0.4 eV to 3 keV*, ORNL-TM-1804 (1967).

3. C. W. Reich and M. S. Moore, *Phys. Rev.* **111**, 929 (1958).

4. G. F. Auchampaugh, Los Alamos Scientific Laboratory Report, LA-4633 (to be published). We are indebted to D. R. Winkler for making the MULTI program operational on the ORNL IBM-360/91 computer and to G. F. Auchampaugh for his many helpful suggestions.

5. M. S. Moore, private communication.

6. *Compilation of Requests for Nuclear Cross Section Measurements*, LA-4652-MS, Request No. 400 (March 1971).

7. G. de Saussure and R. B. Perez, *POLLA, A Fortran Program to Convert R-Matrix-Type Multilevel Resonance Parameters for Fissile Nuclei into Equivalent Kapur-Peierls-Type Parameters*, ORNL-TM-2599 (1969).

8. See Sec. 1.7.

9. D. B. Adler and F. T. Adler, *Proc. Conf. on Breeding Economics and Safety in Large Fast Power Reactors, Oct. 1963*, ANL-6792, p. 695.

10. See Sec. 1.6.

11. J. Blons et al., *Proc. Conf. on Nuclear Data for Reactors, Helsinki*, Vol. II, p. 469 (1970).

1.9 PREPARATIONS FOR PRECISION MEASUREMENTS OF FISSION CROSS SECTIONS FOR ^{235}U AND ^{239}Pu IN THE NEUTRON ENERGY RANGE ABOVE 30 keV

R. W. Peelle L. W. Weston

In the neutron energy region above 20 keV, the spread of credible values for the fission cross sections of ^{235}U and ^{239}Pu is so broad that errors in the evaluated

cross sections may be larger than 5%. To help remedy this undesirable situation, a small experimental program has been started to utilize the strong neutron beam of the Oak Ridge Electron Linear Accelerator for precision measurements of $^{235}U(n,f)$, $^{239}Pu(n,f)$, and the ratio of these cross sections. The plan is to prepare for eventual absolute measurements while obtaining first results using cross-section normalization at thermal or eV neutron energies. Initial measurements will include ratio measurements between the fission cross sections of ^{235}U and ^{239}Pu as well as measurements through 100 keV of each of these against the standard $^{10}B(n,\gamma)$ and $^{6}Li(n,\alpha)$ cross sections. The validity of such relative measurements depends on the proper evaluation of time-dependent backgrounds and upon detector systems which respond to the studied reactions with an efficiency which is independent of energy.

ORELA flight path No. 8 is being readied for this work at 22 m from the target. The collimator and baffle system has been installed and aligned to give a nominal beam umbra 2 in. in diameter. To reduce the scattered intensity outside the optical penumbra, the final section of the collimator has a double taper. The system is constructed of a copper-nickel alloy (70% Cu, 30% Ni) to inhibit neutron penetration at cross-section minima such as the one at 7 keV for copper. As of July 1, 1971, the beam-handling system will be completed except for some of the hardware in the flight station.

A gridded ionization chamber has been designed[1] and constructed in which the central electrode is coated on both sides in its central region with about 10 $\mu g/cm^2$ of ^{10}B. Grid and collector electrodes are arranged symmetrically about this electrode so that the alpha particles will lose all their energy in the region between the boron deposit and the grid, and so that the classic electric field requirements of gridded chambers are met.[2] Timing signals will be obtained from the central electrode, while analysis of the spectra of charge pulses on the collector plates should permit optimum biasing of the system to attain a known energy dependence of the counter's efficiency. The chamber is undergoing early tests.

For measurements of relative fission cross sections, an ionization chamber is being built to house a pair of back-to-back foils, so that a comparison between two target materials can be made with each relative orientation to the beam direction. Principal measurements will be made with foils of ^{239}Pu and ^{235}U about 0.1 g/cm^2 in thickness, but the same chamber can be used to compare energy-dependent count rates for foils of different thicknesses to test the counting efficiency as a function of energy. Plate spacing will be optimized based on approximate calculations of pulse pileup spectra for plutonium fission foils.

Efforts are being made to minimize the mass of material placed in the beam by these chambers. To attain stable operation and near-minimum noise, we plan for timing signals to employ current-mode linear amplifiers with FET inputs.[3]

References

1. F. Gillespie, Instrumentation and Controls Division.
2. O Bunemann, T. E. Cranshaw, and J. A. Harvey, *Can. J. Res.* **27A**, 191 (1949).
3. J. K. Millard, *An Investigation of Broadband Current Preamplification for Obtaining High-Resolution Energy and Time Information from Nuclear Radiation Detectors*, ORNL-TM-3252 (1971).

1.10 NEUTRON FISSION AND CAPTURE CROSS-SECTION MEASUREMENTS FOR URANIUM-233 IN THE ENERGY REGION 0.02 TO 1 eV[1]

L. W. Weston	J. H. Todd[2]
R. Gwin	C. W. Craven[3]
G. de Saussure	R. W. Hockenbury[4]
R. W. Ingle[2]	R. C. Block[4]

The relative neutron capture and fission cross sections in the neutron energy range 0.02 to 1 eV have been simultaneously measured. The data are normalized by means of the previously reported total cross section. The technique used consisted of passing a pulsed neutron beam through a ^{233}U fission chamber placed at the center of a large liquid scintillator. The prompt-neutron capture gamma rays were detected only in the liquid scintillator whereas a fission event was characterized by coincident signals from the liquid scintillator and fission chamber. This technique provides a new method of obtaining eta in this neutron energy range which is not subject to the same type of errors as are associated with a direct measurement. Comparisons with previously published data are given.

References

1. Abstract of *Nucl. Sci. Eng.* **42**, 143 (1970); included in 1969 annual report as abstract of ORNL-TM-2353.
2. Instrumentation and Controls Division.
3. Reactor Division.
4. Rensselaer Polytechnic Institute.

1.11 THE USE OF THE COMPUTER PROGRAM HYFITS TO GENERATE APPROXIMATE RESONANCE PARAMETERS

E. G. Silver R. B. Perez
R. S. Booth[1] G. de Saussure

Many ^{238}U resonances seen in the capture cross-section experiments at ORELA were not listed in the ENDF/B II file. In order to obtain approximate values for the parameters of these resonances to use as input to least-squares calculations, a program called HYFITS, written for the Instrumentation and Controls Division's hybrid computer system, was used in an interactive mode.[2-3] With this code, the self-shielded cross section in capture can be constructed from the resonance parameters presented to the computer as voltages selected by a number of 10-turn helipots. The contructed cross section and the experimental points are then simultaneously displayed on a CRT, and the resonance parameters can be modified to obtain a good visual fit. For data regions consisting of several hundred points and containing five or more resonances, the delay time between input modification and the resulting display modification was only of the order of one second, so that the fitting was easily carried out.

About 60 resonances in the region from 10 to 1200 eV have so far been fitted by this method, and the parameters so obtained proved to be excellent values for use as input guesses in least-squares calculations.

References

1. Instrumentation and Controls Division.
2. R. S. Stone, *The Controls Department Hybrid Computer Hardware and Applications,* ORNL-TM-3101 (1970).
3. R. S. Booth and R. B. Perez, *Interactive Least-Squares Fitting Using the Hybrid Computer,* ORNL-4620, p. 53 (1970).

1.12 INVARIANT IMBEDDING APPROACH TO THE KAPUR-PEIERLS NUCLEAR REACTION FORMALISM

R. B. Perez

Invariant imbedding methods have been shown to be convenient tools for use in obtaining the variation of the R-matrix with respect to the parameters entering in the formalism.[1] The results are given in the form of a Ricatti-type integrodifferential equation whose independent variable is precisely the particular reaction parameter in consideration. This result is a corollary of the well-known Poincaré theorem about the analyticity of the solutions of differential equations (in this case the Schrödinger equation) on the various parameters in the equation.

Because of the emphasis placed in the past few years on the study of the analytical properties of the S-matrix as a function of the energy and angular momentum[2] and the fundamental type of information which can be obtained from even the nonrelativistic wave equation, it seems useful to obtain the variation of the S-matrix in a manner similar to the previously mentioned results concerning the Wigner-Eisenbud R-matrix.[3]

For this endeavor the Kapur-Peierls[4] nuclear reaction formalism is very convenient, in view of the direct connection between the S-matrix and the Green's function describing the wavefield. As is well-known, such a direct relationship arises through the use of complex, momentum-dependent boundary conditions imposed on the nuclear states wave functions. In order to discuss the invariant imbedding method, we shall present here the case of particle scattering by a central potential. The radial wave function is then defined by the equation

$$\left\{ \frac{d^2}{dr^2} + \frac{2M}{\hbar^2} [E - U_\ell(r)] \right\} \psi_\ell(r) = 0 \tag{1}$$

and

$$U_\ell(r) = V(r) + \frac{\hbar^2}{2M} \frac{\ell(\ell+1)}{r^2} . \tag{2}$$

The Green's function is in turn the solution of the equation

$$\left\{ \frac{d^2}{dr^2} + \frac{2M}{\hbar^2} [E - U_\ell(r)] \right\} G_\ell(r|r') = -\delta(r - r') , \tag{3}$$

with the associated boundary condition of regularity at $r = 0$, and

$$\left[\frac{d}{dr} G_\ell(r|r') \right]_a = ik\, G_\ell(a|r') . \tag{4}$$

We now introduce the $S_\ell(r|a,\tau)$ operator in the form

$$\psi_\ell(r,\tau) = I_\ell(r,\tau) - S_\ell(r|a,\tau)\, O_\ell(r,\tau) , \tag{5}$$

where $r = a$ is the radius of the interaction region, τ a given reaction parameter and

$$I_\ell(r,\tau) = \exp \left\{ -i \left[k(\tau)a(\tau) - \frac{1}{2} \pi\, \ell(\tau) \right] \right\} , \tag{6}$$

$$O_\ell(r,\tau) = I_\ell^*(r,\tau)\,, \tag{7}$$

and

$$k^2 = \frac{2M}{\hbar^2} E\,. \tag{8}$$

Upon application of Green's theorem and use of Eq. 5, one obtains the following relationship between the S-operator and the Green's function

$$S(r|a) = e^{-i[\phi_\ell(r,\tau) + \phi_\ell(a,\tau)]} \times [1 + 2ik\, G_\ell(r|a,\tau)]\,, \tag{9}$$

which for $r = a$, reduces to the usual relation for the S-function $S(a|a)$, with

$$\phi_\ell(r,\tau) = k(\tau)a(\tau) - \frac{\pi}{2}\ell(\tau)\,. \tag{10}$$

Equation 10 affords the method to obtain the variation of the S-function in terms of the corresponding variation of the Green's function. To obtain the latter we recur to the invariant imbedding formalism developed previously. The result is

$$\frac{\partial}{\partial\tau} G_\ell(a|a,\tau) = \left\{ i\frac{\partial k}{\partial\tau} - \frac{2M}{\hbar^2} U_\ell(a,\tau)\frac{\partial a}{\partial\tau}\right\} G_\ell^2(a|a,\tau) + 2ik\frac{\partial a}{\partial\tau} G_\ell(a|a,\tau) + \left(\frac{2M}{\hbar^2}\right)\int_0^a dr\, G_\ell(a|r,\tau)\left\{\frac{\partial}{\partial\tau}[E(\tau) - U_\ell(r,\tau)]\right\} G_\ell(r|a,\tau)\,. \tag{11}$$

Upon taking the derivative with respect to the parameter τ in Eq. 10 and introducing the results into the Eq. 11, one obtains for $\tau = a$,

$$2ik\frac{\partial}{\partial a} S_\ell(a) = -\left(\frac{2M}{\hbar^2}\right) U_\ell(a)\, e^{-2i\phi_\ell(a)} + \left(\frac{4M}{\hbar^2}\right) U_\ell(a)\, S_\ell(a) - \left(\frac{2M}{\hbar^2}\right) e^{2i\phi_\ell(a)}\, S_\ell^2(a)\,, \tag{12}$$

and for $\tau \neq a$,

$$2ik\frac{\partial}{\partial\tau} S_\ell(a|a,\tau) = -ie^{-2i\phi_\ell(a)}\frac{\partial k}{\partial\tau} + 4k\left[\frac{\partial}{\partial\tau}\phi_\ell(\tau)\right] S_\ell(a|a,\tau) + ie^{2i\phi_\ell(a)}\frac{\partial k}{\partial\tau} S_\ell^2(a|a,\tau) + \left(\frac{2M}{\hbar^2}\right) e^{-2i\phi_\ell(a)}\int_0^a dr\,\frac{\partial}{\partial\tau}[E(\tau) - U_\ell(r,\tau)] - \left(\frac{4M}{\hbar^2}\right)\int_0^a dr\left\{\frac{\partial}{\partial\tau}[E(\tau) - U_\ell(r,\tau)]\right\} \times e^{+i[\phi_\ell(r) - \phi_\ell(a)]} + \left(\frac{2M}{\hbar^2}\right)\int_0^a dr\, S_\ell(a|r)\, e^{2i\phi_\ell(r)} \times \left\{\frac{\partial}{\partial\tau}[E(\tau) - U_\ell(r,\tau)]\right\} S_\ell(r|a)\,. \tag{13}$$

The result (12) is a Ricatti equation for the S-function. The case $\tau \neq a$ yields a nonlinear integrodifferential equation, which by expansion in the proper set of eigenfunctions leads to a set of Ricatti-matrix equations. In both instances the original boundary value problem involved in the solution of the Schrödinger equation has been converted into the solution of an initial value problem for the S-function. By expressing the S-function in terms of the phase shifts, δ_ℓ, of scattering theory, i.e., $S(a|a,\tau) = e^{2i\delta_\ell(\tau)}$, followed by the introduction of the Green's function expansions,

$$G_\ell(a|a,\tau) = k^{-1}\, e^{i\delta_\ell}\sin[\delta e + \phi_\ell(a)]\, e^{i\phi_\ell(a)} \tag{14}$$

and

$$G_\ell(r|a) = e^{i\delta_\ell}\, e^{i\phi_\ell(a)}\,\psi_\ell(r)\,. \tag{15}$$

In Eq. 10, one obtains from the relation (12)

$$\frac{\partial}{\partial a}\delta_\ell(a) = -k^{-1}\left(\frac{2M}{\hbar^2}\right) U_\ell(a)\sin^2[\delta_\ell(a) + \phi_\ell(a)]\,, \tag{16}$$

or alternatively

$$\frac{\partial}{\partial a}\, tg\,\delta_\ell(a) = -\left(\frac{2Mka^2}{\hbar^2}\right) U_\ell(a)\,[j_\ell(ka) - n_\ell(ka)\, tg\,\delta_\ell(a)]^2\,, \tag{17}$$

where $j_\ell(ka)$ and $n_\ell(ka)$ give the spherical Bessel functions. The above results have been arrived at by other methods by Robinson and Hirschfelder,[5] Devooght,[6] and Calogero.[7]

For the case of $\tau \neq a$, it is found from Eq. 13 that the phase shifts, δ_ℓ, satisfy the rather general equation

$$\frac{\partial}{\partial \tau}[\delta_\ell(\tau) + \phi_\ell(\tau)] = k\left(\frac{2M}{\hbar^2}\right)\int_0^a dr \left\{\frac{\partial}{\partial \tau}\left[E(\tau) - V(\tau) - \frac{\hbar^2}{2M}\frac{\ell(\ell+1)}{r^2}\right]\right\}\psi_\ell^2(r) + \frac{1}{2}\sin\left\{2[\delta_\ell(\tau) + \phi_\ell(a)]\right\}\left(\frac{\partial}{\partial \tau}\ln k\right). \quad (18)$$

Two well-known results of the scattering theory[8] are obtained from the Eq. 17. Identification of τ with the angular momentum ℓ yields

$$\frac{\partial}{\partial \ell}\delta_\ell(\ell) = \frac{\pi}{2} - k(2\ell+1)\int_0^a dr\, r^{-2}\,\psi_\ell^2(r). \quad (19)$$

Alternatively, making $\tau = k$, one obtains the variation of the phase shifts as a function of the linear momentum k, i.e.:

$$2i\frac{\partial}{\partial k}\delta_\ell(k) = 4ik^2\int_0^a dr\,\psi_\ell^2(r) + ik^{-1}\sin 2[\delta_\ell(k) + \phi_\ell(k)] - 2ia. \quad (20)$$

Another important relation is obtained by writing the potential $V(r|\tau)$ in the form $\epsilon V_0(r)$, where ϵ is the coupling constant. Then identification of τ with this parameter leads to

$$\frac{\partial}{\partial \epsilon}\delta_\ell(\epsilon) = -k\left(\frac{2M}{\hbar^2}\right)\int_0^a dr\, V_0(r)\,\psi_\ell^2(r). \quad (21)$$

In conclusion it has been shown that the invariant imbedding formulation of the Kapur-Peierls dispersion theory leads to a general integrodifferential equation for the S-function with the following advantages: (a) It contains, in a neat compact form, the various relations for the phase shifts obtained in scattering theory. (b) The solution of the Schrödinger boundary value problem for the wave function is replaced by an initial value problem for the S-function which is much more closely related to observable magnitudes than is the wave function. (c) The various relationships obtained yield methods by which the analytical properties of the S-function can be studied. (d) The present formalism can easily be extended to the multichannel reaction case.

References

1. A. J. Mockel and R. B. Perez, *Phys. Rev.* **C2**, 1179 (1970).
2. G. F. Chew, *The Analytic S-Matrix*, W. A. Benjamin, Inc., New York, 1966.
3. E. P. Wigner and L. Eisenbud, *Phys. Rev.* **72**, 29 (1947).
4. P. L. Kapur and R. E. Peierls, *Proc. Roy. Soc. (London)* **166**, 277 (1938).
5. P. Robinson and J. Hirschfelder, *Phys. Rev.* **129**, 1391 (1963).
6. J. Devooght, *J. Math. Phys.* **7**, 1764 (1966).
7. F. Calogero, *Variable Phase Approach to Potential Scattering*, Academic Press, New York, 1967.
8. R. G. Newton, *Scattering Theory of Waves and Particles*, McGraw-Hill Book Co., New York, 1966.

1.13 VARIATION OF THE R MATRIX[1]

A. J. Mockel[2] R. B. Perez

The R matrix of Wigner and Eisenbud is a function of a set of parameters (channel radii, boundary numbers, etc.) as well as of the energy of the incoming particle. Invariant imbedding techniques have been applied, which give the variation of the R matrix with respect to changes of the parameters entering into the theory. A generalization of various formulas, derived originally by Wigner and Teichmann and Wigner, to the multichannel case has been obtained. Our general results apply also to deformations of the nucleus other than spherical. An application of the invariant imbedding technique is also shown concerning Robson's theory of the isobaric spin analogs.

References

1. Abstract of *Phys. Rev. C*, 2(4), 1179 (1970).
2. *University of Florida.*

1.14 MSC, A PROGRAM TO EVALUATE MULTIPLE SCATTERING CORRECTIONS IN THICK SAMPLES

N. M. Greene[1] G. de Saussure
R. B. Perez S. K. Penny[1]

Work on the Multiple Scattering Correction Program (MSC)[2] has been continued for the past year. Besides the evaluation of multiple scattering corrections in cross-section measurements, the MSC code is also applicable to the computation of reaction rates necessary for the interpretation of the self-indication ratio

measurements presently being carried out at the Oak Ridge Electron Linear Accelerator by Silver et al.[3] This program employs discrete ordinates theory to calculate the reaction rates in thick foils.

The feasibility of the approach utilized in the program was demonstrated[2] by comparing the results of the program with Monte Carlo calculations made with the MULTSCA code.[4] As previously reported,[2] the original version of MSC was essentially three programs modified for our specific application and tied together with IBM Job Control language. They were:

1. A program which requires as input an arbitrary number of resonance parameters, determines a suitable energy group structure, and generates Doppler-broadened point cross sections over our specified energy range.
2. A program to calculate the group-to-group transfer matrices required by S_n codes.
3. A modified version of the ANISN[5] program to perform an adjoint S_n calculation.

A particular case,[2] which used 100 energy groups in the energy interval from 5 to 8 eV around the 6.67-eV ^{238}U resonance, had the following computation times for the IBM-360/91, corresponding to the three programs above:

1. Generation of Doppler-broadened cross sections, 0.47 sec.
2. Generation of transfer matrices, 94.48 sec.
3. Adjoint S_8P_1 calculation, 20.53 sec.

For realistic cases in which several resonances are considered either for resonance-fitting purposes or for self-indication ratio calculations, the computation time is at a premium when various iterations have to be performed to reach a preset level of accuracy. As shown above, the largest expenditure of time was the calculation of the transfer matrices. For this reason the existing routines to calculate transfer matrices were abandoned in favor of a method which employed analytical expressions, valid within the limits of the following assumptions:

1. The flux within each group exhibits the $1/E$ behavior.
2. The elastic scattering cross section is linear between energy points.
3. The elastic scattering is isotropic in the center of mass system.

The first two assumptions are valid for a reasonably fine energy mesh. The last condition is very well satisfied for heavy elements such as the fertile and fissile elements.

The calculation time was decreased further by combining the three programs entering in the MSC code into a single callable package to minimize unnecessary and redundant operations. The flow chart of the resulting program is shown in Fig. 1.14.1.

The improved package was tested for a realistic case in which ten ^{238}U resonances were considered. The energy region between 500 and 600 eV contained five of the resonances and five additional resonances in the adjoining energy regions were used to define the background. A total of 224 groups with a variable mesh, denser around the resonance peaks and wider in the cross-section valleys, were utilized in this particular problem. The new computation times for IBM 360/91 were found to be 4.2 sec for the generation of all cross sections and 4.8 sec to perform the S_9P_1 adjoint calculation. The results for samples of nominal thicknesses of 1 and 23 mils were compared with similar Monte Carlo calculations by the program MULTSCA[4] in which 3000 energy points were taken into account. The results are displayed in Figs. 1.14.2 and 1.14.3 for the 1- and 23-mil samples, respectively. The agreement between the two methods is excellent around the cross-section peaks. Between resonances, however, the energy mesh used in the present test case is too coarse.

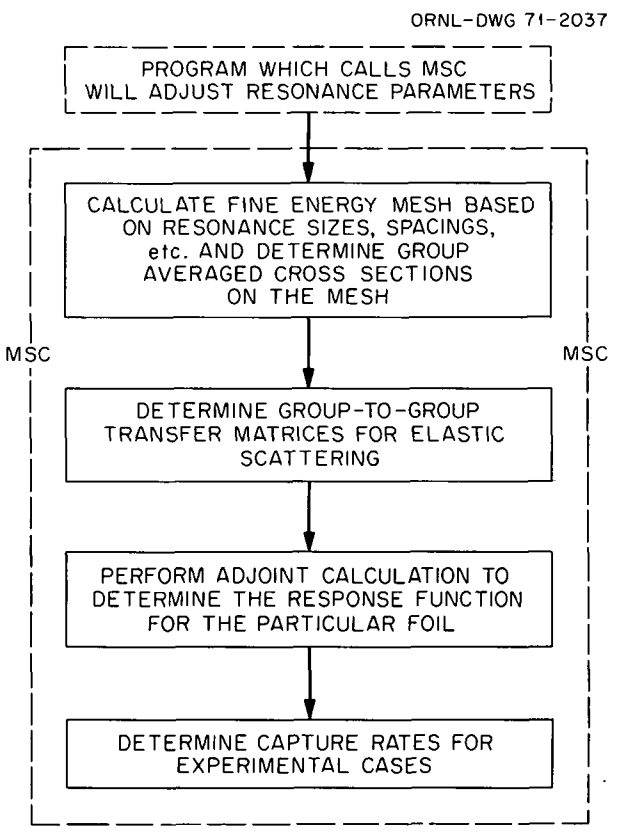

Fig. 1.14.1. Flowchart of the MSC Program.

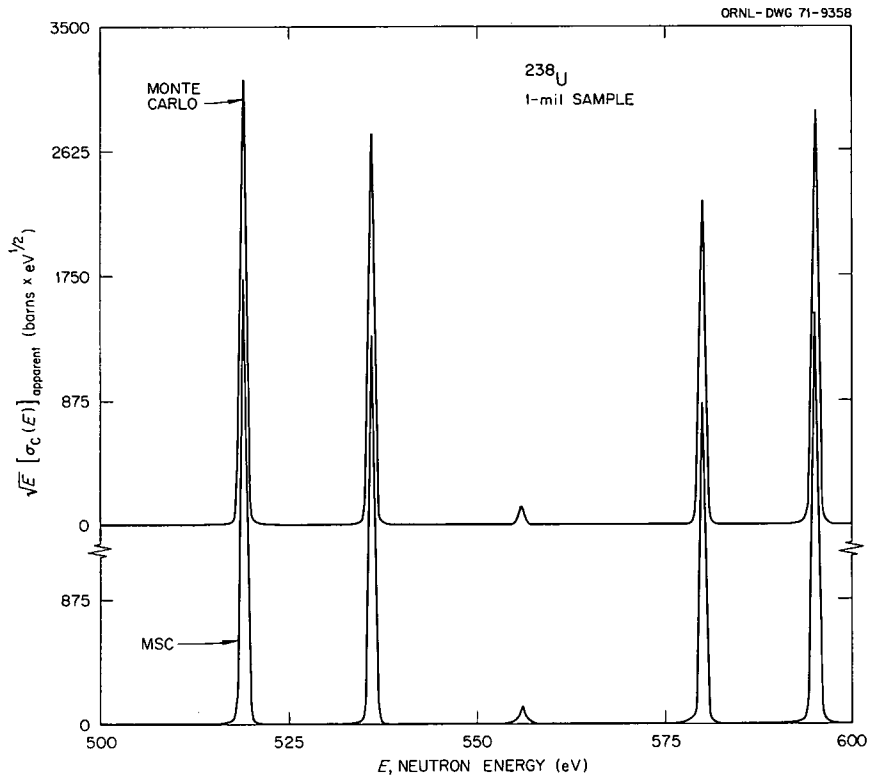

Fig. 1.14.2. Comparison of MSC and Monte Carlo Results for 1-mil ^{238}U Sample.

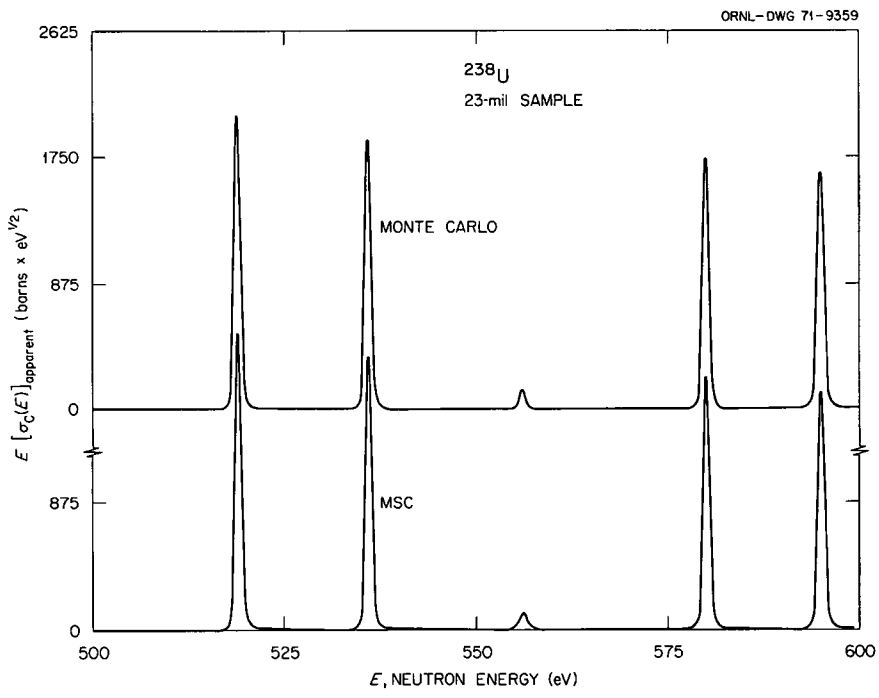

Fig. 1.14.3. Comparison of MSC and Monte Carlo Results for 23-mil ^{238}U Sample.

This is apparent especially in the small resonances but is much less serious for the large ones. Except for the 556-eV resonance the resonance areas agree within 2% for the thinner sample and within 4% for the thick 23-mil sample. For the small resonance at 556 eV, the deviations in the resonance areas are 27% due to the effect mentioned previously. This problem can, however, be easily corrected within reasonable computation times by increasing the number of groups in the cross section valleys.

Work is presently being carried out leading to the incorporation of the MSC code to our least squares resonance fitting programs.

References

1. Mathematics Division.
2. N. M. Greene et al., *Neutron Phys. Div. Ann. Progr. Rept. May 31, 1970,* ORNL-4592, p. 18.
3. See Sec. 1.1.
4. MULTSCA – A Monte Carlo Code to Evaluate Multiple Scattering Corrections, unpublished work of G. de Saussure (1969).
5. W. W. Engle, *A User's Manual for ANISN, A One-Dimensional Discrete Ordinates Transport Code With Anistropic Scattering,* K-1693 (1967).

1.15 HIGH-RESOLUTION INELASTIC CROSS-SECTION MEASUREMENTS FOR Na, Si, AND Fe[1]

F. G. Perey W. E. Kinney
R. L. Macklin[2]

A program of inelastic scattering measurements has been initiated at the Oak Ridge Electron Linear Accelerator. Data are obtained by detecting the de-excitation gamma rays in a 4π geometry with a flight path of 40 m. The present detector is a hydrogen-free carbon fluoride liquid scintillator used in capture cross-section measurements. The initial set of measurements was performed with only a 0.125-nsec/m resolution to investigate the technique. Data were reduced up to the threshold of the second excited state for ^{7}Li, C, Na, Si, and Fe. The carbon data were used for background determination and the ^{7}Li data for flux determination. The data for Na, Si, and Fe will be presented. The cross sections show great resonance structure with peak-to-valley ratios larger than those found in the total cross section. The energy resolution is sufficient to identify all the resonances observed in the inelastic cross sections with resonances in the total cross sections. Various aspects of the experimental technique will be discussed, including extension of these measurements above the threshold of the second excited state.

References

1. Abstract of paper presented at the Third Conference on Neutron Cross Sections and Technology, March 15–17, 1971, Knoxville, Tennessee.
2. Physics Division.

1.16 STATUS REPORT OF THE OAK RIDGE ELECTRON LINEAR ACCELERATOR (ORELA)

N. A. Betz[1] F. C. Maienschein
J. A. Harvey[2] J. W. Reynolds[3]
T. A. Lewis[3] H. A. Todd[3]

1.16.1 ORELA Performance

Operation of the Oak Ridge Electron Linear Accelerator (ORELA) on a 24-hour, 7-day basis (excepting holidays) was generally favorable as is indicated in Table 1.16.1 with one notable exception. A failure on December 15, 1970, of the closure clamp on the slightly pressurized tank (~20 psi of SF_6) which contains the electron gun and its electronic drive circuits interrupted linac operation for about eight weeks. We had identified the "tank system" as the weakest link of the accelerator with respect to probable failure and difficulty of repair. We had started to design and construct a conservatively designed replacement

Table 1.16.1. ORELA Operation from June 3, 1970 Through May 30, 1971

Date	Research Hours
6-3-70 to 6-30-70	369.5
7-1-70 to 7-18-70	237.7
7-19-70 to 8-11-70	[a]
8-12-70 to 8-31-70	313.4
9-1-70 to 9-30-70	437.0
10-2-70 to 10-30-70	321.6
11-1-70 to 12-1-70	559.7
12-1-70 to 12-31-70	278.8[b]
1-1-71 to 1-31-71	0.0[b]
2-1-71 to 2-31-71	273.6[b]
3-1-71 to 3-31-71	506.3
4-1-71 to 4-30-71	573.0
5-1-71 to 5-30-71	529.2
6-3-70 through 5-30-71	4400 Total

[a]Scheduled shutdown for Be-target installation.
[b]Shutdown to repair gun-tank failure.

tank system with modular circuit components which could be substituted and repaired on the bench.[4] Of course, we did not anticipate catastrophic mechanical failure of the tank itself. Repair of the tank and components was greatly delayed because detailed examination before reassembly revealed flaws in the original tank design and construction. Thus virtually the entire tank had to be replaced.

All of the down-time caused by the tank failure was not lost, however, since many maintenance and improvement items on other parts of the accelerator were handled which would have eventually required accelerator down-time in any event. The maintenance schedule normally adopted is two days off after two weeks of steady running.

Major improvement in the operation of the linac has resulted from changes made during this year in heat generation and removal in the modulator boxes. New voltage-supply transformers were installed to allow lower de-Qing and thus dump less heat into the resistor stacks. Additional fans with better filters improved the air flow. Altogether, as soon as the new gun tank is installed, these changes should allow operation at the full design repetition rate of 1000 ppsec rather than at $\leqslant$ 800 ppsec as at present. The heat removal from the present gun tank limits its operation to ~800 ppsec.

Klystron performance continues to be good as is indicated in Table 1.16.2. The experience with electron guns during the past year is reviewed in Table 1.16.3.

1.16.2 Data-Handling System

The concept of multiple use of the linac has been brilliantly fulfilled during this year. Usually, a total of five to six experimenters were taking data or performing preliminary experiments at any time the accelerator was operating. (See Table 1.16.4 for a list of current experiments.) Multiple use is made possible by the design of the facility and the data-handling system. The Phase-I data-acquisition system[5] was placed in general use for multiple, uniquely defined experiments in August, 1970. A maximum of four experiments with total data rates of ~5000 events/sec can simultaneously operate on each computer. The computers can also operate auxiliary programs such as processing paper tape output from other ORELA data-acquisition devices and updating the accelerator inventory list during acquisition.

In March, 1971, routines were put in operation to control changing of samples during an experiment. Such equipment control will be extended to other experiments later.

A ground-isolating data link for transferring data and remotely using the peripherals of the Phase-I SEL 810B was installed between the SEL 810B and the PDP-4 and PDP-9 which are used for data collection. Use of the Phase-I peripherals by the PDP-4 and PDP-9 computers should be possible in June, 1971.

A major effort was made in the continuing program of avoiding instrumental ground loops. Electrical isolation was installed on the computer ends of the scaler and multiplexer connections between experiments and Phase-I data-handling systems. In the absence of the isolation devices, all ground connections have been through the Phase-I data-handling system, an arrangement which has become less and less desirable as more detecting equipment is connected to it.

The Phase-II Data Analysis System with interactive graphics was delivered by Digital Equipment Corporation (DEC) in April, 1971. The extended acceptance tests are scheduled to start in August, 1971, and to be completed in September, 1971. DEC will supply the software for their computers for telephone-line communications among the parts of the system, and they

Table 1.16.2. Klystron Lifetimes

Klystron Number	H. V. Hours	
2002	1447	Available as spare[c]
2004	0[a]	Available as spare
2008	2324.8[b]	March 1970–Oct. 1970
2003	9212.6	Sept. 1969–May 1971
2006	7813.6	Nov. 1969–May 1971
2007	7850.0	Available as spare[c]
2009	3106.3	Available as spare[c]
2010	626.3	April 1971–May 1971
2011	625.5	April 1971–May 1971

[a]Subsequently rebuilt.
[b]End of life.
[c]Removed to test new tubes.

Table 1.16.3. Electron Gun Lifetimes

Gun Number	Beam Hours	Date
5-2	1743	5-29-70 to 10-26-70
4-2	868[a]	10-26-70 to 12-15-70
8-1	598[b]	2-1-71 to 3-13-71
7-1	1466[c]	3-13-71 to 5-30-71

[a]Gun life terminated due to vacuum failure.
[b]Gun life terminated due to HV overcurrents.
[c]Still operating.

Table 1.16.4. Experiments at ORELA

Flight Path Number	Station	Experiment	Reference
1	18 m	Total Cross Sections of Small Samples	ORNL-4659, p. 61
	80 m, 200 m	High Energy Resolution Neutron Total Cross-Section Measurements	ORNL-4513, p. 62
2	10 m	Fission Fragment Asymmetries from Aligned Fissile Nuclides	ORNL-4659, p. 90
	20 m	J-Value Determinations Using Polarized Neutrons	ORNL-4659, p. 32
3	15 m	High Energy Resolution Fission Cross-Section Measurements	ORNL-4659, p. 71
4	20 m	Being prepared for auxiliary experiments for flight paths 5–8	
5	20 m	Neutron Cross-Section Measurements Using Scintillators in Low-Efficiency Geometry	This report, Secs. 1.4, 1.5
	60 m	Fast-Neutron Inelastic-Scattering Measurements[a]	This report, Sec. 1.15
6	40 m	Neutron Cross-Section Measurements Using Scintillator Tank	This report, Secs. 1.1, 1.2, 1.3
		Fast-Neutron Inelastic-Scattering Measurements[a]	This report, Sec. 1.15
	150 m	Neutron Cross-Section Measurements Using Scintillator Tank[b]	
7	40 m	Neutron Capture Cross Sections for Nonfissile Materials in the keV Range	ORNL-4513, p. 33, *Nucl. Instr. Methods* **91**, 565 (1971)
		Fast-Neutron Inelastic-Scattering Measurements[a]	This report, Sec. 1.15
8	20 m	Precision Neutron Cross-Section Measurements	This report, Sec. 1.9
9	30 m, 50 m	Semi-integral Shielding Studies	This report, Secs. 2.12, 2.13
10			
11	10 m	Gamma-Ray Spectral Measurements from Resonance Neutron Capture	ORNL-4659, p. 64
	Target room	Pneumatic Rabbit Irradiation Facility	

[a]These measurements will use one or more of the indicated flight paths, depending upon their availability, which will change with time.

[b]New flight station being readied for use.

will supply the Fortran-accessible graphic primitives. Further development of programs required for data analysis will be carried out by ORNL staff members.

1.16.3 Neutron-Producing Targets

A measurement during the year of the absolute fast-neutron spectrum from the standard ORELA neutron-producing target showed good agreement with the predicted spectrum.[6] The agreement should lend increased credibility to predictions of spectra for new targets. A target designed for improved yield of high-energy neutrons was installed and made operational this year. It uses tantalum for conversion to photons and a separate beryllium neutron source.

The standard ORELA target uses an aluminum can to contain the water moderator. The aluminum introduces unwanted structure into the neutron flux at energies above 30 keV. To eliminate this problem, beryllium has been substituted for the aluminum in the can in a test-model target. This target is scheduled for delivery during the summer of 1971. Since it presents challenging Be fabrication problems, it will be tested as thoroughly as possible before installation and use.

References

1. Mathematics Division.
2. Physics Division.
3. Instrumentation and Controls Division.
4. We anticipate installation of the replacement gun tank in the fall of 1971.
5. N. A. Betz, et al., *Neutron Phys. Div. Ann. Progr. Rept. May 31, 1970,* ORNL-4592, p. 24.
6. C. E. Burgart et al., "The Energy Spectrum of Photoneutrons Produced by 140-MeV Electrons Incident on Tantalum," *Nucl. Sci. Eng.* **42**, 421 (1970).

1.17 PULSE-SHAPE MEASUREMENTS FOR THE OAK RIDGE ELECTRON LINEAR ACCELERATOR WITH GAMMA-RAY DETECTION TECHNIQUES[1]

L. W. Weston J. H. Todd

A study of the pulse-shape characteristics of the Oak Ridge Electron Linear Accelerator was carried out because the resolution of neutron cross section and neutron spectra measurements are directly dependent upon this pulse shape. Gamma-ray detection with techniques commonly used in the neutron time-of-flight experiments was used in the study because of the fidelity with which the pulse shape could be measured.

References

1. Abstract of *Nucl. Instr. Methods* 86, 205 (1970); included in last year's annual as abstract of ORNL-TM-2833 (1970).

1.18 SPECTRUM OF PHOTONS EMITTED IN COINCIDENCE WITH FISSION OF ^{235}U BY THERMAL NEUTRONS[1]

R. W. Peelle F. C. Maienschein

The absolute energy spectrum of prompt photons emitted from the fission of ^{235}U by thermal neutrons was measured in the range from 0.01 to 10 MeV by using single-crystal, Compton, and pair NaI(Tl) scintillation spectrometers. Each was operated in $\leqslant$69-nsec coincidence with a fission chamber exposed to thermal neutrons from a reactor. The pulse-height response functions of the spectrometers were constructed in detail by exposing the spectrometers to radioactive sources of known disintegration rates. These data were used to "unfold" the measured pulse-height spectra to give the absolute differential energy spectrum and its random uncertainties. A careful analysis of systematic uncertainties was also performed. The average number of photons per fission is 8.13 ± 0.35 and the average photon energy release per fission is 7.25 ± 0.26 MeV, both over the energy region from 10 keV to 10.5 MeV. The results obtained here are in approximate agreement with the recent measurement by Verbinski and Sund in the energy region above 140 keV. From 1.5 to 4 MeV the calculations of Zommer, Savel'er, and Prokofiev give results which are close to the measurements. The observed total energy release in photon emission per fission has been predicted by two published calculations which treated statistical evaporation theory in different ways to enhance the emission of photons. The *K*-shell x-ray intensities for the light- and heavy-fragment groups were found to be 0.08 ± 0.02 and 0.23 ± 0.02 photons/fission, respectively. The x-ray intensities are consistent with internal conversion of the observed γ-ray spectrum for various assumed mixtures of $E1$, $E2$, and $M2$ transitions, including roughly equal $E1$-$E2$ mixtures; the intensities are not consistent with all the transitions having any single multipolarity.

References

1. Abstract of *Phys. Rev..C* 3(1), 373 (1971).

1.19 NEUTRON ELASTIC- AND INELASTIC-SCATTERING CROSS SECTIONS FOR YTTRIUM IN THE ENERGY RANGE 4.19 TO 8.56 MeV[1]

F. G. Perey W. E. Kinney

We present numerical values for neutron elastic- and inelastic-scattering cross sections for yttrium for incident neutron energies from 4.19 to 8.56 MeV. Our data are in good agreement with the results of others.

References

1. Abstract of ORNL-4552 (1970).

1.20 ELASTIC AND INELASTIC SCATTERING OF NEUTRONS FROM CARBON IN THE ENERGY RANGE OF 5 – 8.7 MeV

F. G. Perey W. E. Kinney

We have acquired data on elastic and inelastic scattering of neutrons on carbon in the energy range of 5 – 8.7 MeV. Angular distributions (data at 18 angles) were obtained at least every 100 keV on the energy range and when the resonance structure required at every 50 keV. We hope that these data will be adequate to present the resonance structure of elastic and inelastic scattering in this energy region and plan to do an R matrix analysis of this data.

1.21 V NEUTRON ELASTIC- AND INELASTIC-SCATTERING CROSS SECTIONS FROM 4.19 TO 8.56 MeV[1]

F. G. Perey W. E. Kinney

We present numerical values for neutron elastic-scattering cross sections for natural V (99.76% ^{51}V, 0.24% ^{50}V) and cross sections per atom of natural V

for inelastic scattering to levels in ^{51}V for incident neutron energies from 4.19 to 8.56 MeV. Our data are in good agreement with the results of others. The ENDF/B V elastic angular distributions are in good agreement with experimental data at forward angles but are displaced about 10° toward 0° beyond the first minimum. The ENDF/B excitation functions are in good agreement with experiment although the inelastic functions stop at 2.6 MeV. Our data partially fill priority III requests to NCSAC.

References

1. Abstract of ORNL-4551 (1970).

1.22 Al NEUTRON ELASTIC- AND INELASTIC-SCATTERING CROSS SECTIONS FROM 4.19 TO 8.56 MeV[1]

W. E. Kinney F. G. Perey

We present numerical values of Al neutron elastic- and inelastic-scattering cross sections in the incident neutron energy range of 4.19 to 8.56 MeV. Our data are compared with the results of others and found to be consistent with them. The ENDF/B Al elastic angular distributions are in good agreement with experiments at angles less than 60° but are in poor agreement with angles larger than this. The ENDF/B Al inelastic excitation functions could be improved and extended through the use of data which has become available since the evaluation. Our data partially fill priority I and II requests to NCSAC.

References

1. Abstract of ORNL-4516 (1970).

1.23 SCATTERING OF NEUTRONS FROM Fe, Cu, AND Pb

F. G. Perey W. E. Kinney

Neutron inelastic-scattering data have been obtained every 500 keV from 5.5 – 8.5 MeV for ^{54}Fe, ^{63}Cu, ^{65}Cu, ^{206}Pb, ^{207}Pu, and ^{208}Pb. Complete angular distribution data of both elastic and inelastic scattering were obtained for ^{54}Fe, ^{63}Cu, ^{65}Cu, and ^{208}Pb at 5.5, 7, and 8.5 MeV.

1.24 NUCLEON-NUCLEUS OPTICAL MODEL POTENTIAL

F. G. Perey

A paper with the above title was presented at the Third International Symposium on Polarization Phenomena.[1] The methodology for obtaining optical model parameters from elastic-scattering data was reviewed and the impact of polarization data on the parameters discussed.

References

1. *Polarization Phenomena in Nuclear Reactions. Proceedings of the Third International Symposium, Madison 1970*, edited by H. H. Barshall and W. Haebertli, pp. 131-142, The University of Wisconsin Press, Madison, 1971.

1.25 COMPILATION OF OPTICAL MODEL PARAMETERS

C. M. Perey[1]

Periodically the need arises to make use of optical-model parameters which have been determined from the analysis of elastic scattering. Various tabulations have been done in the past, the most recent one being five years old. We have been approached by the editor of Nuclear Data to undertake a compilation of this nature. We agreed to undertake a pilot compilation going back to a few years in order to ascertain the response of the research community to such a need. Previous compilations of optical-model parameters have generally appeared in institutional reports and are not generally available. We are attempting, in this compilation, to perform a certain degree of evaluation of the optical-model parameters.

References

1. Consultant.

1.26 11-MeV PROTON INELASTIC SCATTERING FROM EVEN-EVEN MEDIUM-WEIGHT NUCLEI[1]

C. M. Perey[2] J. K. Dickens
R. J. Silva[3] F. G. Perey

The analysis of inelastic scattering of 11-MeV protons from quadrupole and octupole collective levels of 14 even-even nuclei between ^{48}Ti and ^{76}Ge is reported. The distorted-wave Born approximation is used to calculate the cross sections using the collective-model generalization of the optical model for inelastic scattering. The analysis is performed using both real and complex form factors for the model. A satisfactory description of all the data is obtained when a contribution due to compound-nucleus decay for most of the

octupole levels and a few of the quadrupole levels is included.

References

1. Abstract of *Phys. Rev. C* 2(2), 468 (1970); included in last year's annual as abstract of ORNL-TM-2861 (1970).
2. Consultant.
3. Chemistry Division.

1.27 MEASUREMENTS OF THE NEUTRON FISSION AND ABSORPTION CROSS SECTIONS OF ^{239}Pu OVER THE ENERGY REGION 0.02 eV TO 30 keV, PART II[1]

R. Gwin — J. H. Todd[2]
L. W. Weston — F. E. Gillespie[2]
G. de Saussure — R. W. Hockenbury[3]
R. W. Ingle[2] — R. C. Block[3]

The neutron absorption and fission cross sections for ^{239}Pu have been measured simultaneously over the neutron energy range from 0.02 eV to 30 keV. These cross sections were measured using an ionization chamber containing ^{239}Pu. The differential cross sections derived from these measurements are presented along with a multilevel analysis of the data up to 100 eV. A re-evaluation of data obtained using a metal foil of ^{239}Pu has also been made. Average values of the neutron capture and fission cross sections are presented for ^{239}Pu as obtained using the ionization chamber as well as with the metal foil. A detailed comparison of the present data is made with the results of the ENDF/B evaluation for ^{239}Pu (material 1104). The neutron cross sections presented in this report supersede the results previously reported by the authors.

References

1. Abstract of *Nucl. Sci. Eng.* **45**, 25 (1971) and ORNL-4707 (1971).
2. Instrumentation and Controls Division.
3. Rensselaer Polytechnic Institute.

1.28 FAST FISSION CHAMBER AMPLIFIER-DISCRIMINATOR SYSTEM[1]

R. W. Ingle[2] F. E. Gillespie[2]
L. W. Weston

To measure the fission cross section of ^{233}U as a function of neutron energy, instrumentation with fast pulse rise time and short resolving time characteristics is required. The efficient detection of fission-fragment pulses in the presence of a high alpha background requires these characteristics. A fission detector with an electron collection time of 25 nsec and containing 1 g of ^{233}U, and an amplifier with a rise time of 7 nsec and an over-all gain of 1000 were developed for this measurement. This system, detecting the fast rising current pulse from a parallel plate ionization chamber, is an integral part of the instrumentation used by a group at ORNL engaged in the measurement of the neutron fission and capture cross sections as a function of neutron energy. With this system, the fission cross section of ^{233}U was successfully measured over a neutron energy range from 0.4 to 2000 eV.

References

1. Abstract of *Rev. Sci. Instr.* **41**, 1539 (1970).
2. Instrumentation and Controls Division.

2. Reactor and Weapons Radiation Shielding

2.0 INTRODUCTION

C. E. Clifford

The objectives of the ORNL shielding program, which is largely supported by the Space Electric Power Office (SEPO) project, the Defense Atomic Support Agency (DASA), and the Division of Reactor Development and Technology for the Liquid Metal Fast Breeder Reactor (LMFBR), are the development of basic methods for solving radiation transport problems, the testing of these methods by comparison with experimental results, and the development of data and techniques that engineers can use with a high degree of confidence in designing shields to meet their requirements. Further, the intent is to provide design techniques that are general in nature so that shields can be optimized not only with respect to weight, as required for the SEPO program, but also with respect to cost, radiation heating, radiation damage, or any other requirement or constraint that may be imposed by the design engineers.

The LMFBR shielding development program has continued to increase in scope and has become the major reactor shielding program within the division. Shield design problems for fast-breeder reactors are more complex than those for earlier power reactors due to the unique requirements of the systems. In the proposed LMFBR's, for example, the liquid sodium coolant rules out, for safety reasons, the use of the standard hydrogeneous neutron shields near the core. Also, the very high neutron fluences in these systems will require internal shields to protect reactor structural components from damage. These shields are usually immersed in sodium and must be resistant to high temperatures, a requirement which restricts the choice of materials to elements that have known desirable behavior in the reactor environment. For this limited group of materials the neutron interactions are often not well understood. Also, the secondary gamma-ray production rates are usually unknown, particularly for neutrons in the eV to keV range that dominate the reactor spectrum.

Many of the principal problems in the current designs are dominated by neutron streaming effects. Streaming occurs through voids, insulation space, and sodium coolant passages, and may be enhanced due to the deep valleys in the neutron cross sections for iron. A major problem in piped systems is the activation of the secondary coolant due to neutron streaming in passageways for the primary loop pipes. Prediction of radiation damage in the core support structure is complicated by streaming in the heterogeneous core, reflectors, blankets and shielding. Also streaming in the fission gas plenum, reactor cavity, and head penetrations affect the dose rates and activation rates which are predicted for the environs of the reactor head.

The majority of the effort in the LMFBR shielding program has been directly related to the Fast Test Reactor (FTR) design now in progress at the Westinghouse Advanced Reactor Division. Radiation transport calculations have been performed for a two-dimensional representation of the entire reactor and shield system with the discrete ordinates computer code DOT. The number of specific problems related to the FTR design has required both development in the application of the discrete ordinates method and an experimental program to indicate the validity of the calculational technique. Because of the extremely close coupling between the calculational results obtained by ORNL and the project design at ARD, the results of this program have been documented primarily by monthly reports and by letter reports. Of both short- and long-range interest is a detailed study of neutron transport through iron which has been performed utilizing very recent iron cross-section evaluations in a Monte Carlo calculation of an experiment performed at the Tower Shielding Facility.

The shielding effort being conducted for the Defense Atomic Support Agency (DASA) continues to be concerned with radiation transport through the atmosphere and into heavily shielded military systems. The effort includes the development and application of time-dependent transport methods both for the solution of military design problems and for the analysis of experiments which again are designed to determine the validity of the methods. Recently the emphasis of the program has been directed toward the determination of the sensitivity of specific design problems and integral experiments to differential cross-section data.

The SNAP shielding program has been concerned with the development and verification of basic methods and cross-section data and with the design of a number of optimized shields for particular space missions and reactor configurations. The techniques for optimizing shields has been considerably improved during the past year. A one-dimensional shield optimization code using a perturbation technique has been developed which obtains the first and second dose derivatives from a single forward and adjoint transport calculation for any portion of a many-layered shield. Using ANISN calculations, the new code is hoped to be as accurate as ASOP, which obtains essentially the same information by performing two somewhat independent transport calculations for each variable in the shield design. A significant step forward has been achieved in the shaping of a 4π asymmetric shield based on isodose and constant gamma-ray production contours within the shield which are automatically generated and plotted as part of the DOT calculation. The experimental program at the TSF has included the measurement of the gamma-ray production in shields consisting of combinations of heavy metal and LiH, the heavy metals consisting of iron, tungsten, and ^{238}U. Iron was chosen because all the cross-section data are now reasonably well known and the ability to calculate the neutron transport and secondary gamma-ray production has been well demonstrated. The experiments with uranium are being repeated because of disagreements on the order of a factor of 2 to 3 between the measured and calculated results for laminated shields. Because of a reduced effort in the SNAP program, the analysis of the results may be delayed.

During the past year, Monte Carlo development work has been primarily concerned with the MORSE Monte Carlo code. Revisions have been made in the cross-section module for MORSE to include treatment of the total, scattering, and fission cross sections with point data rather than by groups, as well as to include treatment of neutron upscattering. Investigations have also been made into the coupling of two-dimensional DOT results to MORSE for the solution of the three-dimensional aspects of particular shielding problems.

Importance sampling techniques for Monte Carlo calculations continue to be studied primarily with respect to the biasing of the production of secondary gamma rays utilizing importance functions from discrete ordinates calculations. Russian roulette and splitting, nonabsorption weighting, and biasing gamma-ray generation probabilities were evaluated and found to be useful in improving the efficiency in a MORSE coupled neutron-gamma-ray deep-penetration calculation for concrete.

Production calculations using Monte Carlo techniques have been completed for deep penetration in sodium and iron. Calculated results for the penetration of neutrons through thicknesses of iron ranging up to approximately 90 cm have been compared with experimental results obtained at the TSF. Two recently evaluated iron cross-section sets were used in the calculation to predict measured Bonner ball results and hydrogen and NE-213 spectrometer measurements of the neutron spectra in various locations. The largest variation between the calculated and measured results was less than a factor of two and in many instances less than 10%. The most recent set of cross-section data (ENDF/B Mat 1124) gave the best agreement.

Application of the advanced calculational techniques requires continued improvement in the basic cross-section data needed as input. A sizeable effort has been maintained in both the measurement and calculation of the cross-section data for neutron-induced gamma rays. Experiments conducted at the Oak Ridge Electron Linear Accelerator (ORELA) and at the TSF are used to evaluate the adequacy of existing information for the gamma rays produced in shielding materials, including tantalum, lead, uranium, and tungsten, and the materials found in soils and concrete. These data have been utilized to compare newly evaluated cross-section sets for use in the shielding library. Nuclear model theory continues to be studied as a useful tool for evaluating existing cross-section information and hopefully for extrapolating the data in a systematic way.

2.1 SHIELDING FOR ADVANCED REACTORS IN THE UNITED STATES[1,2]

F. C. Maienschein F. R. Mynatt
C. E. Clifford L. S. Abbott

A shielding technology emerging in the United States for advanced reactor systems is based on detailed solutions of the Boltzmann transport equation with improved versions of the discrete ordinates and Monte Carlo calculational methods. These improved techniques, together with the availability of larger and faster computers and an increasing body of accurate cross-section data, will reduce shield design uncertainties and thereby alleviate excessive costs associated with over-conservatism. The need for such a refined technology becomes imperative as the designs for Liquid Metal Fast Breeder Reactors and reactors for application in space become more advanced. In current efforts to provide

shield design methods required for these reactors, work is being concentrated on adapting the discrete ordinates and Monte Carlo techniques to the unique characteristics of each system and on improving the basic nuclear data for specific materials used in the systems. The validity of the techniques and data, as adapted, is being tested experimentally, with more emphasis on benchmark-type measurements than on mockup-type measurements.

References

1. The ORNL work reviewed in this paper was jointly funded by LMFBR and SEPO projects of the Atomic Energy Commission and the Defense Atomic Support Agency under Subtask PE074.
2. Abstract of *Nucl. Eng. Design* **15**, 241-264 (1970).

2.2 FFTF RELATED STUDIES IN THE ORNL-LMFBR SHIELDING PROGRAM[1,2]

F. R. Mynatt R. E. Maerker
C. E. Clifford M. L. Gritzner
F. J. Muckenthaler L. R. Williams
J. L. Rathbun[3]

The basic goal of the ORNL Liquid Metal Fast Breeder Reactor shielding program is to develop and verify in a timely fashion those calculational techniques which will be capable of providing results suitable for accurate and efficient LMFBR plant design. So that maximum benefit from other shielding programs may be obtained, the transport, shield optimization, and cross-section processing codes which have been and are presently being developed for the Defense Atomic Support Agency and USAEC-SNAP programs are being extended to provide the capability necessary for LMFBR shielding analysis and design. The ability of the resulting transport codes, cross-section data, and data processing codes to provide an accurate determination of radiation distributions must then be verified through intercomparison with integral experiments and other calculations. The problems of the Fast Flux Test Facility reactor have provided a significant stimulus to the LMFBR shielding program by requiring the execution of full transport calculations and experimental verification in support of complex shield designs. The ORNL effort is providing the reactor designers with direct calculational and experimental support and is providing a realistic guide for methods development.

Three major FFTF shielding problems are to predict (1) radiation levels above the head, (2) radiation damage to the core support grid plate, and (3) radiation effects in the heat exchanger rooms. The ORNL effort has been concentrated on the above-core problems leading to a prediction of the radiation levels above the head. The grid-plate shielding problem has received less study, and the problem of determining the effects of radiation streaming to the heat exchanger rooms is yet to be studied.

The design support calculations for the reactor head shielding study were pursued in three steps:

(1) A preliminary analysis of neutron streaming around the rotating plugs was performed with the two-dimensional transport code DOT.[4] The neutron flux incident on the head was obtained with the one-dimensional transport code ANISN[5] using a spherical reactor and pool representation, a special 56-angle quadrature, a 50-group energy grid, and P_3 scattering. The DOT calculations of the rotating plug configuration used a biased 315-angle quadrature so that streaming in the annular slit around the 6-ft-diam. plug would be accurately calculated. Calculations with this model showed that above-head flux intensities were acceptable for several arrangements having double offset clearance gaps which were mechanically suitable.

(2) Two-dimensional calculations of the reactor were made to better determine the radiation distribution incident on the head. A 50-group, S_6P_1 DOT calculation for 11,024 space points in an R-Z geometry described the reactor from the core center to the top of the head and from the centerline to the shield beyond the radial cavity. The importance of streaming in the radial reactor cavity and in the structure surrounding the thermal shield and head was demonstrated by these results. An overlapped sequence of DOT calculations with specially biased angular quadratures in each step was then performed to evaluate the effects of streaming in the fission gas plenum and the sodium pool. The heterogeneous zones were represented by concentric annular rings, giving a conservatively high streaming effect. It was found that the streaming in the fission gas plenum was important.

(3) The two-dimensional calculations in (2) were then coupled with streaming calculations for the rotating plugs in the top head and the vessel support system around the circumference of the head. It was found that the transmission through the head and the relative importance of streaming were very sensitive to the changing spectra across the top of the sodium pool. The transmitted flux was increased so that the relative importance of streaming was reduced, making a single offset geometry gap feasible. The vessel support system calculations showed excessive streaming and additional shielding is required in the support system area or in the reactor cavity.

To establish reliable confidence levels in the complex transport calculations, it is necessary to perform extensive comparisons with relevant integral experiments. Several such experiments have been performed at the ORNL Tower Shielding Facility in support of the FFTF head shielding problem.

Measurements of absolute spectra transmitted through solid iron slabs and stainless steel slabs have been made using both a bare reactor source and a collimated reactor beam source. Comparisons have shown that by using the recent Penny-Kinney[6] iron evaluation with either point cross sections or several hundred tailored energy groups, good (1 to 20%) agreement with the experimental data at deep penetration is achieved.

Experiments have been performed for annular and plane air-filled slots in iron (see Sec. 2.5) and in laminated iron/nickel slabs of thicknesses comparable to the FFTF head. A spectrum modifier consisting of 8 in. of iron and 60 in. of sodium was used to provide a realistic source spectrum. Present results indicate absolute ratios of measured/calculated results varying from 0.96 to 1.36 for a single slit and 1.44 to 1.75 for an offset slit.

References

1. Funded by the LMFBR program of the Atomic Energy Commission.
2. Summary of paper to be presented at American Nuclear Society Meeting, October 17-21, 1971, Miami Beach, Florida.
3. Westinghouse Electric Corp., Advanced Reactor Division, Waltz Mill Site, Madison, Pa.
4. F. R. Mynatt, F. J. Muckenthaler, and P. N. Stevens, *Development of Two-Dimensional Discrete Ordinates Transport Theory for Radiation Shielding,* USAEC Report CTC INF-952 (1969).
5. W. W. Engle, Jr., *A User's Manual for ANISN, A One-Dimensional Discrete Ordinates Code with Anisotropic Scattering,* USAEC Report K-1693 (1967).
6. S. K. Penny and W. E. Kinney, *A Re-Evaluation of Natural Iron Neutron and Gamma-Ray Production Cross Sections – ENDF/B Material 1124,* ORNL-4617 (1971); see also Sec. 2.44, this report.

2.3 MEASUREMENTS OF THE TRANSPORT OF REACTOR NEUTRONS THROUGH IRON SHIELDS[1,2]

C. E. Clifford — L. B. Holland
F. J. Muckenthaler — J. L. Hull
P. N. Stevens[3] — J. J. Manning
K. M. Henry — J. N. Money

An experimental study of neutron transport in iron utilizing a typical reactor leakage spectrum was undertaken at the Tower Shielding Facility for two reasons: calculations of neutron transport in solid steel shields are particularly difficult, and iron is a major constituent in shields for fast, high-temperature reactor systems. The difficulty in calculations for iron lies in the very complex nature of the variation of the neutron cross sections over a broad energy region. This complexity in turn requires detailed representation within the transport calculations and also requires very high resolution measurements of the iron cross sections themselves.

An early indication that problems existed in predicting neutron transport in iron was obtained during the ORNL "broomstick" experiment.[4,5] It was discovered that the total cross-section data available circa 1966 were quite inadequate for predicting the uncollided neutron flux through 12 in. of iron. Analysis of these experiments indicated that the valleys in the cross sections did not extend to low enough levels, as is indicative of total cross sections measured with poor energy resolution. Because of this interpretation, a high-resolution total neutron cross-section measurement for iron was undertaken by Carlson and Cerbone.[6] This total neutron cross-section set gave good agreement in predicting the uncollided flux measured at the Tower Shielding Facility (TSF). However, transport calculations of differential fluxes based on a cross-section set that included these same total cross sections did not agree with measurements made in a spherical bulk iron experiment conducted by Cerbone. In order to provide additional experimental data for comparison with the calculations the TSF measurements of the spectral and angular distributions of neutrons transmitted through various thicknesses of iron shields were made. The spectral measurements were made over the entire energy range with the boron spectrometer, hydrogen counter, NE-213 spectrometer, and the Bonner ball counter. The results were obtained for both very thin

and very thick iron shields in order to test all parts of the iron cross-section data. These data, which will be presented in a forthcoming report in tabular form, and also as plotted curves, should provide an adequate test of the transport methods as well as the cross-section sets.

References

1. Funded by LMFBR program of Atomic Energy Commission.
2. The results of this experiment will be published as ORNL-TM-3511.
3. Consultant, University of Tennessee.
4. C. E. Clifford *et al., Nucl. Sci. Eng.* **27**, 299 (1967).
5. E. A. Straker, *Nucl. Sci. Eng.* **34**, 114 (1968).
6. R. J. Cerbone, *Measurement of Neutron Penetration Standards. Vol. II. High Resolution Measurements of the Total Neutron Cross Sections of Nitrogen and Iron,* GA-9149 (1969).

2.4 COMPARISON OF MONTE CARLO CALCULATIONS WITH MEASUREMENTS OF NEUTRON TRANSPORT IN IRON[1,2]

R. E. Maerker G. W. Morrison[3]
R. Q. Wright[3] R. M. Freestone, Jr.
M. B. Emmett[3]

Calculations have been performed with the Monte Carlo multigroup code MORSE to test two neutron cross-section sets for iron. The results from these calculations were compared with measurements performed at the Tower Shielding Facility[4] in order to determine which of the two sets is the better and in what energy regions disagreement with the measurements still exists. The two sets were ENDF/B MAT 1101, evaluated by Irving and Straker,[5] and MAT 1124, evaluated by Penny and Kinney.[6] The two sets basically differ in only two energy regions: in the neighborhood of the 24-keV window where $\sigma_{min} \cong 0.3$ barns for MAT 1124 and $\cong 0.65$ barns for MAT 1101, and in the greater detail of the inelastic scattering cross section described in MAT 1124. Since the differences in the results from the two sets are not extensive, only the 1124 results are shown.

Multigroup cross-section sets weighted $1/E\sigma_T$ were used through P_3 expansion in the scattering angular distribution for 215 groups in the Irving-Straker set and 218 groups in the Penny-Kinney set, the groups being chosen to reproduce in good detail the peaks and valleys in the point cross-section structure. In addition, a set of ~6600 point total cross sections was used to calculate the uncollided contribution exactly; the total cross sections were also incorporated into MORSE to sample collision points and calculate next-flight statistical estimates. Only mild biasing (path-length stretching parameter = 0.5, together with nonleakage from the transmitting face) was found to be necessary in the calculations, and statistics in the neutron fluxes transmitted through the windows, which dominate the answers, averaged better than 10%.

The neutron field incident on the iron slabs was composed of a free-field component (determined with the aid of measurements using a Blosser spectrometer, a set of hydrogen counters, and an NE-213 spectrometer with no iron present), and an enhancement component arising from reflection off the incident face of the iron slabs followed by subsequent reflection by the reactor collimator-iron collar system back into the iron slabs. This latter component was calculated by MORSE and added into the free-field component but with a cosine angular distribution rather than a near-normal one. Since the iron slabs were flush with the outside of the collimator, the enhancement component was considerable and contributed 33% more neutrons in the range above 0.4 eV, leading to responses of the order of 15% higher for detectors located off the centerline behind the iron slabs.

No significant calculated differences in the neutron fluxes above 0.8 MeV transmitted through 6 and 12 in. of iron were observed between the two sets of cross sections. Both agreed well with experiment if the calculated fluxes were smeared with the resolution function of the NE-213 spectrometer. Figures 2.4.1–2.4.3 show a comparison of the smeared calculations based on the Penny-Kinney set with the experiment for the NE-213 detector at three locations behind 12 in. of iron. The ratio of the calculated flux to the measured flux integrated over all energies above 0.8 MeV is 0.97 on the centerline, 1.01 at an angle of 15° from the centerline, and 0.79 at an angle of 45°. Since approximately 88% of the flux above 0.8 MeV calculated at the centerline detector is uncollided, the centerline measurement is a good test of the total cross sections down to 0.8 MeV. A reasonable explanation for the significant disagreement between the calculated and the experimental fluxes in the region between 0.8 and 1.5 MeV at 45° is that the angular distribution of inelastic scattering for energies above 1 MeV is incorrect as used by MORSE. This does not necessarily mean that the angular distributions in MAT 1124 are wrong, however, since the processing code used to change the point data to multigroup data, SUPERTOG, treats all inelastic

scattering as isotropic. The only remaining significant disagreement, which is more or less common to all three detector locations, is the overestimation of the flux in the region between 1.6 and 2.0 MeV, but this disagreement probably lies within acceptable bounds. The apparent disagreement from 2.5 to 3.5 MeV for the

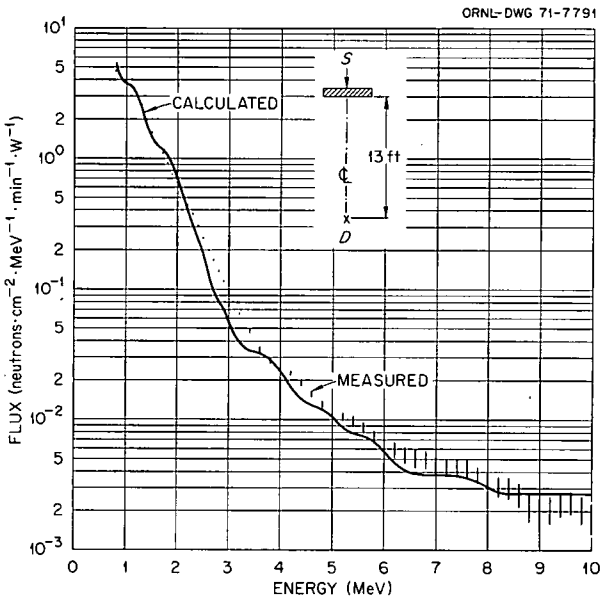

Fig. 2.4.1. Comparison of Calculated and Measured Neutron Fluxes Behind 12 in. of Iron: Detector on Centerline.

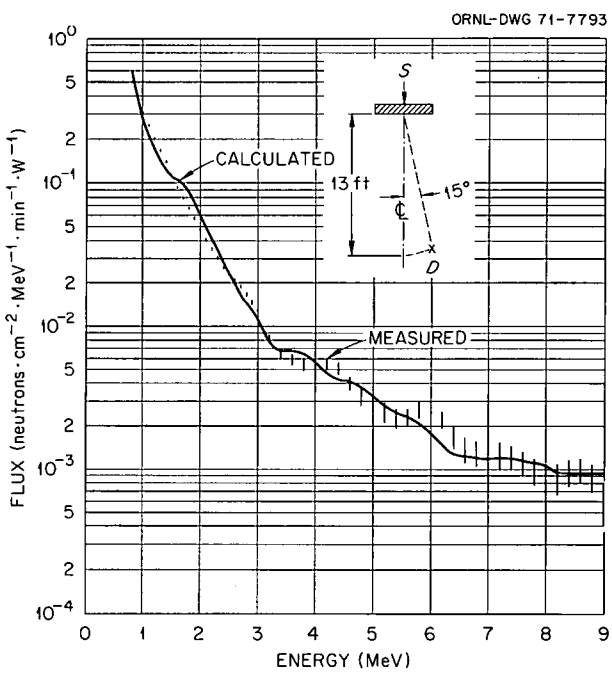

Fig. 2.4.2. Comparison of Calculated and Measured Neutron Fluxes Behind 12 in. of Iron: Detector 15° Off Centerline.

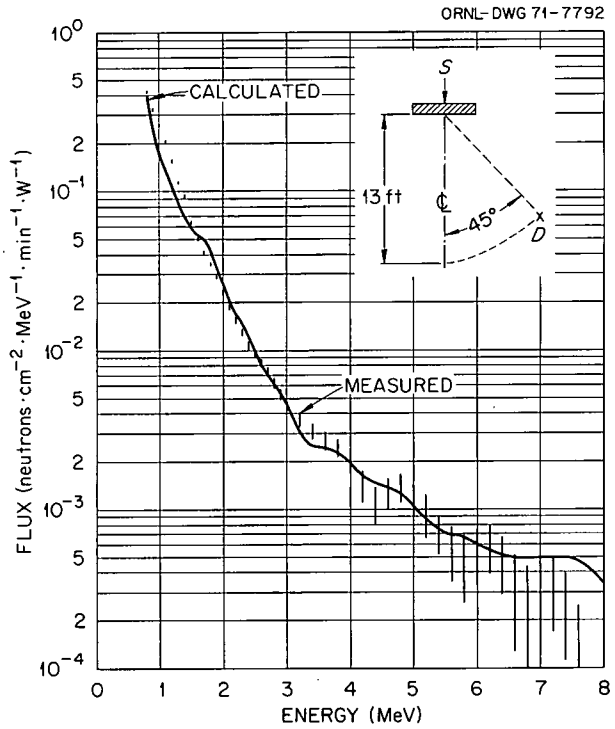

Fig. 2.4.3. Comparison of Calculated and Measured Neutron Fluxes Behind 12 in. of Iron: Detector 45° Off Centerline.

centerline detector is most probably due to the fact that the calculations contained only two broad groups in this region. The overall agreement is considered satisfactory for fast neutrons.

Tables 2.4.1 and 2.4.2 show similar comparisons behind 12 in. of iron in the region from ~80 keV to ~1.5 MeV. The experimental data were obtained with a set of hydrogen proportional counters located 10 in. behind the slab, one set along the centerline where the calculated uncollided contribution was 0.21 of the total flux and the other 12 in. off the centerline where the uncollided contribution was negligible. No smearing of the calculations with the resolution function of the hydrogen counter was performed, and no point cross sections were used for these particular calculations. The bracketing of the bins shown in the last column is an attempt to smooth the data. No significant differences were found using the two sets of cross sections. The overall agreement in this energy region is also considered satisfactory.

Measurements were also made with three cadmium-covered Bonner balls at several positions behind 1-1/2, 12, 24, and 36 in. of iron. The spectral response of each ball was determined by a 100-group adjoint ANISN calculation,[7] and the overall counting efficiencies meas-

Table 2.4.1. Comparison of Calculated and Measured Fluxes on the Centerline Behind 12 in. of Iron

Energy Bin[a] (keV)	Flux (neutrons·cm^{-2}·min^{-1}·kW^{-1}) Measured	Calculated Free Field	Calculated Enhancement	Calculated Sum	Calc./Meas.
1270–1500	6.58(+3)[b]	3.54(+3)	3.4(+1)	3.57(+3)	0.60
1082–1270	9.06(+3)	5.71(+3)	8.0(+1)	5.79(+3)	
915–1082	1.017(+3)	6.63(+3)	1.0(+2)	6.73(+3)	0.64
785–915	8.84(+3)	5.37(+3)	1.6(+2)	5.53(+3)	
664–785	1.720(+4)	9.00(+3)	3.1(+2)	9.31(+3)	0.88
562–664	1.770(+4)	2.018(+4)	1.13(+3)	2.131(+4)	
478–562	1.049(+4)	9.94(+3)	9.2(+2)	1.086(+4)	0.99
434–478	5.59(+3)c	4.69(+3)	4.4(+2)	5.13(+3)	
365–434	1.495(+4)	8.05(+3)	8.9(+2)	8.94(+3)	1.02
314–365	1.771(+4)	2.163(+4)	2.77(+3)	2.440(+4)	
267–314	1.558(+4)	1.428(+4)	2.38(+3)	1.666(+4)	1.04
224–267	9.60(+3)	7.99(+3)	1.51(+3)	9.50(+3)	
190–224	7.89(+3)	5.89(+3)	1.10(+3)	6.99(+3)	1.01
179–190	3.22(+3)[c]	3.56(+3)	7.0(+2)	4.26(+3)	
153–179	9.41(+3)	1.140(+4)	2.31(+3)	1.371(+4)	1.12
129–153	1.118(+4)	7.74(+3)	1.70(+3)	9.44(+3)	
110–129	3.67(+3)	4.64(+3)	1.37(+3)	6.01(+3)	1.43
93.6–110	2.49(+3)	3.91(+3)	1.19(+3)	5.10(+3)	
79.4–93.6	3.42(+3)	1.95(+3)	6.2(+2)	2.57(+3)	
Total	1.848(+5)	1.561(+5)	1.97(+4)	1.758(+5)	0.95

[a]Hydrogen counter region.
[b]Read: 6.58×10^3.
[c]Average over two counters in an overlap region.

Table 2.4.2. Comparison of Calculated and Measured Fluxes off the Centerline Behind 12 in. of Iron

Energy Bin[a] (keV)	Flux (neutrons·cm^{-2}·min^{-1}·kW^{-1}) Measured	Calculated Free Field	Calculated Enhancement	Calculated Sum	Calc./Meas.
1106–1300	2.09(+3)[b]	1.50(+3)	4.2(+1)	1.54(+3)	0.73
939–1106	2.82(+3)	1.84(+3)	4.5(+1)	1.89(+3)	
791–939	3.38(+3)	2.54(+3)	1.2(+2)	2.66(+3)	
680–791	5.17(+3)	3.06(+3)	1.6(+2)	3.22(+3)	0..90
578–680	7.17(+3)	7.30(+3)	5.9(+2)	7.89(+3)	
486–578	5.76(+3)	5.93(+3)	5.4(+2)	6.47(+3)	1.07
412–486	4.69(+3)	4.31(+3)	4.4(+2)	4.75(+3)	
356–412	5.47(+3)	3.69(+3)	4.4(+2)	4.13(+3)	1.14
337–356	2.44(+3)[c]	4.19(+3)	7.2(+2)	4.91(+3)	
286–337	8.64(+3)	9.69(+3)	1.73(+3)	1.142(+4)	1.26
243–286	5.79(+3)	5.76(+3)	1.08(+3)	6.84(+3)	
210–243	3.75(+3)	3.14(+3)	6.1(+2)	3.75(+3)	1.11
176–210	4.42(+3)	4.39(+3)	9.4(+2)	5.33(+3)	
150–176	3.70(+3)	5.78(+3)	1.36(+3)	7.14(+3)	1.70
144–150	1.18(+3)[c]	1.03(+3)	2.8(+2)	1.31(+3)	
123–144	4.39(+3)	3.38(+3)	9.1(+2)	4.29(+3)	1.26
104–123	1.79(+3)	2.67(+3)	8.2(+2)	3.49(+3)	
88–104	1.92(+3)	1.93(+3)	6.1(+2)	2.54(+3)	1.18
74–88	2.24(+3)	1.76–(+3)	6.0(+2)	2.36(+3)	
Total	7.68(+4)	7.39(+4)	1.20(+4)	8.59(+4)	1.12

[a]Hydrogen counter region.
[b]Read: 2.09×10^3.
[c]Average over two counters in an overlap region.

ured with a calibrated ^{252}Cf source.[8] The absolute responses so obtained were then checked for consistency with an antimony-beryllium photoneutron source to test any strong spectral dependence of the upscattering effect in the polyethylene of Bonner balls.[8] No dependence was observed, so that the absolute responses should be very accurate for all incident energies above ~10 keV, that is, they can be safely used to predict all measured counting rates in the iron experiment with the possible exception of the free-field 3-in.- and 4-in.-diam. Bonner ball measurements, where more than half the counts are due to incident neutrons below 10 keV.

Preliminary calculations showed that using the Irving-Straker data resulted in an underestimate of the 3-in.-diam Bonner ball counting rates by about a factor of two for iron thicknesses of 24 in. or greater. The calculations with the Penny-Kinney data gave much better agreement, however, indicating that the cross sections in the neighborhood of the 24-keV window are well represented by the MAT-1124 data since over half of the calculated counts recorded by the 3-in.-diam Bonner ball are due to neutrons emerging from the iron slab in the vicinity of 24 keV for slab thicknesses of 12 in. or greater. It should be pointed out that the presence of 0.6 wt.% manganese and 0.25 wt.% carbon measured in the iron slabs perturbs the 24-keV window significantly, and must be incorporated into the macroscopic cross sections.

Table 2.4.3 presents the comparisons between the measured and calculated counting rates for the Bonner balls using MAT-1124 data. The location of the detectors was similar to the geometry illustrated for the NE-213 counter in Figs. 2.4.1-2.4.3, the difference being that the uncollided flux at the Bonner ball location on the centerline comprised approximately 99% of the total flux above 0.4 eV behind 1-1/2 in. of iron, 80% behind 12 in., 50% behind 24 in., and 30% behind 36 in. The biggest disagreement in Table 2.4.3 is a calculated/measured value of 0.63, i.e., the calculation is 37% low. In general, the agreement is considered adequate, thus verifying the general acceptability of the MAT-1124 neutron data. However, there does seem to be an indication that the windows in the region from ~100 keV to ~1.5 MeV are not quite deep enough, since the calculated uncollided contribution for the centerline 6- and 10-in.-diam balls is apparently somewhat low.

Table 2.4.4 indicates a measure of the shape of the response functions for the three balls by presenting the

Table 2.4.3. Comparison of Calculated and Measured Counting Rates for Bonner Balls

Bonner Ball Diameter (in.)	Detector Position	Counting Rate ($counts \cdot min^{-1} \cdot W^{-1}$) Measured	Calculated	Calc./Meas.
		Free Field		
3	CL	469.1	559.8	1.19
4	CL	1007	1154	1.14
6	CL	1980	2078	1.05
8	CL	2159	2272	1.05
10	CL	1699	1803	1.06
12	CL	1215	1291	1.06
		Behind 1 1/2 in. of Iron		
3	CL	57.8	64.8	1.12
	15°	1.02	1.015	1.00
	45°	0.680	0.680	1.00
6	CL	607.4	636.4	1.05
	15°	5.22	4.61	0.88
	45°	2.82	2.865	1.02
10	CL	586.8	617.9	1.05
	15°	4.737	4.178	0.88
	45°	1.986	2.193	1.10
		Behind 12 in. of Iron		
3	CL	2.32	2.29	0.99
	15°	0.577	0.610	1.06
	45°	0.411	0.426	1.04
6	CL	18.5	14.4	0.78
	15°	3.54	3.46	0.98
	45°	2.39	2.37	0.99
10	CL	9.89	7.19	0.73
	15°	1.58	1.45	0.92
	45°	1.03	0.963	0.93
		Behind 24 in. of Iron		
3	CL	0.604	0.607	1.00
	45°	0.245	0.254	1.04
6	CL	3.49	2.63	0.75
	45°	1.13	1.01	0.89
10	CL	1.40	0.883	0.63
	45°	0.405	0.301	0.74
		Behind 36 in. of Iron		
3	CL	0.243	0.250	1.03
	45°	0.128	0.132	1.03
6	CL	1.08	0.873	0.81
	45°	0.475	0.439	0.92
10	CL	0.368	0.238	0.65
	45°	0.151	0.112	0.74

Table 2.4.4. Percentage of Calculated Counts Due to Various Energy Ranges of Neutrons Incident on the Centerline Bonner Balls

ΔE	Percent of Counts											
	3-in.-diam Detector				6-in.-diam Detector				10-in.-diam Detector			
	0 in.[a]	12 in.	24 in.	36 in.	0 in.	12 in.	24 in.	36 in.	0 in.	12 in.	24 in.	36 in.
8–10 MeV	0.0	0.0	0.0	0.0	0.3	0.0	0.0	0.0	0.8	0.1	0.0	0.0
6–8	0.1	0.0	0.0	0.0	1.2	0.0	0.0	0.0	3.5	0.2	0.0	0.0
4–6	0.6	0.0	0.0	0.0	5.6	0.1	0.0	0.0	13.4	0.3	0.0	0.0
2.6–4	1.5	0.1	0.0	0.0	11.9	0.4	0.0	0.0	22.3	1.3	0.0	0.0
1.6–2.6	2.7	0.7	0.0	0.0	18.5	2.8	0.1	0.1	27.3	7.3	0.4	0.0
1.0–1.6	2.2	2.7	0.3	0.0	11.2	8.2	1.1	0.2	12.4	16.1	3.2	0.6
0.7–1.0	1.7	4.2	1.0	0.2	6.7	10.0	3.3	0.8	5.6	14.9	7.2	2.3
0.43–0.7	2.2	10.2	3.7	1.1	6.7	18.6	9.5	3.6	4.4	21.4	16.0	7.5
0.25–0.43	2.4	16.1	10.1	4.8	5.3	21.6	19.4	11.4	2.6	18.7	24.4	17.7
0.11–0.25	2.9	12.9	13.0	8.7	4.6	12.5	17.9	14.8	1.7	8.2	17.2	17.5
30–110 keV	4.8	4.6	7.6	6.1	5.2	3.1	7.1	7.1	1.5	1.6	5.3	6.5
10–30	4.7	46.1	56.0	64.9	3.8	22.1	38.3	55.1	1.0	9.7	24.6	43.4
3.7–10	4.6	0.5	2.3	2.9	3.0	0.2	1.2	2.0	0.7	0.1	0.7	1.4
1.14–3.7	6.1	0.5	2.6	6.4	3.1	0.1	1.2	3.6	0.6	0.1	0.6	2.3
0.32–1.14	7.1	0.2	0.4	0.7	2.9	0.1	0.2	0.3	0.5	0.0	0.1	0.2
88–320 eV	7.8	0.3	0.6	1.4	2.5	0.1	0.2	0.5	0.4	0.0	0.1	0.3
24.4–88	9.5	0.3	1.0	1.1	2.2	0.1	0.2	0.3	0.4	0.0	0.1	0.2
6.8–24.4	11.5	0.3	0.8	1.3	2.1	0.0	0.3	0.2	0.4	0.0	0.1	0.1
1.9–6.8	13.4	0.2	0.3	0.3	1.8	0.0	0.0	0.1	0.3	0.0	0.0	0.0
0.4–1.9	14.2	0.1	0.3	0.1	1.4	0.0	0.0	0.0	0.2	0.0	0.0	0.0

[a]Thickness of iron.

percentage of the calculated counts due to various energy ranges of the neutrons incident on the centerline detectors.

References

1. Funded by the LMFBR program of the Atomic Energy Commission.
2. This work will be discussed along with the measurements, in ORNL-TM-3511.
3. Mathematics Division.
4. See Sec. 2.3, this report.
5. D. C. Irving and E. A. Straker, *Evaluation of the Cross Sections of Iron: ENDF/B MAT 1101,* ORNL-TM-2891 (ENDF-138) (1970); see also Sec. 3.20, this report.
6. S. K. Penny and W. E. Kinney, *A Re-Evaluation of Natural Iron Neutron and Gamma-Ray Production Cross Sections - ENDF/B Material 1124,* ORNL-4617 (ENDF-139) (1971); see also Sec. 2.30.
7. R. E. Maerker, L. R. Williams, F. R. Mynatt, and N. M. Greene, *Response Functions for Bonner Ball Neutron Detectors,* ORNL-TM-3451 (1971); see also Sec. 2.9, this report.
8. R. E. Maerker, F. J. Muckenthaler, J. J. Manning, J. L. Hull, J. N. Money, K. M. Henry, and R. M. Freestone, Jr., *Calibration of the Bonner Ball Neutron Detectors Used at the Tower Shielding Facility,* ORNL-TM-3465 (1971); see also Sec. 2.10, this report.

2.5 MEASUREMENTS OF THE TRANSPORT OF REACTOR NEUTRONS THROUGH IRON SHIELDS CONTAINING PLANE AND ANNULAR SLITS[1,2]

C. E. Clifford — L. B. Holland
F. J. Muckenthaler — J. L. Hull
P. N. Stevens[3] — J. J. Manning
K. M. Henry — J. N. Money

An experimental program recently performed at the Tower Shielding Facility was designed to study neutron streaming in the gaps around the stepped iron plugs in the top head of the Fast Flux Test Facility. This streaming may be important because the neutrons incident on the underside of the shield have been moderated and the effect of the "window" in the iron cross section decreases for the softened spectrum.

Therefore, the existence of the air slits in the iron shield may compromise an otherwise adequate shield design.

The radiation source for these experiments was provided by the TSR-II reactor.[4] The normal reactor spectrum was modified by 8 in. of iron and 60 in. of sodium in order to simulate the spectrum that would be incident on the reactor head. The characteristics of this "modified source" were carefully studied and this effort comprised the first phase of this program. The second (or plate-slit) phase consisted of measuring the transmission of neutrons through straight and stepped plane slits in iron for a variety of slit widths and offsets. Similar measurements were also performed (the third phase) for straight and stepped annular slits in iron. Most of the measurements in the latter two phases were made with the Bonner ball spectrometer.

The results will be presented in a forthcoming report[2] in tabular form for the Bonner ball responses (cpm/100 kW) as plotted transmission profiles and, in some cases, as unfolded flux spectra. These results should provide a means for evaluating calculational techniques as well as for forming the basis for making some empirical design decisions.

References

1. Funded by the LMFBR program of the Atomic Energy Commission.
2. The details of this experiment will be published as ORNL-TM-3513.
3. Consultant from the University of Tennessee.
4. C. E. Clifford and L. B. Holland, *Design for a Spherical Tower Shielding Reactor (TSR-II)*, Chapter 3.1 in ORNL-2389 (1957).

2.6 EXPERIMENTAL INVESTIGATION OF NEUTRON STREAMING THROUGH THE GRID PLATE SHIELD OF THE FAST FLUX TEST FACILITY[1,2]

C. E. Clifford — L. B. Holland
F. J. Muckenthaler — J. L. Hull
P. N. Stevens[3] — J. J. Manning
K. M. Henry — J. N. Money

A series of measurements were made at the Tower Shielding Facility to determine the importance of neutrons streaming through various geometric arrangements of coolant passages in the reactor grid-plate shield of the Fast Flux Test Facility. The TSR-II neutron spectrum filtered through 12 in. of stainless steel, 1 in. of polyethylene and 1/4 in. of boral was used as a source, and the flux transmitted through the grid-plate "mockup" was measured with a 5-in.-diam Bonner ball total-fluence detector. The results for the various experimental configurations will be presented in a forthcoming report[2] as count rates (counts$\cdot$min$^{-1}\cdot$W^{-1}), and a comparison of the count rates will indicate the relative intensities of the transmitted total fluxes for the various configurations. Spectral measurements of the radiation emerging from the reactor spectrum modifier were made with a hydrogen counter, an NE-213 spectrometer, and a Bonner ball counter. Unfolded hydrogen counter and NE-213 spectra will be presented graphically and the Bonner ball results will be reported as count rates corresponding to the full series of Bonner ball sphere configurations.

References

1. Funded by LMFBR program of the Atomic Energy Commission.
2. The details of this experiment will be published as ORNL-TM-3514.
3. Consultant from the University of Tennesssee.

2.7 CALCULATED NEUTRON FLUX DISTRIBUTION RESULTING FROM A FISSION SOURCE LOCATED AT THE CENTER OF A 10-METER-DIAM SPHERE OF SODIUM[1,2]

C. L. Thompson[3]

A Monte Carlo calculation using the O6R code was made to determine the neutron flux distribution resulting from a point isotropic fission source located at the center of a 10-meter-diameter sphere of sodium. The purpose was to obtain data that will be helpful in evaluating the accuracy of calculations involving neutron transport in sodium.

References

1. Funded by the LMFBR program of the Atomic Energy Commission.
2. Abstract of ORNL-TM-3156 (Oct. 27, 1970).
3. Mathematics Division.

2.8 THE LOW-ENERGY NEUTRON SPECTRUM OF THE ORNL TOWER SHIELDING REACTOR BEAM[1,2]

R. M. Freestone, Jr. — K. M. Henry
F. J. Muckenthaler — C. E. Clifford

An estimate of the spectrum of neutrons having energies between 0.4 and 1.5 MeV emitted by the

ORNL Tower Shielding Reactor (TSR-II) has been made. Spherical, hydrogen-filled proportional counters were used to obtain the data. The unfolded result of the measurement is presented as a histogram of flux vs energy.

References

1. Funded by the LMFBR program of the Atomic Energy Commission.
2. Abstract of ORNL-TM-3098 (1970).

2.9 RESPONSE FUNCTIONS FOR BONNER BALL NEUTRON DETECTORS[1,2]

R. E. Maerker F. R. Mynatt
L. R. Williams N. M. Greene[3]

Response functions applicable to measurements conducted at the Tower Shielding Facility are presented for Bonner ball neutron detectors consisting of polyethylene spheres surrounding BF_3 proportional counters and covered on the outside by cadmium.

References

1. Funded by the LMFBR program of the Atomic Energy Commission.
2. Abstract of ORNL-TM-3451 (June 18, 1971).
3. Mathematics Division.

2.10 CALIBRATION OF THE BONNER BALL NEUTRON DETECTORS USED AT THE TOWER SHIELDING FACILITY[1,2]

R. E. Maerker J. L. Hull
F. J. Muckenthaler J. N. Money
J. J. Manning K. M. Henry
R. M. Freestone, Jr.

Efficiencies of the Bonner ball neutron detectors in use at the Tower Shielding Facility were determined from measurements performed with a calibrated ^{252}Cf neutron source. Additional measurements with a monoenergetic ~30-keV neutron source indicate that the efficiencies are spectrum independent down to ~10 keV. Further measurements in a soft spectrum indicate that upscattering effects in the thermalization process rendered by the polyethylene may be spectrum dependent below incident energies of ~10 keV.

References

1. Funded by the LMFBR program of the Atomic Energy Commission.
2. Abstract of ORNL-TM-3465 (June 30, 1971).

2.11 THE ENERGY SPECTRUM OF PHOTONEUTRONS PRODUCED BY 140-MeV ELECTRONS INCIDENT ON TANTALUM[1,2]

C. E. Burgart T. A. Love
E. A. Straker R. M. Freestone, Jr.

The neutron energy spectrum produced by 140-MeV electrons incident on tantalum has been measured at the Oak Ridge Electron Linear Accelerator by time of flight in the 0.7- to 20-MeV energy range. This energy spectrum normalized per incident electron is in excellent agreement with previous calculations.

References

1. Funded by the Defense Atomic Support Agency under Subtask PE075.
2. Abstract of *Nucl. Sci. Eng.* **42**, 421 (1970) and of ORNL-TM-3022 (1970).

2.12 SIMULTANEOUS DETERMINATION OF FAST-NEUTRON SPECTRA BY TIME-OF-FLIGHT AND PULSE-HEIGHT UNFOLDING TECHNIQUES[1,2]

E. A. Straker T. A. Love
C. E. Burgart R. M. Freestone, Jr.

Proton-recoil spectrometers have frequently been used in the past few years to measure spectra for neutron energies greater than approximately 1 MeV with the results depending strongly on the adequacy of the response matrix used in unfolding pulse-height spectra. By simultaneously measuring a fast-neutron spectrum by time-of-flight and by pulse-height unfolding, the adequacy of the response matrix and unfolding code could be determined. Spectra of several shapes and measurements with different time-of-flight resolution were used to validate the spectra obtained by unfolding the pulse-height spectrum.

References

1. Funded by the Defense Atomic Support Agency under Subtask PE075.
2. Abstract of ORNL-TM-3371 (April 5, 1971) and of paper submitted for journal publication.

2.13 MEASUREMENTS AND CALCULATIONS OF THE TIME-DEPENDENT SPECTRA OF GAMMA RAYS EMERGING FROM POLYETHYLENE SLABS PULSED WITH NEUTRONS[1]

C. E. Burgart T. A. Love
E. A. Straker G. L. Morgan
R. M. Freestone, Jr.

Measurements of the time-dependent secondary gamma rays from polyethylene due to a neutron source produced at the Oak Ridge Electron Linear Accelerator (ORELA) have been made to provide an experiment to test time-dependent transport codes. In the past few years, several time-dependent transport codes have been written; however, there are few experiments that may be used to validate these codes.

Measurements have been made at the ORELA Shielding Facility to provide data useful in testing time-dependent transport codes. The linac neutron source is produced by 140-MeV electrons incident on a tantalum target. Slabs of polyethylene and borated polyethylene were positioned 48.5 m from the linac target and at an angle of 45° from the nearly parallel beam of neutrons. A 12.7- by 12.7-cm NaI crystal was utilized to detect the emerging gamma rays. The crystal was located in a lead and lithiated paraffin shield 188 cm from the polyethylene at an angle of 125° from the neutron beam. Two-parameter pulse-height versus time-of-flight data, as well as higher resolution time-dependent count-rate data, were acquired by a PDP-9 computer.

The time-dependent count rate per source neutron for a 15.24-cm-thick slab is shown in Fig. 2.13.1. Prior to 1.6 μsec, the 4.43-MeV gamma ray from neutron inelastic scattering in carbon dominates the gamma-ray spectrum. The structure in the time-dependent count rate at early times results from the structure in the neutron inelastic scattering cross section in carbon. For times greater than 1.6 μsec, the 2.22-MeV hydrogen capture gamma ray dominates. The buildup and decay of the hydrogen capture gamma rays is due entirely to the time-dependent slowing down of high-energy neutrons in the slab since there are no low-energy neutrons incident on the slab.

Coupled neutron-gamma-ray calculations for the experimental configurations have been performed with the MORSE multigroup Monte Carlo code[2] using a

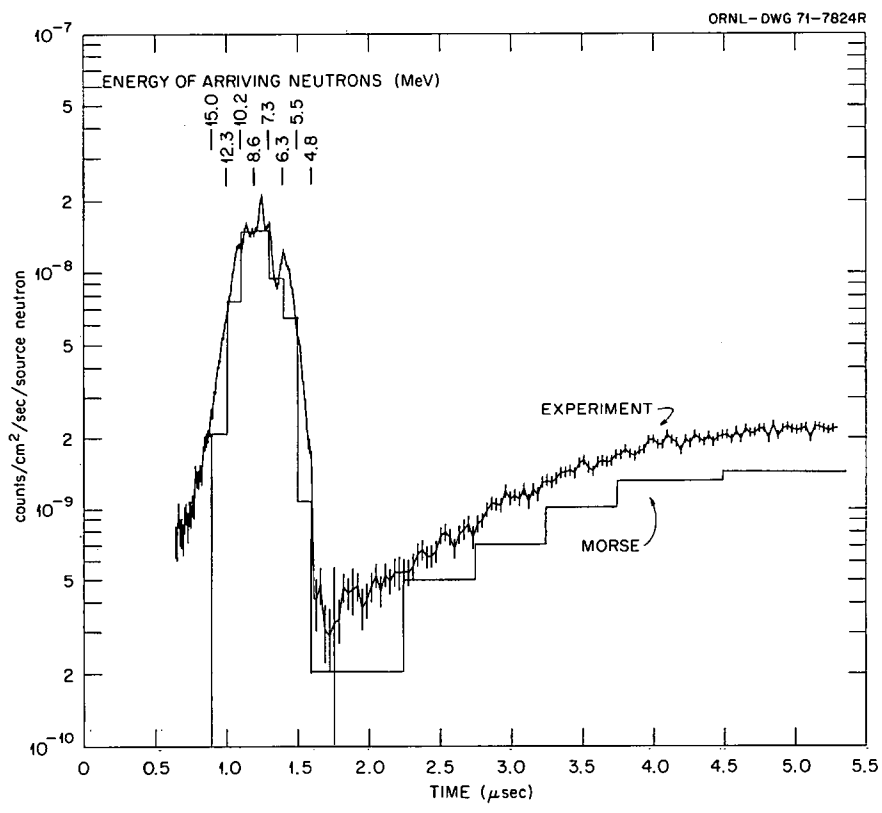

Fig. 2.13.1. Time-Dependent Gamma-Ray Count Rate for a 15.24-cm-thick Slab of Polyethylene Pulsed with Neutrons: Comparison of Experiment and Monte Carlo MORSE Calculation.

revised cross-section module.[3] [A comparison between time-dependent ANISN (TDA) and MORSE for a similar configuration has previously been reported,[4] and the agreement for that comparison was quite good.] The neutron multigroup cross-section sets used included both a set having a single thermal group and a set having multithermal groups with upscattering. Several sets of secondary gamma-ray yields from the POPOP4 library were utilized,[5] and in all cases the secondary gamma-ray production was assumed to be isotropic. Comparisons between the experiments and calculations were made for pulse-height spectra integrated over an observation time, time-dependent count rates, and pulse-height spectra for various time-of-flight bins. The experimental and calculated results agree quite well in shape for neutrons below 15 MeV for both the carbon inelastic and hydrogen capture gamma-ray time dependence. The apparent difference in magnitude requires further investigation.

References

1. Funded by the Defense Atomic Support Agency under Subtasks PE074 and PE075.

2. E. A. Straker, P. N. Stevens, D. C. Irving, and V. R. Cain, *The MORSE Code – A Multigroup Neutron and Gamma-Ray Monte Carlo Transport Code,* ORNL-4585 (1970).

3. E. A. Straker and M. B. Emmett, *MORSEC, A Revised Cross-Section Module for the MORSE Multigroup Monte Carlo Code,* ORNL-4716 (1971); see also Sec. 3.26, this report.

4. C. E. Burgart and W. W. Engle, Jr., "Time-Dependent Coupled Neutron-Gamma Calculations in Polyethylene," *ANS Trans.* 13(2), 861-862 (1970).

5. Walter E. Ford, III, and David H. Wallace, *POPOP4, A Code for Converting Gamma-Ray Spectra to Secondary Gamma-Ray Production Cross Sections,* CTC-12, Computing Technology Center, Union Carbide Corporation (1969).

2.14 TAKER – DATA ACQUISITION PROGRAM FOR A PDP-9 COMPUTER[1]

C. E. Burgart R. M. Freestone, Jr.

The data acquisition program for a PDP-9 computer[2] has been improved and its capabilities expanded. Called TAKER, the principal purpose of the program is to acquire two-parameter pulse-height versus time-of-flight data on a PDP-9 computer at the ORELA Shielding Facility. In addition to acquiring data, TAKER controls the experiment by starting and stopping the external scalers, automatically reading into the computer values from the external scalers and checking the values, and stopping and restarting the data acquisition based on an external count-rate meter.

An addition to the data-acquisition subroutines has proved to be useful with hydrogen-filled spherical proportional counters. Discrimination against gamma rays in the low-keV region is a problem with this type of detector. One of the most sophisticated techniques requires that the linear pulse height be divided by a signal proportional to the rise time of the linear pulse to obtain a variable for discrimination. A two-parameter data-acquisition subroutine was written for the PDP-9 which quite simply performs the above division of two input pulse heights. If the value of this quotient is greater than a preset value, a count is stored in a location corresponding to the linear pulse height. Thus, a one-dimensional discriminated pulse-height spectrum may be obtained. In addition to the pulse-height spectrum, two-parameter data (quotient versus pulse height) are stored both for the purpose of enlightenment and for subsequent detailed analysis.

The addition of a communications link to the central data acquisition computers (DAC's) at ORELA has made possible several significant improvements in the TAKER system,[3] the most important being the ability to accumulate large two-parameter data arrays on the fixed head disks on the DAC's. Arrays of up to 750,000 channels are possible. One- and two-parameter data with a reduced number of channels are simultaneously acquired on the PDP-9. When data is acquired on a DAC, the PDP-9 data acquisition is handled via the accumulator rather than the data channel. Thus, the data are sorted one event at a time, and high peak data rates associated with sorting a buffer of events are avoided.

The DAC link has also made possible the rapid listing of data on the line printer and the writing of data on IBM-compatible magnetic tapes. Previously, DEC tape has been used for storage of raw data, while punched paper tape was the only true output from the PDP-9. This paper tape was interpreted by a CDC-160-A or a DAC and punched on cards for subsequent reduction. Needless to say, this process is quite tedious when more than 4,000 channels of data are utilized.

References

1. Funded by the Defense Atomic Support Agency under Subtask PE075.

2. R. M. Freestone, Jr. and C. E. Burgart, "On-Line Data Acquisition and Treatment Programs for a PDP-9

Computer," Sec. 2.39 in *Neutron Phys. Div. Ann. Progr. Rept. May 31, 1970,* ORNL-4592.

3. A line-printer handler utilizing the link has also been added to the Digital Equipment Corp. software system, thus providing the capability of quickly obtaining assembly listings of the programs on DAC-II. This has proved to be of great value in writing and debugging TAKER.

2.15 A STUDY OF THE OVERLAP CONDITIONS REQUIRED IN SEQUENTIAL DISCRETE ORDINATES TRANSPORT CALCULATIONS FOR A 14-MeV NEUTRON SOURCE IN A 5000-m RADIUS CYLINDER OF AIR[1,2]

J. V. Pace, III[3] F. R. Mynatt
L. S. Abbott

Because of computer storage limitations, the two-dimensional discrete ordinates code DOT cannot be applied to the calculation of the transport of radiation over large distances in an air-over-ground geometry unless the problem is divided in space and run in series so that the results of one run are used as the source in the succeeding one. With this technique the runs must be sufficiently overlapped to remove the effects caused by the assumption in each run that the outer boundary of the region being calculated is followed by a vacuum. The overlap conditions have been studied in a series of calculations with the one-dimensional code ANISN for the case of an infinitely long cylinder of air and a 14-MeV neutron source on the cylinder axis. Radial distances out to 5000 m were covered both in a single ANISN run and in a series of runs for a central cylindrical core and several successive cylindrical annuli. The results showed that for this problem a 500-m overlap is required unless boundary albedos are introduced in the runs, in which case the overlap is reduced to 30 m. The boundary albedos are based on the incoming and outgoing currents determined for the boundary locations in the single ANISN run. For a large DOT calculation involving a source spectrum, using the albedos would substantially reduce the number of runs required to complete the calculation.

References

1. Funded by the Defense Atomic Support Agency under Subtask PE080.

2. Abstract of ORNL-TM-3269 (1971); included in last year's annual as abstract of Computer Technology Center report CTC-40.

3. Mathematics Division.

2.16 NEUTRON AND SECONDARY GAMMA-RAY INDUCED HEAT IN THE GROUND DUE TO POINT 12.1-15-MeV AND FISSION SOURCES AT AN ALTITUDE OF 50 FEET[1,2]

E. A. Straker M. B. Emmett[3]
M. L. Gritzner

The energy deposited in ground due to neutrons and the secondary gamma rays has been determined as a function of range, ground depth, and time from an instantaneous point neutron source with either a fission spectrum or a 12.2- to 15-MeV energy band. In all cases, the source was at a height of 50 ft above the air/ground interface. Discrete ordinates and Monte Carlo calculations illustrated that there is a significant effect on the energy deposited due to source energy distribution, but little effect due to small differences in ground composition. The importance of gamma rays produced by low-energy neutrons was found to be small for the 12.1- to 15-MeV source, but large for the fission source.

References

1. Funded by the Defense Atomic Support Agency under Subtask PE080.

2. Abstract of ORNL-4626 (1970); included in last year's annual as abstract of ORNL-TM-3003.

3. Mathematics Division.

2.17 NEUTRON AND GAMMA-RAY FLUENCES TRANSMITTED THROUGH A SLAB OF BORATED POLYETHYLENE[1,2]

C. E. Burgart

A multigroup Monte Carlo code, a two-dimensional discrete ordinates code, and a one-dimensional discrete ordinates code were each used with identical multigroup cross sections for the same transport calculation as a rigorous test of the transport methods. The calculated results were neutron energy spectra and neutron and gamma-ray fluences behind a slab of borated polyethylene on which a line beam of neutrons with a ^{235}U fission spectrum was normally incident. The slab was followed by a vacuum and the points for which the spectra and fluences were calculated were located at large distances beyond the slab. The methods yielded nearly identical results for points located within 30° of a normal to the slab. The agreement becomes less satisfactory at greater angles; however, possible explanations for the observed discrepancies are given.

References

1. Funded by the Defense Atomic Support Agency under Subtask PE074.
2. Abstract of ORNL-TM-3517 (to be published).

2.18 GAMMA-RAY SPECTRA ARISING FROM FAST-NEUTRON INTERACTIONS IN ELEMENTS FOUND IN SOILS, CONCRETES, AND STRUCTURAL MATERIALS[1,2]

R. E. Maerker F. J. Muckenthaler

Measurements have been made at the Tower Shielding Facility of the spectra of secondary gamma rays arising from fast-neutron interactions in samples of natural iron, aluminum, copper, zinc, titanium, potassium, calcium, sodium, silicon, nickel, barium, sulfur, and a type-321 stainless steel. The absolute spectra are expressed as values of $\sigma(\Delta E_\gamma) = 4\pi\, d\sigma/d\Omega(\Delta E_\gamma, 90°)$, where $\sigma(\Delta E_\gamma)$ is the production cross section in millibarns averaged over an incident neutron spectrum from 1 to 14 MeV for 0.5-MeV wide gamma-ray intervals lying between approximately 1 and 6.5 MeV in gamma-ray energy. These data are intended primarily as integral checks on existing and future production cross-section sets which are differential in both the gamma-ray energy and the neutron energy. Agreement with existing sets of data is adequate for iron, nickel, chromium, calcium, and aluminum. The agreement is fair to poor for the remaining elements for which comparisons could be made.

References

1. Funded by the Defense Atomic Support Agency under Subtask PE075.
2. Abstract of *Nucl. Sci. Eng.* 42, 335 (1970); included in last year's annual as abstract of ORNL-4475.

2.19 GAMMA-RAY SPECTRA ARISING FROM THERMAL-NEUTRON CAPTURE IN ELEMENTS FOUND IN SOILS, CONCRETES, AND STRUCTURAL MATERIALS[1,2]

R. E. Maerker F. J. Muckenthaler

Gamma-ray spectra arising from the capture of thermal neutrons have been measured for several naturally occurring elements of interest to the shielding community. The spectral intensities in units of photons per 100 captures are presented as sums over 0.5 MeV intervals. These results have an estimated accuracy of ±15% and include the contributions from both discrete and continuum gamma rays. The present results do not go below 1 MeV, but when the relatively small contributions from energies less than 1 MeV are added to them, binding energy checks averaging within ±5% are obtained.

References

1. Funded by the Defense Atomic Support Agency under Subtask PE075.
2. Abstract of *Nucl. Eng. Design* 13, 455 (1970); included in last year's annual as abstract of a paper prepared for journal submission.

2.20 TIME-DEPENDENT NEUTRON AND PHOTON TRANSPORT CALCULATIONS USING THE METHOD OF DISCRETE ORDINATES[1,2]

S. A. Dupree[3] G. E. Hansen[4]
H. A. Sandmeier[4] W. W. Engle, Jr.
F. R. Mynatt

This report describes the time-dependent discrete ordinates radiation transport computer program, Time-Dependent ANISN (TDA). The results of application of the code to several nonphysical problems having approximate analytical solutions and to the real problem of a neutron-pulsed subcritical ^{239}Pu sphere are presented and discussed. In the latter problem, neutron and photon leakage rates are presented as functions of energy and time. The neutronic response time of this pure metal system is 10 to 20 nsec. In all cases considered, the TDA code performed well, within the discrete limitation, provided that care was taken to assure proper convergence of the S_n iteration scheme.

References

1. Funded by the U. S. Navy and the Defense Atomic Support Agency under Subtask PE080.
2. Abstract of LA-4557 (ORNL-4662) (May 1971).
3. Naval Weapons Evaluation Facility, Albuquerque, New Mexico.
4. Los Alamos Scientific Laboratory.

2.21 BRACKETING THE PEAK PRIMARY GAMMA-RAY DOSE RATE FROM NUCLEAR DEVICES BY STEADY-STATE TRANSPORT CALCULATIONS[1,2]

H. C. Claiborne W. W. Engle, Jr.

Electronic components can be affected by the dose rate from gamma rays delivered during the first few

shakes of an exploding nuclear device. Determining such dose rates generally requires expensive time-dependent calculations. This paper demonstrates that relatively inexpensive steady-state transport calculations can be used to bracket the time-dependent peak dose rates with meaningful upper and lower limits.

The model configuration consisted of a sphere of air surrounded by a spherical annulus of concrete with an isotropic source of gamma rays from fissioning ^{235}U located at the geometric center. Steady-state calculations were made with the discrete ordinates code ANISN and time-dependent calculations with TDA (time-dependent ANISN). The upper limit dose rates were obtained by dividing the steady-state total dose by the pulse width of the device. This is equivalent to assuming that the uncollided and air-scattered fluxes arrive at the shield simultaneously. For a lower limit calculation, only the uncollided flux was considered incident on the shield.

Calculations were made for a 120-cm-thick concrete shield for ranges of 500, 1000, and 5000 m and for step-function burst pulse widths of 1 through 8 shakes. The results from the steady-state calculations generally bracketed the peak time-dependent dose rates within an acceptably narrow band except for the 500-m range at the back end of the shield where the peak time-dependent dose rates were highest for all pulse widths. This apparent anomaly is explained on the basis of using a moving boundary condition in the time-dependent solution and the effect is shown to be of no consequence.

References

1. Funded by the U. S. Corps of Engineers, Huntsville Division, Huntsville, Alabama.
2. Abstract of ORNL-TM-3462 (1971).

2.22 THE Ca($n,x\gamma$) REACTION AT E_n = 5.9 MeV[1,2]

J. K. Dickens F. G. Perey

Gamma-ray production cross sections have been measured for 5.9-MeV neutrons interacting with calcium. Cross-section data are in reasonable agreement with previously reported neutron inelastic scattering cross sections.

References

1. Funded by the Defense Atomic Support Agency under Subtask PC068.
2. Abstract of paper to be published in proceedings of *Third Conference on Neutron Cross Sections and Technology, March 15-17, 1971,* Knoxville, Tennessee.

2.23 Pb($n,x\gamma$) REACTIONS FOR E_n BETWEEN 4.9 AND 8.0 MeV[1]

J. K. Dickens

Spectra of gamma rays produced by neutrons interacting with Pb have been obtained for $4.9 \leqslant E_n \leqslant 8.0$ MeV in approximately 0.5-MeV steps for $\theta_\gamma = 125°$. Three samples were used: a 67-g sample enriched in ^{208}Pb; a 136-g sample enriched in ^{207}Pb; and a 67-g sample of radiogenic Pb (88% ^{206}Pb). These spectra were obtained using a 48-cc Ge(Li) detector and appear to be of good quality. Discrete high-energy gamma rays are observed in the ^{208}Pb spectra, in particular E_γ = 4.085, 4.839, and 5.286 MeV. Spectra for ^{206}Pb and ^{207}Pb do not exhibit strong, discrete, high-energy gamma rays, but indicate a "continuum" of unresolved, weakly excited gamma radiation with energies between 3 and 5 MeV.

References

1. Funded by the Defense Atomic Support Agency under Subtask PC068.

2.24 SURVEY OF ($n,x\gamma$) GAMMA PRODUCTION CROSS SECTIONS FOR E_n = 6 MeV[1]

J. K. Dickens

A survey study of gamma rays produced by 6-MeV neutron interactions with samples having priority I request[2] was initiated. Samples studied include Ti(^{nat}Ti, and samples enriched in ^{46}Ti and ^{48}Ti), Ni (^{nat}Ni and ^{60}Ni), Cu (^{63}Cu and ^{65}Cu), Zn (^{64}Zn and ^{68}Zn), Nb and Bi. The samples of ^{nat}Ti, ^{63}Cu, ^{65}Cu, ^{nat}Ni, ^{60}Ni, and Bi were metallic cylinders, and the Nb sample was a metallic plate. The materials enriched in ^{46}Ti, ^{48}Ti, ^{64}Zn, and ^{68}Zn could be obtained only in oxide form. The samples were fabricated by compacting the powder in thin-walled aluminum cans. A similar sample fabricated with BeO powder was used to provide the background data. This sample revealed a number of background lines which may interfere with weaker transitions in the element under study.

These data have not yet been completely analyzed.

References

1. Jointly funded by the Defense Atomic Support Agency under Subtask PC068 and the Reactor Development Technology Division of the Atomic Energy Commission.

2. *Compilation of Requests for Nuclear Cross Section Measurements,* Los Alamos Scientific Laboratory Report NCSAC-35 (March 1971).

2.25 DETERIORATION OF LARGE Ge(Li) DIODES CAUSED BY FAST NEUTRONS[1]

P. H. Stelson[2] J. K. Dickens
S. Raman[2] R. C. Trammell[3]

Large (and expensive) Ge(Li) gamma-ray detectors have become a powerful tool for nuclear research. Unfortunately these detectors are quite susceptible to fast-neutron damage and this makes it difficult to decide whether or not to risk using the detectors to investigate nuclear reactions at accelerators where fast neutrons are inevitably present. After ruining two diodes by neutron damage we decided to investigate the problem in a controlled way.

A 30-cm^3 diode furnished by Oak Ridge Technical Enterprises Corporation (ORTEC) was systematically irradiated by neutrons from a plutonium-beryllium source. An increase in the width of the 2.614-MeV gamma-ray peak from ThC″ was first detected after an irradiation of 5×10^7 neutrons/cm^2. When the total irradiation had reached 5×10^8 neutrons/cm^2, the peak width had increased by 50%. Two different values of amplifier time constants were used. The irradiated detector was then processed by ORTEC to remove the damage. The reprocessed detector exhibited essentially complete recovery in terms of peak width. The diode was again subjected to neutron irradiation. The second curve of resolution deterioration as a function of neutron flux was identical to the first. This is a very encouraging result since reprocessing a detector costs only about 10 percent of the initial price. A method was also developed for evaluating the amount of neutron flux incident on the detector from the gamma-ray spectrum itself. The number of counts in the prominent 693-keV peak (from n,n' of ^{72}Ge in the detector) can be multiplied by 20 to get a rough measure of the neutron flux in neutrons/cm^2.

References

1. Jointly funded by the Defense Atomic Support Agency under Subtask PC068 and the Reactor Development Technology Division of the Atomic Energy Commission.

2. Physics Division.
3. Oak Ridge Technical Enterprises Corporation, Inc., Oak Ridge, Tennessee.

2.26 EVALUATION OF NATURAL LEAD NEUTRON AND GAMMA-RAY PRODUCTION CROSS SECTIONS[1]

C. Y. Fu[2] F. G. Perey

Neutron and gamma-ray production cross sections for natural lead up to 20 MeV have been thoroughly investigated. In the course of this investigation, we have had discussions with physicists who are currently measuring lead cross sections with improved techniques. New data far better than those presently existing in certain energy regions and reactions will be available soon. We have, therefore, completed the evaluation with such precaution that when these data become available corrections and/or additions to the ENDF/B file can be made with minimum effort.

In certain cases, measured data points were too few in the required energy region to define the cross sections adequately and we had to rely heavily on calculations for interpolations and extrapolations. Prominent examples of such cases are angular distributions of elastically and inelastically scattered neutrons, energy distributions of secondary neutrons from $(n,2n)$ and $(n,3n)$ reactions, and gamma-ray spectra and production cross sections from fast neutrons. To facilitate review and re-evaluation, a rather detailed report is being written.

As an illustration, the evaluated cross sections $\sigma(n,x)$, $\sigma(n,x\gamma)$, $\sigma(n,n')$, $\sigma_L(n,n')$, $\sigma_C(n,n)$, $\sigma(n,2n)$, and $\sigma(n,3n)$ are given in Fig. 2.26.1, with the subscripts L and C denoting "level" and "continuum" respectively. For conciseness of presentation, no experimental data points are shown. Of these cross sections, only $\sigma(n,x)$ could be defined by measured data. The agreement between calculated and measured $\sigma(n,x)$ was so good that the calculated results were adopted which clearly showed the threshold effects of various lead isotopes. Separate calculations were made for $\sigma(n,n'\gamma)$, $\sigma(n,2n\gamma)$, and $\sigma(n,3n\gamma)$ and for each of the three major lead isotopes. These cross sections were then combined to define $\sigma(n,x\gamma)$ for natural lead. $\sigma_L(n,n')$ contains 35 levels, each representing one or more levels from 48 levels in ^{206}Pb, 49 in ^{207}Pb, and 22 in ^{208}Pb up to 4.4 MeV of excitation energy. Direct-interaction contributions were included in 10 of the 35 levels. No measurement has been made for $\sigma(n,3n)$, which is therefore purely theoretical.

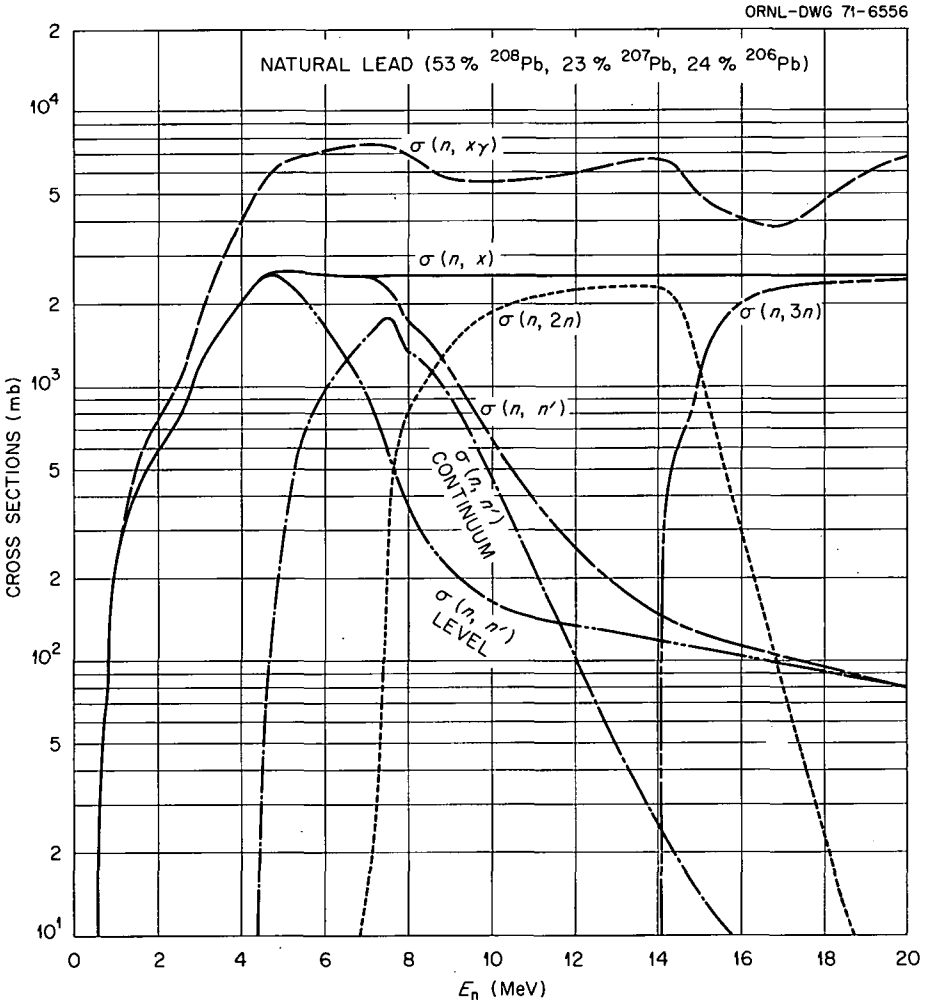

Fig. 2.26.1. Evaluated Natural Lead Nonelastic Cross Sections, Their Various Components, and Gamma-Ray Production Cross Sections.

References

1. Funded by the Defense Atomic Support Agency under Subtask PC103.
2. University of Tennessee.

2.27 A CALCULATION OF NEUTRON ENERGY-DEPENDENT CAPTURE GAMMA-RAY YIELD SPECTRA FOR IRON AND COMPARISONS WITH EXPERIMENTS[1,2]

J. E. White[3] C. Y. Fu[4]
K. J. Yost

The spin-dependent gamma-ray cascade model DUCAL has been applied to calculate neutron and energy-dependent capture gamma-ray spectra in iron. There are significant variations in the capture gamma-ray yield spectra with neutron energy. The results have been compared with a series of integral gamma-ray yield measurements above 1 MeV and the agreement found was reasonably good. The yield data are presented in a neutron energy format that would facilitate the preparation of the capture component of the secondary gamma-ray production cross section for iron.

References

1. Funded by the Defense Atomic Support Agency under Subtask PC103.
2. Abstract of ORNL-TM-3442 (to be published).
3. Mathematics Division.
4. University of Tennessee.

2.28 Fe(n,$x\gamma$) REACTION FOR E_n BETWEEN 4.0 AND 9.0 MeV[1]

J. K. Dickens F. G. Perey

The study of production cross sections of gamma rays produced by the interaction of neutrons with Fe, first

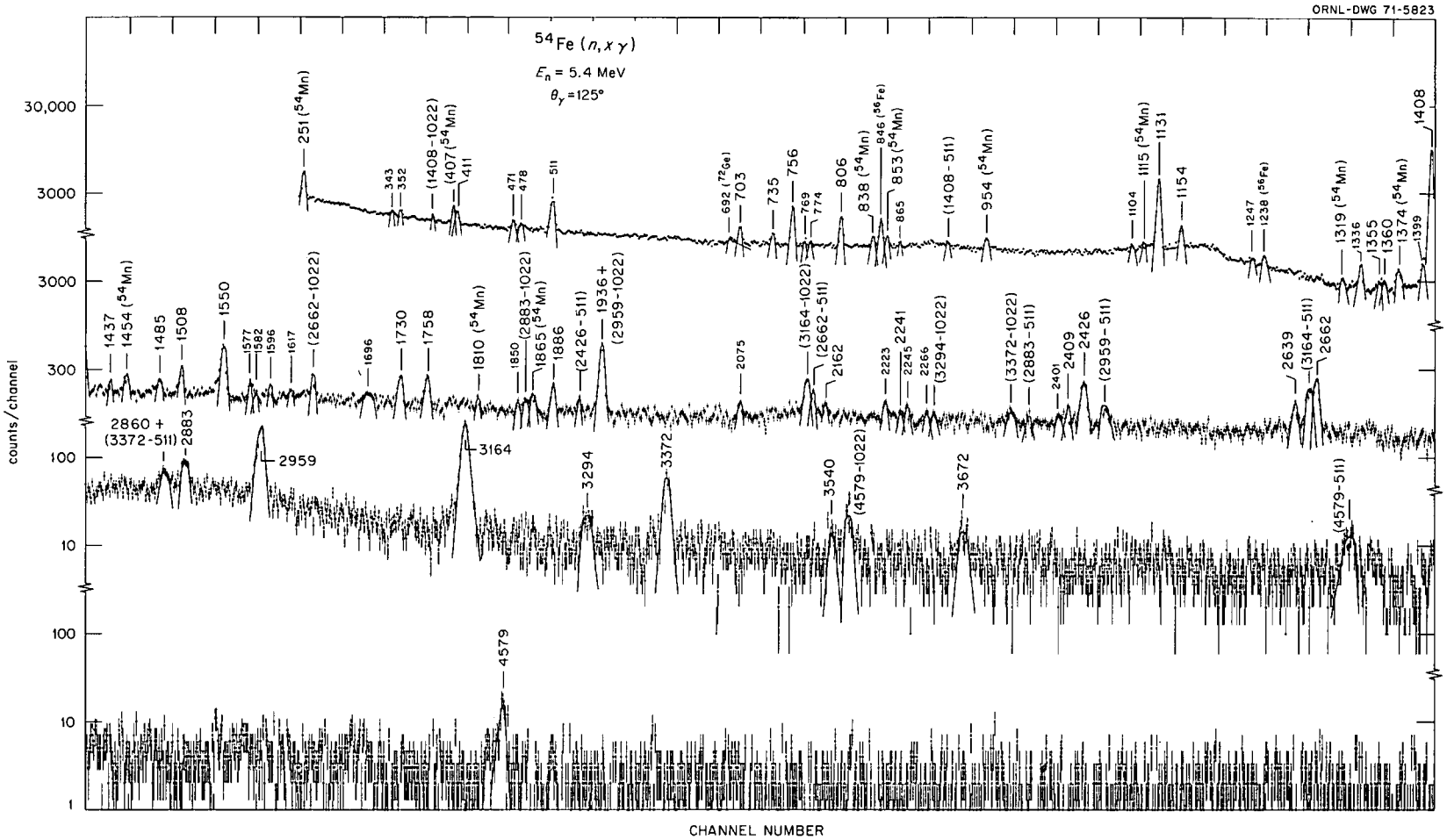

Fig. 2.28.1. Spectrum of Gamma Rays Produced by the Bombardment of ^{54}Fe with 5.4-MeV Neutrons. Peaks are labelled with the energy of the detected gamma ray. Escape peaks are indicated by (E_γ − 511) and (E_γ − 1022) labels. Isotope symbols indicate gamma radiation emanating from nuclei other than ^{54}Fe. Smaller labels indicate gamma radiation of either background or unknown origin.

reported last year,[2] has continued. Emphasis has been on obtaining data for gamma rays with energy >3.6 MeV. In addition, several spectra were obtained for an Fe sample enriched to 97% in the isotope ^{54}Fe. The spectrum obtained for E_n = 5.4 MeV is shown in Fig. 2.28.1. These data are being studied to obtain accurate cross sections for gamma rays seen in the spectra using ^{nat}Fe due to the 6% ^{54}Fe isotope.

References

1. Funded by the Defense Atomic Support Agency under Subtask PC068.

2. J. K. Dickens and F. G. Perey, *Neutron Phys. Div. Ann. Progr. Rept. May 31, 1970,* ORNL-4592, p. 32.

2.29 WEAPONS RADIATION SHIELDING HANDBOOK: STATUS REPORT[1]

L. S. Abbott, H. C. Claiborne,
and C. E. Clifford, Editors

During the past year Chap. 7 of the Handbook, "Engineering Method for Designing Initial Radiation Shields for Blast-Hardened Underground Structures," was distributed, increasing the number of published chapters to six. In addition, Chap. 3, "Methods for Calculating Neutron and Gamma-Ray Attenuation," was revised and enlarged and the new draft was forwarded to the Defense Atomic Support Agency for classification review prior to its release. Following the completion of these two chapters the Handbook effort was somewhat reduced, delaying the final editing and publication of Chap. 8, which it now appears will be the concluding chapter of the Handbook.

References

1. Funded by the Defense Atomic Support Agency under Subtask PE033.

2.30 A RE-EVALUATION OF NATURAL IRON NEUTRON AND GAMMA-RAY PRODUCTION CROSS SECTIONS – ENDF/B MATERIAL 1124[1,2]

S. K. Penny W. E. Kinney

Recent data and good agreement between calculated and experimental cross sections prompted the re-evaluation of natural iron neutron and gamma-ray production cross sections for ENDF/B use with the aim of improving angular distributions and extending inelastic level excitation cross sections. Calculations are described and are shown to be in good agreement with experiment. Below 2 MeV, neutron elastic scattering cross sections and cross sections for inelastic scattering to levels in ^{56}Fe are obtained from experimental results. Above 2 MeV, neutron elastic scattering cross sections and cross sections for inelastic scattering to levels in ^{56}Fe up to an excitation energy of 4.116 MeV are obtained from calculations. Cross sections for inelastic scattering to the continuum are obtained from fits to experimental results. The total cross sections are the evaluated cross sections of Irving and Straker from 330 keV to 15 MeV and those of the U.K. evaluation DFN-91 from 10^{-5} eV to 330 keV. The (n,p) and (n,α) cross sections were taken from the U.K. evaluation DFN-91, while the $(n,2n)$ cross sections are those of ENDF/B material 1122. The (n,γ) cross sections were taken from U.K. DFN-91. The gamma-ray production cross sections and associated gamma-ray spectra were calculated from the evaluated (n,n') and (n,γ) cross sections together with known and assumed branching ratios. The evaluated cross sections are presented in graphical form.

References

1. Funded by the Defense Atomic Support Agency under Subtask PC103.

2. Abstract of ORNL-4617 (1971); included in last year's annual as abstract of ORNL-TM-3100.

2.31 EVALUATION OF THE CROSS SECTIONS OF IRON: ENDF/B MAT 1101[1,2]

D. C. Irving E. A. Straker

The neutron cross sections for iron have been evaluated and placed in the ENDF/B format with the material (MAT) number 1101. The total cross section was evaluated from recent experimental measurements and is compatible with measurements from very thick sample penetration made at the Tower Shielding Facility. Other data were taken from evaluations by J. J. Schmidt as contained in the UKAEA Nuclear Data File, DFN 64.

References

1. Jointly funded by the Defense Atomic Support Agency under Subtask PC103 and the SEPO project of the Atomic Energy Commission.

2. Abstract of ORNL-TM-2891 (ENDF-138) (1970).

2.32 ENERGY CALIBRATION OF A PROTON-RECOIL PROPORTIONAL COUNTER[1,2]

G. L. Morgan E. A. Straker
T. A. Love R. M. Freestone, Jr.
C. E. Burgart

Three methods for calibration of proton-recoil proportional counters have been investigated. These are the $^{14}N(n,p)^{14}C$ reaction, an internally mounted alpha-particle source, and observations of resonances in a neutron spectrum. Calibrations based on each method were compared and found to be consistent to within 2%. The variation of the gas amplification as a function of counter voltage was measured and was found to be in good agreement with the formula of Diethorn.

References

1. Jointly funded by the Defense Atomic Support Agency under Subtask PE075 and the SEPO project of the Atomic Energy Commission.
2. Abstract of ORNL-TM-3347 (Mar. 15, 1971).

2.33 INTRIGUE-II: AN IBM-360 SUBROUTINE PACKAGE FOR MAKING LINEAR, LOGARITHMIC AND SEMILOGARITHMIC GRAPHS USING THE CALCOMP PLOTTER[1,2]

M. B. Emmett[3]

The plotting package INTRIGUE which was previously reported has been greatly modified to add greater flexibility for use on the IBM-360 system. It facilitates the plotting of data on linear, logarithmic and semilogarithmic graphs using the CALCOMP pen and ink plotter. The subroutines accomplish the necessary computations and prepare a magnetic tape for use by the plotter. The modifications include variable height, dashed lines for connecting points, placement of a legend within the grid lines, and insertion of a numerical value or a Greek letter symbol in the titles. This package supersedes the previous INTRIGUE for the IBM-360.

References

1. Jointly funded by the Defense Atomic Support Agency under Subtask PE074 and the SEPO project of the Atomic Energy Commission.
2. Abstract of ORNL-4664 (1971).
3. Mathematics Division.

2.34 A CALCULATION OF NEUTRON-INDUCED PHYSICAL DOSES IN HUMAN TISSUES[1,2]

J. J. Ritts M. Solomito[3]
P. N. Stevens[3]

Improved multicollision neutron fluence-to-dose conversion factors have been calculated for a phantom exposed to neutrons with energies from 15 MeV down to thermal. The phantom was a 30-cm-thick slab composed of the 11 most common elements in the standard man. The calculations consisted of the simultaneous solution of the neutron and secondary gamma-ray transport problem with the ANISN computer code for both a beam source and an isotropic flux source, and for a slab having both infinite and finite transverse dimensions. The fluence-to-dose conversion factors were based on new neutron fluence-to-kerma factors and improved secondary gamma-ray yields determined from the individual elements comprising the slab. The neutron and gamma-ray cross sections used in the calculations are from the ENDF/B file and the OGRE library, respectively.

References

1. Jointly funded by the Defense Atomic Support Agency under Subtask PE074 and the SEPO project of the Atomic Energy Commission.
2. Abstract of *Nucl. Tech.* **11**, 246 (1971); included in last year's annual as abstract of ORNL-TM-2991 (1970).
3. University of Tennessee.

2.35 HEAT GENERATION BY NEUTRONS IN SOME MODERATING AND SHIELDING MATERIALS[1,2]

H. C. Claiborne M. Solomito[3]
J. J. Ritts[4]

For all practical purposes, the heat deposited by neutron interactions in moderating and shielding materials of a nuclear reactor is less than or equal to the kerma (kinetic energy released in materials). Kerma factors (kerma rate/unit flux) were calculated for neutron energies between 0.22 eV and 10 MeV for concrete, water, LiH, ^{6}LiH, ^{7}LiH, BeO, Be, C, and Fe. Plots of these kerma factors are presented in units of (watts/g)/(neutrons/cm^2 sec) as a function of neutron energy. The maximum heat generation rate at any point is simply the sum of the products of the kerma factors

read from the plots and the neutron fluxes for the energy groups at the point in question. These plots should be useful in the design of shields for nuclear reactors.

References

1. Jointly funded by the Defense Atomic Support Agency under Subtask PE074 and the SEPO project of the Atomic Energy Commission.
2. Abstract of *Nucl. Eng. Design* **15**, 232 (1971) and of ORNL-TM-3157 (1970).
3. University of Tennessee.
4. Now at Westinghouse Electric Co., Madison, Pa.

2.36 USE OF THE DISCRETE ORDINATES S_n METHOD IN RADIATION SHIELDING CALCULATIONS[1,2]

P. N. Stevens[3]

Recent developments have led to the widespread use of the "discrete ordinates" method in the deep-penetration shielding calculation. Events leading to this breakthrough in technology are described. A detailed derivation of the discrete ordinates difference equations is presented along with a review of the calculational procedures which are peculiar to the shielding problem. Advantages and disadvantages of the method are discussed and a list of current computer codes is included.

References

1. The development of the discrete ordinates method was jointly supported by the Defense Atomic Support Agency under Subtask PE074 and the SEPO project of the Atomic Energy Commission.
2. Abstract of *Nucl. Eng. Design* **13**, 395 (1970).
3. University of Tennessee.

2.37 MORSEC, A REVISED CROSS-SECTION MODULE FOR THE MORSE MULTIGROUP MONTE CARLO CODE[1,2]

E. A. Straker M. B. Emmett[3]

The cross-section module for the MORSE neutron and gamma-ray Monte Carlo transport code has been revised to treat upscattering, to handle point total, scattering, and fission cross sections and to output a processed cross-section tape for use on subsequent problems. Several other minor changes in the logic have also been made to improve the overall capabilities of the code.

References

1. Jointly funded by the Defense Atomic Support Agency under Subtask PE074 and the SEPO project of the Atomic Energy Commission.
2. Abstract of ORNL-4716 (1971).
3. Mathematics Division.

2.38 METHODS OF BIASING SECONDARY GAMMA-RAY PRODUCTION IN COUPLED NEUTRON GAMMA-RAY MONTE CARLO CALCULATIONS[1,2]

M. Solomito[3] E. A. Straker
P. N. Stevens[3] C. E. Burgart
S. N. Cramer[4]

Methods for applying importance sampling techniques to secondary gamma-ray generation in coupled neutron-gamma-ray Monte Carlo transport calculations have been developed and evaluated. The Boltzmann transport equation is presented in an integral-matrix form which defines a set of coupled neutron-gamma-ray multigroup equations and provides the basis for the coupled Monte Carlo random walk. Three methods of biasing the production of secondary gamma rays which make use of importance functions obtained from discrete ordinates adjoint calculations are formalized. These methods employ importance sampling techniques which include alteration of the gamma-ray generation probabilities, nonabsorption weighting, and a combination of splitting and Russian roulette. These three methods are evaluated using the multigroup Monte Carlo code MORSE in the solution of a deep-penetration shielding problem in concrete. All three methods were shown to be more efficient than the standard method of biasing the secondary gamma-ray production in the MORSE code. The methods varied from a factor of 1.3 to 40.0 better than the standard method based on the running time of the code and the variance of the answer obtained.

References

1. Jointly funded by the Defense Atomic Support Agency under Subtask PE080 and the SEPO project of the Atomic Energy Commission.
2. Abstract of thesis submitted to the University of Tennessee in partial fulfillment of the requirements for the degree of doctor of philosophy; also to be issued as ORNL-TM-3530.
3. University of Tennessee.
4. Mathematics Division.

2.39 A GENERAL METHOD OF IMPORTANCE SAMPLING THE ANGLE OF SCATTERING IN MONTE CARLO CALCULATIONS[1,2]

C. E. Burgart P. N. Stevens[3]

The application of the Monte Carlo method to the solution of deep-penetration radiation transport problems requires the use of "importance sampling." A systematic approach to obtaining an importance function is to calculate the solution of the inhomogeneous adjoint transport equation (using the Monte Carlo estimator of the answer of interest as the source term) and to use this adjoint flux (or value function) as the importance function. The adjoint flux is calculated for simplified geometries using one-dimensional discrete ordinates methods.

In three-dimensional deep-penetration Monte Carlo calculations the alteration of both the transport and the collision kernel is desirable. The exponential transform is quite useful for altering the transport kernel. However, selection from the altered collision kernel is much more difficult. The approach taken here is to introduce an angular grid with 30 discrete directions fixed in the laboratory coordinate system, along which particles are required to travel. After determining appropriate scattering probabilities and values of the importance function for each of the discrete directions, the selection of the outgoing direction and, hence, energy from the resulting discrete distribution is easily performed.

The effects of the discrete angular grid and the capability of angular-biased Monte Carlo have been investigated for neutron transport by comparison with standard Monte Carlo and discrete ordinates calculations, experiment, and exact analytic solutions for several configurations. In all cases the discrete grid alone (no angular biasing) was observed to have no significant effect on the results. Monte Carlo calculations were performed utilizing the exponential transform, nonleakage, source energy biasing, Russian roulette, and splitting plus the angular biasing. The results of these calculations illustrate the general usefulness of this discrete grid approach to angular biasing in several ways. First, meaningful results were obtained with angular biasing at much greater distances from the source than were practically possible with the earlier biasing techniques. The answers, variances, and computer times were all on the same order or better than those obtained with the earlier biasing techniques. Finally, this method utilizing the discrete grid to incorporate angular biasing requires very little human interaction once the adjoint configuration is selected.

References

1. Jointly funded by the Defense Atomic Support Agency under Subtask PE074 and the SEPO project of the Atomic Energy Commission.

2. Abstract of *Nucl. Sci. Eng.*, **42**, 306 (1970); included in last year's annual as abstract of ORNL-TM-2890 (1970).

3. University of Tennessee.

2.40 COLLISION DENSITY PLOTTING ROUTINES AND COLLISION DENSITY FLUENCE ESTIMATES FOR THE MORSE MONTE CARLO CODE[1,2]

E. A. Straker M. B. Emmett[3]

Routines for use with the Monte Carlo transport code MORSE have been written to provide collision density plots – that is, plots of the locations of collisions occurring during the random walk process. The plots can be made either on the on-line printer or, through a collision tape, on a pen and ink or cathode-ray plotter. The user must decide what type of events and over what spatial range the collisions are to be plotted. Also, an output routine has been added to take advantage of the collision counter information in MORSE in providing a region-averaged estimate of the fluence. Printer plots of the resulting energy spectra for both neutrons and gamma rays are part of the output. This output may be obtained for both forward and adjoint calculations. These routines can also be utilized in other Monte Carlo codes.

References

1. Jointly funded by the Defense Atomic Support Agency under Subtask PE080 and the SEPO project of the Atomic Energy Commission.

2. Abstract of ORNL-4722 (to be published).

3. Mathematics Division.

2.41 XCHEKR – A MULTIGROUP CROSS-SECTION EDITING AND CHECKING CODE[1,2]

C. E. Burgart E. A. Straker

XCHEKR is a multigroup cross-section editing and checking code. Cross sections in either ANISN or DTF-IV format may be read from cards or binary magnetic tape. They may be neutron cross sections only, gamma-ray cross sections only, or coupled neutron-gamma-ray cross sections with full or partial downscatter and/or upscatter. XCHEKR produces a

highly readable edit of the P_0 portion of the cross sections, as well as tables of evaluated angular distributions for each group-to-group transfer. Checks are performed to determine if the Legendre coefficients are possible.

References

1. Jointly funded by the Defense Atomic Support Agency under Subtask PE074 and the SEPO project of the Atomic Energy Commission.
2. Abstract of ORNL-TM-3518 (to be published).

2.42 NNNGAM: A CODE FOR CALCULATING GAMMA-RAY SPECTRA FROM COMPETING (n,n') AND $(n,2n)$ REACTIONS[1]

C. Y. Fu[2]

During the course of evaluation of natural lead neutron and gamma-ray production cross sections, lack of experimental data has led to the development of a code for calculating gamma-ray spectra from competing (n,n') and $(n,2n)$ reactions. The inclusion of gamma rays from $(n,2n)$ reactions is particularly significant in lead because of its low $(n,2n)$ threshold (6.733 MeV). The code also contains a method, employing the concept of modified level density, for approximating gamma-ray yields for $(n,3n)$ reactions from those for $(n,2n)$ reactions for the same residual nuclei.

The program is based on the statistical model theory of neutron reactions and scattering[3] and gamma-ray cascade theory[4] with the following exceptions:

1. Level excitation cross sections from experiment or Hauser-Feshbach model calculations[5] for (n,n') reactions may be used as an option to replace those from statistical model predictions.

2. Direct interaction cross sections from distorted wave Born approximation calculations[6] may be included. In general, these cross sections are small, but they influence the strong gamma rays most, and, therefore, are not negligible from a shielding point of view.

3. Gamma-ray cascades are made spin and parity dependent. Discrete-to-discrete branching ratios, if not known experimentally, are filled by $E1$ selection rules. Levels that cannot be de-excited by $E1$ transitions are allowed to decay by $M\lambda$, $E\lambda$ transitions with the smallest possible λ. Continuum-to-discrete transitions are assumed to be proportional to

$$\{\exp[-I^2/2\sigma^2] - \exp[-(I+1)^2/2\sigma^2]\},$$

where I is spin of a discrete level and σ is an energy-dependent parameter.

Details of the code will be reported.

References

1. Jointly funded by the Defense Atomic Support Agendy under Subtask PC103 and the SEPO project of the Atomic Energy Commission.
2. University of Tennessee.
3. See, for example, H. Goldstein, "Statistical-Model Theory of Neutron Reactions and Scattering," in *Fast-Neutron Physics*, edited by J. B. Marion and J. L. Fowler, Interscience Publishers, New York (1963).
4. E. S. Troubetzkoy, *Phys. Rev.* **122**, 212 (1961).
5. S. K. Penny, *HELENE – A Computer Program to Calculate Nuclear Cross Sections Employing the Hauser-Feshbach Model, Porter-Thomas Width Fluctuations, and Continuum States,* ORNL-TM-2590 (1969).
6. R. H. Bassel, R. M. Drisko, and G. R. Satchler, *The Distorted-Wave Theory of Direct Nuclear Reactions, and the Codes SALLY and JULIE,* ORNL-3240 (1962) and Supplement(1966).

2.43 A COMPARISON OF FOLDING AND UNFOLDING TECHNIQUES FOR DETERMINING THE GAMMA SPECTRUM FROM THERMAL NEUTRON CAPTURE IN ALUMINUM[1,2]

R. S. Booth

The gamma-ray spectrum above 1 MeV resulting from thermal-neutron capture in aluminum is determined by both a folding and an unfolding analysis of data taken at the Tower Shielding Facility. This results in a comparison of the relative merits of the two analysis techniques and demonstrates the accuracy that can be obtained in unfolding a complex spectrum. It is concluded that the accuracy of the final photon spectrum is not governed by the technique employed to unfold the measured counts.

References

1. Jointly funded by the Defense Atomic Support Agency under Subtask PE037 and the SEPO project of the Atomic Energy Commission.
2. Abstract of *Nucl. Instr. Methods* 85, 69 (1970); included in last year's annual as abstract of TM-2898 (1970).

2.44 THE ORNL-SNAP SHIELDING PROGRAM[1,2]

F. R. Mynatt F. J. Muckenthaler
C. E. Clifford M. L. Gritzner

The effort in the ORNL-SNAP shielding program is directed toward the development and verification of computer codes using numerical solutions to the transport equation for the design of optimized radiation shields for SNAP power systems. A brief discussion is given for the major areas of the SNAP shielding program which are cross-section development, transport code development, and integral experiments. Detailed results are presented for the integral experiments utilizing the TSF-SNAP reactor. Calculated results are compared with experiment for neutron and gamma-ray spectra from the bare reactor and as transmitted through slab shields.

References

1. Funded by the SEPO project of the Atomic Energy Commission.
2. Abstract of paper presented at the National Symposium on Natural and Manmade Radiation in Space, Las Vegas, Nevada, March 1-5, 1971; also abstract of ORNL-TM-3364 (1971).

2.45 THE DESIGN OF ASYMMETRIC 4π SHIELDS FOR SPACE REACTORS[1,2]

W. W. Engle, Jr. R. L. Childs[3]
F. R. Mynatt

A one-dimensional shield optimization program based on the method of discrete ordinates has been developed and is used to determine material thicknesses used in asymmetric 4π shields for space power reactors. The two-dimensional discrete ordinates program DOT is used to check the design and the information generated in the DOT calculation is used as a guide in shaping the shield which may be considered a first step in two-dimensional shield optimization.

References

1. Funded by SEPO project of the Atomic Energy Commission.
2. Abstract of paper presented at the National Symposium on Natural and Manmade Radiation in Space, Las Vegas, Nevada, March 1-5, 1971; also abstract of ORNL-TM-3368 (1971).
3. Mathematics Division.

2.46 OPTIMIZATION OF A SHIELD FOR A HEAT-PIPE-COOLED FAST REACTOR DESIGNED AS A NUCLEAR ELECTRIC SPACE POWER PLANT[1,2]

W. W. Engle, Jr. F. R. Mynatt
R. L. Childs [3] L. S. Abbott

A reactor shield optimization procedure based on the ASOP shield optimization computer code and the DOT radiation transport code was used to determine a minimum-weight shield for a small fast reactor designed for a space nuclear electric power plant. The reactor, cylindrical in shape, is fueled with uranium nitride and cooled by potassium circulating through a matrix of stainless steel heat pipes embedded in the core; the design power is 450 kWt. The surrounding shield is typically asymmetric, having the overall shape of a truncated 90-deg cone whose thick base is positioned between one end of the reactor and the crew compartment. The heat pipes emerge from the opposite end of the reactor, penetrating through the apex of the shield. The dose constraints are 3 mrem/hr at all 100-ft radii falling within the shadow cast by the base of the cone and 300 mrem/hr at all other 100-ft radii. The optimized shield consists of alternate layers of tungsten and lithium hydride, the thick bottom section extending out to a radius of 112 cm and the tapered side decreasing to a radius of 89 cm. The top heat-pipe shield region consists of a 59-cm-thick inner layer of a stainless-steel-B_4C mixture and a 30.5-cm-thick outer layer of a BeO-B_4C mixture. The total shield weight is 25,589 lb. A partially optimized shield having a 45-deg cone angle and a higher dose constraint for positions outside the cone shadow (100 rem/hr) has a total weight of 14,708 lb. These shield weights include an allocation for 3.5 vol% of stainless steel structure in the LiH regions.

References

1. Funded by SEPO project of the Atomic Energy Commission.
2. Abstract of ORNL-TM-3449 (1971).
3. Mathematics Division.

2.47 DEVELOPMENT OF SHIELD OPTIMIZATION TECHNIQUES[1]

R. L. Childs[2]

The one-dimensional shield optimization code, ASOP, has been used extensively in the design of space reactor shields. The outstanding advantage of this code is that it

incorporates ANISN transport calculations directly into the optimization procedure. A disadvantage of the ASOP method is that a relatively large number of transport calculations are required. Also, the method is difficult to apply to two-dimensional problems.

Another approach to the shield optimization problem is to use perturbation theory. A small change in layer thickness can be approximated by a small change in the density of the layer. If the change in density is not large enough to substantially distort the flux, the change in dose rate can be calculated if both the forward flux and the adjoint flux are known. With this technique, the dose-weight derivatives, which ASOP calculates from several forward transport calculations, can be calculated from one forward and one adjoint calculation.

A one-dimensional shield optimization code which utilizes the perturbation theory method is presently under development. Preliminary calculations indicate that the new method obtains essentially the same results as ASOP with significantly less computation. For shields with six layers, as is now common, the new code has proven to be at least five times faster than ASOP.

Future plans include an investigation of the application of perturbation theory to two-dimensional shield optimization. Two-dimensional shield optimization is a very difficult problem for a number of reasons. Instead of one dose constraint, a two-dimensional problem usually has a number of constraints for detectors in different positions. Also, the amount of computation and data storage required is much greater for two-dimensional problems than for similar one-dimensional problems.

References

1. Funded by the SEPO project of the Atomic Energy Commission.
2. Mathematics Division.

2.48 MORSE MONTE CARLO SHIELDING CALCULATIONS FOR THE ZIRCONIUM HYDRIDE REFERENCE REACTOR[1,2]

C. E. Burgart

Verification of DOT-SPACETRAN transport calculations of a lithium hydride and tungsten shield for a SNAP reactor has been performed using the MORSE Monte Carlo code. Transport of both neutrons and gamma rays was considered. Several forms of importance sampling were utilized in the MORSE calculations. Quantities internal to the shield, as well as doses at several points outside the configuration, were in satisfactory agreement with the DOT calculations of the same.

References

1. Funded by the SEPO project of the Atomic Energy Commission.
2. Abstract of paper presented at the National Symposium on Natural and Manmade Radiation in Space, Las Vegas, Nevada, March 1-5, 1971; also abstract of ORNL-TM-3366 (to be published).

2.49 APPLICATION OF DOT-MORSE COUPLING TO THE ANALYSIS OF THREE-DIMENSIONAL SNAP SHIELDING PROBLEMS[1,2]

E. A. Straker R. L. Childs[3]
M. B. Emmett[3]

Many radiation transport problems can best be solved by using both discrete ordinates and Monte Carlo techniques with a coupling between the two techniques occurring at a geometry interface. A general discussion of two possible coupling schemes is given. The calculation of the reactor radiation scattered from a docked service and command module is used as an example of coupling discrete ordinates (DOT) and Monte Carlo (MORSE) calculations.

References

1. Funded by the SEPO project of the Atomic Energy Commission.
2. Abstract of paper presented at the National Symposium on Natural and Manmade Radiation in Space, Las Vegas, Nevada, March 1-5, 1971; also abstract of ORNL-TM-3365 (1971).
3. Mathematics Division.

2.50 COMPARISONS OF MONTE CARLO CALCULATIONS TO MEASUREMENTS OF NEUTRON LEAKAGE FROM THE TSF-SNAP REACTOR[1,2]

V. R. Cain

The TSF-SNAP reactor is being used at ORNL as a realistic source for investigations of the light-weight shields required for space power systems. As part of this program, experimental and analytical determinations have been made of the energy and angular distribution of neutrons leaving an area roughly equal to 10% of the

reactor lower surface. The agreement between experiment and Monte Carlo calculations was found to be quite good when the reactor was described in sufficient detail in the calculations.

References

1. Funded by the SEPO project of the Atomic Energy Commission.

2. Abstract of *Nucl. Sci. Eng.* **41**, 320 (1970); included in last year's annual as abstract of paper submitted for journal publication.

2.51 EXAMINATION OF THE CODE ERF (EXTENDED R-MATRIX FORMALISM) WITH A COUPLED SQUARE-WELL POTENTIAL[1]

C. Y. Fu[2]

The core-coupling nuclear structure code KK[3,4] and the extended R-matrix program ERF[5] were designed to be used as one package (called KKERF) for studying neutron reactions and scattering from a microscopic view of the compound nucleus structure. An effort in applying the code KKERF for neutron scattering cross sections of ^{12}C has met with substantial difficulty, and it was not immediately clear whether the ERF code had been completely debugged, whether the extended R-matrix formalism[6] was sufficiently accurate in the few-level approximation, or whether the nuclear wave functions provided by the code KK were adequate for the purpose. The present study is an attempt to answer some of these questions.

As a first step, the code ERF was checked against the theory,[6] and several inconsistencies between the code and the theory have been found and removed. To ensure that the code ERF was completely debugged, a simple problem of a neutron in a coupled square well was solved on the harmonic oscillator basis to replace the role of the code KK. The Hamiltonian of the potential well may be written as

$$H = \begin{pmatrix} T + V_1(r) & V_{12}(r) \\ V_{12}(r) & T + V_2(r) + Q \end{pmatrix}$$

where T is the usual kinetic energy operator, the V's are all square-well potentials, and Q is the energy of an excited state in the second well. With the same number of oscillator bases and potential strengths, the wave functions were checked in terms of reduced level widths against the tabulation of Purcell,[7] guaranteeing that the solutions obtained were correct.

Elastic and inelastic cross sections of s-wave neutrons scattered from the potential were then calculated with the code ERF with several sets of potential strengths, all used previously by other authors.[8-10] Reasonable results were obtained in each case, indicating that the code ERF was a working one. While the extended R-matrix formalism in the few-level approximation is by no means perfect, it is sufficiently accurate if one considers the far more approximate nature of nuclear wave functions obtainable with the current knowledge of nuclear structure. Figure 2.51.1 illustrates one set of the approximate and the exact cross sections obtained with the following parameters:

$V_1 = -42$ MeV

$V_2 = -39$ MeV

$V_{12} = 1.0$ MeV

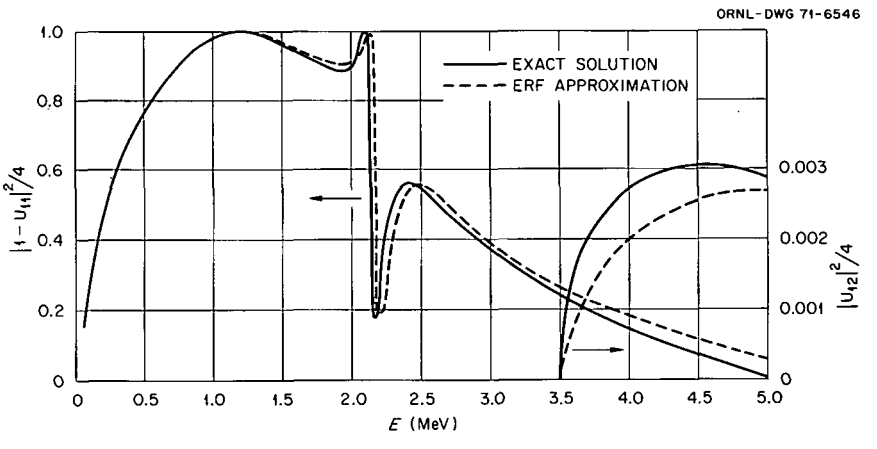

Fig. 2.51.1. Elastic ($|1 - U_{11}|^2 \pi/k^2$) and ($|U_{12}|^2 \pi/k^2$) Cross Section of Neutrons Scattered from a Coupled Square-Well Potential.

$Q = 3.5$ MeV

radius of well = 6 F

channel radii = 7 F

mass of target = 10,000 Amu

mass of neutron = 1 Amu

harmonic oscillator length = 2 F

number of basis functions = 5

Shown in the figure are $|1 - U_{11}|^2/4$ and $|U_{12}|^2/4$, which are elastic and inelastic cross sections multiplied by $k^2/4$, where k is the wave number of incident neutrons.

While considerable effort has gone into the refinement of the codes KK and ERF separately, a combined study of the two together has yet to be done. We think that this approach is still a promising one and could prove to be very useful, together with other theories, in performing evaluations of nuclear data. We plan to continue this investigation.

References

1. Funded by the SEPO project of the Atomic Energy Commission.
2. University of Tennessee.
3. K. Kumar, "A Bootstrap Method for the Calculation of High-Lying Nuclear Levels and Electromagnetic Moments (I). Theory," submitted for journal publication.
4. K. Kumar, K. J. Yost, and C. Y. Fu, "A Bootstrap Method for the Calculation of High-Lying Nuclear Levels and Electromagnetic Moments (II). Application to ^{13}C and ^{209}Pb," Sec. 2.21 in *Neutron Phys. Div. Ann. Progr. Rept. May 31, 1970*, ORNL-4592.
5. K. J. Yost and P. H. Pitkanen, "The Application of Extended R-Matrix Theory to Elastic Scattering of Neutrons by ^{12}C," Sec. 2.18 in *Neutron Phys. Div. Ann. Progr. Rept. May 31, 1970*, ORNL-4592.
6. L. Garside and W. Tobocman, *Phys. Rev.* **173**, 1047 (1968).
7. J. E. Purcell, *Application of Generalized R-Matrix Theory to Simple Scattering Models*, Case Institute of Technology, Department of Physics, Technical Report (1966).
8. L. Garside and W. Tobocman, *Ann. Phys.* **53**, 115 (1967).
9. W. Romo, *Nucl. Phys.* **A142**, 300 (1970).
10. F. Schmittroth and W. Tobocman, *Phys. Rev.* **C3**, 1010 (1971).

2.52 A UNIFIED MODEL OF DEFORMED ODD-ODD NUCLEI FOR NUCLEAR DATA GENERATION AND ANALYSIS[1,2]

C. Y. Fu[3] K. J. Yost

A unified model of deformed odd-odd nuclei has been formulated as an aid in nuclear data generation and evaluation. The model employs products of single-particle Nilsson wave functions as basis functions. The coupling of angular momenta of the odd nucleons is assumed to obey the Gallagher-Moszkowski coupling rules. The matrix elements of the proton-neutron residual interaction potential are evaluated with the use of oscillator brackets. The validity of the model has been established by computing and comparing with experimental data nuclear-energy levels and/or gamma-ray transition probabilities for ^{23}Na, ^{28}Al, ^{166}Ho, ^{182}Ta, and ^{238}Np. The calculated results compare quite well with experiment. Special attention has been given to the establishment of an efficient computational method.

References

1. Funded by the SEPO project of the Atomic Energy Commission.
2. Abstract of *Nucl. Sci. Eng.* **41**, 193 (1970); included in last year's annual as abstract of ORNL-TM-2832 (1970).
3. University of Tennessee.

2.53 THE POPOP4 LIBRARY AND CODES FOR PREPARING SECONDARY GAMMA-RAY PRODUCTION CROSS SECTIONS[1,2]

W. E. Ford, III[3]

The POPOP4 code for converting secondary gamma-ray yield data to multigroup secondary gamma-ray production cross sections and the POPOP4 library of secondary gamma-ray yield data are described. Recent results in the "testing" of uranium and iron data sets from the POPOP4 library are given. The data sets were tested by comparing calculated secondary gamma-ray pulse-height spectra with spectra measured at the ORNL TSR-II reactor.

References

1. Funded by the SEPO project of the Atomic Energy Commission.
2. Abstract of paper presented at the National Symposium on Natural and Manmade Radiation in

Space, Las Vegas, Nevada, March 1-5, 1971; also abstract of ORNL-TM-3367 (1971).

3. Mathematics Division.

2.54 THE TESTING OF ^{238}U SECONDARY GAMMA-RAY PRODUCTION DATA SETS FROM THE POPOP4 LIBRARY[1,2]

W. E. Ford, III[3] J. S. Gillen[3]

The ^{238}U nonfission capture, fission capture, and inelastic-scattering data sets included in the POPOP4 library of neutron-induced secondary gamma-ray yield and cross-section data were tested for use in the preparation of ^{238}U secondary gamma-ray production cross sections (SGRPXS's). The data sets were tested over various neutron energy ranges by comparing calculated secondary gamma-ray pulse-height spectra with previously measured spectra resulting from the exposure of a 30-mil-thick, depleted uranium foil to bare, thermal, Cd-, ^{10}B-, (Cd-^{10}B)-, and (Cd-1.377^{10}B)-filtered neutron beams from the ORNL TSR-II reactor. ^{235}U fission capture and inelastic scattering data sets 925801 and 925301, respectively, were found to be suitable for use in the preparation of ^{238}U SGRPXS's. ^{238}U nonfission capture data sets 928109, 928112, and 928113 and the total SGRPXS data set 928901 are adequate for use in shielding calculations when used over the neutron and gamma-ray energy ranges for which the data are defined.

References

1. Funded by the SEPO project of the Atomic Energy Commission.
2. Abstract of ORNL-TM-3482 (to be published).
3. Mathematics Division.

2.55 GAMMA-RAY SPECTRA FROM INELASTIC NEUTRON SCATTERING IN ^{181}Ta[1]

C. Y. Fu[2] K. J. Yost

The spectra of gamma rays produced by neutron inelastic scattering in ^{181}Ta have been calculated on the basis of the statistical-model theory of neutron reactions[3] and gamma-ray cascade assumptions[4] for neutron energies up to 15 MeV. Level density consistent with neutron evaporation data of Tsukada et al.[5] was used. Using the same calculated cross sections for compound nucleus formation[6] as those used in the analysis of neutron evaporation data for obtaining level densities[5] essentially reproduced the experimental secondary neutron distributions of Tsukada et al. Gamma-ray spectra were then obtained by performing gamma-ray cascade calculations[4] with those secondary neutron distributions. Part of the results are compared in Fig. 2.55.1 with some experimental data[7,8] and an empirical formalism.[9] Details of the calculated data are available in the POPOP4 library.[10]

References

1. Funded by the SEPO project of the Atomic Energy Commission.
2. University of Tennessee.
3. See, for example, H. Goldstein, "Statistical-Model Theory of Neutron Reactions and Scattering," *Fast Neutron Physics,* J. B. Marion and J. L. Fowler, Eds., Interscience Publishers, New York (1963).
4. E. S. Troubetzkoy, *Phys. Rev.* **122**, 212 (1961).
5. K. Tsukada et al., *Nucl. Phys.* **78**, 369 (1966).
6. J. R. Beyster et al., Los Alamos Scientific Laboratory, LA-2199 (1957).

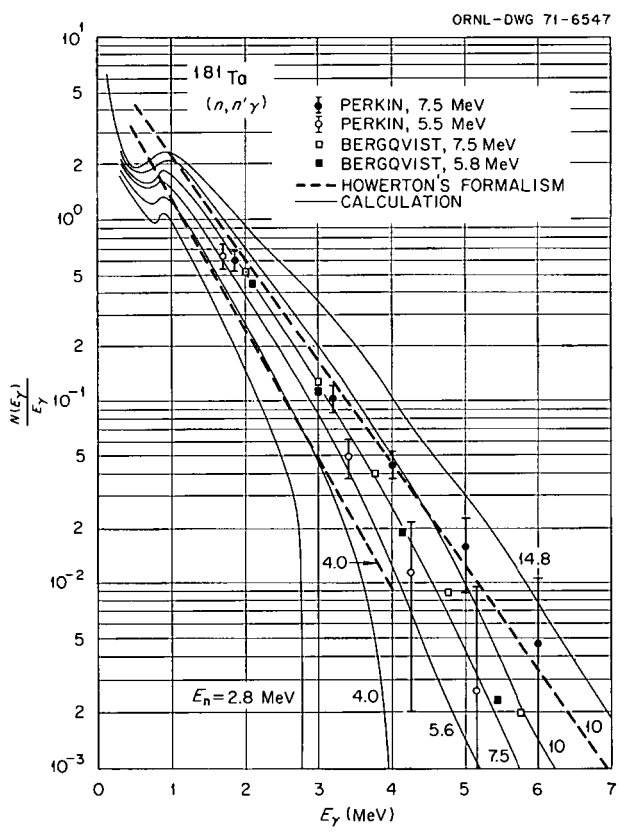

Fig. 2.55.1. $N(E_\gamma)/(E_\gamma)$ vs. E_γ for ^{181}Ta. $N(E_\gamma)$ is the number of gamma rays per MeV per inelastic scattering.

7. J. L. Perkin and N. Starfelt, *Nucl. Phys.* **63**, 526 (1965).
8. I. Bergqvist et al., *Nucl. Phys.* **80**, 198 (1966).
9. R. J. Howerton and E. F. Plechaty, *Nucl. Sci. Eng.* **32**, 178 (1968).
10. W. E. Ford, III, *The POPOP4 Library of Neutron-Induced Secondary Gamma-Ray Yields and Cross-Section Data*, CT-42 (1970).

2.56 NEUTRON ENERGY-DEPENDENT CAPTURE GAMMA-RAY YIELDS IN TANTALUM AND TUNGSTEN[1,2]

K. J. Yost C. Y. Fu[4]
J. E. White[3] W. E. Ford, III[3]

Gamma-ray yields as a function of neutron energy for tantalum and tungsten have been calculated with the cascade code DUCAL. The results are presented in a format that would facilitate use in coupled neutron gamma-ray transport calculations. In the case of tungsten, pronounced variations in the capture yield spectra were noticed above 3.0 MeV. On the other hand, only slight variations in the yield spectra were evident for tantalum. The results have been compared with integral gamma-ray yield measurements, and the agreement is favorable.

References

1. Funded by the SEPO project of the Atomic Energy Commission.
2. Abstract of ORNL-TM-3436 (1971).
3. Mathematics Division.
4. University of Tennessee.

2.57 THE TOTAL GAMMA-RAY ENERGY SPECTRUM ABOVE 1 MeV FROM NEUTRON INTERACTIONS IN ^{235}U AND ^{238}U[1,2]

R. S. Booth F. J. Muckenthaler

The total gamma-ray energy spectra above 1 MeV from neutron interactions in ^{235}U and ^{238}U were measured to test the accuracy of model calculations and to improve the accuracy of shielding calculations by reducing the uncertainty in the source term.

The general structure of the gamma-ray energy spectrum above 1 MeV from fission was independent of the isotope in which the fission occurred and the energy of the neutron that caused the fission. This total fission spectrum was approximated to an accuracy of 20% by a simple empirical expression which, between 1 and 5.12 MeV, is twice the spectrum from prompt fission.

The gamma-ray energy spectrum from all neutron interactions in ^{235}U was dominated by the total fission spectrum. The photon spectrum obtained as a result of reactor neutrons striking ^{235}U had the same shape as the photon spectrum obtained from the same neutron beam filtered with cadmium. When the reactor spectrum was filtered with ^{10}B, a photon spectrum due to interactions other than fission was evident for photon energies between 1 and 3 MeV. Our measured photon spectrum from thermal-neutron interactions in ^{235}U was compatible with previous estimates and measurements.

The photon energy spectra from ^{238}U were isolated from the measurements and presented on an absolute basis for three situations: (1) capture of thermal neutrons, (2) interactions with a $1/E$ spectrum of intermediate-energy neutrons, and (3) interactions with a fission spectrum of neutrons. The first two spectra were used to determine parameters in model calculations of differential yield data which were compared to measured differential yield data.

The relative photon spectra from neutron interactions in ^{233}U and ^{239}Pu were measured in preliminary experiments. The shapes of these spectra were quite similar to spectra obtained with ^{235}U.

References

1. Funded by the SEPO project of the Atomic Energy Commission.
2. Abstract of ORNL-4691 (1971); included in last year's annual as ORNL-TM-3060.

2.58 CALCULATED PERTURBATIONS IN THRESHOLD FOIL MEASUREMENTS DUE TO NEUTRON INTERACTIONS IN B_4C SHELLS[1,2]

W. E. Ford, III[3] J. S. Gillen[3]

Calculations were made to determine expected perturbation effects to the measured neutron flux in B_4C shielded threshold foils resulting from neutron interactions in the B_4C. Results indicated that there is a significant increase in the measured flux below the source energy of monoenergetic neutron beams due to scattering.

The activities in a series of threshold foils encased within a B_4C shell were calculated for exposure of the shell to monoenergetic 13.57- and 1.01-MeV neutron beams incident at 0° with respect to the shell axis.

Calculations were also made to determine if there would be a significant change in the measured threshold foil activities if the detector were inadvertently positioned "upside down" (beam incident at 180°) during an experiment. The difference between the 0° and 180° activities was not sufficient to distinguish which end of the detector was oriented toward the beam.

References

1. Work funded by Army Nuclear Defense Laboratory.
2. Abstract of ORNL-TM-3519 (to be published).
3. Mathematics Division.

2.59 Al($n,x\gamma$) REACTIONS FOR $5.3 \leqslant E_n \leqslant 9.0$ MeV[1,2]

J. K. Dickens

Interactions of neutrons with aluminum have been studied by measuring gamma-ray-production cross sections. Spectra were obtained for incident mean neutron energies E_n = 5.35, 5.85, 6.4, 6.9, 7.45, 7.95, 8.5, and 9.0 MeV. The gamma rays were detected using a coaxial Ge(Li) detector of 30 cm^3 active volume. Data were obtained for gamma-ray scattering angles of 55 deg for all E_n, of 90 deg for all E_n except 5.35 MeV, and of 75 deg for E_n = 6.4 and 7.45 MeV. Time-of-flight was used with the detector to discriminate against pulses due to neutrons and background radiation.

The gamma-ray spectra were reduced using a computer system based upon visual display of the data and estimation of the peak area using an interactive light pen. A simple algorithm which does not require *a priori* knowledge of the spectrum was used to estimate the underlying Compton distribution.

Absolute cross sections for production of gamma rays were obtained for the incident neutron energies quoted above. The cross sections have been compared, where possible, with previous measurements with good agreement. The spectra were studied for gamma rays which could be associated with de-excitation of nuclear levels having unknown decay modes. Gamma rays were found having energies appropriate for ground-state decay of levels at excitation energies E_x = 5.155, 5.414, 5.434, 6.514, 6.821, 6.956, 7.920, 7.411, 7.471, 7.56 (doublet), 7.655, 8.148, and 8.184 MeV.

References

1. Partially funded by Defense Atomic Support Agency under Subtask PC068.
2. Abstract of ORNL-TM-3284 (1971).

2.60 $^{28-30}$Si($n,x\gamma$) REACTIONS FOR $5.3 \leqslant E_n \leqslant 9.0$ MeV[1,2]

J. K. Dickens

Interactions of neutrons with silicon have been studied by measuring gamma-ray-production cross sections. For incident mean neutron energies E_n = 5.35, 5.85, 6.4, 6.9, 7.45, 7.95, 8.5, and 9.0 MeV spectra were obtained for a natural silicon sample. The gamma rays were detected using a coaxial Ge(Li) detector of 30 cm^3 active volume. Data were obtained for gamma-ray scattering angles of 55 and 90 deg for all E_n, 35 deg for E_n = 7.45 and 8.5 MeV, and 75 deg for E_n = 6.4 and 7.45 MeV. Time-of-flight was used with the detector to discriminate against pulses due to neutrons and background radiation. Data were also obtained at E_n = 5.9 MeV, θ_γ = 55 deg for a sample of $^{29}SiO_2$ enriched to 95% in ^{29}Si, and for a similarly enriched sample of $^{30}SiO_2$. These data have been studied to obtain absolute cross sections for production of gamma rays for the incident neutron energies quoted above. The cross sections have been compared, where possible, with previously measured values with fair agreement.

The spectra were studied for gamma rays which could be associated with deexcitation of nuclear levels having unknown decay modes. For ^{29}Si gamma rays were found having energies appropriate for decay of levels at excitation energies E_x = 4.736, 4.836, 4.893, and 5.249 MeV. For ^{30}Si gamma rays were found for decay of levels at excitation energies $E_x \geqslant 4.826$ MeV. The spin of the 4.826-MeV state in ^{30}Si is reasonably limited to 2, 3, or 4. No previously unknown transitions were found for ^{28}Si or ^{25}Mg; for ^{28}Al the evidence suggests that the 1.624-MeV level is a doublet of 3 keV separation.

References

1. Partially funded by Defense Atomic Support Agency under Subtask PC068.
2. Abstract of *Phys. Rev.* 2(3), 990 (1970); included in last year's annual as abstract of ORNL-TM-2883.

2.61 A MONOENERGETIC 6130-keV GAMMA-RAY SOURCE FOR DETECTOR CALIBRATION[1,2]

J. K. Dickens R. D. Baybarz[3]

A monoenergetic 6130-keV gamma-ray source based upon the reaction $^{13}C(\alpha,n)^{16}O$ has been fabricated using ^{244}Cm as the alpha source.

References

1. Funded by the Defense Atomic Support Agency under Subtask PC068.
2. Abstract of *Nucl. Instr. Methods* **85**, 143 (1970); included in last year's annual as abstract of ORNL-TM-2958.
3. Chemical Technology Division.

2.62 PAIRING-PLUS-QUADRUPOLE MODEL CALCULATION OF BAND-MIXING ANOMALIES IN ^{152}Sm[1]

Krishna Kumar

The pairing-plus-quadrupole model is improved and extended to $I = 6$ states. This microscopic theory gives the parameters of the first-order band-mixing theory of Bohr and Mottelson, as well as most of the higher order corrections revealed by the recent measurements of $E2$ matrix elements. The increase in the intra-ground-band transitions as well as the depression of the ground-band levels compared with their rotational-model values are reproduced.

References

1. Abstract of *Phys. Rev. Letters* **26**(5), 269 (1971).

2.63 THE ADJOINT BOLTZMANN EQUATION AND ITS SIMULATION BY MONTE CARLO[1,2]

D. C. Irving

The Boltzmann equation for neutron transport is discussed in both integro-differential and integral form. The 'value' or 'importance' equation is derived and shown to be equivalent, in the integral form, to the adjoint of the collision density. However, the value is also equivalent to the adjoint of the flux when the adjoint operation is carried out on the integro-differential equations. Possible ways of simulating both the forward and adjoint equations by Monte Carlo are discussed. Because the value equation is a 'flux-like' equation, direct simulation of it proves to be unwieldy. Instead, a 'collision density' for adjoint particles, equal to the value of adjoint flux times the total cross section, is introduced. The equation for this adjuncton collision density may be simulated by the same routines as were used for the forward calculation and only the cross sections need to be changed. The extension of this to problems involving multiplying media is also included.

References

1. Funded by the Defense Atomic Support Agency under Subtask PE080.
2. Abstract of *Nucl. Eng. Design* **15**(3), 273 (1971).

2.64 LEGCK, A SUBROUTINE TO ANALYZE LEGENDRE COEFFICIENTS FOR NEGATIVITY IN THE ANGULAR DISTRIBUTION[1,2]

D. C. Irving

LEGCK is a subroutine package designed to analyze Legendre expansions of angular distributions for negative regions. The analysis is divided into two portions. The first check determines if the Legendre coefficients are 'possible,' that is, if any negativity is due only to the truncation of the Legendre expansion. The second test determines if there are regions of negativity in the truncated expansion and where such negative regions are. The report describes the subroutines in the package and discusses the operations performed by each subroutine.

References

1. Funded by the Defense Atomic Support Agency under Subtask PE074.
2. Abstract of ORNL-TM-2903 (1970).

3. Radiation Shielding Information Center

3. RADIATION SHIELDING INFORMATION CENTER

3.1 INTRODUCTION, FUNCTIONS, AND SUMMARY OF OPERATIONS

B. F. Maskewitz
R. W. Roussin
H. C. Claiborne
J. Gurney
H. E. Comolander
H. R. Hendrickson
J. B. Wright
M. W. Landay
M. P. Guthrie
V. A. Jacobs
A. B. Gustin
C. M. Anthony
J. D. Needham

The Radiation Shielding Information Center (RSIC) is a technical institute serving the international scientific community. It serves those engaged in research and development for the design of shields that provide protection from biological and physical damage due to penetrating ionizing radiation. The Center is sponsored by the Atomic Energy Commission (AEC), the Defense Atomic Support Agency (DASA), and the National Aeronautics and Space Administration (NASA). In serving the interests of these agencies, RSIC is concerned with the shielding of radiation from nuclear reactors, nuclear weapons, radioisotopes, accelerators, and radiation present in space.

3.1.1 Current Statement of the Information Analysis Functions

RSIC continues to function in all the normal areas of an information analysis center. Specific research areas and publications are noted separately. In general, the work performed can be described as follows:

1. Examining and analyzing radiation shielding literature, including categorizing and abstracting the literature selected for inclusion in the RSIC computerized Storage and Retrieval Information System (SARIS).[1] The system is used to retrieve information to answer an inquiry, to compile bibliographies, to write state-of-the-art reviews, and/or to routinely disseminate selected information to fill individual needs indicated by a customer profile. An archival microfiche file of the literature store is maintained and made available on request.

2. Collecting, examining, packaging, and disseminating digital computer codes designed for shielding calculations. Effort is expended to collect useful programs, to acquire complete documentation, to run sample problems, and to acquire enough experience with each to advise requesters on the operability of each code at their computer facility. Abstracts of the code packages are written and published.[2,3] RSIC staff members are available on request to make recommendations, to answer inquiries, and to trouble-shoot on problems connected with the code collection. The current collection includes 165 complex shielding code packages and 29 packages of codes peripheral to shielding calculations.

3. Collecting useful shielding data and preparing and documenting data packages for dissemination. Abstracts of the data sets are also prepared and published.[4] The current data collection consists of 16 packages.

4. Cooperating with the National Neutron Cross Section Center (NNCSC) and with the Cross Section Evaluation Working Group (CSEWG) in the interests of the shielding community, and performing some checking and testing of data for the CSEWG Shielding Subcommittee. RSIC also acts as a clearinghouse in the DASA cross section evaluation program, assisting in Phase I testing and in other data testing functions.

5. Publishing an informal monthly newsletter on current activities, including an accession list of all the literature examined in the previous month, news of current work and problems in the shielding community, additions and corrections to the data and code collections, announcements of meetings of interest to the shielding community, and general shielding information. The "current work and problems" series, which describes briefly problems being considered at various installations, was reactivated during the year. The emphasis is on communication and exchange of ideas among workers in the shielding community, hoping that experience in solving certain problems at one installation may benefit other workers with similar problems.

6. Sponsoring seminar-workshops for the purpose of evaluating and discussing the theory and state-of-the-art of a particular calculational method and the application of the method as it is employed in particular codes. The seminar-workshops are arranged in answer to the needs shown by inquiries from the shielding community over a period of time. They have proved to be a practical and efficient way to transfer a great deal of information to a large number of potential users in a small amount of time and are held at least once a year. Leading experts are invited to present papers which are collected, edited, and published as a state-of-the-art review. One seminar-workshop was sponsored by RSIC in 1970 – on the Monte Carlo calculational method and selected computer codes.[5]

7. Cooperating with efforts to set standards that will promote interchangeability of computer programs,[6,7] avoid duplication of effort and improve the state-of-the-art of shielding in general. In this connection, RSIC cooperates in collecting and publishing information on benchmark problems for use in testing computational methods.[8] RSIC also promotes the efforts of the American Nuclear Society (ANS) Standards Committee through representation on the ANS-6 Shielding Subcommittee and on the ANS-10 Mathematics and Computation Subcommittee.

3.1.2 Annual Summary of Operations and Services

Government-sponsored information analysis centers are required to review periodically their distribution lists and to purge from the lists the names of those no longer interested in receiving information. This annual review, together with the addition of new names, causes the RSIC distribution lists to fluctuate somewhat over the years, but on an average they remain fairly constant. Currently, more than 1000 people receive the RSIC Newsletter, each of whom may also be on one or more categories of the RSIC distribution. Approximately 270 people have furnished individual profiles so that they will routinely receive shielding information of interest to them through RSIC's SDI service.

During the 12 months of 1970 RSIC made the following additions to the literature store and to the code and data collections:

604 bibliographic entries were made to the storage and retrieval system.

44 computer codes were packaged.

25 code packages in the collection were updated, several of which included major modifications and extensions to the program.

11 new hardware versions of existing code packages were fed back into RSIC by installations where conversions were made.

5 additional data library sets were collected and packaged with documentation.

3 updates to existing data packages were made.

During this same period, RSIC received 2149 letters of request – approximately 179/month. Of these 1343 letters requested information on data or code packages or the packages themselves, and 806 letters requested general shielding information. An analysis of the more than 5000 activities required to prepare responses to these letters is as follows:

1. Activities connected with the codes collection:

   573 fully documented code packages were shipped.

   74 packages of updating material were shipped.

   12 source programs in the form of computer listings were mailed.

   151 sample problems (input and output) were mailed, including some special problems run by the RSIC staff members to satisfy a particular customer request.

   64 abstracts of shielding code packages were sent.

   202 cases in which staff members spent considerable time in trouble-shooting specific codes as a requester was learning how to use a code and in giving advice on the input preparation.

   542 instances in which assistance was given in the selection of the computer code to fit the requester's problem, his computer, and his capabilities.

2. Activities connected with data-handling:

   185 separate data packages were shipped, including documentation.

   131 separate data-handling activities involving the use of the computer were carried out in connection with NNCSC and the CSEWG subcommittee and with the ORNL cross section steering committee (CSSC).

3. Other activities:

   900 RSIC publications were furnished to requesters.

   1245 additional shielding documents (841 of which were code documents) were mailed to requesters.

   86 packets of RSIC introductory literature were mailed to possible new subscribers.

499 instances were logged in which time was spent in assisting the requester to solve his problem – general advice and counsel.

702 separate miscellaneous requests were filled.

79 separate requests for literature searches were processed.

One hundred ten visitors were welcomed to the Radiation Shielding Information Center, excluding those attending seminar-workshops sponsored by RSIC. Twenty of these visitors were from foreign countries.

3.1.3 Literature Review and Indexing

Scanning of the literature for publications of radiation shielding papers and related articles and for announcements of such publications continued. References to the articles that seem pertinent based on the title are given in each RSIC monthly newsletter.

Approximately 700 papers, reports, and books on reactor and weapons shielding were announced in the Newsletter and subsequently reviewed. About half of them, along with about 150 articles on space and accelerator shielding (also included in the Newsletter), were indexed according to the RSIC subject category lists ("Weapons and Reactor Shielding" and "Space and Accelerator Shielding") and entered into the computerized Storage and Retrieval System (SARIS).

In addition to the above literature, 215 documents describing computer programs for use in shielding research were reviewed, indexed, and announced in the Newsletter.

3.1.4 Storage and Retrieval Information System (SARIS)

Final documentation of the RSIC Storage and Retrieval Information System (SARIS) has been completed[1] and the system is in full operation. A central Authority File permits the system to be used in connection with customers and with documentation. The File contains the following information: the names of the countries identifying the customer and/or documentation, the work area of a customer, the telephone area code of a customer, the names of corporations as customer or as origin of documentation, the names of journals as origin of documentation, and indexing categories for radiation shielding information.

The system includes programs for handling the RSIC distribution lists; it is used to print lists, to print labels for mailing, and to include names and addresses on SDI's and on special questionnaires as required. A Customer Update program is used routinely to add new names or to delete existing ones, and to change addresses and/or telephone numbers when necessary. The Customer Search Program is used to produce various lists which may be sorted alphabetically, numerically, by corporation, by country, or by any combination of these. A computer-produced directory of RSIC customers, printed periodically, is found to be very useful.

As a service to the American Nuclear Society (ANS) Shielding and Dosimetry Division, RSIC maintains an annual membership listing of the Division. It has been useful in membership retention and, in combination with RSIC customer listings, has assisted the Division workers in new membership drives.

The SARIS Document Update and SDI programs produce new bibliographic master files and bibliographies and abstract listings of the updated material for the individual customer profile. The Document Search program produces bibliographies and/or related abstracts for special inquiries upon request.

Two comprehensive bibliographies are published during the year.[9,10] Two changes will be noted in these new documents. For the sake of economy, blank spaces and pages have been "squeezed" and dual columns with a 60% reduction have been inaugurated. For the convenience of the user, the Author Index Edit now lists the pertinent subject categories in ascending order, each category followed by all related accession numbers.

Formerly, each bibliography was complemented by a book of abstracts of the same literature.[11] Since retrospective searches are now available, in addition to the routine SDI service, the publishing of the abstracts as a routine matter has been discontinued. As an additional economy move, RSIC-originated publications are now distributed on a request basis only and are not sent routinely to all customers who have indicated a special interest in that particular field. These publications will continue to be announced in the RSIC Newsletter as available from RSIC and will be announced in Nuclear Science Abstracts (NSA) as available from the National Technical Information Service (NTIS).

With the advent of SARIS, the SDI program was extended to provide summary cards which serve as a quick subject index to the associated SDI abstracts. When filed to precede the abstract, the card is a useful reference. The SDI service is currently in routine operation with estimated cost at $0.04-$0.05 per drop, where the drop often includes two cards of output.

As a standard procedure, the SDI service distribution is reviewed annually. Existing profiles are mailed to the individuals concerned for review and possible revision.

All RSIC customers are apprised of the SDI service and each is invited to submit an individual profile of primary interests. Currently, 264 profiles are serviced through SARIS, an increase of 18% during the year.

Input to the system is either keypunched or typed on the MT/ST typewriter and run through the Digi-Data Converter, whichever way is deemed faster at a given time. Information prepared by both methods may be mixed through the MT/ST Conversion program. Either tape or card input is permitted. SARIS now will allow, through proper setup, several operations to be performed by one pass through the computer. The input data conversion may now be followed by updates to the customer and to the document files, which in turn may be followed by searches and edits as required.

3.1.5 Computer Code Collection (CCC)

The computer code collection continues to grow. Thirty-five new shielding code packages and 21 packages of codes peripheral to shielding have been added since last reporting.

The Center continues to provide computer tools and assistance in their use directly to the individual scientist who performs radiation transport calculations. Shipments to requesters averaged 2.5 packages per working day during the year. In addition, much time and effort was given by RSIC staff members in answering technical inquiries concerned with calculational methods, computer codes, and problem solving in general.

A summary of the new shielding codes is given in Table 3.1.1.

3.1.6 The Data Library Collection (DLC)

Three new data libraries were added and several existing ones were updated and improved during the past year. A total of 185 separate shipments of these data sets were made during the year. Abstracts of the current series are being published.[4]

The philosophy behind the packaging and distributing of these data libraries is to preserve and make available in an easily useable form data which may be useful to those utilizing or performing radiation transport calculations. Since this usually involves the use of large computer programs, several of these libraries are multigroup cross sections in the format utilized by many such programs. In addition, a data library may consist of voluminous results from such programs or input data that can be used to reproduce benchmark calculations.

Data libraries on magnetic tape or in other forms are packaged, maintained, and distributed in a manner analogous to computer code distribution. Each library carries a Data Library Collection (DLC) number and is packaged as a unit. In addition to the data, the package contains a handling program and documentation, including an RSIC-prepared abstract. Additions to and revisions of the DLC's are announced in the RSIC Newsletter.

A summary of the DLC data sets is given in Table 3.1.2.

3.1.7 DASA Data Center (DDC) Activities

A representative of RSIC attended the DASA Cross Section Working Group meeting at LASL at which plans were formulated for the development and maintenance of the DASA Cross Section Working Library.

RSIC began serving as a depository for the DASA data, which will be a working library (in ENDF format) subject to modification and revision at as fast a rate as necessary. The key to this approach is the selected evaluator, a person responsible who will authorize the document changes in evaluations for particular elements.

The clearinghouse for the program is RSIC. Initial versions of evaluations are received, processed through checking codes to eliminate obvious format errors, and modified as necessary in collaboration with the evaluator. RSIC is implementing a DASA Phase I data testing program whereby selected reviewers will be provided with listings, output from checking codes, graphics, etc., and asked to perform a review of the data and feed back their comments. These will be relayed to the evaluator and, upon his instruction, appropriate changes will be made.

The data, along with available documentation, are sent to DASA contractors upon request. The users are asked to feed back any comments they have through using the data.

The official DASA library will be maintained at RSIC. Changes to it will be initiated only by the evaluator and each change will be documented so that users can, at any time refer to an identifiable data set when reporting results of their calculations.

It is anticipated that essentially all of the data in the DASA library will eventually be submitted to CSEWG for consideration as input to the ENDF/B master file.

3.1.8 ORNL Cross Section Steering Committee (ORNL-CSSC)

RSIC plays an active role in the ORNL Cross Section Steering Committee (CSSC), which has as its charter the promotion of information exchange and the reduction of duplication of effort in manipulating and using

Table 3.1.1. Computer Code Packages Added to RSIC Collection

CCC No./ Code Name	Contributor[a]	Language and Computer	Radiation Type	Method	Geometry	Ref.	Comments
CCC-131/ANTE 2	MAGI	FORTRAN IV, (A) CDC 6600 (B) IBM 360 (ANTE-BELLM)	n	Adjoint Monte Carlo	Complex, 3-dimens.	DASA-2396, MR-7003, MR-7004/2	Time dependent; combinatorial geometry; reads ENDF/B version I data.
CCC-132/ATTOW	UKAEA/RISLEY	FORTRAN IV & MAP, IBM 7090	n	Multigroup Spinney	2-dimens.	TRG-1466(R)	Removal diffusion; output includes flux prints, neutron currents and detector activations.
CCC-133/UNCSAM 3	UNC	FORTRAN, (A) CDC 6600 (B) CDC 1604	n,γ	Monte Carlo	Complex, 3-dimens.	UNC-5157 & Suppl., UNC-5243	Package includes ENDT, which reads ENDF/B version I cross-section data; time dependent.
CCC-134/2DBS	BNWL	FORTRAN IV, UNIVAC 1108	n	Multigroup diffusion	2-dimens.	BNWL-1291	2-dimensional diffusion-burnup code (2DB) for fast reactor analysis modified for shielding (see also BNWL-640 and 831).
CCC-135/GAMMON	NBS & AI	FORTRAN, (A) IBM 360 (both codes) (B) CDC 1604 (NBS code only)	γ	Moments	Infinite homogeneous medium	NAA-SR-MEMO-11653, NBS Informal Notes	Includes an NBS elementary FORTRAN routine for evaluating coefficient moments and SPENCER to reconstitute a function from a finite number of its moments.
CCC-136/COLLIMATOR	UI	FORTRAN IV & MAP, IBM 7090	γ	Monte Carlo	Finite cylinders with multiregions symmetric about the axis	NRDL-TRC-68-6	Collimated ^{60}Co source; energy spectrum and angular distribution calculations.
CCC-137/RIBD	BNWL	FORTRAN, UNIVAC 1108	γ	Fission-product inventory	Point calculation	BNWL-962, DUN-4136, RL-NRD-610	RIBD library incorporates fast fission yield factors and fast-neutron burnup cross sections; general purpose, multiple path, multiple chain, grid processor.
CCC-138/PIGG	IFA/Norway ENEA CPL	FORTRAN 63, CDC 3600	n	Multigroup spherical harmonics	1-dimens., slabs or cylinders	KR-129	P_1 radiation transport code similar to P1MG; differs in resonance absorption treatment; includes epithermal spectrum part of BIGG II.
CCC-139/CONSTRIP V	RTI	FORTRAN IV, IBM 360	γ	Numerical integration	Vertical barrier, finite plane source	R-OU-266	Uses Monte Carlo differential dose transmission data in structure analysis of fallout studies.
CCC-140/DIPHO	CLA/France ENEA CPL	FORTRAN IV, IBM 360	γ	Monte Carlo with exponential transformation	Isotropic point source in infinite medium	ORNL-tr-2349	Differential energy flux calculation in a photon scattering problem.
CCC-141/RAC	JAERI/Japan ENEA CPL	FORTRAN II, IBM 7090	n,γ	Spinney	Multiregion slabs or cylinders	Informal notes	Removal diffusion; attenuation and heat generation.
CCC-142/MERCURE 3	CEA/FAR/France	FORTRAN IV, IBM 360	γ	Kernel integration	3-dimens.	ORNL-tr-1812 (CEA-R-3264)	Straight-line attenuation.

Table 3.1.1. Computer Code Packages Added to RSIC Collection

CCC No./ Code Name	Contributor[a]	Language and Computer	Radiation Type	Method	Geometry	Ref.	Comments
CCC-143/GREAT-GRASS	RRA	FORTRAN IV, (A) IBM 1130 (B) IBM 360	γ	Monte Carlo	2 regions with cylindrical symmetry	RRA-T78, RRA-T79, RRA-M84	Fallout shielding; portions of procedure taken from COHORT; Performs γ-ray scattering calculations in air-ground geometry.
CCC-144/TIMOC	EURATOM ENEA CPL	FORTRAN II & FAP, IBM 7090 (TIMOC); FORTRAN IV IBM 360 (CODAC)	n	Monte Carlo	Complex, 3-dimens.	EUR-4536, EUR-4519, EUR-4521	Includes O5R geometry routine; solves energy and time-dependent, homogeneous or inhomogeneous transport equation; treats absorption and commonly used scattering kernels; includes CODAC data processor from ENDF/B file.
CCC-145/SORS	UCRL	FORTRAN IV, CDC 6600 (A) Photon version (B) Neutron version	γ,n	Monte Carlo	Complex, 2- or 3-dimens.	UCRL-50358, UCRL-50532	Code version (A), photon calculation, version (B), neutrons; splitting with Russian roulette is only variance-reduction technique used.
CCC-146/UNAMIT	NASA/LRC	FORTRAN IV, (A) IBM 7090 and (B) IBM 360 (C) CDC 1604	n,γ	Shield weight optimization	1-dimens., spherical	NASA-TM-X-2048	Code uses an exponential attenuation, secondary-production analytic model.
CCC-147/EXDOSE	BNWL	FORTRAN, UNIVAC 1108	γ	Fission-product inventory and numerical integration	Plane	BNWL-811	RIBD (CCC-137) is built into the program for fission-product inventory; dose is calculated at a downwind point; designed for estimating accident consequences.
CCC-148/SPARES	BSRL/Seattle	FORTRAN IV, IBM 360				AS-2807	Space radiation environment and shielding code system.
Several codes							
(A) ELMC		FORTRAN IV, IBM 360	e	Monte Carlo	Multilayer slab	AS-2807	Calculates electron flux penetrating a shield; produces data for input to EPEN.
(B) EPEN		FORTRAN IV, IBM 360	e	Kernel integration	1-dimens.	AS-2807	Calculates the absorbed dose at a point caused by electrons penetrating a shielding system.
(C) BREMS		FORTRAN IV, IBM 360	brems.	Kernel integration	Multilayer slab	AS-2807	Calculates the dose absorbed at points in a space system from bremsstrahlung produced by the incident electrons.
(D) HEVAPART		FORTRAN IV, IBM 360	nucleon	Straightahead scattering	Multilayer slab	AS-2807	Calculates the absorbed radiation dose and energy spectrum resulting from heavy charged particles that penetrate a shield.
(E) SECPRO		FORTRAN IV, IBM 360	sec.p, n,γ; nucleon	Kernel integration	Multilayer slab	AS-2807	Calculates radiation dose absorbed from radiation resulting from a proton-flux incident on a radiation shield; secondary proton penetration calculation.
(F) TANDE		FORTRAN IV, IBM 360	p,e	Trajectory and environment		AS-2807	Trajectory and environment code; calculates proton and electron flux or dose encountered by earth-orbiting satellites.

Table 3.1.1. Computer Code Packages Added to RSIC Collection

CCC No./ Code Name	Contributor[a]	Language and Computer	Radiation Type	Method	Geometry	Ref.	Comments
CCC-149/GASOUT	ANL	FORTRAN IV, IBM 360		Fission-product inventory		ANL-7534	Calculates gaseous fission-product release for a ZPR-6 and -9 basis accident; time dependence.
CCC-150/MAP	WANL	FORTRAN IV, CDC 6600, (Compatible with IBM 360 and UNIVAC 1108)	n,γ	Numerical integration	Complex	WANL-TME-2706	MAP solves for the nuclear radiation transport to a detector surface from an energy- and angular-dependent surface source defined by the surface leakage data of a DOT (CCC-89C) discrete ordinate transport solution in r,z geometry; photon absorption data from GAMLEG or other generator.
CCC-151/DOT2DB	GE/Sunnyvale	FORTRAN IV, GE 635	n,γ	Multigroup discrete ordinates and diffusion	2-dimens.	GEAP-13537 & informal notes	DOT (CCC-89) and 2DBS (CCC-134) linked; either calculational option may be used with a single cross-section library and identical input format; can generate a flux guess from the diffusion calculation for the transport theory calculation; may use transport theory for some energy groups and diffusion theory for the remainder.
CCC-152/ALGAM	ORNL	FORTRAN IV, IBM 360	γ	Monte Carlo	Truncated elliptic cylinders and cones	ORNL-2250, ORNL-4584, & informal notes	Includes DLC-7C cross-section library; estimation of internal dose in a phantom man.
CCC-153/ASFIT	BARC/India	FORTRAN, CDC 3600	n,γ	Semi-analytic technique	Multilayer slab	Informal notes	Solves the Boltzmann transport equation for finite 1-dimensional systems with severe anisotropy in the scattering process.
CCC-154/ANDYMG3	LASL	FORTRAN IV, CDC 6600 and UNIVAC 1108	n,γ	Multigroup Monte Carlo	Complex	LA-4539	Solves time-dependent particle and photon transport for general geometries; cross sections are read in S_n format with scattering up to P_3; particle splitting and termination routines permit negative weights; library of reaction cross sections provided.
CCC-155/ELTRAN	Sandia	FORTRAN, CDC 3600	e	Monte Carlo	Multilayer slab	SC-TM-68-713	Computes energy deposition distribution of stopped electrons or the spectral properties of electrons transmitted by a thin slab.
CCC-156/MECC-3	ORNL-N	FORTRAN IV, IBM 360	p,n; charged pions	Monte Carlo intranuclear cascade	General	ORNL-4564	Medium-energy intranuclear cascade; incident particles are protons or neutrons (100–3500 MeV) or charged pions (1–2500 MeV).
CCC-157/MEVDP	AFWL, NAR, MM/Denver	FORTRAN IV, CDC 6600	p,α and (areal density) data for secondaries	Straightahead scattering	Complex	AFWL-TR-69-68, -161	MEVDP generates spatially oriented arrays of material type and associated thicknesses which are encountered by radiation traveling toward a dose point within any complex geometry shielding configuration; the computerized Anatomical Model Man is included in the package.

Table 3.1.1. Computer Code Packages Added to RSIC Collection

CCC No./ Code Name	Contributor[a]	Language and Computer	Radiation Type	Method	Geometry	Ref.	Comments
CCC-158/MAGNA	IFA/Norway ENEA CPL	FORTRAN, CDC 1604 and 3600	γ	Kernel integration	Point, cylinder cylindrical shells	KR-111, IFA-RPS-82	Dose rates are calculated at points in and around a complex arrangement of point or cylindrical γ-ray sources and slab, cylinder, or cylindrical shell shields; multilayer buildup factor used.
CCC-159/ORPHEE VI	CEA/FAR/France	FORTRAN IV, IBM 360	n	Kernel integration	Cylinders	ORNL-tr-2357 (CEA-N-1224)	Fast-neutron attenuation in a structure consisting of layers of water and dense material.
CCC-160/PICA	ORNL-N	FORTRAN IV, IBM 360	photon	Monte Carlo intranuclear cascade	General	Informal notes	Designed to handle photon-nucleus (atomic number > 4) collisions in approximate energy range of 30–450 MeV.
CCC-161/NMTC	ORNL-N	FORTRAN IV, IBM 360	p,n,π^+; π^-,π^+,π^-	Monte Carlo intranuclear cascade	General	ORNL-4606	Computes transport of nucleons <3.5 GeV and muons and charged pions <2.5 GeV; includes modified O5R, and MECC-3 and EVAP-4 as subroutines.
CCC-162/FPIP	WANL	FORTRAN IV, CDC 6600	γ,β	Fission-product inventory		WANL-TME-537 Rev.1	Used to predict fission-product inventories and source strengths associated with operation of the NERVA reactor.
CCC-163/FISSP-CLOUD	Sandia	FORTRAN IV, (A) CDC 6600 (B) IBM 360	γ	Fission-product inventory and kernel integration	Simple, 3-dimens.	SC-RR-70-338	For calculating dose from radioactivity released to the atmosphere; FISSP and CLOUD are packaged together.
CCC-164/NAC	NASA/LRC	FORTRAN IV, (A) IBM 360 (B) IBM 7090/94	n,γ activation source	Analytical solution of activation equations		NASA-TM-X-52460	A data library is included; used to calculate post-irradiation activation of an experimental capsule irradiated in a test reactor.
CCC-165/DOSE1	ORNL-P	FORTRAN IV, IBM 360	γ	Kernel integration	Arbitrary finite geometry of source, absorber and target	ORNL-TM-3398	Dosimetry calculation.

[a]Contributors: AFWL, Air Force Weapons Laboratory, Kirtland Air Force Base, Albuquerque, N.M.; AI, Atomics International, Canoga Park, California.; ANL, Argonne National Laboratory, Chicago, Ill.; BARC/India, Bhabha Atomic Research Centre, Bombay, India. BNWL, Battelle Memorial Institute, Pacific Northwest Laboratory, Richland, Wash.; BSRL/Seattle, Boeing Space Research Laboratory, Seattle, Wash.; CEA/FAR/France, CEA/CEN Fontenay-aux-roses Nuclear Research Center, France; CLA/France, Central Laboratory and Schools of Armament, Ministry of the Army, France; ENEA CPL, European Nuclear Energy Agency (ENEA) Computer Programme Library, Ispra, Italy; EURATOM, European Atomic Energy Community (EURATOM), Joint Research Centre (CCR), Ispra, Italy; GE/Sunnyvale, General Electric, Sunnyvale, Calif.; IFA/Norway, Institutt for Atomenergi, Kjeller Research Establishment, Kjeller, Norway; JAERI/Japan, Japan Atomic Energy Research Institute, Tokai, Iberaki, Japan; LASL, Los Alamos Scientific Laboratory, Los Alamos, N.M.; MAGI, Mathematical Applications Group, Inc., White Plains, N.Y.; NBS, National Bureau of Standards, Washington, D.C.; ORNL, Oak Ridge National Laboratory, Oak Ridge, Tenn.; ORNL-N, ORNL Neutron Physics Division; ORNL-P, ORNL Physics Division; RRA, Radiation Research Associates, Inc., Fort Worth, Tex.; RTI, Research Triangle Institute, Research Triangle Park, N.C.; Sandia, Sandia Laboratories, Albuquerque, N.M.; UCRL, University of California, Lawrence Radiation Laboratory, Livermore, Calif.; UI, University of Illinois, Urbana, Ill.; UKAEA/Risley, United Kingdom Atomic Energy Agency, Risley Establishment, Warrington, Lancs.; UNC, United Nuclear Corporation, Elmsford, N.Y.; WANL, Westinghouse Electric, Astronuclear Laboratory, Pittsburgh, Pa.

Table 3.1.2. Summary of RSIC-DLC Data Sets

Data Library Designation	Contributor[a]	Form	Data Type/Computer Code/Component
DLC-1/LEP	ORNL-N	16-mm microfilm, magnetic tape, machine listings	Bertini's low-energy intranuclear cascade results; output from ANALYSIS Codes I and II from EVAP (ORNL-3433).
DLC-2/99G	ORNL-N	Magnetic tape	99-group $\leq P_8$-expanded neutron cross sections for input to ANISN/DOT/DTF-IV/MORSE; produced from ENDF/B category I version II data by SUPERTOG (1971); energy range from 14.92 MeV to 0.414 eV.
DLC-4/HPIC	ORNL-N	Magnetic tape	Gama-ray photoelectric and pair-production data in OGRE format (ORNL-3805); data same as in DLC-7.
DLC-5/HALLMARK	ORNL-N	Magnetic tape	Output from DOT, O5R-ACTIFK, and OGRE; Straker's time-dependent air-over-ground results for point isotropic sources; handling energy spectrum; neutron sources range from 15 MeV to 3.3 keV; results include neutron and secondary gamma-ray fluxes (ORNL-4289, vol. II).
DLC-7/HPIC	LRL	Magnetic tape	Livermore gamma-ray interaction data in ENDF/B format; recommended as ENDF/B reference data; covers elements having Z values of 83, 86, 90, 92, and 94, and gamma rays having energies in the range from 1 keV to 100 MeV (UCRL-50400, vol. VI; UCRL-50174 Sect. II, May 1969).
DLC-8A/BP-3	ORNL-N	Cards	22-group P_5-expanded cross sections for air in the ANISN/DOT/MORSE format; data used by Straker for Benchmark Problem No. 3; neutron spectrum constructed from point sources in infinite air covering energy ranges from 15 MeV to thermal (ORNL-RSIC 25).
DLC-9/FARS	ORNL-N, CTC	Magnetic tape	P_8-expanded coupled cross sections (104 neutron groups, 18 gamma-ray groups) for H, C, N, O, Mg, Al, Si, Ca, and Fe; data format for ANISN/DOT/DTF-IV/MORSE; compiled by F. Schmidt for concrete calculations (ORNL-RSIC-26); neutron energy range, 15 MeV to thermal; gamma-ray energy range, 10-0.02 MeV.
DLC-10/AVKER	ORNL-N	Magnetic tape	Data library of neutron fluence-to-kerma factors for many elements; retrieval program will compute energy group values for any composition for use with group fluence to calculate dose or heating (ORNL-TM-2558); neutron energy ranges from 19.2 MeV to 0.023 eV.
DLC-11/RITTS	ORNL-R ORNL-N CTC	Magnetic tape	P_3-expanded coupled microscopic cross sections (100 groups, 21 gamma-ray groups) for H, C, O, N, Na, Mg, P, S, Cl, K, and Ca; 100-group neutron cross-section set alone also provided, plus coupled macroscopic cross sections for standard man, skin, bone, tissue, brain, lung, red marrow, and muscle; data format for ANISN/DOT/MORSE; neutron energy range, 15 MeV to thermal; gamma-ray energy range, 14 to 0.01 MeV (ORNL-TM-2291).
DLC-12/POPLIB	CTC ORNL-N	Magnetic tape	Compendium of neutron-induced secondary gamma-ray yield and production cross-section data; data library for PSR-11/POPOP4 code; current library has 233 data sets (1971) (CTC-INF-1004).
DLC-13/GARLIB	NASA-LE	Magnetic tape	32-group resonance-region neutron capture and scattering cross sections for moderated tungsten and uranium slabs; produced by by the GAROL code; group fluxes calculated by GAROL also included for further collapsing of the group structure; energy range, 1.234 keV to 0.414 eV (NASA TM X-1909).
DLC-14/AIR	ORNL-N	Magnetic tape	ANISN input data for a P_5S_{16} coupled (22 neutron groups, 18 gamma-ray groups) transport calculations for a 12.2- to 15-MeV point source in air; output from ANISN run also provided; allows users to repeat the Straker-Gritzner infinite-air calculations (ORNL-4464).
DLC-15/STORM-ISRAEL	LASL	Magnetic tape	Los Alamos gama-ray interaction data in ENDF format for elements from Z=1 to 100; energy range, 1 keV to 100 MeV; essentially equivalent to DLC-7 but has additional data for many derived cross sections (Nuclear Data, A7, 565-681).
DLC-16/COBB	ORNL-R ORNL-M	Magnetic tape	123-group P_3-expanded neutron cross sections for input to XSDRN; produced from ENDF/B category I version II data by SUPERTOG-THERMOS (30 thermal groups); energy range, 14.92 MeV to thermal.

[a]Library contributors: CTC, Computing Technology Center, Union Carbide Corp., Oak Ridge, Tenn.; NASA-LE, NASA Lewis Research Center, Cleveland, Ohio; ORNL-M, Mathematics Division, ORNL-N, Neutron Physics Division; ORNL-R, ORNL Reactor Division; LRL, Lawerence Radiation Laboratory, Livermore, Calif. LASL, Los Alamos Scientific Laboratory, Los Alamos, N. M.

cross-section data at ORNL. Its membership consists of personnel from the Mathematics, Neutron Physics, and Reactor Divisions. The membership includes ORNL representatives to the CSEWG and thus a substantial proportion of the work sponsored by CSSC is related to tasks for CSEWG, described in a following section.

An example of the type of effort sponsored by CSSC is the INDEX System[12] now available at ORNL. The contents of several neutron data libraries in production use at ORNL have been compiled into a data library index. This information has been entered into the computer in a form accessible to a search and manipulation program.

RSIC acts as the local clearinghouse for all ENDF data and codes distributed to ORNL by NNCSC. The Center also promotes, through CSSC, the various computer programming efforts which are useful to the program of the Shielding Subcommittee of CSEWG. For example, as a means of acquiring evaluated data in the UKAEA Nuclear Data Library, the computer code UKE was modified to translate data in UK format to ENDF/B Version II format.

3.1.9 Shielding Subcommittee, Cross-Section Evaluation Working Group

RSIC continues to collaborate with NNCSC at Brookhaven National Laboratory and the CSEWG Shielding Subcommittee. The Center's role in this activity is to assist in the acquisition, checkout, and review of "shielding" cross sections in ENDF format which will ultimately be placed in the ENDF/B file. In this context, "shielding" cross sections are evaluations performed in the shielding radiation effects or weapons community which are likely to have an emphasis on gamma-ray production cross sections, gamma-ray interaction cross sections, and neutron cross sections in the energy range of interest for shielding with detailed energy and angular distribution resolution.

Thus far, ten evaluations have been received by RSIC, processed through checking codes, modified to conform to the ENDF Version II format[13] as necessary, and forwarded to NNCSC, which will prepare and distribute a packet for Phase I testing. To assist in preparation of Phase I testing materials, RSIC, through the ORNL-CSSC, helped coordinate the updating of computer codes PLOTFB and CHECKER to handle gamma-ray production data (ENDF files 12-16) in the new formats. The revised codes are now at NNCSC.

The future efforts of the Shielding Subcommittee will focus on Phase II Integral Data testing of the "shielding" evaluations.

References

1. J. G. Jones, D. K. Trubey, and J. Gurney, *RSIC Storage and Retrieval Information System (SARIS)*, ORNL-TM-2719 (1971); J. G. Jones and R. O. Green, *Radiation Shielding Information Center Program Set-Up Instruction Manual*, CTC-INF-1017 (1971); J. G. Jones, R. O. Green, and S. L. Yount, *RSIC User Documentation*, CTC-48 (1971).

2. Betty F. Maskewitz, *Abstracts of Digital Computer Code Packages Assembled by the Radiation Shielding Information Center*, ORNL-RSIC-13, Volumes I, II, and III.

3. B. F. Maskewitz, *Abstracts of the Peripheral Shielding Code Packages Assembled by the Radiation Shielding Information Center*, ORNL-RSIC-31 (1971).

4. R. W. Roussin and J. B. Wright, *Abstracts of the Data Library Packages Assembled by the Radiation Shielding Information Center*, ORNL-RSIC-30 (1971).

5. B. F. Maskewitz and V. Z. Jacobs, *A Review of the Monte Carlo Method for Radiation Transport Calculations (Collected Papers of a Seminar, October 5-7, (1970)*, ORNL-RSIC-29 (1971).

6. *ANS Standard – A Code of Good Practices for the Documentation of Digital Computer Programs*, prepared by Subcommittee 10, ANS Standards Committee. ANS-STD-2-1967. Approved December 5, 1967.

7. *ANS Standard – Recommended Programming Practices to Facilitate the Interchange of Digital Computer Programs*, prepared by Subcommittee 10, ANS Standards Committee. ANS-STD-3-1971. Approved April 1, 1971.

8. A. E. Profio, editor, *Shielding Benchmark Problems*, ORNL-RSIC-25 Supp. 1 (ANS-SD-9 Supp 1) (1970).

9. H. C. Claiborne, R. W. Roussin, and J. Gurney, *Bibliography, Subject Index, and Author Index of the Literature Examined by the Radiation Shielding Information Center (Reactor and Weapons Radiation Shielding)*, Vol. III, ORNL-RSIC-5 (1971).

10. M. P. Guthrie, R. G. Alsmiller, Jr., and J. Gurney, *Bibliography, Subject Index, and Author Index of the Literature Examined by the Radiation Shielding Information Center, Space and Accelerator Shielding*, ORNL-RSIC-11, Rev. 2 (1970).

11. *Abstracts of the Literature Examined by the Radiation Shielding Information Center (Space and Accelerator Shielding)*, ORNL-RSIC-12, Vol. 1, Rev. (1970).

12. J. L. Lucius, J. D. Jenkins, and R. Q. Wright, *The INDEX Data System: An Index of Nuclear Data Libraries Available at ORNL*, ORNL-TM-3334 (March 29, 1971).

13. M. K. Drake, Editor, *Data Formats and Procedures for the ENDF Neutron Cross Section Library,* BNL 50274 (ENDF 102, Vol. 1); and D. J. Dudziak, *ENDF/B Formats and Procedures for Photon Production and Interaction Data,* LA-4549 (ENDF-102, Vol. II).

3.2 THE SPACE SHIELDING HANDBOOK[1]

R. T. Santoro H. C. Claiborne
R. G. Alsmiller, Jr. J. Barish[2]

Preparation of the Space Shielding Handbook, which will summarize the available information on the shielding of manned space vehicles against protons and alpha particles in space, has continued. The handbook is intended primarily for nonexperts and is expected to be most useful to mission planners who must decide with little effort whether a radiation hazard is likely to exist during a specific mission. It will also serve as a useful starting point for obtaining more adequate information about the shielding required when a radiation hazard is thought to exist on a specific mission.

Many space shielding calculations have been published and are available, but to ensure uniformity and consistency throughout the handbook, a large majority of the calculated results that will be contained in the handbook are being generated specifically for the handbook. The calculational model that is being used is that of a 300-cm inside diameter spherical shell shield of a specified material and thickness with a 30-cm-diameter tissue sphere at the center. This configuration simulates only very approximately a manned space vehicle, but it does serve to illustrate many of the significant features in spacecraft shield design.

Calculations in this configuration are being made to estimate the absorbed dose and dose equivalent at the center of the simulated astronaut (tissue sphere) when solar-flare protons and alpha particles and Van Allen belt protons are incident on the shield. The calculations are being made with two computer codes: the Nucleon-Meson Transport Code NMTC[3] and the Transport of Alpha and Proton Primaries Code TRAPP.[4]

NMTC makes use of Monte Carlo methods to take into account secondary-particle production and transport, and gives the absorbed dose and dose equivalent at the center of the tissue sphere when protons are incident on the shield. NMTC does not, however, treat incident alpha particles. Contributions to the dose arising from the primary ionization and the secondary-radiation components, including secondary protons, heavy ions, charged and neutral pions, muons, electrons, positrons, and photons, are computed. These calculations provide an accurate and detailed description of the dose received by the "astronaut."

TRAPP gives the absorbed dose and dose equivalent at the center of the tissue sphere for incident protons and alpha particles. In this code, only the contribution to the dose from primary ionization is considered; that is, particle production by nuclear interactions is neglected. Results may be obtained showing the effects of absorption of the incident radiation through nuclear interactions of the radiation both in the shield and in tissue. For all elements except hydrogen, nonelastic proton and alpha-particle cross sections are used. For hydrogen, absorption is treated by using the total cross section.

Examples of typical results for inclusion in the handbook are shown in Fig. 3.2.1 and in Table 3.2.1. Figure 3.2.1 gives the dose equivalent at the center of the tissue sphere vs shield thickness when a solar-flare proton spectrum, with 100 MV characteristic rigidity and 10^9 protons/cm^2 with energy >30 MeV, is incident on an aluminum shield. The solid and dashed lines give the results obtained using TRAPP and show the effects of exclusion and inclusion of the absorption due to nuclear interactions, respectively. Also plotted are the dose equivalent due to primary ionization and the total dose from primary plus all secondary radiation, computed with NMTC for aluminum shield thicknesses of 5, 20, and 35 g/cm.[2] The error bars on these data are due to the statistics of the Monte Carlo calculation. These data represent the dose equivalent averaged over a 3-cm-radius sphere at the center of the tissue sphere.

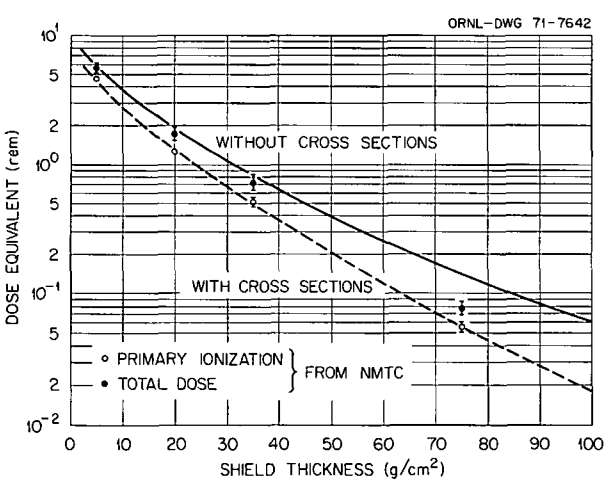

Fig. 3.2.1. Dose Equivalent at the Center of the Tissue Sphere vs. Aluminum Shield Thickness for an Incident Solar-Flare Proton Spectrum with a Characteristic Rigidity of 100 MV and 10^9 protons/cm^2 with Energy > 30 MeV.

Table 3.2.1. Absorbed Dose and Dose Equivalent at the Center of the Tissue Ball for Incident Solar-Flare and Van Allen Belt Spectra

Incident Spectrum	Shield	Thickness (g/cm^2)	NMTC[a]				TRAPP[b]			
			Absorbed Dose		Dose Equivalent		Absorbed Dose		Dose Equivalent	
			Primary	Total	Primary	Total	With Cross Sections	Without Cross Sections	With Cross Sections	Without Cross Sections
			(rads)		(rems)		(rads)		(rems)	
100-MV Solar Flare	Al	20	1.08	1.26	1.22	1.73	1.15	1.70	1.32	1.96
	Al	35	0.46	0.54	0.52	0.73	0.43	0.73	0.48	0.83
			(rads/day)		(rems/day)		(rads/day)		(rems/day)	
1500-NM VAB[c] 30° Circular Orbit	Poly[d]	20	5.72	6.89	6.22	8.61	5.91	9.20	6.52	10.15
240-NM VAB[c] 30° Circular Orbit	Al	20	0.016	0.022	0.018	0.027	0.018	0.026	0.019	0.029

[a]Nucleon-Meson Transport Code.
[b]Transport of Alpha and Proton Primaries Code.
[c]Van Allen Belt.
[d]Polyethylene.

For the values of shield thickness studied with NMTC, the total dose falls between the curves obtained using TRAPP. Thus, at least for the cases shown in Fig. 3.2.1, a conservative estimate of the dose equivalent may be obtained from the primary-ionization contribution, ignoring the effects of particle absorption through nuclear interactions. However, this may not always be the case.[5,6]

Summarized in Table 3.2.1 are the absorbed dose and dose equivalent at the center of the tissue sphere for selected solar-flare and Van Allen belt spectra obtained using TRAPP and NMTC. The incident Van Allen belt spectra were obtained from the code TRECO.[7] The NMTC results represent the dose averaged over the 3-cm-radius sphere at the center of the tissue sphere. In all cases shown in Table 3.2.1, the absorbed dose and dose equivalent computed using TRAPP and neglecting nuclear absorption represent a conservative estimate of the absorbed dose and dose equivalent as given by NMTC.

References

1. Work funded by the National Aeronautics and Space Administration under Orders W-12792 and H-38280A.
2. Mathematics Division.
3. W. A. Coleman and T. W. Armstrong, *The Nucleon-Meson Transport Code NMTC,* ORNL-4606 (1970).
4. This code is not yet available for general distribution.
5. K. A. More and O. L. Tiffany, "Comparison of Monte Carlo and Ionization Calculations for Spacecraft Shielding," *Proceedings of the Symposium on the Protection Against Radiation Hazards in Space, Gatlinburg, Tennessee, November 5-7, 1962,* TID-7652, p. 682.
6. K. A. More and O. L. Tiffany, "Cosmic-Ray Shower Production in Manned Space Vehicles – Copper," *Second Symposium on Protection Against Radiations in Space, Gatlinburg, Tennessee, October 12-14, 1964,* NASA-SP-71, p. 183.
7. "Data Users' Note: TRECO, An Orbital Integration Computer Program for Trapped Radiation," National Space Science Data Center, Goddard Space Flight Center, NASA, NSSDC-68-02 (1968).

3.3 BIBLIOGRAPHY, SUBJECT INDEX, AND AUTHOR INDEX OF THE LITERATURE EXAMINED BY THE RADIATION SHIELDING INFORMATION CENTER (REACTOR AND WEAPONS RADIATION SHIELDING)[1]

H. C. Claiborne J. Gurney
R. W. Roussin A. B. Gustin

An indexed bibliography is presented of literature selected by the Radiation Shielding Information Center

in the area of Radiation Transport and Shielding against radiation from nuclear reactors, X-ray machines, radioisotopes, nuclear weapons (including fallout), and low energy accelerators. The bibliography was printed by computer from magnetic tape files. In addition to lists of literature titles by subject category, author and key-word indexes are given.

Most of the literature selected was published in the years 1968-1970.

References

1. Abstract of ORNL-RSIC-5 (Vol. III) (July 1971); work partly funded by Defense Atomic Support Agency under subtask PE055.

3.4 BIBLIOGRAPHY, SUBJECT INDEX, AND AUTHOR INDEX OF THE LITERATURE EXAMINED BY THE RADIATION SHIELDING INFORMATION CENTER (SPACE AND ACCELERATOR SHIELDING)[1]

M. P. Guthrie J. Gurney
R. G. Alsmiller, Jr. A. B. Gustin

This bibliography replaces the one previously published as ORNL-RSIC-11 (Rev. 1) in 1967. All of the material included in the previous bibliography, as well as much additional material, is included in this volume. The categories remain the same. In the areas of "space radiation sources" and "cross-section data" only review- and summary-type articles are included, since the literature in these areas is so voluminious that it is impossible to consider all of it. In the areas of "particle transport," "shielding," and "accelerator shielding," it is hoped that all pertinent literature has been included. In the areas of "space shielding," only the literature published after January 1962 has been included since most of the literature published prior to 1962 has been superseded by later work.

The "dose" category is intended to include calculations and experiments on physical dose and calculations on biological dose, that is, flux-to-dose conversions, etc. It specifically does not include the large amount of very significant experimental work that is being done in the general area of radiation effects on biological systems.

References

1. Abstract of ORNL-RSIC-11, Rev. 2 (May 1970); work partly funded by National Aeronautics and Space Administration.

3.5 ABSTRACTS OF THE LITERATURE EXAMINED BY THE RADIATION SHIELDING INFORMATION CENTER (SPACE AND ACCELERATOR SHIELDING)[1]

M. P. Guthrie J. Gurney
R. G. Alsmiller, Jr. A. B. Gustin

The abstracts included in a loose-leaf binder cover all the space and accelerator shielding documents that are both in the literature store of the Radiation Shielding Information Center and in an RSIC bibliography for these fields. Although most of the abstracts were taken directly from the published documents, some were written by the reviewers for RSIC. These are limited to documents which either did not contain abstracts or contained abstracts that were not sufficiently informative. Only unclassified abstracts are included; all are subject to revision or replacement.

References

1. Abstract of ORNL-RSIC-12, Vol. I, Rev. (May 1970); work partly funded by National Aeronautics and Space Administration.

3.6 A REVIEW OF THE MONTE CARLO METHOD FOR RADIATION TRANSPORT CALCULATIONS (COLLECTED PAPERS OF A SEMINAR, OCTOBER 5-7, 1970)[1]

B. F. Maskewitz V. Z. Jacobs
Compilers

This review consists of 18 papers presented at the Monte Carlo Seminar-Workshop held at Oak Ridge, Tennessee, October 5-7, 1970. The papers constitute a current statement of the state-of-the-art of the Monte Carlo method as used to calculate radiation transport and establish the fact that only this method of solving the Boltzmann transport equation is routinely applied to three-dimensional problems.

Several computer codes utilizing the Monte Carlo method were reported. These include: POKER (CEA), ANDY, MONA, and MCP (LASL), FASTER (ART), ANTE (MAGI), ESP and MORSE (ORNL). Currently, FASTER, ANTE and MORSE are available in the Radiation Shielding Information Center for routine distribution. It is expected that others may be included in the near future.

References

1. Abstract of ORNL-RSIC-29 (1970); work partly funded by Defense Atomic Support Agency.

3.7 RECENT DEVELOPMENTS IN THE SHIELDING OF NEUTRON SOURCES[1]

H. C. Claiborne

This paper on recent developments in the shielding of neutron sources is basically composed of two parts. In the first part, the impact of ^{252}Cf on shielding of neutron sources is discussed, the newer methods used for coupled neutron and gamma-ray shielding calculations and shield weight optimization are reviewed, and some shipping cask designs for ^{252}Cf and other transplutonium elements are discussed.

The second part consists of a summary and discussion of the six papers on neutron source shielding that were contributed to the American Nuclear Society Topical Meeting on Neutron Sources and Applications at Augusta, Georgia, 1971. Two papers are about the attenuation properties of various materials for the neutrons from ^{252}Cf and other neutron sources; one compares measurements and calculations for ten different shielded containers for ^{252}Cf; two involve the design of portable neutron source facilities; and one describes the use of tissue equivalent proportional counters for thin shield studies.

References

1. Abstract of ORNL-RSIC-32 (1971); work partially supported by Defense Atomic Support Agency under Subtask PEO55.

3.8 SHIELDING AGAINST NEUTRONS IN THE ENERGY RANGE 15 TO 75 MeV[1]

R. W. Roussin R. G. Alsmiller, Jr.
J. Barish[2]

Coupled neutron and gamma-ray transport calculations have been performed for monoenergetic neutrons normally incident on an infinite slab shield of concrete with 5.5% water content by weight. The composition of concrete is the same as that used in ref. 3 and the method of calculation is the same as that used in ref. 4. The transport of gamma rays produced in interactions by neutrons with energy greater than 15 MeV was ignored but the transport of gamma rays produced by neutrons with energies less than 15 MeV was explicitly treated. In Fig. 3.8.1, for incident neutron energies of 15, 25, 50, and 75 MeV, results of total and gamma-ray dose equivalents are given as a function of relative depth into the slab. For the 50- and 75-MeV incident neutron energies, the gamma-ray dose equivalent was found to be no more than 5% of the total dose equivalent. For the 15- and 25-MeV incident neutron energies, however, the gamma-ray dose equivalent dominates at greater depths into the slab. A conservative

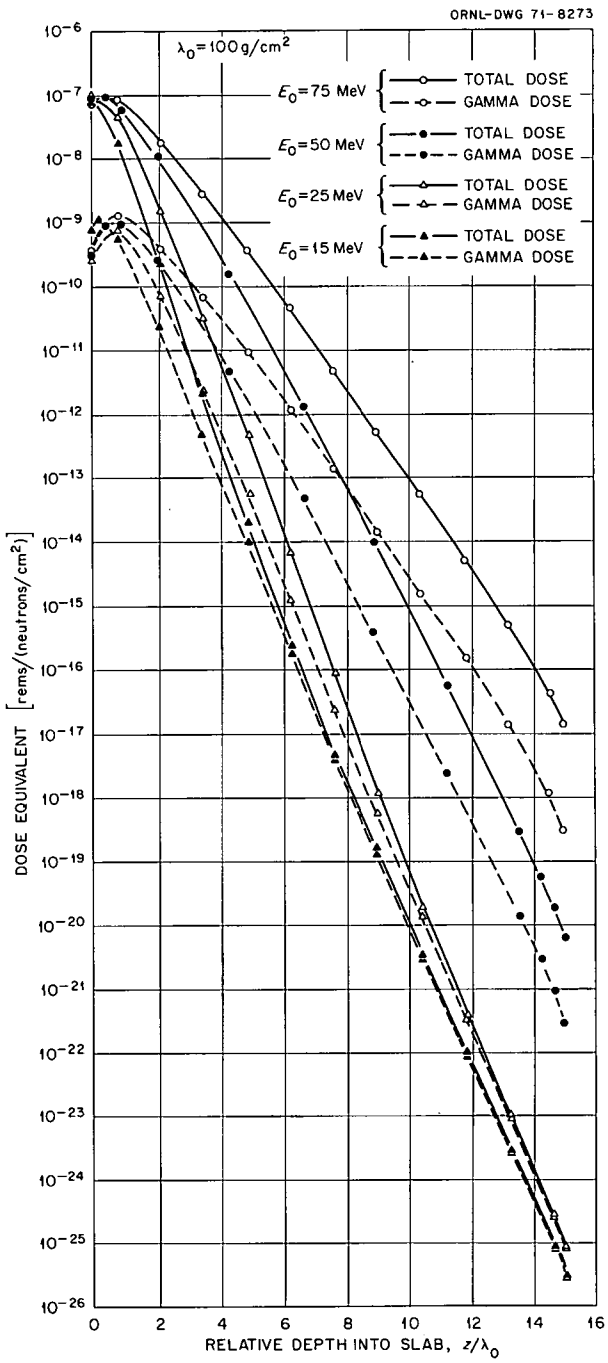

Fig. 3.8.1. Total and Gamma-Ray Dose Equivalents as a Function of Relative Depth in a 650-cm-Thick Concrete Slab for Normally Incident Neutrons of Energies 15, 25, 50, and 75 MeV.

estimate of the effect of including gamma rays produced in interactions with neutrons of energy greater than 15 MeV indicates that the calculated total dose equivalent would increase by no more than 2%.

Réferences

1. Partially funded by Defense Atomic Support Agency under Subtask PEO5501.
2. Mathematics Division.
3. R. W. Roussin and F. A. R. Schmidt, "Adjoint S_n Calculations of Coupled Neutron and Gamma-Ray Transport Through Concrete Slabs," *Nucl. Eng. Des.* **15**, 319-343 (1971).
4. R. G. Alsmiller, Jr., et al. "Shielding Against Neutrons in the Energy Range 50 to 400 MeV," *Nucl. Sci. Eng.* **72**, 213 (1969).

3.9 COMPUTER CODES FOR SHIELDING CALCULATIONS – 1970[1]

B. F. Maskewitz D. K. Trubey

An extensive library of computer codes useful for radiation transport or shielding calculations is available from the Radiation Shielding Information Center (RSIC) at Oak Ridge National Laboratory. In addition to the point kernel, Monte Carlo, and discrete ordinates codes used for neutron and gamma-ray transport calculations, the collection includes cross-section libraries and codes for processing cross sections, for calculating fission product inventories, proton penetration of spacecraft, and electron-photon transport and for analyzing neutron activation detector data to determine spectra.

References

1. Abstract of *Nucl. Eng. Design* **13**, 448 (1970); work partially funded by Defense Atomic Support Agency and National Aeronautics and Space Administration.

3.10 THE INDEX DATA SYSTEM: AN INDEX OF NUCLEAR DATA LIBRARIES AVAILABLE AT ORNL[1]

J. L. Lucius[2] J. D. Jenkins[3]
R. Q. Wright[2]

The contents of several of the basic neutron data libraries in production use at ORNL have been compiled into a data library index. The information has been entered into the computer in a form accessible to a search and manipulation program. A description of the computer program, INDEX, a brief description of the libraries, and an index of the contents of each is given.

References

1. Abstract of ORNL-TM-3334 (1971).
2. Mathematics Division.
3. Reactor Division.

3.11 ADJOINT S_n CALCULATIONS OF COUPLED NEUTRON AND GAMMA-RAY TRANSPORT THROUGH CONCRETE SLABS[1,2]

R. W. Roussin F. A. R. Schmidt[3]

The use of the discrete ordinates computer code ANISN to obtain solutions to the adjoint Boltzmann Equation is discussed. These solutions allow the calculation of transmission factors which give the tissue dose equivalent from particles transmitted through a concrete slab due to an incident source particle in a given energy-angle bin. A coupled set of multigroup (22 neutron, 18 gamma-ray) cross sections allowed the consideration of primary neutron, secondary gamma-ray, and primary gamma-ray transport. Tables of transmission factors are presented which allow the calculation of dose equivalent transmission through concrete slabs from 15 to 200 cm thick for any arbitrary neutron or gamma-ray source energy and angular distribution. The use of these factors is illustrated and comparisons are made with other calculations.

References

1. Research partially sponsored by the U.S. Defense Atomic Support Agency under Subtask PBO5203.
2. Abstract of *Nucl. Eng. Design* **15**, 319 (1971); included in last year's annual as submitted paper.
3. Present address: Institut für Kernenergetik, Universität Stuttgart, Germany.

3.12 PREPARATION OF DATA SETS IN ENDF FORMAT FOR Na, Mg, Cl, AND K FOR USE IN SHIELDING CALCULATIONS[1]

R. W. Roussin V. A. Singletary[2]
S. K. Penny[2] J. B. Wright

Neutron interaction and gamma-ray production cross sections for sodium, magnesium, potassium, and chlorine, which were originally evaluated by Drake et al.,

have been placed in the currently approved ENDF/B formats. This involved a format change for the neutron files and two format changes for the gamma-ray production files. Gamma-ray interaction cross sections were then added to the neutron interaction and gamma-ray production data to obtain a reasonably complete set of data for use in shielding calculations.

References

1. Abstract of ORNL-TM-3429; work partially supported by Defense Atomic Support Agency under Subtask PEO55.
2. Mathematics Division.

3.13 USER'S MANUAL FOR PROGRAMS TO EDIT AND COMBINE DLC-5/HALLMARK CALCULATIONAL RESULTS OF NEUTRON AND SECONDARY GAMMA-RAY TRANSPORT IN AIR-OVER-GROUND GEOMETRY[1]

C. L. Thompson[2] I. J. Brown
R. W. Roussin

The DOT and O5R-ACTIFK-OGRE results generated by E. A. Straker for point isotropic neutron sources in air-over-ground geometry are now being distributed on magnetic tape by the Radiation Shielding Information Center. The format of this data and the six retrieval programs for editing and combining these results are described.

References

1. Abstract of ORNL-TM-3129; work partially supported by the Defense Atomic Support Agency under Subtask PEO5501.
2. Mathematics Division.

3.14 ACTIVITIES OF THE ANS-6 SUBCOMMITTEE ON RADIATION SHIELDING STANDARDS[1]

H. C. Claiborne D. J. Dudziak[2]
N. M. Schaeffer[3]

This is a special report on the activities of the ANS-6 Subcommittee on Radiation Shielding Standards that was prepared for presentation at the special session entitled "Current Status of Nuclear Standards Development" at the 1970 winter meeting of the American Nuclear Society at Washington, D. C.

Included in this report is a brief discussion of the history, organization, and philosophy of the ANS-6 Subcommittee and a report on the accomplishments and current activities of the existing working groups, which include:

ANS-6.1: Shielding Cross Section Standards
ANS-6.2: Benchmark Problems
ANS-6.3: Shield Performance Evaluation
ANS-6.4: Shield Materials
ANS-6.5: Shielding Nomenclature

References

1. Abstract of ORNL-TM-3251; work partially supported by the Defense Atomic Support Agency under Subtask PEO55.
2. Los Alamos Scientific Laboratory, Los Alamos, New Mexico.
3. Radiation Research Associates, Fort Worth, Texas.

3.15 A COMPUTER CODE CENTER – EXPERIENCE AND OPERATIONS[1]

B. F. Maskewitz

The history of organized computer codes exchange within the nuclear industry from 1956 to the present is briefly cited. The Radiation Shielding Information Center (RSIC) experience in collecting, making operable, testing, evaluating, packaging, abstracting and publicizing computer codes is outlined. Emphasis is given to organization, work procedures, and operating philosophy as a guide to the establishment of new computer technology centers.

References

1. Paper presented at the Nuclear Medicine Society *Symposium on the Sharing of Computer Programs and Technology in Nuclear Medicine,* Proceedings published as ORAU-114 (September 1971).

3.16 KERNEL METHODS FOR RADIATION SHIELDING CALCULATIONS[1,2]

D. K. Trubey

A review is given of the development and use of kernel methods in solving problems of radiation shield design and radiation transport. Two classes of kernels are identified: empirical and computational. An analysis of the various techniques is made and examples are given. The relevant computer codes in the collection of the Radiation Shielding Information Center are listed and briefly described.

It is concluded that kernel methods are valuable for quick estimates, hand calculations, checks of transport computer code results, and engineering parameter studies. However, the method can give underestimates for situations which the applied kernel cannot treat properly.

References

1. Research partially supported by the U.S. Defense Atomic Support Agency under Subtask PBO5203.

2. Abstract of *Nucl. Eng. Design* **13**, 423 (1970); included in last year's annual as submitted paper.

3.17 GAMMA-RAY BUILDUP FACTOR COEFFICIENTS FOR CONCRETE AND OTHER MATERIALS[1]

D. K. Trubey

Coefficients for the Berger formula gamma-ray buildup factor are given for ordinary, magnetite, and barytes concrete, air, sand, wood, and lithium hydride. The original data can be reproduced using these coefficients with an error for source energies greater than 2 MeV to generally less than about 5%. Errors for energies 0.5 to 2 MeV may be of the order of 20%.

References

1. Abstract of *Nucl. Appl. Tech.* **9**, 439 (1970); included in last year's annual as submitted paper.

4. Theoretical Studies for Medium- and High-Energy Radiation Shielding

4.0 INTRODUCTION

R. G. Alsmiller, Jr.

In this section theoretical studies of medium- and high-energy particle transport are described. The work is primarily directed at the shielding of manned space vehicles and high-energy accelerators, but the transport methods that are developed for shielding purposes are also applicable in areas other than shielding, and some calculated results in these peripheral areas are also presented. For example, calculations pertaining to the use of π^- mesons in cancer radiotherapy are described.

The major obstacle to performing high-energy nucleon transport calculations is the lack of information on particle-production cross sections from nucleon-nucleus and pion-nucleus collisions, so theoretical studies directed at obtaining more reliable data than those presently available are pursued on a continuing basis. The intranuclear-cascade model of nuclear reactions has been used extensively at energies of less than 3 GeV, and satisfactory results have been obtained. Substantial progress has been made in writing a code to calculate particle-production cross sections at energies greater than 3 GeV using the intranuclear-cascade model, but comparisons between the results obtained with the code and experimental data have not yet been obtained. For space shielding purposes, it is necessary to consider the transport of alpha particles and heavier nuclei through matter, and some very preliminary results on predicting the particle production from high-energy alpha-particle-nucleus collisions have been obtained.

In the area of particle transport, much of the effort during the past year has gone into exploiting the nucleon-meson transport code HETC which became operable just at the beginning of the year. This code, which uses Monte Carlo techniques, is capable of treating particles at energies of the order of several hundred GeV. The differential particle-production cross sections for nucleon-nucleus and pion-nucleus collisions at energies greater than 3 GeV are obtained by extrapolation and must be considered to be very approximate, but calculated results obtained with the code are in good agreement with experimental data on the cascade induced in iron by 29.4-GeV/c protons. The code HETC has been used for both accelerator shielding and space shielding applications. For several years the accelerator shielding program has been directed almost entirely toward providing shield design data for the accelerator under construction at the National Accelerator Laboratory, and the existence of HETC has made it possible to do a variety of calculations for NAL which previously could not be done. In the areas of space shielding and space physics, the code has been used to do several calculations involving galactic cosmic rays. In particular, it has been used to estimate the induced activity and photon albedo spectrum arising from cosmic-ray bombardment of the moon.

The transport of low-energy (of the order of a few MeV) electrons through matter is important in the shielding of manned space vehicles against Van Allen belt electrons. Studies of low-energy electron transport by means of Monte Carlo techniques are available, but because of the poor statistical accuracy which can be obtained in some cases, a nonstatistical method of calculation is needed. To fill this need, studies are in progress to adapt the method of discrete ordinates, which has been used extensively in the low-energy neutron shielding program, to the transport of low-energy electrons.

4.1 CALCULATION OF NUCLEAR REACTIONS FOR INCIDENT NUCLEONS AND π-MESONS IN THE ENERGY RANGE 30 TO 2700 MeV[1,2]

H. W. Bertini

The two-step intranuclear-cascade evaporation approach is used in the calculation of nuclear reactions for incident nucleons and π-mesons in the energy range where the production of π-mesons is important. The model of the target nuclei includes the effects of the diffuse nuclear boundary, the motion of the bound

nucleons, and the exclusion principle. The calculated inelastic cross sections, particle multiplicities, energy spectra, angular distributions, and radiochemical cross sections are compared with experiment, and reasonable agreement is found, in general, over broad incident-particle energy ranges and target mass values. Even through the agreement found in the present set of comparisons is very encouraging, additional comparisons must be made to clearly delineate the areas in which the model may or may not reproduce experimental results.

References

1. Work partially funded by the National Aeronautics and Space Administration under Order H-38280A.

2. Abstract of paper in *Proceedings of the Second International Conference on Accelerator Dosimetry and Experience, Stanford Linear Accelerator Center, Stanford, Calif., Nov. 3-5, 1969*, USAEC Division of Technical Information, CONF-691101, p. 42; included in last year's annual as abstract of a submitted paper.

4.2 RESULTS FROM MEDIUM-ENERGY INTRANUCLEAR-CASCADE CALCULATIONS[1,2]

H. W. Bertini M. P. Guthrie

An appreciable quantity of data has been generated using a medium-energy intranuclear-cascade calculation. Reactions were calculated for incident neutrons, protons, and charged pions on five elements ranging from oxygen to lead. The energy range of the incident nucleons was from 500 to 3000 MeV in 500-MeV steps and, similarly, the energy range of the incident pions was from 500 to 2500 MeV. Data from the cascade and evaporation phases are available. A preliminary version of the computer programs used to generate the data is also available. The final version of the programs will be made available in the near future.

References

1. Work partially funded by the National Aeronautics and Space Administration under Order H-3828OA.

2. Abstract of ORNL-TM-3336 (August 10, 1970); to be published in *Nuclear Physics.*

4.3 HECC-1, A CODE TO CALCULATE HIGH-ENERGY PARTICLE-NUCLEUS REACTIONS BY THE METHOD OF INTRANUCLEAR CASCADES[1]

H. W. Bertini N. B. Gove[2]
A. H. Culkowski[2] M. P. Guthrie

The code HECC-1 (high-energy cascade calculation, version 1) is a preliminary version of a program for calculating the interactions of high-energy (hundreds of GeV) nucleons and π-mesons with complex nuclei via the intranuclear-cascade model. A general description of the approach is given elsewhere.[3] A brief summary and short history are given here.

The basic assumption in the model is that nuclear reactions involving incident particles with sufficient energy (>100 MeV) can be described in terms of individual particle-particle collisions that take place within the nucleus. The life history of every particle that becomes involved in these collisions is followed, using statistical sampling techniques, until the particles escape from the nucleus, or until their energies become so low that they are assumed to be trapped inside. The individual particle-particle collisions are assumed to be free-particle collisions, and free-particle experimental cross sections, when available, are used to calculate the points of collision, the types of collision, and the angles of emission. The types of collision that are included are simple-scattering collisions, charge-exchange scatterings, pion production, and pion absorptions. When free-particle data are not available, either they are calculated, as in the case of the π^0-nucleon reactions,[4] or they are estimated. Various models, described below, are used in the calculation of the pion production processes. Since each one of the particles that emanate from every collision can also collide during its lifetime, a cascade of particles is created within the nucleus as the reaction progresses. In the past, the depletion of nuclear matter during the development of the cascade was not taken into account; i.e., when a collision occurred, a bound nucleon, from those making up the nucleus, was knocked out of the bound state and was added to the cascade, but the resulting change in the density of bound nucleons was not taken into account.

This model yielded reasonable agreement with experimental data for incident particles with energies $\leqslant 3$ GeV.[5,6] But when it was applied at higher energies (>5 GeV), a serious discrepancy with experiment was observed in that many more low-energy particles were predicted than were measured.[7] An attempt to resolve this discrepancy is made in HECC-1 by including the

effects of the depletion of the bound nucleons during the course of the cascade. To this end, the nucleus is divided into a number of regions. The number and the size of the regions are variable and are determined by the input to the code. When a collision occurs in a region, the density therein (and where necessary the density in neighboring regions also) is reduced to account for the fact that one bound nucleon has been removed from that region. It is clear that in order to ascertain which of the cascade particles are affected by this local density reduction, the cascade-particle histories must be followed as a function of time, and hence each history is followed in time as well as through space. Former versions of the model followed each history in space only.[4,5]

With respect to the nuclear properties of the target that are accounted for in the program, only the diffuseness of the nuclear edge is included. The Fermi motion and the nuclear potentials are not taken into account, although they were previously.[4,5] Their incorporation requires a major effort, and they were not put into the present version of HECC because their effects should not greatly influence the answer to the main question to be satisfied by HECC-1; i.e., whether the incorporation of nuclear depletion will resolve the discrepancy observed at energies >5 GeV described above.[7]

Two models are used to describe the particle-particle pion-production reactions. At energies below 3.5 GeV the Sternheimer-Lindenbaum isobar model is used[8,9] and at higher energies the empirical formulas of Ranft are used.[10]

The status of HECC-1 is that the coding is completed, but the program has not yet been tested.

References

1. Work partially funded by the National Aeronautics and Space Administration under Order H-38280A.
2. Mathematics Division.
3. N. B. Gove et al., *High Energy Nuclear Cascades,* ORNL-TM-2627 (June 26, 1970).
4. Hugo W. Bertini, *Phys. Rev.* **131**, 1801 (1963).
5. H. W. Bertini, *Phys. Rev.* **188**, 1711 (1969).
6. K. Chen et al., *Phys. Rev.* **166**, 949 (1968).
7. V. S. Barashenkov, K. K. Gudima, and V. D. Toneev, *Acta Phys. Polon.* **36**, 887 (1969).
8. R. M. Sternheimer and S. J. Lindenbaum, *Phys. Rev.* **123**, 333 (1961); **109**, 1723 (1958); and **105**, 1874 (1957).
9. H. W. Bertini, M. P. Guthrie, and A. H. Culkowski, *Phenomenologically Determined Isobar Angular Distributions for Nucleon-Nucleon and Pion-Nucleon Reactions Below 3 GeV,* ORNL-TM-3132 (1970); see abstract 5.4 in this report.
10. J. Ranft and T. Borak, *Improved Nucleon-Meson Cascade Calculation,* NAL Report FN-193, 1100.0 (Nov. 21, 1969).

4.4 CALCULATION OF THE PHOTON-PRODUCTION SPECTRUM FROM PROTON-NUCLEUS COLLISIONS IN THE ENERGY RANGE 15 TO 150 MeV AND COMPARISON WITH EXPERIMENT[1,2]

Y. Shima[3] R. G. Alsmiller, Jr.

Calculations of the differential photon-production cross sections from proton-nucleus collisions in the energy range 15 to 150 MeV have been carried out and compared with experimental measurements on ^{12}C, ^{16}O, ^{27}Al, and ^{56}Fe. The calculations are based on the intranuclear-cascade evaporation model of nuclear reactions and simple assumptions about the deexcitation of excited nuclei. The calculated total photon-production cross sections are within roughly a factor of 2 of the experimental values, but the calculated photon spectra are not in good agreement with the experimental spectra.

References

1. Work partially funded by the National Aeronautics and Space Administration under Order H-38280A.
2. Abstract of *Nucl. Sci. Eng.* **41**, 47 (1970); included in last year's annual as abstract of ORNL-TM-2908 (1969).
3. Present address: Soreq Nuclear Research Center, Yavne, Israel.

4.5 AN APPROXIMATE HIGH-ENERGY ALPHA-PARTICLE-NUCLEUS-COLLISION MODEL[1,2]

T. A. Gabriel R. T. Santoro
R. G. Alsmiller, Jr.

An alpha-particle-nucleus-collision model, which assumes that the nucleons within the alpha particle can be treated separately and independently except for their relative spatial locations when they enter the nucleus, is described. Because of the assumptions that are made, calculations based on the model can be carried out using the intranuclear-cascade code of Bertini. Calculated data on the energy and angular distribution of emergent nucleons and on the cross sections for the

production of various residual nuclei from alpha-particle-nucleus collisions are found to be in very approximate agreement with existing experimental data.

References

1. Work partially funded by the National Aeronautics and Space Administration under Order H-38280A.
2. Abstract of ORNL-TM-3153 (Oct. 1, 1970); *Nucl. Sci. Eng.* **44**, 104 (1971).

4.6 PHENOMENOLOGICALLY DETERMINED ISOBAR ANGULAR DISTRIBUTIONS FOR NUCLEON-NUCLEON AND PION-NUCLEON REACTIONS BELOW 3 GeV[1,2]

H. W. Bertini M. P. Guthrie
A. H. Culkowski[3]

The angular distribution of the isobars in the Lindenbaum-Sternheimer isobar model was determined phenomenologically for single and double π-meson production in nucleon-nucleon collisions and for single π-meson production in π-nucleon collisions in the energy region below a few GeV. It was assumed that only the 3/2,3/2 isobar was excited and that it experienced s-wave decay in its own rest system. The entire range of mass values, consistent with conservation of energy, was assumed to be available to the isobars. The isobar angular distribution was constructed by first comparing experimental data with results from a calculation in which it was assumed that the isobar was created with an isotropic angular distribution. Then the same experimental data were compared with results from an identical calculation except that it was assumed that the isobar was created with a forward-backward distribution. Using different percentages of each distribution for different energies and incident particles, composite distributions were then formed by judgment in an attempt to obtain reasonable representations of the experimental data.

References

1. Work partially funded by the National Aeronautics and Space Administration under Order H-38280A.
2. Abstract of ORNL-TM-3132 (Dec. 7, 1970).
3. Mathematics Division.

4.7 INSTRUCTIONS FOR THE OPERATION OF CODES ASSOCIATED WITH MECC-3, A PRELIMINARY VERSION OF AN INTRANUCLEAR-CASCADE CALCULATION FOR NUCLEAR REACTIONS[1,2]

H. W. Bertini M. P. Guthrie
O. W. Hermann[3]

Instructions for the operation of MECC-3 and associated editing codes are given in this report. MECC-3 will operate over the range of 1 to 3500 MeV for incident nucleons and 1 to 2500 MeV for incident π^+ and π^- mesons for targets ranging from ^{4}He to ^{239}Pu. However, the calculation is expected to be valid only over the range from about 100 to 2000 MeV for targets heavier than carbon. The programs operate on the IBM 360/75 and 360/91 computers.

References

1. Work partially funded by the National Aeronautics and Space Administration under Order No. H-38280A.
2. Abstract of ORNL-4564 (May 1971).
3. Mathematics Division.

4.8 EVAP-4: ANOTHER MODIFICATION OF A CODE TO CALCULATE PARTICLE EVAPORATION FROM EXCITED COMPOUND NUCLEI[1,2]

M. P. Guthrie

EVAP-4 is a Monte Carlo computer program that calculates the types, multiplicities, and energy distributions of particles evaporated from excited compound nuclei. It is identical to its predecessor, EVAP-3, except that an "improved-termination" feature has been added. This permits evaporation to continue as long as energetically possible by removing a pairing-energy correction to the excitation energy of the compound nucleus after the initial rounds of evaporation have stopped. EVAP-4 is written in FORTRAN IV for the IBM-360 computer. The input card and printed output for a sample case are shown.

References

1. Work partially funded by the National Aeronautics and Space Administration under Order H-38280A.
2. Abstract of ORNL-TM-3119 (Sept. 10, 1970).

4.9 INSTRUCTIONS FOR THE OPERATION OF THE PROGRAM PACKAGE PICA, AN INTRANUCLEAR-CASCADE CALCULATION FOR HIGH-ENERGY (30 TO 400 MeV) PHOTON-INDUCED NUCLEAR REACTIONS[1]

T. A. Gabriel M. P. Guthrie
O. W. Hermann[2]

Operating instructions for the program package PICA, which calculates the differential particle spectra and distribution of residual nuclei following high-energy photon-nucleus collisions, are given in this report. The photon energy range in which the calculations are applicable is $30 \lesssim E_\gamma \lesssim 400$ MeV. All target nuclei with mass numbers >4 are possible; however, the calculations have more validity with mass numbers $\gtrsim 10$. The program can accommodate incident monoenergetic photons as well as several types of photon spectra. The program is written in FORTRAN IV for the IBM 360/75 and 360/91 computers. Input and output for a sample problem are given.

References

1. Abstract of ORNL-4687 (in press).
2. Mathematics Division.

4.10 THE NUCLEON-MESON TRANSPORT CODE NMTC[1,2,3]

W. A. Coleman[4] T. W. Armstrong

The nucleon-meson transport code NMTC computes the transport of nucleons below 3.5 GeV and muons and charged pions below 2.5 GeV. Monte Carlo methods are employed to provide a detailed description of the transport process. High-energy nucleon-nucleus and pion-nucleus collisions are treated using the intra-nuclear-cascade-evaporation model. Virtually arbitrary geometries can be specified. The code is written in FORTRAN IV for the IBM 360/75 and 360/91 computers.

In this report, the method of calculation used by the code is discussed, and the code input is described. Also, input and output for a sample problem are given.

References

1. Work partially funded by the National Aeronautics and Space Administration under Order No. H-38280A.
2. Abstract of ORNL-4606 (October 1970).
3. See also the Computer Code Abstract, *Nucl. Sci. Eng.* **43**, 353-354 (1971).
4. Present address: Science Applications, Inc., P. O. Box 3251, La Jolla, California, 92037.

4.11 ELECTROMAGNETIC- AND NUCLEAR-CASCADE CALCULATIONS AND THEIR APPLICATION IN SHIELDING AND DOSIMETRY[1,2]

R. G. Alsmiller, Jr.

Some of the more recent studies conducted at the Oak Ridge National Laboratory in the areas of high-energy shielding and dosimetry are reviewed. The subjects considered are electron-photon cascades, photonucleon and photopion production, nucleon-meson cascades, and muon transport.

Calculated results on the dose in tissue from electrons in the energy range 0.1 to 20 GeV and from photons in the energy range 0.01 to 20 GeV are presented, and the calculated dose as a function of depth for 5.2-GeV electrons normally incident on a tissue slab is compared with experimental dose-vs-depth results.

An essential element in calculating the shielding requirements of electron accelerators is the determination of the energy and angular distributions of nucleons and pions from high-energy photon-nucleus nonelastic collisions. A model for calculating these distributions is briefly described, and calculated results are presented and compared with experimental results for photons in the energy range 50 to 350 MeV.

Nucleon-meson cascade calculations carried out using Monte Carlo techniques are described. In particular, the determination of the radioactive residual nuclei induced in matter by a high-energy nucleon-meson cascade is discussed, and comparisons between experimental and calculated data for 1- and 3-GeV protons incident on a very thick iron target are given. Calculated results on the energy deposition in tissue for 525-MeV neutrons are also presented and compared with experimental data.

The use of Monte Carlo methods to study the properties of nucleon cascades is often unsatisfactory because of the poor statistical accuracy which can be achieved in deep-penetration problems. To avoid these statistical difficulties, the applicability of the method of discrete ordinates to the study of nucleon cascades has been considered. Results obtained using the method of discrete ordinates are presented and compared with similar results obtained using Monte Carlo methods.

In the shielding of high-energy electron accelerators, it is often necessary to consider the transport of very high-energy muons through matter. Muon-transport calculations are discussed, and calculated results ob-

tained with several approximations are presented and compared with experimental data on the transport of photomuons produced by 18-GeV electrons in a thick copper target through a thick iron shield.

References

1. Work partially funded by the National Aeronautics and Space Administration under Order H-38280A.

2. Abstract of paper in *Proceedings of the Second International Conference on Accelerator Dosimetry and Experience, Stanford Linear Accelerator Center, Stanford, Calif., Nov. 3–5, 1969,* USAEC Division of Technical Information, CONF-691101, p. 166; included in last year's annual as abstract of submitted paper and of ORNL-TM-2722 (1969).

4.12 AN APPROXIMATE DENSITY-EFFECT CORRECTION FOR THE IONIZATION LOSS OF CHARGED PARTICLES[1,2]

T. W. Armstrong R. G. Alsmiller, Jr.

An approximate density-effect correction for determining the stopping power and range of high-energy charged particles is discussed and evaluated. For a variety of materials and all particle energies, using the approximate density-effect correction, which can be easily computed for both elements and compounds, overestimates the stopping power by $\lesssim$6% and underestimates the range by $\lesssim$4%. This error should be acceptable in many practical problems that involve materials for which the correct density effect has not been evaluated.

References

1. Work partially funded by the National Aeronautics and Space Administration under Order H-38280A.

2. Abstract of *Nucl. Instr. Methods* 82, 289 (1970); included in last year's annual as abstract of ORNL-TM-2868 (1970).

4.13 THE ABSORBED DOSE AND DOSE EQUIVALENT FROM NEUTRONS IN THE ENERGY RANGE 60 TO 3000 MeV AND PROTONS IN THE ENERGY RANGE 400 TO 3000 MeV[1,2]

R. G. Alsmiller, Jr. T. W. Armstrong
W. A. Coleman[3]

Nucleon-meson cascade calculations have been carried out for monoenergetic neutrons (60 to 3000 MeV) and protons (400 to 3000 MeV) normally incident on a semiinfinite slab of tissue 30 cm thick, and the absorbed dose and dose equivalent as a function of depth in the tissue are presented. The calculated absorbed doses from 180- and 525-MeV incident neutrons and 660- and 730-MeV protons are compared with experimental data. For 525-MeV incident neutrons, the experimental and calculated absorbed doses are in good agreement, but this is not the case with the other comparisons.

References

1. Work partially funded by the National Aeronautics and Space Administration under Order H-38280A.

2. Abstract of *Nucl. Sci. Eng.* 42, 367 (1970); included in last year's annual as abstract of ORNL-TM-2924 (1970).

3. Work done while at the U.S. Army Nuclear Defense Laboratory, Edgewood Arsenal, Md. Present address: Science Applications, Inc., La Jolla, Calif.

4.14 CALCULATION OF THE ABSORBED DOSE AND DOSE EQUIVALENT INDUCED BY MEDIUM-ENERGY NEUTRONS AND PROTONS AND COMPARISON WITH EXPERIMENT[1,2]

T. W. Armstrong B. L. Bishop

Monte Carlo calculations have been carried out to determine the absorbed dose and dose equivalent for 592-MeV protons incident on a cylindrical phantom and for neutrons from 580-MeV proton-Be collisions incident on a semi-infinite phantom. For both configurations, the calculated depth dependence of the absorbed dose is in good agreement with experimental data.

References

1. Work partially funded by the National Aeronautics and Space Administration under Order H-38280A.

2. Abstract of ORNL-TM-3304 (Feb. 5, 1971); to be published in *Radiation Research.* Also presented at the National Symposium on Natural and Manmade Radiation in Space, Las Vegas, Nevada, March 1-5, 1971.

4.15 THE ABSORBED DOSE AND DOSE EQUIVALENT FROM NEGATIVELY AND POSITIVELY CHARGED PIONS IN THE ENERGY RANGE 10 TO 2000 MeV[1,2]

R. G. Alsmiller, Jr. T. W. Armstrong
B. L. Bishop

Nucleon-meson cascade calculations have been carried out for broad beams of monoenergetic negatively and

positively charged pions normally incident on a semi-infinite slab of tissue 30-cm thick, and the absorbed doses and dose equivalents as a function of depth in the tissue are presented. Results are given for incident energies of 10, 30, 84, 150, 500, 1000, and 2000 MeV. For the lower incident energies ($\leqslant$84 MeV), the pion range is <30 cm in tissue, and peaks in the absorbed dose and dose equivalents due to the reaction products produced by the nuclear capture of the stopped negatively charged pions and to the decay products of the stopped positively charged pions are clearly evident.

References

1. Work partially funded by the National Aeronautics and Space Administration under Order H-38280A.

2. Abstract of ORNL-TM-3105 (Aug. 24, 1970) and *Nucl. Sci. Eng.* **43**, 257-266 (1971).

4.16 CALCULATION OF DEPTH-DOSE DISTRIBUTIONS PRODUCED IN TISSUE BY NEGATIVE PIONS[1]

T. W. Armstrong R. G. Alsmiller, Jr.
K. C. Chandler[2]

The use of negative pions in cancer radiotherapy offers unique advantages over currently employed radiations primarily because of the very favorable depth-dose patterns that can be produced by negative pions. To obtain quantitative information for assessing the merits of negative pions for radiotherapy applications and to provide data to aid in the design of the biomedical pion channel for the meson facility under construction at the Los Alamos Scientific Laboratory, detailed calculations have been carried out to determine the spatial distribution of the absorbed dose and dose equivalent produced in tissue by negative-pion beams.

The calculations have been made for infinitely broad beams of pions incident normally on a slab of tissue 60 cm thick. The energy spectra of the beams were taken to be Gaussian in shape, and results have been obtained for beams having mean energies of 53, 82, and 108 MeV. (These energies produce peak doses at tissue depths of approximately 10, 20, and 30 cm, respectively.)

The calculations have been carried out using the nucleon-meson transport code NMTC.[3] The details of the method of calculation are the same as described previously for calculations involving monoenergetic pions[4] except that multiple Coulomb scattering by the primary pions is taken into account in the present calculations. The multiple Coulomb scattering theory used[5] is based on Fermi's joint distribution function for angular and lateral spread and Rutherford's single-scattering cross-section formula.

Figures 4.16.1 and 4.16.2 show the depth dependence of the contributions to the absorbed dose and dose equivalent, respectively, by various kinds of particles for the case of σ = 1.38 MeV and $\bar{E}$ = 82 MeV, where σ is the standard deviation of the Gaussian energy distribution of the beam and $\bar{E}$ is the mean beam energy. The total absorbed dose and the total dose equivalent are obtained by adding all of the contributions in each figure. In Fig. 4.16.1 the histogram labeled "primary pion ionization" gives the absorbed dose from the ionization and excitation of atomic electrons by those incident pions that have not undergone nuclear interaction. The histogram labeled "protons" gives the absorbed dose from the excitation and ionization of atomic electrons by protons produced by nonelastic nucleon-nucleus and pion-nucleus collisions and from the elastic collisions of nucleons and pions with hydrogen nuclei. The histogram labeled "heavy nuclei" gives the absorbed dose from particles with mass number >1 produced from nonelastic nucleon-nucleus and pion-nucleus collisions and the absorbed dose from the recoiling nuclei produced from elastic neutron-nucleus collisions and from nonelastic nucleon-nucleus and pion-nucleus collisions. The histogram labeled "secondary charged pions" gives the absorbed dose from the excitation and ionization of atomic electrons by both negatively and positively charged pions produced from nuclear interactions. The histogram labeled "photons from neutral pions" gives the absorbed dose from the electron-photon cascade produced by the photons that arise from the decay of neutral pions. The histogram labeled "electrons, positrons, and photons" gives the absorbed dose from the electrons and positrons that arise from the decay of muons and the absorbed dose from the photons produced from nonelastic nucleon-nucleus and pion-nucleus collisions. The histogram labeled "muons" gives the absorbed dose from the ionization and excitation of atomic electrons by both negatively and positively charged muons. In Fig. 4.16.2 the histograms have similar meanings but give the dose equivalents from the various kinds of particles.

The ratios of the peak absorbed dose to the absorbed dose at the surface of the tissue for negative-pion beams with $\bar{E}$ = 53, σ = 0.69; $\bar{E}$ = 82, σ = 1.38; and $\bar{E}$ = 108, σ = 1.75 MeV are approximately 14, 8, and 5, respectively. The corresponding ratios for the dose equivalent are approximately 72, 31, and 18.

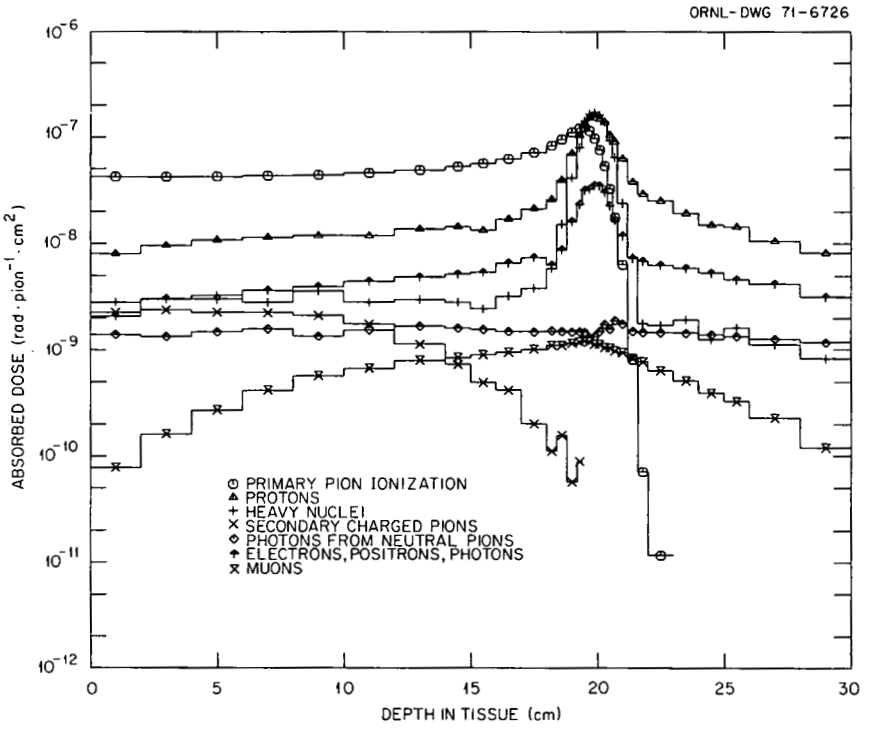

Fig. 4.16.1. Depth Dependence of the Contributions to the Absorbed Dose by Various Kinds of Particles for Incident Negative Pions with $\bar{E}$ = 82 MeV (σ = 1.38 MeV).

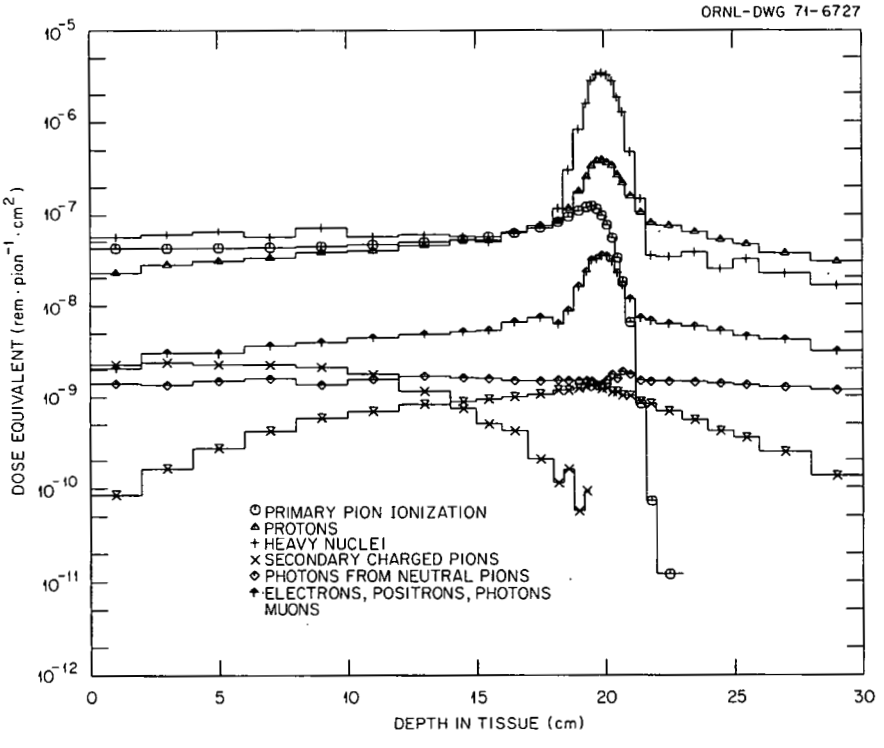

Fig. 4.16.2. Depth Dependence of the Contributions to the Dose Equivalent by Various Kinds of Particles for Incident Negative Pions with $\bar{E}$ = 82 MeV (σ = 1.38 MeV).

The quality-factor (QF) dependence upon linear energy transfer (LET) used to compute the dose equivalent is the same as described in Ref. 5. However, the spatial dependence of the energy deposition spectra for each type of charged particle having a QF > 1 (muons, charged pions, protons, deuterons, ^{3}He's, alpha particles, and recoil nuclei comprised of lithium, beryllium, boron, carbon, nitrogen, and oxygen) has also been computed. From this information, LET spectra may be obtained so that QF-LET relations different from those used here may be applied to compute the dose equivalent.

References

1. Work funded by the Los Alamos Scientific Laboratory under Order CMI-7364-1.
2. Mathematics Division.
3. W. A. Coleman and T. W. Armstrong, *Nucl. Sci. Eng.* **43**, 353-354 (1971).
4. R. G. Alsmiller, Jr., T. W. Armstrong, and Barbara L. Bishop, *Nucl. Sci. Eng.* **43**, 257-266 (1971).
5. Bruno Rossi, *High Energy Particles,* Prentice Hall, Inc., Englewood Cliffs, N. J. (1952), p. 71.

4.17 CALCULATION OF THE RADIATION HAZARD AT SUPERSONIC AIRCRAFT ALTITUDES PRODUCED BY AN ENERGETIC SOLAR FLARE – II[1,2]

T. W. Armstrong H. S. Moran

Calculations have been carried out to estimate the absorbed-dose and dose-equivalent rates at various depths in the atmosphere produced by an energetic solar flare – the flare of Feb. 23, 1956. The dose rates were determined both by computing flux spectra in air only and applying flux-to-dose conversion factors and by computing the dose rates in tissue for an air-tissue-air arrangement. The two methods of calculation are in reasonable agreement when the flux-to-dose factors are applied to the forward-flux spectra, but the calculations indicate that previous results obtained using omni-directional-flux spectra overestimate the dose rates. Also, the effect of the fuel carried by a supersonic aircraft on the dose received by the passengers in the event of a solar flare has been considered and found not to be substantial.

References

1. Work partially funded by the National Aeronautics and Space Administration under Order H-38280A.
2. Abstract of *Nucl. Sci. Eng.* **42**, 41 (1970); included in last year's annual as abstract of ORNL-TM-2844 (1969).

4.18 CALCULATION OF THE DOSE, RADIONUCLIDE PRODUCTION, AND DELAYED PHOTON LEAKAGE DUE TO SOLAR-PROTON BOMBARDMENT OF TISSUE WITH APPLICATION TO ASTRONAUT DOSIMETRY[1,2]

T. W. Armstrong K. C. Chandler[3]

Calculations have been carried out to determine the dose (absorbed dose and dose equivalent), induced radionuclides, and time-dependent photon leakage spectrum due to solar-proton bombardment of a slab of tissue 30 cm thick. Proton spectra with characteristic rigidities of P_0 = 50, 100, and 200 MV are considered. The induced nucleon-meson cascade and the photon transport are calculated using Monte Carlo methods. The radionuclide production is determined by using calculated nucleon spectra and available production cross sections. The purpose of the calculations is to investigate the possibility of determining the whole-body dose received by astronauts in case of solar-flare exposure from measurement of the photons from the decay of radionuclides induced in the astronaut's body.

References

1. Work funded by the National Aeronautics and Space Administration under Order H-38280A and Order T-85613.
2. Abstract of ORNL-TM-3452 (in press); also to be submitted for journal publication.
3. Mathematics Division.

4.19 PRIMARY- AND SECONDARY-PARTICLE CONTRIBUTIONS TO THE DEPTH-DOSE DISTRIBUTION IN A PHANTOM SHIELDED FROM SOLAR-FLARE AND VAN ALLEN PROTONS[1,2]

R. T. Santoro H. C. Claiborne
R. G. Alsmiller, Jr.

Calculations have been made using the nucleon-meson transport code NMTC to estimate the absorbed-dose and dose-equivalent distributions in "astronauts" inside space vehicles bombarded by solar-flare and Van Allen protons. A spherical shell shield of specific radius and thickness with a 30-cm-diam tissue ball at the geometric center was used to simulate the spacecraft-astronaut configuration. The absorbed dose and the dose equivalent from primary protons, secondary protons, heavy

nuclei, charged pions, muons, photons, positrons and electrons are given as a function of depth in the tissue phantom. Results are given for solar-flare protons with a characteristic rigidity of 100 MV and for Van Allen protons in a 240-nautical-mile circular orbit at 30 deg inclination angle incident on both 20-g/cm^2-thick aluminum and polyethylene spherical shell shields.

References

1. Work funded by the National Aeronautics and Space Administration under Order H-38280A.

2. Abstract of ORNL-TM-3320 (Feb. 18, 1971); also presented at the National Symposium on Natural and Manmade Radiation in Space, Las Vegas, Nevada, March 1-5, 1971.

4.20 CALCULATION OF COSMOGENIC RADIONUCLIDES IN THE MOON AND COMPARISON WITH APOLLO MEASUREMENTS[1,2]

T. W. Armstrong R. G. Alsmiller, Jr.

Calculations have been carried out to determine the time and spatial dependence of the production of various radionuclides in the moon from solar and galactic proton bombardment. The calculational method utilizes Monte Carlo techniques to obtain a detailed description of the induced nucleon-meson cascade. All required spallation cross sections are computed using the intranuclear-cascade-evaporation model. The calculated depth dependence of ^{26}Al and ^{22}Na is in good agreement with Apollo 11 and 12 measurements. The depth-dependent neutron spectra are also directly available from the calculations. The calculated thermal-neutron flux is in good agreement with the flux obtained from measured ^{60}Co concentrations. Irradiation ages obtained from the calculated thermal flux and the thermal fluence based on measured gadolinium concentrations are consistent with the ages determined by other methods.

References

1. Work funded by the National Aeronautics and Space Administration under Order T-85613.

2. Abstract of ORNL-TM-3267 (Dec. 31, 1970); also presented at the Lunar Science Conference, Houston, Texas, January 11-14, 1971; will also be in the proceedings to be published in *Geochim. Cosmochim. Acta.*

4.21 CALCULATION OF THE LUNAR PHOTON ALBEDO AND INDUCED DOSE RATE FROM GALACTIC AND SOLAR PROTON BOMBARDMENT[1,2]

T. W. Armstrong

The lunar photon albedo due to cosmogenic and primordial photon sources has been calculated. The individual photon leakage spectra from prompt photons produced by galactic cosmic-ray (GCR) and solar cosmic-ray (SCR) induced nuclear interactions, from the decay of GCR- and SCR-induced radionuclides and from the decay of naturally occurring radionuclides are given. An approximate estimate of the leakage from the photon-electron cascade initiated by the decay of neutral pions is also given. The depth-dependence of the absorbed dose and dose equivalent in the moon resulting from GCR and SCR bombardment is calculated. The calculations have been carried out using Monte Carlo methods to determine the nucleon-meson cascade and discrete ordinates methods for the photon and low-energy neutron transport.

References

1. Work funded by the National Aeronautics and Space Administration under Order T-85613.

2. Abstract of ORNL-TM-3268 (in press) and to be submitted for journal publication.

4.22 MONTE CARLO CALCULATIONS OF HIGH-ENERGY NUCLEON-MESON CASCADES AND APPLICATIONS TO GALACTIC COSMIC-RAY TRANSPORT[1,2]

T. W. Armstrong R. G. Alsmiller, Jr.
K. C. Chandler[3]

Results obtained using a recently developed calculational method for determining the nucleon-meson cascade induced in thick materials by high-energy nucleons and charged pions are presented. The calculational method uses the intranuclear-cascade-evaporation model to treat nonelastic collisions by particles with energies $\lesssim 3$ GeV and an extrapolation model at higher energies. The following configurations are considered: (*a*) 19.2-GeV/c protons incident on iron, (*b*) 30.3-GeV/c protons incident on iron, (*c*) solar and galactic protons incident on the moon, and (*d*) galactic protons incident on tissue. For the first three configurations, experimental results are available and comparisons between the experimental and calculated results are given.

References

1. Work partially funded by the National Aeronautics and Space Administration under Order H-38280A.
2. Abstract of ORNL-TM-3319 (Feb. 22, 1971); also presented at the National Symposium on Natural and Manmade Radiation in Space, Las Vegas, Nevada, March 1-5, 1971.
3. Mathematics Division.

4.23 THE LATERAL SPREAD OF HIGH-ENERGY (≤400-MeV) NEUTRON BEAMS AND EARTHSHINE[1]

R. G. Alsmiller, Jr. M. L. Gritzner
F. R. Mynatt J. V. Pace[2]
J. Barish[2]

Calculated results obtained with the method of discrete ordinates are presented for the cases of zero-width beams of 100- and 400-MeV neutrons normally incident along the axis of a cylindrical shield of silicon dioxide with 5% water by weight. The results include the omnidirectional neutron flux per unit energy as a function of depth and radius in the shield and the neutron and photon dose equivalents as a function of depth and radius in the shield.

In the vicinity of well-shielded target areas of high-energy accelerators, the neutrons and photons which diffuse through the ground under the shield, "earthshine," often pose a radiation hazard. Calculated results of the earthshine in a specific geometry are presented and discussed.

References

1. Abstract of *Nucl. Instr. Methods* **89**, 53 (1970); included in last year's annual as abstract of ORNL-TM-3025 (1970).
2. Mathematics Division.

4.24 CALCULATED ACTIVATION OF COPPER AND IRON BY 3-GeV PROTONS[1]

T. W. Armstrong J. Barish[2]

An estimate of the residual photon dose rate and the neutron leakage induced in an accelerator magnet by a beam of 3-GeV protons is computed. The magnet is approximated as an infinite cylinder of copper surrounded by a layer of iron, with the proton beam located on the cylinder axis. Monte Carlo methods are used to determine the development of the nucleon-meson cascade, the residual nuclei production, and the photon transport.

References

1. Abstract of *Nucl. Sci. Eng.* **41**, 443 (1970); included in last year's annual as abstract of ORNL-TM-2902 (1970).
2. Mathematics Division.

4.25 CALCULATION OF THE LONG-LIVED INDUCED ACTIVITY IN SOIL PRODUCED BY 200-MeV PROTONS[1]

T. A. Gabriel

Calculations have been carried out to obtain the time and spatial dependence of the long-lived induced activity in soil produced by 200-MeV protons incident on a small cylinder of graphite buried in soil. Only radioactive nuclei with half lives greater than or equal to that of ^{7}Be (0.147 year) were considered. Monte Carlo methods were applied to determine the induced neutron flux which was combined with both calculated and experimental radiochemical cross sections to determine the rate of residual-nuclei production. Through the use of the results of the calculations, a procedure has been established whereby the approximate contribution of each target nucleus to the production of a particular radioactive nucleus can be obtained. The results of the calculations are also used to approximate the long-lived induced activity in soil when the small cylinder of graphite is embedded first in another material, such as iron, which is in turn surrounded by soil.

References

1. Abstract of *Nucl. Appl. Tech.* **9**, 605 (1970); included in last year's annual as abstract of ORNL-TM-2848 (1970).

4.26 CALCULATION OF THE LONG-LIVED INDUCED ACTIVITY IN THE SOIL AROUND HIGH-ENERGY ACCELERATOR TARGET AREAS[1]

T. A. Gabriel

Nucleon-meson cascade calculations have been carried out and estimates of the induced activity in the soil surrounding high-energy accelerator target areas have

been obtained. Results on the contribution to the induced activity from various residual nuclei are presented for a specific irradiation time and as a function of time after beam shutdown for a 3-GeV and a 200-GeV proton accelerator. Because of the lack of particle production data at very high energies, the calculated results for the 200-GeV incident proton beam are much more approximate than those for the 3-GeV incident proton beam.

References

1. Abstract of *Nucl. Instr. Methods* **91**, 67 (1970); included in last year's annual as abstract of ORNL-TM-3033 (1970).

4.27 CALCULATION OF THE LONG-LIVED INDUCED ACTIVITY IN THE SOIL AROUND HIGH-ENERGY ACCELERATOR TARGET AREAS – II[1]

T. A. Gabriel R. G. Alsmiller, Jr.
J. Barish[2]

Nucleon-meson cascade calculations have been carried out and estimates of the induced activity in the soil surrounding high-energy accelerator target areas have been obtained. Results are presented for 200- and 500-GeV protons incident on a lead target and for 500-GeV protons incident on a beryllium target. The calculated results include the induced activity as a function of position and time after the proton beam is turned off for an assumed irradiation time of 25 years. In order to carry out the calculations, many *ad hoc* assumptions have been made, and therefore the results must be considered to be very approximate.

References

1. Abstract of ORNL-4599 (1970).
2. Mathematics Division.

4.28 CALCULATION OF THE LONG-LIVED ACTIVITY IN SOIL PRODUCED BY 500-GeV PROTONS[1]

T. A. Gabriel R. T. Santoro

Calculations have been made to estimate the time and spatial dependence of the long-lived ($\tau_{1/2} \geqslant 1$ day) activity in the soil surrounding a semi-infinite beam target tunnel. The activity distributions are given for 500-GeV protons incident on a Be target positioned in the tunnel for an irradiation time of 25 years at 10^{13} protons per second and at a time after shutdown of one month. The distributions are presented as a function of the radial distance from the tunnel axis for the spatial regions along the tunnel and at the end of the tunnel. The activity arising from selected nuclides is given for selected spatial points. Curves showing the decrease in activity as a function of shutdown time are given. Included is the calculated integrated activity along the tunnel axis.

Reference

1. Abstract of ORNL-TM-3262 (Dec. 21, 1970); to be published in *Nuclear Instruments and Methods.*

4.29 NUCLEON AND PION STAR PRODUCTION FROM HIGH-ENERGY (>40 GeV) PROTONS INCIDENT ON IRON[1]

R. T. Santoro T. A. Gabriel

Nucleon and pion star production from 40- to 1000-GeV protons incident on iron has been calculated. Star yields above cutoff energies of 15 and 100 MeV are reported.

Reference

1. Abstract of ORNL-TM-3335 (March 18, 1971); to be published in *Nuclear Instruments and Methods.*

4.30 CALCULATION OF THE NUCLEON- AND PION-INDUCED STAR AND FLUX DISTRIBUTIONS FROM 400-GeV PROTON INTERACTIONS IN IRON[1]

R. T. Santoro T. A. Gabriel

Monte Carlo calculations have been made to estimate the nucleon- and pion-induced star and flux distributions from the interactions of 400-GeV protons in iron. Laterally integrated and radially dependent star distributions as a function of depth in the iron are presented. Omnidirectional nucleon and charged-pion fluxes and energy-dependent flux distributions are also included.

Reference

1. Abstract of ORNL-4673 (in press).

4.31 NUCLEON AND CHARGED-PION ALBEDO SPECTRA IN AN ACCELERATOR CAVE FROM 200-GeV PROTON INTERACTIONS IN IRON[1]

T. A. Gabriel R. T. Santoro

Nucleon and charged-pion albedo flux distributions in an accelerator cave resulting from the interaction of

200-GeV protons have been calculated. The spectra are given as a function of secondary-particle energy and of radial position and distance from the point where the beam is dumped into the iron. Comparisons beteween the omnidirectional and "backward" flux distributions are presented.

Reference

1. Abstract of ORNL-TM-3437 (in press); to be submitted for journal publication.

4.32 MUON TRANSPORT AND THE SHIELDING OF HIGH-ENERGY (≤500 GeV) PROTON ACCELERATORS[1]

R. G. Alsmiller, Jr. J. Barish[2]
F. S. Alsmiller Y. Shima[3]

Calculated results on the muon shielding required around high-energy (200 GeV and 500 GeV) proton accelerator targets are presented. The calculations differ from those presented previously in that, in addition to the angular scattering of the muons due to Coulomb elastic collisions, an estimate of the angular scattering of the muons due to bremsstrahlung production, pair production, and nonelastic nuclear collisions is included. It is found that the angular scattering of the mouns due to bremsstrahlung production, pair production, and nonelastic nuclear collisions does not have a pronounced effect on the shield dimensions and therefore for many design purposes may be neglected.

The calculations also differ from those presented previously in that the case of laminated shields is considered.

References

1. Abstract of ORNL-TM-3353 (April 12, 1971); also presented at the International Congress on Protection Against Accelerator and Space Radiation, CERN, Geneva, April 26-30, 1971.
2. Mathematics Division.
3. Present address: Soreq Nuclear Research Center, Yavne, Israel.

4.33 LOW-ENERGY ELECTRON TRANSPORT WITH THE METHOD OF DISCRETE ORDINATES[1,2]

D. E. Bartine[3] F. R. Mynatt
R. G. Alsmiller, Jr. W. W. Engle, Jr.
J. Barish[3]

Efforts have been in progress for some time to treat the transport of low-energy (≲10 MeV) electrons by the method of discrete ordinates. In principle, the discrete ordinates transport code ANISN[4] may be used to simulate the transport of electrons by the simple expedient of introducing into the code the differential cross sections for electron-nucleus elastic collisions, electron-nucleus bremsstrahlung-producing collisions, and electron-atomic-electron collisions. In practice, these cross sections are quite different from those that occur in neutron transport where the method of discrete ordinates has been used extensively, and it is not clear to what extent the method may be used to successfully transport electrons. Furthermore, some of the differential cross sections that are needed, particularly the cross section for electron-atomic-electron collisions, are not well established, and the extent to which this lack of information will prevent a successful application of the method is also not known.

In the work reported here, the differential cross sections for electron-nucleus elastic scattering and the electron-nucleus bremsstrahlung-producing collisions have been taken from standard sources,[5,6] and the differential cross section for electron-electron collisions that result in large energy transfers is taken from the work of Møller.[5,7] This Møller cross section applies to collisions between free electrons and presumably does not accurately describe electron-atomic-electron collisions that result in energy transfers of the order of the atomic binding energies. To describe electron-electron collisions involving small energy transfers, two methods have been used. In method one (ANISN with Møller cross section), which is due to Spencer and Fano,[8] the Møller cross section is assumed to be valid even for small energy transfers, and the lowest energy transfer that is allowed in an electron-electron collision is determined by the requirement that the energy loss per unit distance from all electron-electron collisions corresponds to the well-established total energy loss per unit distance.[9] In method two (ANISN with continuous slowing down), the effects of electron-electron collisions, which result in small energy transfers, are included in the transport equation by introducing a term which corresponds to a continuous slowing down of the electrons being transported. The stopping power that is used in the continuous slowing-down term is obtained by subtracting the energy loss per unit distance due to large energy-transfer collisions from the well-established total energy loss per unit distance.[9] In the calculations reported below, the continuous slowing down in ANISN was used to describe all electron-electron collisions that result in an energy loss of $<10\ I$, where I is the average ionization potential of aluminum and is equal to 163 eV.

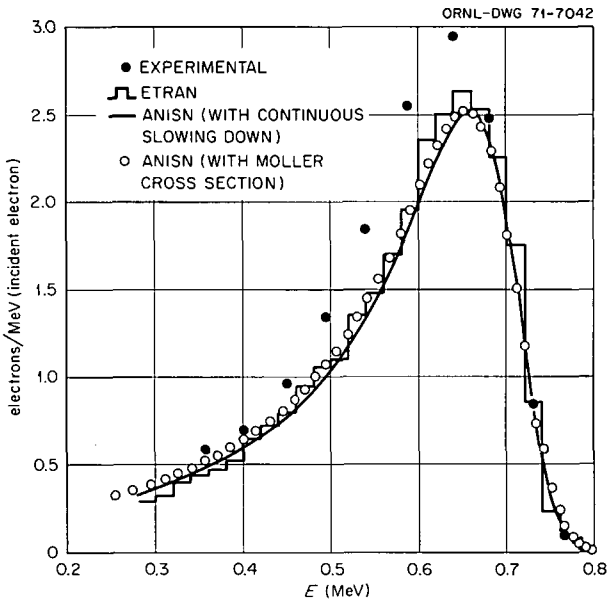

Fig. 4.33.1. Transmitted Electron Current Per Unit Energy from 1-MeV Electrons Normally Incident on a 0.22-g/cm^2-Thick Aluminum Slab.

In Fig. 4.33.1 the transmitted currents per unit energy calculated with ANISN using both methods one and two above are compared with the measured[10] transmitted current per unit energy for 1-MeV electrons normally incident on a 0.22-g/cm^2-thick aluminum slab. Also shown in the figure are the calculated results of Rester and Derrickson[11] obtained with the Monte Carlo code ETRAN of Berger and Seltzer.[12] The two different ANISN calculations are in excellent agreement with each other and are in good agreement with the Monte Carlo calculations. All of the calculations, however, are lower than the experimental data over much of the energy range shown in the figure.

References

1. Work funded by the National Aeronautics and Space Administration under Order H-38280A.

2. For comparisons other than those given here see D. E. Bartine et al., *Low-Energy Electron Transport with the Method of Discrete Ordinates,* ORNL-TM-3318 (Feb. 22, 1971); also presented at the National Symposium on Natural and Manmade Radiation in Space, Las Vegas, Nevada, March 1-5, 1971.

3. Mathematics Division.

4. W. W. Engle, Jr., *A Users Manual for ANISN, A One-Dimensional Discrete Ordinates Transport Code with Anisotropic Scattering,* K-1693, Computing Technology Center, Union Carbide Corp., Oak Ridge, Tenn. (1967).

5. C. D. Zerby and F. S. Keller, *Nucl. Sci. Eng.* **27**, 190 (1967).

6. H. W. Koch and J. W. Motz, *Rev. Mod. Phys.* **31**, 920 (1959).

7. C. Møller, *Ann. Physik* **14**, 531 (1932).

8. L. V. Spencer and U. Fano, *Phys. Rev.* **93**, 1172 (1954).

9. M. J. Berger and S. M. Seltzer, *Tables of Energy Losses and Ranges of Electrons and Positrons,* NASA-SP-3012 (1964).

10. D. H. Rester, *Comparisons of Experimental and Calculated Electron Transmission and Bremsstrahlung Spectra for Electron Energies Below 3.0 MeV,* Ling-Temco-Vought, Inc. Report No. 0-71100/OR-6 (1970).

11. D. H. Rester and J. H. Derrickson, *J. Appl. Phys.* **42**, 714 (1971).

12. M. J. Berger and S. M. Seltzer, *ETRAN, Monte Carlo Code System for Electron and Photon Transport Through Extended Media,* National Bureau of Standards reports NBS-9836 (1968) and NBS-9837 (1968).

4.34. ENERGY DEPOSITION BY 45-GeV PHOTONS IN Be AND Al[1]

R. G. Alsmiller, Jr. H. S. Moran

Electron-photon cascade calculations have been carried out for zero-width beams of 45-GeV photons normally incident on semi-infinite slabs of beryllium and aluminum, and the energy deposition is given as a function of both depth and radius in the slabs.

References

1. Abstract of ORNL-4631 (1970).

5. Medium-Energy Nucleon Spectroscopic Studies

5.0 INTRODUCTION

R. W. Peelle

The work in this area now consists of the reduction and reporting of experimental data obtained during earlier periods. Accumulation of additional data is not possible within the current budget.

The experimental work on the neutron spectrum near the top of the atmosphere has shown that above 25 MeV the intensity is too low at the latitude of Texas to be studied by low-pressure balloons with a conventional liquid scintillator technique. Our data for energies from about 5 to 30 MeV have been released based on preliminary pulse-height spectra from the July 1969 flight. Difficulties have been encountered in obtaining final pulse-height spectra from the analog data tapes, and this work may not be completed for lack of funds.

Except for the data on targets of C and O, the publication of final tabular data is now complete for the experiments on charged secondaries from 30- to 60-MeV protons and 60-MeV alpha particles on a series of targets (Al, ^{59}Fe, ^{56}Fe, ^{88}Y, ^{120}Sn, Au, and Ba). The results offer a wealth of information on the detailed behavior of the cross sections in this energy region where solar cosmic rays and trapped protons are very intense, but where the predictions of the intranuclear cascade model cannot be expected to be very accurate. Considerable effort is yet required for appropriate publication of the significant trends shown by the data and of sets of comparisons against the model cross sections from the intranuclear cascade plus evaporation theory. In the case of the analogous cross sections for 60-MeV alpha particles on carbon and ^{54}Fe, an intranuclear cascade theory does not exist and comparisons with the evaporation theory are not entirely appropriate because forward-peaked continua at high energies are seen for all secondary particles. Comparisons which have been made with evaporation theory indicate that the predicted alpha-particle intensity is far too low using the Monte Carlo evaporation theory based on the work of Dostrovski, but can be made approximately correct by use of optical-model inverse cross sections rather than the analytic ones now built into the program.

Analysis of the data on secondary neutron cross sections from 40- and 60-MeV protons on several nuclei is proceeding with the gradual resolution of the tricky questions involved with spectrometer efficiency determinations. Though few in number the neutron spectra under analysis are sufficiently unique that they can have great weight in the assessment of the cascade model in the energy region below 100 MeV.

5.1 EXPERIMENTAL NUCLEAR CROSS SECTIONS FOR SPACECRAFT SHIELD ANALYSIS[1,2]

R. W. Peelle[3]

Experiments have been performed to validate and to supplement the intranuclear cascade model as a method for estimating cross sections of importance to spacecraft shield design. The experimental situation is inconclusive particularly for neutron-producing reactions, but is relatively sound for reaction cross sections and for proton spectra at several hundred MeV at medium forward angles. Secondary photon contributions are imprecisely known.

References

1. Research partially funded by the National Aeronautics and Space Administration under Order L-12,186.

2. Abstract of ORNL-TM-3376 and of paper to be published in the Proceedings of the National Symposium on Natural and Manmade Radiation in Space, March 1, 1971, Las Vegas, Nevada.

3. Associate authors: F. E. Bertrand, W. R. Burrus (Tennecomp Inc.), W. A. Gibson (Tennecomp Inc.), N. W. Hill, T. A. Love, F. C. Maienschein, R. T. Santoro, R. J. Scroggs (ORTEC), J. H. Todd, V. V. Verbinski (Gulf General Atomic), J. W. Wachter, and W. Zobel.

5.2 NEUTRON SPECTRAL MEASUREMENTS IN THE UPPER ATMOSPHERE[1,2]

W. Zobel J. T. Delorenzo[3]
T. A. Love C. O. McNew[3]

An experiment to measure neutrons in the upper atmosphere has been performed on a balloon flight from

Palestine, Texas, at an altitude of about 32 km. The experimental arrangement is discussed briefly, and results of a preliminary analysis of the data for neutrons in the energy range 3 to 30 MeV are given.

References

1. Flight costs and telemetry support provided by the NASA Office of Space Science and Applications and the George C. Marshall Space Flight Center.
2. Abstract of paper to be published in the Proceedings of the National Symposium on Natural and Manmade Radiation in Space, March 1, 1971, Las Vegas, Nevada.
3. Instrumentation and Controls Division.

5.3 HYDROGEN AND HELIUM PARTICLES PRODUCED BY 59-MeV ALPHA PARTICLE BOMBARDMENT OF ^{12}C, ^{16}O, AND ^{54}Fe[1,2]

F. E. Bertrand[3] R. W. Peelle

Differential cross sections are presented for the production of protons, deuterons, tritons, and alpha particles from ^{12}C and ^{54}Fe bombarded by 58.8-MeV alpha particles. Spectra are presented for the same particles from ^{16}O, but with rather large uncertainty. Continuum cross sections in 1- or 2-MeV wide bins are listed for 5-6 angles and with low-energy cutoffs which range from ~ 2-7 MeV, dependent on the type of exit particle. Angle-integrated and energy-integrated cross

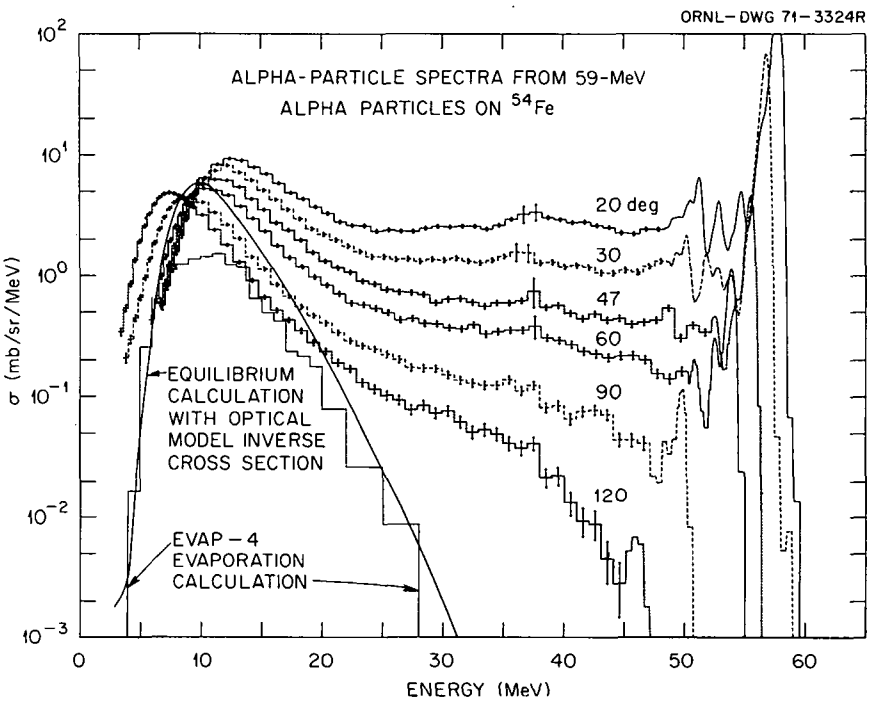

Fig. 5.3.1. Alpha Particle Spectra Observed for the $^{54}Fe(\alpha,x\alpha')$ Reaction for 59-MeV Alpha Particles. Note the angular distribution of the high-energy continuum, the shift in the position of the evaporation peak with angle due to kinematic effects, and the minimum in the strength of evaporation at 90 deg [consistent with Benveniste, *Phys. Rev.* C2, 500 (1970)]. The evaporation calculations are normalized to a nonelastic cross section of 1700 mb based on optical-model calculations, and should be compared with the 90-deg spectrum to reduce kinematic effects. The EVAP-4 (M. Guthrie, ORNL-TM-3119, September 1970) Monte Carlo calculation utilizes analytic inverse cross sections while the preliminary analytic equilibrium calculation used optical-model inverse cross sections for protons, neutrons, and alpha particles. The same level density, pairing correction, and binding energy formulations are included in both programs. The analytic program, modified from one by Blann [*Phys. Rev.* 133, B707 (1964)], does not share kinetic energy with the residual nucleus. The corresponding comparison for secondary protons shows both calculations ~60% higher than experiment.

sections are also given. Total integral cross sections are given for emission of the five hydrogen and helium ions. Comparisons are shown between the $(\alpha,x\alpha)$ and (p,xp) reaction in ^{54}Fe and ^{12}C for E_α and E_p about 60 MeV. (See Fig. 5.3.1.)

References

1. Work funded by the National Aeronautics and Space Administration under NASA Order L-12,186.
2. Abstract of ORNL-4694.
3. Physics Division (Nuclear Data Group).

5.4 DIFFERENTIAL CROSS SECTIONS AT FORWARD ANGLES FOR HYDROGEN AND HELIUM PARTICLES FROM 62-MeV PROTONS INCIDENT ON ^{60}Ni[1,2]

R. W. Peelle F. E. Bertrand[3]

Tabulated differential cross sections are presented for the production, at angles of 15, 20, 25, and 40 deg, of proton, deuteron, triton, helium-3, and alpha particles from ^{60}Ni bombarded by 62-MeV protons. Continuum cross sections are listed in ~1-MeV bins for energies above lower cutoffs which range from 4 to 15 MeV for the different types of exit particles. For a considerable energy range within each spectrum, only the integral cross section is known. The proton-, deuteron-, and alpha-particle cross sections are the same in the continuum region above the evaporation peak as those cross sections previously observed for ^{54}Fe and ^{56}Fe, but the corresponding yield of tritons is higher from ^{60}Ni and ^{56}Fe than from ^{54}Fe. (See Fig. 5.4.1.)

References

1. Work funded by the National Aeronautics and Space Administration under NASA Order L-12,186.
2. Abstract of ORNL-4698.
3. Physics Division (Nuclear Data Group).

5.5 CROSS SECTIONS FOR HYDROGEN AND HELIUM PARTICLES PRODUCED BY 62- AND 39-MeV PROTONS ON ^{209}Bi[1,2]

F. E. Bertrand[3] R. W. Peelle

Tabulated differential cross sections are presented for the production spectra of proton, deuteron, triton,

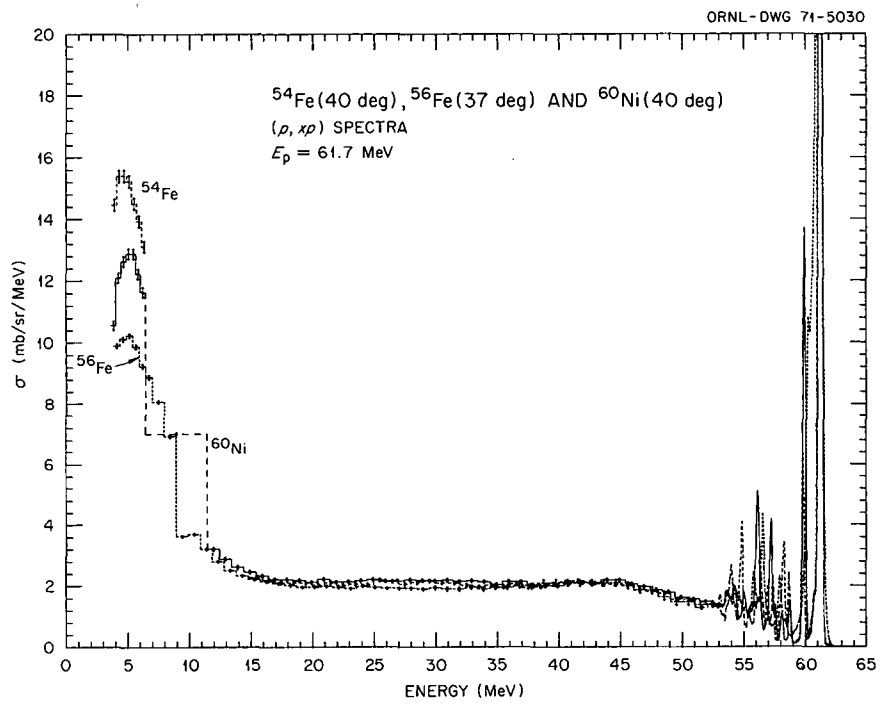

Fig. 5.4.1. A Comparison of Experimental (p,xp) Cross Sections at ~40 deg from the Neighboring Nuclei ^{54}Fe, ^{56}Fe, and ^{60}Ni. Between the evaporation region and the resolved structure from inelastic scattering exciting low-lying levels of the residual nucleus, the cross sections agree with each other in accord with the concepts of the cascade model. The broad histogram at 6-12 MeV for ^{60}Ni shows the integral of the cross section in this region. The break in the ^{54}Fe curve represents an energy region (6-16 MeV) in which the cross section is not known.

helium-3, and alpha particles from ^{209}Bi bombarded by 62-MeV protons, and for all particles but ^{3}He for incident 39-MeV protons. Continuum cross sections in ~1-MeV bins are listed for 18 angles for 62-MeV incident protons, and for four angles for 39-MeV protons. The low-energy cutoffs range from 4 to 15 MeV for the different exit particle types. Angular distributions for 62-MeV incident protons are given for excitations in ^{209}Bi at 0, 1.62, 2.65, 3.15, 3.56, 3.96, 4.29, 5.20, and 5.49 MeV, and comparisons are made with DWBA theory. The energies, strengths, and angular momentum transfers obtained for the ^{209}Bi collective groups approximate those for the collective levels of ^{208}Pb. In ^{208}Bi angular distributions are given for multiplets observed with 62-MeV protons at excitation energies of 0.030, 0.635, 1.02, 1.73, 2.42, and 3.48 MeV. Only elastic scattering cross sections are given for incident 38.8-MeV protons, since there is an inadequate amount of data for angular distributions. Definite

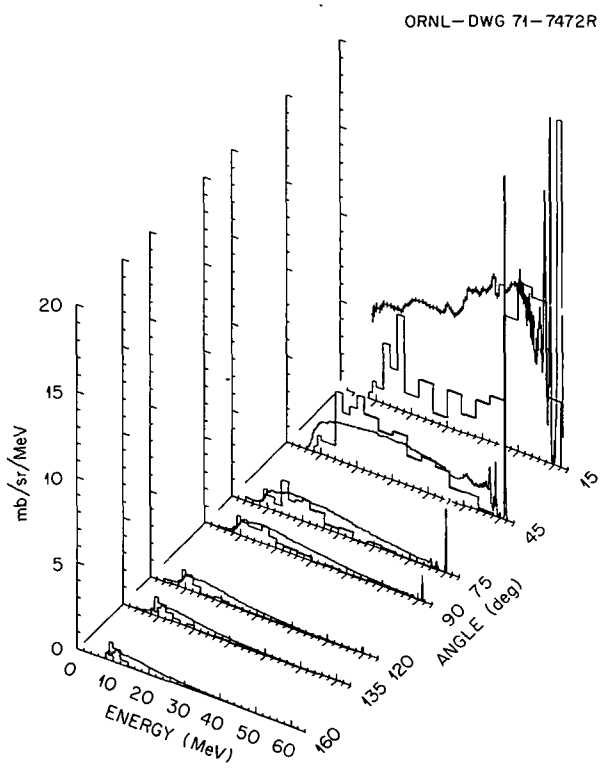

Fig. 5.5.1. Differential Cross Sections at Several Angles for Protons from 62-MeV Protons on ^{209}Bi. For targets in this range of atomic numbers the "evaporation" peak is not evident. Note that the gently variable continuum above 20 MeV extends to backward angles, but rises sharply at angles below 30 deg. The histogram with broad steps illustrates estimates from the Bertini model of the intranuclear cascade plus evaporation reactions.

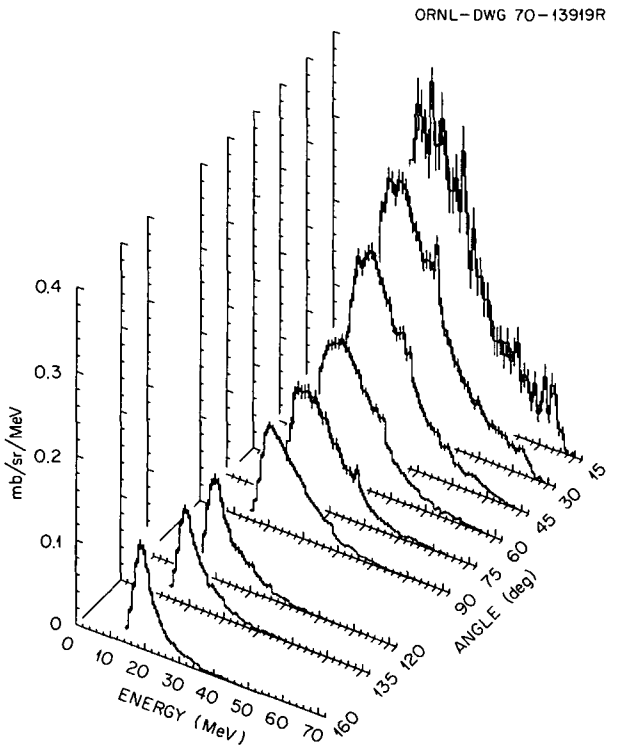

Fig. 5.5.2. Differential Cross Sections at Several Angles for Alpha Particles from 62-MeV Protons on ^{209}Bi. The structure near 35 MeV is caused by imperfect correction for the effect of the nickel foil which covered the Ge(Li) stopping counter. Note the high-energy components at forward angles and the strong angular distribution even near the lowest energies observed.

evidence is found for $(p,n\bar{p})$ reactions in the 90-deg proton spectrum for 39-MeV incident protons, and a value for the ^{209}Po - ^{209}Bi Coulomb displacement energy of 18.9 ± 0.1 MeV is obtained from these data. (See Figs. 5.5.1 and 5.5.2.)

References

1. Work funded by the National Aeronautics and Space Administration under NASA Order L-12,186.
2. Abstract of ORNL-4638.
3. Physics Division (Nuclear Data Group).

5.6 EVIDENCE FROM 62-MeV PROTON SCATTERING FOR EXTENDING THE WEAK COUPLING MODEL IN ^{209}Bi[1,2]

F. E. Bertrand[3] M. B. Lewis[3]

The reaction ^{209}Bi(p,p') has been studied at a bombarding energy of 61.7 MeV. Differential cross sections were obtained between 15 and 75 deg for

various groups of collective levels in ^{209}Bi and for the 1.62-MeV single- particle level. The data were compared with DWBA calculations, and the L-values and deformation parameters so determined were compared with those for corresponding excitations in ^{208}Pb. The results are consistent with the excitation of at least six core (^{208}Pb) excitation multiplets in ^{209}Bi. The observed angular distribution for excitation of the 1.62-MeV level indicates a small L = 3 + (5) admixture in this predominantly $i_{13/2}$ proton state.

References

1. Research partially funded by the National Aeronautics and Space Administration under Order L-12,186.
2. Abstract of *Nucl. Phys.* **168**, 259 (1971).
3. Physics Division (Nuclear Data Group).

5.7 DIFFERENTIAL CROSS SECTIONS FOR NEUTRONS FROM 40- AND 60-MeV PROTONS ON NUCLEI[1]

J. W. Wachter T. A. Love
R. T. Santoro W. Zobel

The energy spectra of secondary neutrons emitted by targets bombarded by 40- and 60-MeV protons were measured at the Oak Ridge Isochronous Cyclotron (ORIC) with a time-of-flight neutron spectrometer sensitive to energies from maximum down to 5 MeV. The measurements were made on ^{12}C, ^{27}Al, ^{54}Fe, and ^{208}Pb at angles of observation of 0, 20, 45 (or 40), 60, 90, and 135 deg.

The experiments were described previously.[2] The neutron spectrometer was a 3 in. by 3 in. NE-213 liquid scintillator viewed by an RCA-4522 photomultiplier tube. This detector observes pulses of light emitted by charged particles arising from interactions between the incident neutrons and the materials of the detector. Pulses from charged particles incident on the face of the detector were rejected by means of a thin NE-102 detector mounted in front of the NE-213 detector and operated in anticoincidence with it. Both neutrons and gamma rays were detected in the NE-213, and the slow-light characteristics of the neutron reactions were used to distinguish between pulses originating from neutrons and gamma rays. Pulse-shape discrimination was achieved with a cross-over timing circuit.

The energy of each neutron was inferred from its time of flight from the target by using a time-to-amplitude converter (TAC), which measured the time from the detection of the event in the detector to a fiducial pulse derived from the rf oscillator of the cyclotron.

To minimize errors in the timing circuits and to facilitate data handling, the TAC output, the pulse height from the scintillator, and the output of the pulse-shape discriminator were fed to an on-line PDP-8 computer. The computer processed all incoming data and continuously recorded on magnetic tape all neutron events and a sample of gamma events. To guard against bias drifts in the electronics, all gamma events near the gamma-neutron decision line were retained. Likewise, all gamma events in which the pulse height corresponded to an energy greater than about 10 MeV were recorded, since high-energy protons produced by neutrons in the scintillator have slow/fast light characteristics more nearly like those of electrons than of lower energy protons.

Analysis of these data tapes involved several phases. Initially, the raw data for the experimental and calibration runs were scanned to obtain pulse height, time of flight, and slow/fast light distributions as initially measured. Analysis of these data enabled correction factors to be determined for changes in the pulse-height calibration due to instrumental drift and for timing errors due to time slewing. In addition, software bias levels were determined to enable the separation of neutron and gamma events on the basis of specific ranges of each of the three variables measured. The data tapes were then reanalyzed to obtain 512 by 512 matrices that summarize the distribution in time and pulse height of the neutrons detected in the experiment.

The second phase of the analysis was directed toward matching the relative response functions for the NE-213 detector as found by calculation and by measurement. The measured response was obtained by partitioning the flight time vs pulse-height matrix into bins labeled by neutron energy, rather than time of flight, so that the pulse-height distribution within such a bin was a relative measure of the light output of the detector when irradiated with neutrons of energy corresponding to the midpoint of the bin. This distribution was then compared with the distribution calculated from the O5S Monte Carlo code,[3] and smeared to match the true response of the scintillator.[4]

Figure 5.7.1 illustrates such a comparison of theoretical and measured response functions. The agreement shown here results from using cross sections in the Monte Carlo calculations that were modified to match the results of a scintillator-efficiency experiment performed here to establish the response at 40 MeV in a detector of smaller size (Cohen et al.[5]). The agreement

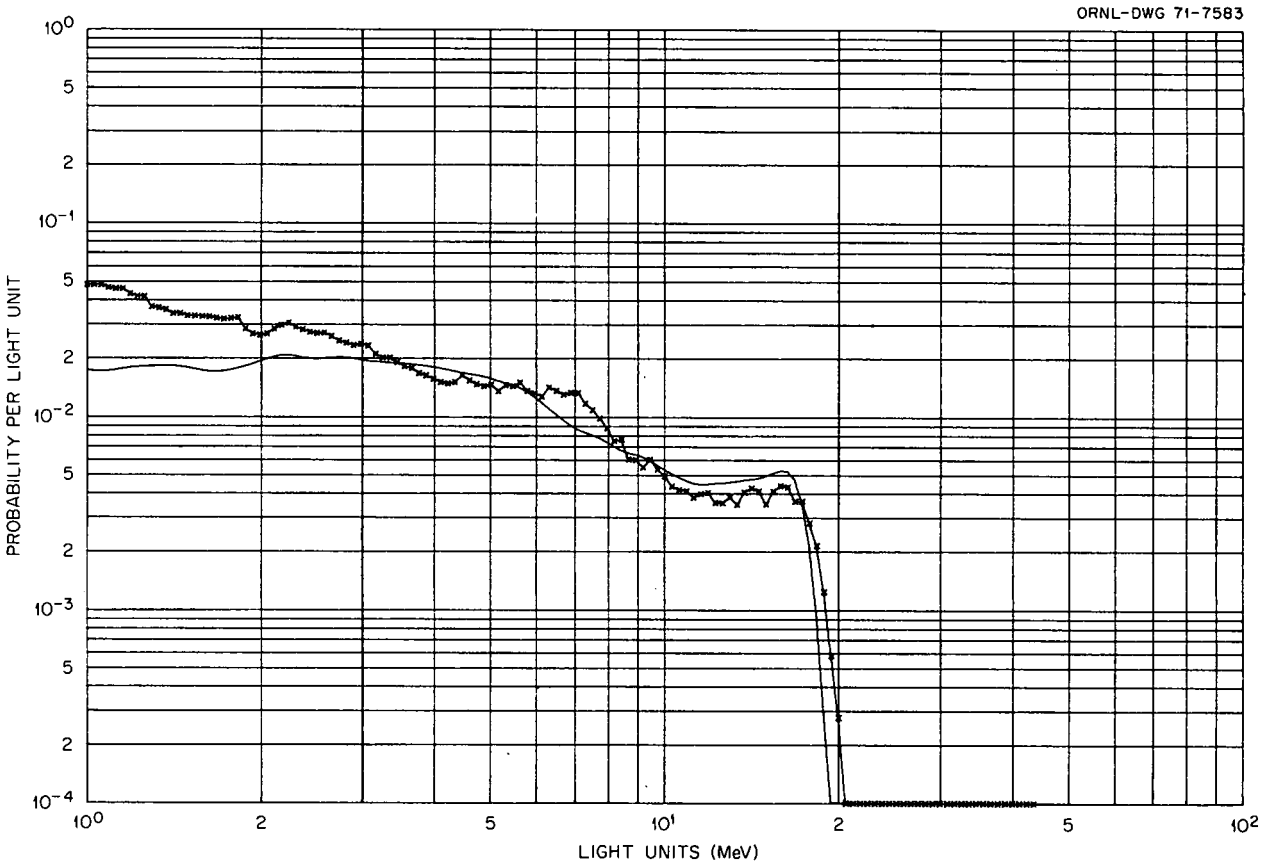

Fig. 5.7.1. Comparison of Theoretical and Measured Response Functions for a 3 in. by 3 in. NE-213 Liquid Scintillator Irradiated by Monoenergetic 30-MeV Neutrons. The theoretical curve was calculated using the 05S Monte Carlo code. The experimental results (x'd line) were inferred using appropriate time intervals from the secondary-neutron measurements of ^{7}Li bombarded by 60-MeV protons and observed at 0 deg. The data were normalized to the 05S results in the range between 3 and 30 light units.

above 30 MeV remains poor, and efforts are being continued to improve the match by further adjustment of the O5S cross-section parameters.

The spectrometer efficiency will be obtained by comparison of these experimental spectra with the calculated response spectra which are assumed to be absolute near the full neutron energy. Based on the comparison, a lower pulse-height limit can be established for each flight time such that the experimental and theoretical responses above this limit are in agreement. The Monte Carlo estimate of the efficiency above this bias point will then be found, and the TOF analysis will be based upon only those counts that fall in the pulse-height region for which the efficiency will best be established. Figure 5.7.2 shows a preliminary analysis of the $^{12}C(p,xn)$ data for 60-MeV protons based upon initial comparisons of the response functions. In the figure, the high-energy peak at each angle of observation corresponds to the $^{12}C(p,n)^{12}N$ ground-state reaction (Q = −18.3). Final cross sections will incorporate efficiency determinations using adjusted cross-section values for the O5S computation.

References

1. Work funded by the National Aeronautics and Space Administration under Order L-12,186.

2. J. W. Wachter, R. T. Santoro, T. A. Love, and W. Zobel, *Neutron Phys. Div. Ann. Progr. Rept. May 31, 1970,* ORNL-4592, p. 104.

3. R. E. Textor and V. V. Verbinski, *O5S: A Monte Carlo Code for Calculating Pulse-Height Distributions Due to Monoenergetic Neutrons Incident on Organic Scintillators,* ORNL-4160 (1968).

4. R. T. Santoro, W. Zobel, and R. E. Textor, *SMOOTHIE: A Program for Smoothing O5S Histogram Output,* ORNL-TM-2597 (1969).

5. L. D. Cohen, T. A. Love, R. T. Santoro, J. W. Wachter, and W. Zobel, *Neutron Phys. Div. Ann. Progr. Rept. May 31, 1969*, ORNL-4433, p. 108.

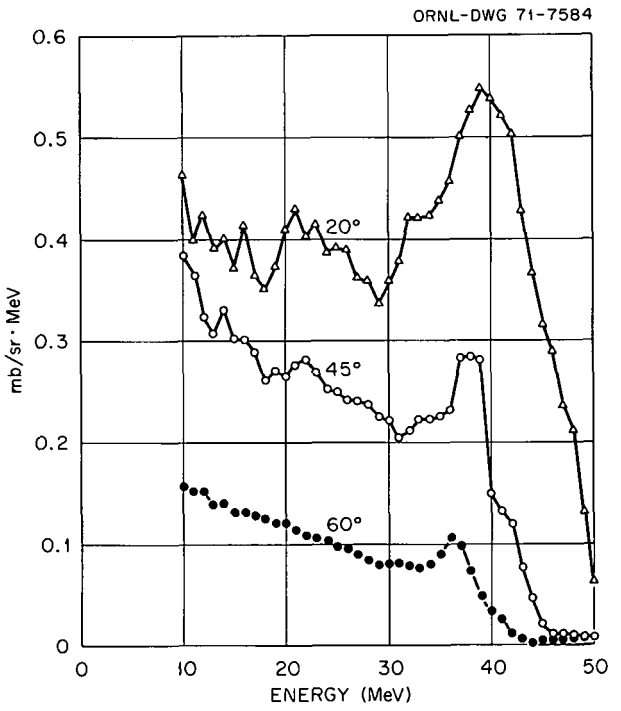

Fig. 5.7.2. Differential Cross Section for Secondary Neutrons from 60-MeV Protons on ^{12}C at 20, 45, and 60 deg (Preliminary Data).

5.8 A PRE-TARGET MONITOR FOR THE INTENSITY AND TIME DISTRIBUTION OF A PROTON BEAM[1,2]

R. T. Santoro J. W. Wachter
T. A. Love

A relative proton beam monitor is described which measures the intensity and time distribution of a proton beam using an ionization chamber and a plastic scintillator. Protons are scattered into the monitor detectors by a mylar film sufficiently thin that the beam and the radiation background are not adversely affected. The beam time spread is inferred from the time distribution of protons and is measured relative to the phase of the cyclotron rf accelerating voltage. Typical results obtained with a 40-MeV proton beam are presented, which show a response reproducibility of 1-4% over a three-decade range in beam intensity.

References

1. Work funded by the National Aeronautics and Space Administration under Order L-12,186.

2. Abstract of ORNL-TM-3249 and *Nucl. Instr. Methods* **93**, 371 (1971).

Publications and Papers Presented at Scientific Meetings

PUBLICATIONS

ALSMILLER, R. G., Jr., F. S. ALSMILLER, J. BARISH, and Y. SHIMA
"Muon Transport and Shielding of High-Energy (≤500 GeV) Proton Accelerators," ORNL-TM-3353 (April 12, 1971). (4.32)*

ALSMILLER, R. G., Jr., T. W. ARMSTRONG, and W. A. COLEMAN
"The Absorbed Dose and Dose Equivalent from Neutrons in the Energy Range 60 to 3000 MeV and Protons in the Energy Range 400 to 3000 MeV," *Nucl. Sci. Eng.* **42**, 367 (1970). (4.13)

ALSMILLER, R. G., Jr., T. W. ARMSTRONG, and Barbara L. BISHOP
"The Absorbed Dose and Dose Equivalent from Negatively and Positively Charged Pions in the Energy Range 10 to 2000 MeV," *Nucl. Sci. Eng.* **43**, 257 (1971); ORNL-TM-3105 (Aug. 24, 1970). (4.15)

ALSMILLER, R. G., Jr., and H. S. MORAN
"Energy Deposition by 45-GeV Photons in Be and Al," ORNL-4631 (November 1970). (4.34)

ALSMILLER, R. G., Jr., F. R. MYNATT, M. L. GRITZNER, J. V. PACE, and J. BARISH
"The Lateral Spread of High-Energy (≤400 MeV) Neutron Beams and Earthshine," *Nucl. Instr. Methods* **89**, 53 (1970); ORNL-TM-3025 (Aug. 3, 1970). (4.23)

ARMSTRONG, T. W.
"Calculation of the Lunar Photon Albedo and Induced Dose Rate from Galactic and Solar Proton Bombardment," ORNL-TM-3268 (June 7, 1971). (4.21)

ARMSTRONG, T. W., and R. G. ALSMILLER, Jr.
"Calculation of Cosmogenic Radionuclides in the Moon and Comparison with Apollo Measurements," ORNL-TM-3267 (Dec. 31, 1970). (4.20)

ARMSTRONG, T. W., R. G. ALSMILLER, Jr., and K. C. CHANDLER
"Monte Carlo Calculations of High-Energy Nucleon-Meson Cascades and Applications to Galactic Cosmic-Ray Transport," ORNL-TM-3319 (Feb. 22, 1971). (4.22)

ARMSTRONG, T. W., and J. BARISH
"Calculated Activation of Copper and Iron by 3-GeV Protons," *Nucl. Sci. Eng.* **41**, 443 (1970). (4.24)

ARMSTRONG, T. W., and B. L. BISHOP
"Calculation of the Absorbed Dose and Dose Equivalent Induced by Medium- Energy Neutrons and Protons and Comparison with Experiment," ORNL-TM-3304 (Feb. 5, 1971). (4.14)

ARMSTRONG, T. W., and K. C. CHANDLER
"Calculation of the Dose, Radionuclide Production, and Delayed Photon Leakage Due to Solar-Proton Bombardment of Tissue with Application to Astronaut Dosimetry," ORNL-TM-3452 (June 1971). (4.18)

ARMSTRONG, T. W., and H. S. MORAN
"Calculation of the Radiation Hazard at Supersonic Aircraft Altitudes Produced by an Energetic Solar Flare - II," *Nucl. Sci. Eng.* **42**, 41 (1970). (4.17)

---

*Abstract of paper published in this report under this number.

BARTINE, D. E., R. G. ALSMILLER, Jr., F. R. MYNATT, W. W. ENGLE, Jr., and J. BARISH
"Low-Energy Electron Transport with the Method of Discrete Ordinates," ORNL-TM-3318 (Feb. 22, 1971).

"Low-Energy Electron Transport by the Method of Discrete Ordinates," ORNL-TM-3438 (Aug. 18, 1971). (4.33)

BERTINI, H. W.
"Charge-Exchange Reactions of Stopped π^--Mesons," *Phys. Rev. C* 2(3) (Aug. 1970).

BERTINI, Hugo W., and Miriam P. GUTHRIE
"Results from Medium-Energy Intranuclear-Cascade Calculation," ORNL-TM-3336 (Aug. 10, 1970). (4.2)

BERTINI, Hugo W., Miriam P. GUTHRIE, and Arline H. CULKOWSKI
"Phenomenologically Determined Isobar Angular Distributions for Nucleon-Nucleon and Pion-Nucleon Reactions Below 3 GeV," ORNL-TM-3132 (Dec. 7, 1970). (4.6)

BERTINI, H. W., M. P. GUTHRIE, and O. W. HERMANN
"Instructions for the Operation of Codes Associated with MECC-3, a Preliminary Version of an Intranuclear-Cascade Calculation for Nuclear Reactions," ORNL-4564 (May 1971). (4.7)

BERTRAND, F. E., and M. B. LEWIS
"Evidence from 62-MeV Proton Scattering for Extending the Weak Coupling Model in ^{209}Bi," *Nucl. Phys.* **168**, 259 (1971). (5.6)

BERTRAND, F. E., and R. W. PEELLE
"Cross Sections for Hydrogen and Helium Particles Produced by 62- and 39-MeV Protons on ^{209}Bi," ORNL-4638 (Jan. 1971). (5.5)

"Hydrogen and Helium Particles Produced by 59-MeV Alpha Particle Bombardment of ^{12}C, ^{16}O, and ^{54}Fe," ORNL-4694 (July 1971). (5.3)

BOOTH, R. S.
"A Comparison of Folding and Unfolding Techniques for Determining the Gamma Spectrum from Thermal Neutron Capture in Aluminum," *Nucl. Instr. Methods* **85**, 69 (1970). (2.43)

BURGART, C. E.
"O6R-D, A Discrete Scattering Version of O6R with Importance Sampling of the Angle of Scatter," ORNL-TM-3031 (Aug. 13, 1970).

BURGART, C. E., and P. N. STEVENS
"A General Method of Importance Sampling the Angle of Scattering in Monte Carlo Calculations," *Nucl. Sci. Eng.* **42**, 306 (1970). (2.39)

BURGART, C. E., E. A. STRAKER, T. A. LOVE, and R. M. FREESTONE, Jr.
"The Energy Spectrum of Photoneutrons Produced by 140-MeV Electrons Incident on Tantalum," *Nucl. Sci. Eng.* **42**, 421 (1970). (2.11)

CAIN, V. R.
"Comparisons of Monte Carlo Calculations to Measurements of Neutron Leakage from the TSR-SNAP Reactor," *Nucl. Sci. Eng.* **41**, 310 (1970). (2.50).

CLAIBORNE, H. Clyde
"Recent Developments in the Shielding of Neutron Sources," ORNL-RSIC-32 (June 1971). (3.7).

CLAIBORNE, H. Clyde, Donald J. DUDZIAK, and Norman M. SCHAEFFER
"Activities of the ANS-6 Subcommittee on Radiation Shielding Standards," ORNL-TM-3251 (December 1970). (3.12)

CLAIBORNE, H. C., and W. W. ENGLE, Jr.
"Bracketing the Peak Primary Gamma-Ray Dose Rate from Nuclear Devices by Steady-State Transport Calculations," ORNL-TM-3462 (June 11, 1971). (2.21)

CLAIBORNE, H. C., R. W. ROUSSIN, J. GURNEY, and A. B. GUSTIN, Editors
"Bibliography, Subject Index, and Author Index of the Literature Examined by the Radiation Shielding Information Center (Reactor and Weapons Radiation Shielding)," ORNL-RSIC-5 (Vol. III) (July 1971). (3.3)

CLAIBORNE, H. C., M. SOLOMITO, and J. J. RITTS
"Heat Generation by Neutrons in Some Moderating and Shielding Materials," *Nucl. Eng. Design* **15**, 232 (1971); ORNL-TM-3157 (Sept. 25, 1970). (2.35)

CLARK, F. H., B. F. MASKEWITZ, J. GURNEY, and M. W. LANDAY, Compilers
"Proceedings of Symposium on Sharing of Computer Programs and Technology in Nuclear Medicine (Collected Papers of a Seminar, April 2-3, 1971)," ORAU-114 (September 1971).

CLIFFORD, C. E., F. R. MYNATT, H. C. CLAIBORNE, V. R. CAIN, R. G. GRAF, M. L. GRITZNER, J. L. HULL, F. J. MUCKENTHALER, E. A. STRAKER, C. L. THOMPSON, and L. R. WILLIAMS
"Preliminary Evaluation of Techniques for Predicting the Spectra of Neutrons Transmitted by Grid Plate Shields," ORNL-TM-2896 (July 31, 1970).

COLEMAN, W. A., and T. W. ARMSTRONG
"NMTC, A Nucleon-Meson Transport Code," ORNL-4606 (October 1970); *Nucl. Sci. Eng.* **43**, 353 (1971). (4.10)

DICKENS, J. K.
"A Monoenergetic 6130-keV Gamma-Ray Source for Detector Calibration," *Nucl. Instr. Methods* **85**, 143 (1970). (2.61)

$^{28-30}$Si($n,x\gamma$) Reactions for $5.3 \leqslant E_n \leqslant 9.0$ MeV," *Phys. Rev.* 2(3), 990 (Sept. 1970). (2.60)

"Al($n,x\gamma$) Reactions for $5.3 \leqslant E_n \leqslant 9.0$ MeV," ORNL-TM-3284 (Jan. 18, 1971). (2.59)

DUPREE, S. A., H. A. SANDMEIER, G. E. HANSEN, W. W. ENGLE, Jr., and F. R. MYNATT
"Time-Dependent Neutron and Photon Transport Calculations Using Method of Discrete Ordinates," LA-4557 (ORNL-4662) (May 1971). (2.20)

EMMETT, M. B.
"INTRIGUE-II: An IBM-360 Subroutine Package for Making Linear, Logarithmic, and Semilogarithmic Graphs Using the Calcomp Plotter," ORNL-4664 (March 1971). (2.33)

ENGLE, W. W., Jr., R. L. CHILDS, and F. R. MYNATT
"The Design of Asymmetric 4π Shields for Space Reactors," ORNL-TM-3368 (April 1, 1971). (2.45)

ENGLE, W. W., Jr., R. L. CHILDS, F. R. MYNATT, and L. S. ABBOTT
"Optimization of a Shield for a Heat-Pipe-Cooled Fast Reactor Designed as a Nuclear Electric Space Power Plant," ORNL-TM-3449 (June 1971). (2.46)

FORD, W. E., III
"The POPOP4 Library and Codes for Preparing Secondary Gamma-Ray Production Cross Sections," ORNL-TM-3367 (April 1, 1971). (2.53)

FREESTONE, R. M., Jr., F. J. MUCKENTHALER, K. M. HENRY, Jr., and C. E. CLIFFORD
"The Low-Energy Neutron Spectrum of the ORNL Tower Shielding Reactor Beam," ORNL-TM-3098 (Aug. 24, 1970). (2.8)

FU, C. Y. and K. J. YOST
"A Unified Model of Deformed Odd-Odd Nuclei for Nuclear Data Generation and Analysis," *Nucl. Sci. Eng.* **41**, 193 (1970). (2.52)

GABRIEL, T. A.
"Calculation of the Long-Lived Induced Activity in the Soil Around High-Energy Accelerator Target Areas," *Nucl. Instr. Methods* **91**, 67 (1971); ORNL-TM-3033 (Aug. 12, 1970). (4.26)

"Calculation of the Long-Lived Induced Activity in Soil Produced by 200-MeV Protons," *Nucl. Appl. Tech.* **9**, 605 (Oct. 1970). (4.25)

GABRIEL, T. A., R. G. ALSMILLER, Jr., and J. BARISH
"Calculation of the Long-Lived Induced Activity in the Soil Around High-Energy Accelerator Target Areas – II," ORNL-4599 (Oct. 1970). (4.27)

GABRIEL, T. A., M. P. GUTHRIE, and O. W. HERMANN
"Instructions for the Operation of the Program Package PICA, an Intranuclear-Cascade Calculation for High-Energy (30 to 400 MeV) Photon-Induced Nuclear Reactions," ORNL-4687 (1971). (4.9)

GABRIEL, T. A., and R. T. SANTORO
"Calculation of the Long-Lived Activity in Soil Produced by 500-GeV Protons," ORNL-TM-3262 (Dec. 21, 1970). (4.28)

"Nucleon and Charged-Pion Albedo Spectra in an Accelerator Cave from 200-GeV Proton Interactions in Iron," ORNL-TM-3437 (1971). (4.31)

GABRIEL, T. A., R. T. SANTORO, and R. G. ALSMILLER, Jr.
"An Approximate High-Energy Alpha-Particle-Nucleus-Collision Model," *Nucl. Sci. Eng.* **44**, 104 (1971); ORNL-TM-3153 (Oct. 1, 1970). (4.5)

GUTHRIE, M. P.
"EVAP-4: Another Modification of a Code to Calculate Particle Evaporation from Excited Compound Nuclei," ORNL-TM-3119 (Sept. 10, 1970). (4.8)

GUTHRIE, M. P., R. G. ALSMILLER, Jr., J. GURNEY, and A. B. GUSTIN (Editors)
"Bibliography, Subject Index, and Author Index of the Literature Examined by the Radiation Shielding Information Center (Space and Accelerator Shielding)," ORNL-RSIC-11 (Rev. 2) (May 1970). (3.4)

"Abstracts of the Literature Examined by the Radiation Shielding Information Center (Space and Accelerator Shielding)," ORNL-RSIC-12, Vol. I Rev. (May 1970). (3.5)

GWIN, R., L. W. WESTON, G. de SAUSSURE, R. W. INGLE, J. H. TODD, F. E. GILLESPIE, R. W. HOCKENBURY, and R. C. BLOCK
"Measurements of the Neutron Fission and Absorption Cross Sections of ^{239}Pu Over the Energy Region 0.02 eV to 30 keV, Part II," *Nucl. Sci. Eng.* **45**, 25 (1971); ORNL-4707 (June 1971).

INGLE, R. W., F. E. GILLESPIE, and L. W. WESTON
"Fast Fission Chamber Amplifier-Discriminator System," *Rev. Sci. Instr.* **41**, 1539 (1970). (1.32)

IRVING, D. C.
"LEGCK, A Subroutine to Analyze Legendre Coefficients for Negativity in the Angular Distribution," ORNL-TM-2903 (Sept. 10, 1970). (2.64)

"The Adjoint Boltzmann Equation and Its Simulation by Monte Carlo," *Nucl. Eng. Design,* Vol. 15, No. 3, 273 (1971). (2.63)

IRVING, D. C., and E. A. STRAKER
"Evaluation of the Cross Sections of IRON: ENDF/B Mat 1101," ORNL-TM-2891 (ENDF-138) (Sept. 10, 1970). (2.31)

KINNEY, W. E., and F. G. PEREY
"Al Neutron Elastic- and Inelastic-Scattering Cross Sections from 4.19 to 8.56 MeV," ORNL-4516 (Oct. 1970). (1.22)

KUMAR, Krishna
"Pairing-Plus-Quadrupole Model Calculations of Band-Mixing Anomalies in ^{152}Sm," *Phys. Rev. Letters* Vol. 26, No. 5 (1971). (2.62)

LUCIUS, J. L., J. D. JENKINS, and R. Q. WRIGHT
"The INDEX Data System: An Index of Nuclear Data Libraries Available at ORNL," ORNL-TM-3334 (1971). (3.10)

MAERKER, R. E., and F. J. MUCKENTHALER
"Gamma-Ray Spectra Arising from Thermal-Neutron Capture in Elements Found in Soils, Concretes, and Structural Materials," *Nucl. Eng. Design* **13**, 455 (1970). (2.19)

"Gamma-Ray Spectra Arising from Fast-Neutron Interactions in Elements Found in Soils, Concretes, and Structural Materials," *Nucl. Sci. Eng.* **42**, 335 (1970). (2.18)

MAERKER, R. E., F. J. MUCKENTHALER, J. J. MANNING, J. L. HULL, J. N. MONEY, K. M. HENRY, and R. M. FREESTONE, Jr.
"Calibration of the Bonner Ball Neutron Detectors Used at the Tower Shielding Facility," ORNL-TM-3465 (June 30, 1971). (2.10)

MAERKER, R. E., L. R. WILLIAMS, F. R. MYNATT, and N. M. GREENE
"Response Functions from Bonner Ball Neutron Detectors," ORNL-TM-3451 (June 4, 1971). (2.9).

MAIENSCHEIN, F. C., C. E. CLIFFORD, F. R. MYNATT, and L. S. ABBOTT
"Shielding for Advanced Reactors in the United States," *Nucl. Eng. Design* **15**, 241 (1971). (2.1)

MASKEWITZ, B. F., and V. Z. JACOBS (Compilers)
"A Review of the Monte Carlo Method for Radiation Transport Calculations (Collected Papers of a Seminar, Oct. 5-7, 1970)," ORNL-RSIC-29 (Feb. 1971). (3.6)

MASKEWITZ, B. F., and D. K. TRUBEY
"Computer Codes for Shielding Calculations - 1970," *Nucl. Eng. Design* **13**, 448 (1970). (3.9)

MOONEY, L. G., M. B. WELLS, and H. C. CLAIBORNE
"Engineering Method for Designing Initial Radiation Shields for Blast-Hardened Underground Structures," Chap. 7 of *Weapons Radiation Shielding Handbook*, L. S. Abbott, H. C. Claiborne, and C. E. Clifford, Editors, DASA-1892-6 (1970) (Classified).

MORGAN, G. L., T. A. LOVE, E. A. STRAKER, R. M. FREESTONE, Jr., and C. E. BURGART
"Energy Calibration of a Proton-Recoil Proportional Counter," ORNL-TM-3347 (March 15, 1971). (2.32)

MOCKEL, A. J., and R. B. PEREZ
"Variation of the R-Matrix," *Phys. Rev. C* 2, 1179 (1970). (1.13)

MYNATT, F. R., C. E. CLIFFORD, F. J. MUCKENTHALER, and M. L. GRITZNER
"The ORNL-SNAP Shielding Program," ORNL-TM-3364 (April 1, 1971). (2.44)

MYNATT, F. R., R. G. ALSMILLER, Jr., and L. R. WILLIAMS
"A Study of Mine Detection by Means of Neutron-Induced Gamma Rays," ORNL-TM-3305 (Jan. 11, 1971).

PACE, J. V., III, F. R. MYNATT, and L. S. ABBOTT
"A Study of the Overlap Conditions Required in Sequential Discrete Ordinates Transport Calculations for a 14-MeV Neutron Source in a 5000-m Radius Cylinder of Air," ORNL-TM-3269 (CTC-40) (June 1971). (2.15)

PEELLE, R. W.
"Experimental Nuclear Cross Sections for Spacecraft Shield Analysis," ORNL-TM-3376 (April 1971). (6.1)

PEELLE, R. W., and F. E. BERTRAND
"Differential Cross Sections at Forward Angles for Hydrogen and Helium Particles from 62-MeV Protons Incident on ^{60}Ni," ORNL-4698 (June 1971). (5.4)

PEELLE, R. W., and F. C. MAIENSCHEIN
"Spectrum of Photons Emitted in Coincidence with Fission of ^{235}U by Thermal Neutrons," *Phys. Rev.* C 3(1), 373 (1971). (1.18)

PENNY, S. K., and W. E. KINNEY
"A Re-Evaluation of Natural Iron Neutron and Gamma-Ray Production Cross Sections - ENDF/Material 1124," ORNL-4617 (April 1971). (2.30)

PEREY, C. M., R. J. SILVA, J. K. DICKENS, and F. G. PEREY
"11 MeV Proton Inelastic Scattering from Even-Even Medium Weight Nuclei," *Phys. Rev.* C 2(2), 468 (1970). (1.26)

PEREY, F. G., and W. E. KINNEY
"V Neutron Elastic- and Inelastic-Scattering Cross Sections from 4.18 to 8.56 MeV," ORNL-4551 (October 1970). (1.21)

"Neutron Elastic- and Inelastic-Scattering Cross Sections for Yttrium in the Energy Range 4.18 to 8.56 MeV," ORNL-4552 (December 1970). (1.19)

PEREZ, R. B.
"Reciertes Avances En La Theoria De La Fision Nuclear (Recent Developments in the Theory of Fission Energia Nuclear)," *Journal of the 'Juntake Energia Nuclear'* XIV(67) (1970) Madrid, Spain.

RITTS, J. J., M. SOLOMITO, and P. N. STEVENS
"A Calculation of Neutron-Induced Physical Doses in Human Tissues," *Nucl. Tech.* **11**, 246 (1971). (2.34)

ROUSSIN, R. W., and F. A. R. SCHMIDT
"Adjoint S_n Calculations of Coupled Neutron and Gamma-Ray Transport Through Concrete Slabs," *Nucl. Eng. Design* **15**, 319 (1971). (3.11)

ROUSSIN, R. W., S. K. PENNY, V. A. SINGLETARY, and J. B. WRIGHT
"Preparation of Data Sets in ENDF Format for Na, Mg, Cl, and K for Use in Shielding Calculations," ORNL-TM-3429 (ENDF-151) (May 27, 1971). (3.10)

SANTORO, R. T., H. C. CLAIBORNE, and R. G. ALSMILLER, Jr.
"Primary- and Secondary-Particle Contributions to the Depth-Dose Distribution in a Phantom Shielded from Solar-Flare and Van Allen Protons," ORNL-TM-3320 (Feb. 18, 1971). (4.19)

SANTORO, R. T., and T. A. GABRIEL
"Calculation of the Nucleon- and Pion-Induced Star and Flux Distributions from 400-GeV Proton Interactions in Iron," ORNL-4673. (4.30)

"Nucleon and Pion Star Production from High-Energy (> 40 GeV) Protons Incident on Iron," ORNL-TM-3335 (March 18, 1971). (4.29)

SANTORO, R. T., J. W. WACHTER, and T. A. LOVE
"A Pre-Target Monitor for the Intensity and Time Distribution of a Proton Beam," *Nucl. Instr. Methods* **93**, 371 (1971); ORNL-TM-3249 (Dec. 1, 1970). (5.8)

SCHMIDT, F. A. R.
"The Attenuation Properties of Concrete for Shielding of Neutrons of Energy Less than 15 MeV," ORNL-RSIC-26 (Aug. 1970).

STEVENS, P. N.
"Use of the Discrete Ordinates S_n Method in Radiation Shielding Calculations," *Nucl. Eng. Design* **13**, 395 (1970). (2.36)

STRAKER, E. A.
"Status of Neutron Transport in the Atmosphere," ORNL-TM-3065 (July 29, 1970).

STRAKER, E. A., C. E. BURGART, T. A. LOVE, and R. M. FREESTONE, Jr.
"Simultaneous Determination of Fast-Neutron Spectra by Time-of-Flight and Pulse-Height Unfolding Techniques," ORNL-TM-3371 (April 5, 1971). (2.12)

STRAKER, E. A., R. L. CHILDS, and M. B. EMMETT
"Application of DOT-MORSE Coupling to the Analysis of Three-Dimensional SNAP Shielding Problems," ORNL-TM-3365 (April 1, 1971). (2.49)

STRAKER, E. A., M. B. EMMETT, and M. L. GRITZNER
"Neutron and Secondary Gamma-Ray Induced Heat in the Ground Due to Point 12.2-15 MeV and Fission Sources at an Altitude of 50 Feet," ORNL-4626 (Nov. 1970). (2.16)

STRAKER, E. A., P. N. STEVENS, D. C. IRVING, and V. R. CAIN
"The MORSE Code - A Multigroup Neutron and Gamma-Ray Monte Carlo Transport Code," ORNL-4585 (September 1970).

THOMPSON, C. L.
"Calculated Neutron Flux Distribution Resulting from a Fission Source Located at the Center of a 10-Meter-Diameter Sphere of Sodium," ORNL-TM-3156 (Oct. 27, 1970).

THOMPSON, C. L., I. J. BROWN, and R. W. ROUSSIN
"User's Manual for Programs to Edit and Combine DLC-5/Hallmark Calculational Results of Neutron and Secondary Gamma-Ray Transport in Air-Over-Ground Geometry," ORNL-TM-3129 (September 1970). (3.11)

TRUBEY, D. K.
"Kernel Methods for Radiation Shielding Calculations," *Nucl. Eng. Design* **13**, 423 (1971). (3.16)

"Gamma-Ray Buildup Factor Coefficients for Concrete and Other Materials," *Nucl. Appl. Tech.* **9**, 439 (1970). (3.17)

WESTON, L. W., R. GWIN, G. de SAUSSURE, R. W. INGLE, J. H. TODD, C. W. CRAVEN, R. W. HOCKENBURY, and R. C. BLOCK
"Neutron Fission and Capture Cross-Section Measurements for ^{233}U in the Energy Region 0.02 to 1 eV," *Nucl. Sci. Eng.* **42**, 143 (1970). (1.10)

WESTON, L. W., and J. H. TODD
"Pulse-Shape Measurements for the Oak Ridge Electron Linear Accelerator with Gamma-Ray Detection Techniques," *Nucl. Instr. Methods* **86**, 205 (1970). (1.17)

"Neutron Multiplicity for ^{239}Pu Resonance Fission," ORNL-TM-3331 (April 1971). (1.4)

YOST, K. J., J. E. WHITE, C. Y. FU, and W. E. FORD, III
"Neutron Energy-Dependent Capture Gamma-Ray Yields in Tantalum and Tungsten," ORNL-TM-3436 (June 7, 1971). (2.56)

PAPERS

Second IAEA International Conference on Nuclear Data for Reactors, Helsinki, Finland, June 15-19, 1970.

G. de SAUSSURE, R. B. PEREZ, and H. DERRIEN: "Multilevel Analysis of the ^{233}U and ^{235}U Capture and Fission Cross Sections and Statistical Properties of the Kapur-Peierls Type Resonance Parameters for the S-Wave Cross Sections of the Fissile Isotopes."

American Nuclear Society Meeting, Los Angeles, California, June 28-July 2, 1970; Trans. Am. Nucl. Soc. 13(1) (1970).

R. G. ALSMILLER, Jr., T. W. ARMSTRONG, and W. A. COLEMAN: "Absorbed Dose and Dose Equivalent from High Energy (<3000 MeV) Neutrons and Protons."

T. W. ARMSTRONG, R. G. ALSMILLER, Jr., and H. S. MORAN: "Photon Leakage from the Moon Due to Solar-Flare Bombardment."

C. Y. FU and K. J. YOST: "A Unified Model of Deformed Odd-Odd Nuclei for Nuclear Data Generation and Analysis."

K. KUMAR and K. J. YOST: "An Adaptation of the Core-Quasi-Particle Coupling Model for Neutron Cross-Section Generation and Analysis."

R. E. MAERKER and F. J. MUCKENTHALER: "Gamma-Ray Spectra Arising from Fast-Neutron Interactions in Iron, Aluminum, Copper, Zinc, and Titanium."

R. W. PEELLE, F. C. MAIENSCHEIN, and W. ZOBEL: "Prompt Gamma Rays from Thermal Fission of Uranium-235."

S. K. PENNY: "Calculation of Cross Sections for Gamma-Ray Production Via Neutron Inelastic Scattering in ^{56}Fe."

R. W. ROUSSIN and F. A. R. SCHMIDT: "Adjoint S_n Calculations of Coupled Neutron, Gamma-ray Transport Through Concrete Slabs."

E. G. SILVER, R. W. INGLE, R. B. PEREZ, and G. de SAUSSURE: "Neutron Capture Cross Sections of ^{238}U Below 100 keV."

E. A. STRAKER: "Status of Neutron Transport in the Atmosphere."

12th Meeting of the European-American Committee on Reactor Physics, Richland, Washington, July 7-9, 1970.

Fred C. MAIENSCHEIN: "Advanced Reactor Shielding in the United States."

Gordon Conference on Nuclear Structure Physics, July 27-31, 1970, Tilton, New Hampshire.

K. KUMAR: "Present Status of the Calculation of Nuclear Deformation."

International Conference on Properties of Nuclei Far from the Region of Beta-Stability, Leysin, Switzerland, August 31-September 4, 1970; CERN Report No. 70-30, Geneva, November 1970, pp. 779-812.

K. KUMAR: "New Aspects of Intermediate Nuclei."

Third International Symposium on Polarization Phenomena in Nuclear Reactions, Madison, Wisconsin, August 31-September 4, 1970.

F. G. PEREY: "Nucleon-Nucleus Optical Model Potential."

American Physical Society Meeting, Houston, Texas, October 15-17, 1970; Bull. Am. Phys. Soc. Ser. II, 15(12) (1970)

F. E. BERTRAND and R. W. PEELLE: "Protons, Deuterons, Tritons, and Alpha Particles Produced in Bombardment of ^{54}Fe by 59-MeV Alpha Particles."

R. B. PEREZ and G. de SAUSSURE: "Multilevel Effects in Fissile Cross Sections."

American Nuclear Society Meeting, November 15-19, 1970, Washington,D. C.; Trans. Am. Nucl. Soc. Vol. 13, No. 2 (1970).

C. E. BURGART and W. W. ENGLE, Jr.: "Time-Dependent Coupled Neutron-Gamma Calculations in Polyethylene."

H. C. CLAIBORNE, D. J. DUDZIAK, and N. M. SCHAEFFER: "Activities of the ANS-6 Subcommittee on Radiation Shielding Standards."

G. de SAUSSURE, R. B. PEREZ, E. G. SILVER, R. W. INGLE, and H. WEAVER: "Simultaneous Measurements of the Fission and Capture Cross Sections of ^{235}U up to 100 keV."

R. B. PEREZ, G. de SAUSSURE, E. G. SILVER, and R. W. INGLE: "Measurements of the Capture Cross Section of ^{238}U up to 100 keV."

E. A. STRAKER, C. E. BURGART, T. A. LOVE, and R. M. FREESTONE, Jr.: "Simultaneous Fast-Neutron Spectral Measurements by Time-of-Flight and Pulse-Height Unfolding Techniques."

K. J. YOST and P. H. PITKANEN: "The Application of Extended R-Matrix Theory to Elastic Scattering of Neutrons by ^{12}C."

K. J. YOST, J. E. WHITE, and C. Y. FU: "Neutron Energy-Dependent Capture Gamma-Ray Yields for ^{238}U and ^{181}Ta."

37th Meeting of the Southeastern Section of the American Physical Society, November 23-25, 1970.

R. E. MAERKER and F. J. MUCKENTHALER: "Neutron Inelastic Scattering from the 4.43-MeV Level in ^{12}C and the 6.13-MeV Level in ^{16}O."

Specialists Panel on Reactor Shielding on "The Physics Problems of Reactor Shielding," Held Jointly by the IAEA and the ENEA, Paris, France, December 8-10, 1970.

F. C. MAIENSCHEIN, C. E. CLIFFORD, F. R. MYNATT, and L. S. ABBOTT: "Shielding for Advanced Reactors in the United States."

Second Lunar Science Conference on Manned Spacecraft Center (NASA), Houston, Texas, January 11, 1971.

T. W. ARMSTRONG, and R. G. ALSMILLER, Jr.: "Calculation of Cosmogenic Radionuclides in the Moon and Comparison with Apollo Measurements."

American Physical Society Meeting, February 1-4, 1971, New York; Bull. Am. Phys. Soc., Ser. II, 16(1) (1971).

Krishna KUMAR: "Pairing-Plus Quadrupole Model Calculations for the Transitional Nuclei $^{150-152}$Sm."

National Symposium on Natural and Manmade Radiation in Space, Las Vegas, Nevada, March 1-5, 1971.

T. W. ARMSTRONG, R. G. ALSMILLER, Jr., and K. C. CHANDLER: "Monte Carlo Calculations of High-Energy Nucleon-Meson Cascades and Applications to Galactic Cosmic-Ray Transport."

T. W. ARMSTRONG and B. L. BISHOP: "Calculations of the Absorbed Dose and Dose Equivalent Induced by Medium-Energy Neutrons and Protons and Comparison with Experiment."

D. E. BARTINE, R. G. ALSMILLER, Jr., F. R. MYNATT, W. W. ENGLE, Jr., and J. BARISH: "Low-Energy Electron Transport with the Method of Discrete Ordinates."

C. E. BURGART: "MORSE Monte Carlo Shielding Calculations for the Zirconium Hydride Reference Reactor."

W. W. ENGLE, Jr., R. L. CHILDS, and F. R. MYNATT: "The Design of Asymmetric 4π Shields for Space Reactors."

W. E. FORD, III: "The POPOP4 Library and Codes for Preparing Secondary Gamma-Ray Production Cross Sections."

F. R. MYNATT, C. E. CLIFFORD, F. J. MUCKENTHALER, and M. L. GRITZNER: "The ORNL-SNAP Shielding Program."

R. W. PEELLE: "Experimental Nuclear Cross Sections for Spacecraft Shield Analysis."

R. T. SANTORO, H. C. CLAIBORNE, and R. G. ALSMILLER, Jr.: "Primary- and Secondary-Particle Contributions to the Depth-Dose Distribution in a Phantom Shielded from Solar-Flare and Van Allen Protons."

E. A. STRAKER, R. L. CHILDS, and M. B. EMMETT: "Application of DOT-MORSE Coupling to the Analysis of Three-Dimensional SNAP Shielding Problems."

W. ZOBEL, T. A. LOVE, J. T. DELORENZO, and C. O. McNEW: "Neutron Spectral Measurements in the Upper Atmosphere,"

Third Conference on Neutron Cross Sections and Technology, Knoxville, Tennessee, March 15-17, 1971.

J. K. DICKENS and F. G. PEREY: "The Ca($n,x\gamma$) Reaction at E_n = 5.9 MeV."

W. E. KINNEY and F. G. PEREY: "Comparisons of ENDF/B Evaluated Neutron Scattering Cross Sections for Eight Elements with Recent Experimental Data from 1 to 8.5 MeV."

S. K. PENNY and W. E. KINNEY: "A Re-Evaluation of Natural Iron Neutron and Gamma-Ray Production Cross Sections ENDF/B Material 1124."

F. G. PEREY, W. E. KINNEY, and R. L. MACKLIN: High Resolution Inelastic Cross Section Measurements for Na, Si, and Fe."

E. G. SILVER, G. de SAUSSURE, R. B. PEREZ, and R. W. INGLE: "Measurement of Neutron Cross Sections in ^{238}U and ^{235}U Below 100 keV at the ORELA."

L. W. WESTON and J. H. TODD: "Neutron Multiplicity of ^{239}Pu Resonance Fission."

Symposium on Sharing of Computer Programs and Technology in Nuclear Medicine, April 2-3, 1971; proceedings published as ORAU-114 (Sept. 1971).

B. F. MASKEWITZ: "A Computer Code Center – Experience and Current Operations." (Topical Meeting of the Society of Nuclear Medicine, Inc.)

American Nuclear Society National Topical Meeting on Neutron Sources and Applications, Augusta, Georgia, April 19-22, 1971.

H. C. CLAIBORNE: "Recent Developments in the Shielding of Neutron Sources."

International Congress on Protection Against Accelerator and Space Radiation, CERN, Geneva, April 26-30, 1971.

R. G. ALSMILLER, Jr., J. BARISH, F. S. ALSMILLER, and Y. SHIMA: "Muon Transport and the Shielding of High-Energy ($\leqslant$500 GeV) Proton Accelerators."

ORNL-4705
UC-34 – Physics

INTERNAL DISTRIBUTION

1. L. S. Abbott
2. F. S. Alsmiller
3. R. G. Alsmiller, Jr.
4. T. W. Armstrong
5. J. Barish
6. H. W. Bertini
7. F. E. Bertrand
8. N. A. Betz
9. B. L. Bishop
10. A. L. Boch
11. R. S. Booth
12. C. E. Burgart
13. V. R. Cain
14. K. C. Chandler
15. G. T. Chapman
16. H. C. Claiborne
17. F. H. S. Clark
18. C. E. Clifford
19. H. E. Comolander
20. S. N. Cramer
21. C. W. Craven
22. A. H. Culkowski
23. F. L. Culler
24. J. T. DeLorenzo
25. G. de Saussure
26. J. K. Dickens
27. M. B. Emmett
28. W. W. Engle, Jr.
29. W. E. Ford III
30. F. L. Fowler
31. R. M. Freestone, Jr.
32. C. Y. Fu
33. T. A. Gabriel
34. J. S. Gillen
35. F. E. Gillespie
36. L. W. Gilley
37. J. H. Gillette
38. N. B. Gove
39. N. M. Greene
40. M. L. Gritzner
41. Jane Gurney
42. M. P. Guthrie
43. R. Gwin
44. J. A. Harvey
45. H. R. Hendrickson
46. K. M. Henry, Jr.
47. O. W. Hermann
48. R. F. Hibbs
49. N. W. Hill
50. L. B. Holland
51. J. L. Hull
52. R. W. Ingle
53. J. D. Jenkins
54. W. H. Jordan
55. R. Keubbing
56. W. E. Kinney
57. C. O. Le Rigoleur
58. J. Lewin
59. M. B. Lewis
60. T. A. Lewis
61. T. A. Love
62. J. L. Lucius
63. R. L. Macklin
64. H. G. MacPherson
65. E. Madden
66. R. E. Maerker

67–141. F. C. Maienschein

142. J. J. Manning
143. B. F. Maskewitz
144. J. W. McConnell
145. C. O. McNew
146. J. K. Millard
147. G. L. Morgan
148. F. J. Muckenthaler
149. F. R. Mynatt
150. D. O. Nellis
151. C. E. Newlon
152. J. V. Pace

153–154. R. B. Parker

155. J. W. Paul
156. R. W. Peelle
157. S. K. Penny
158. C. M. Perey
159. F. G. Perey
160. R. Perez
161. H. P. Ramon
162. J. W. Reynolds
163. R. W. Roussin
164. R. D. Sabin
165. R. T. Santoro
166. G. R. Satchler
167. R. J. Silva
168. E. G. Silver
169. M. J. Skinner

170. G. G. Slaughter
171. A. H. Snell
172. P. H. Stelson
173. J. R. Stockton
174. D. A. Sundberg
175. C. L. Thompson
176. H. A. Todd
177. J. H. Todd
178. D. K. Trubey
179. T. J. Tyrell
180. J. W. Wachter
181. D. R. Ward
182. H. Weaver
183. A. M. Weinberg
184. L. W. Weston
185. J. E. White
186. L. R. Williams
187. D. R. Winkler
188. H. A. Wright
189. J. B. Wright
190. R. Q. Wright
191. K. Yamada
192. G. Young
193. W. Zobel
194. H. Feshbach (consultant)
195. H. Goldstein (consultant)
196. C. R. Mehl (consultant)
197. H. T. Motz (consultant)
198. RSIC Library
199. Biology Library
200–202. Central Research Library
203. ORNL–Y-12 Technical Library Document Reference Section
204–253. Laboratory Records Department
254. Laboratory Records, ORNL RC

EXTERNAL DISTRIBUTION

255–621. Given external distribution
622. P. B. Hemmig, Reactor Development & Technology, U.S. Atomic Energy Commission, Washington, D.C. 20545
623. W. H. Hannum, Reactor Development & Technology, U.S. Atomic Energy Commission, Washington, D.C.
624. K. O. Laughon, AEC Site Representative, ORNL
625. C. P. McCallum, Division of Space Nuclear Systems, U.S. Atomic Energy Commission, Washington, D.C. 20545
626. Morton F. Fleishman, Space Nuclear Propulsion Office, U.S. Atomic Energy Commission, Washington, D.C. 20545
627. R. L. Detterman, Atomics International, 8900 Desota Street, Box 309, Canoga Park, California
628. J. G. Gallagher, Manager, Thermal & Nuclear Design, Westinghouse Astronuclear Laboratory, P.O. Box 10864, Pittsburgh, Pa. 15236
629. G. A. Graves, N-2 Division, Los Alamos Scientific Laboratory, P.O. Box 1663, Los Alamos, New Mexico 87544
630. H. Derrien, Centre d'Etudes Nucleaires de Saclay, France
631. W. Kolar, Central Bureau for Nuclear Measurements, Euratom, Geel, Belgium
632. A. J. Mockel, University of Florida, Gainesville
633. J. L. Rathbun, The Westinghouse Electric Corp., Advanced Reactor Division, Waltz Mill Site, Madison, Pa.
634. S. A. Dupree, Naval Weapons Evaluation Facility, Albuquerque, New Mexico
635. G. E. Hansen and H. A. Sandmeier, Los Alamos Scientific Laboratory, Los Alamos, New Mexico
636. R. C. Trammell, Oak Ridge Technical Enterprises Corp., Inc., Oak Ridge, Tenn.
637. D. J. Dudziak, Los Alamos Scientific Laboratory, Los Alamos, New Mexico
638. N. M. Schaeffer, Radiation Research Associates, Fort Worth, Texas
639. A. E. Profio, University of California, Santa Barbara, California
640. F. A. R. Schmidt, Institute for Kernenergetik, Stuttgart, Germany
641. J. J. Ritts, Westinghouse Advanced Reactor Division, Waltz Mill Site, Madison, Pa. 15663
642. D. C. Irving, 816 Legare Road, Aiken, South Carolina 29081
643. L. G. Mooney, Radiation Research Associates, Inc., 3550 Hulen Street, Fort Worth, Texas 76107

644. K. J. Yost, Department of Nuclear Engineering, Purdue University, Lafayette, Indiana 47907
645. M. Solomito, 3699 South Galloway Drive, Memphis, Tenn.
646. E. A. Straker, Science Applications, Inc., Clinton Bldg., Suite 432, 2109 Clinton Avenue West, Huntsville, Alabama 35805
647. K. Kumar, Physics Department, Stevenson Science Center, Vanderbilt University, 21st Avenue South, Nashville, Tenn. 37203
648. P. N. Stevens, Oregon State University, Radiation Center, Corvallis, Oregon 97331
649. J. A. Swartout, Union Carbide Corporation, New York, N.Y. 10017
650–652. Director, Division of Reactor Licensing
653–654. Director, Division of Reactor Standards
655–659. Executive Secretary, Advisory Committee on Reactor Safeguards
660. Laboratory and University Division, AEC, ORO
661. Patent Office, AEC, ORO
662–895. Given distribution as shown in TID-4500 under Physics category (25 copies – NTIS)